SYNTHESIS OF OLIGOMERS, POLYMERS AND CUCURBITURIL-BASED POLYROTAXANES TOWARDS POLYMER LIGHT EMITTING DIODE AND PHOTODYNAMIC THERAPY APPLICATION

A THESIS SUBMITTED TO

THE DEPARTMENT OF CHEMISTRY

AND THE GRADUATE SCHOOL OF ENGINEERING AND SCIENCE

OF BILKENT UNIVERSITY

IN PARTIAL FULFILLMENT OF THE REQUIREMENTS

FOR THE DEGREE OF

MASTER OF SCIENCE

By

Muazzam Idris

June 2014

I certify that I have read this thesis and have found that it is fully adequate, in scope and in quality, as a thesis for the degree of Master of Science.

_____

Assoc. Prof. Dr. Dönüş Tuncel
Supervisor

I certify that I have read this thesis and have found that it is fully adequate, in scope and in quality, as a thesis for the degree of Master of Science.

_____

Prof. Dr. Ahmet M. Önal
Examining Committee Member

I certify that I have read this thesis and have found that it is fully adequate, in scope and in quality, as a thesis for the degree of Master of Science.

_____

Assist. Prof. Dr. Ferdi Karadaş
Examining Committee Member

Approval of the Graduate School of Engineering and Science

_____

Prof. Dr. Levent Onural
Director of the Institute

ABSTRACT

SYNTHESIS OF OLIGOMERS, POLYMERS AND CUCURBITURIL-BASED POLYROTAXANES TOWARDS POLYMER LIGHT EMITTING DIODE AND PHOTODYNAMIC THERAPY APPLICATION

MUAZZAM IDRIS

M.S. in Chemistry

Supervisor: Assoc. Prof. Dr. Dönüş Tuncel

June 2014

In the first part of this study, porphyrin-thiophene monomers, oligomers and polymer are synthesized for photodynamic therapy application. Water solubility and the ability of a photosensitizer to generate singlet oxygen for tumor destruction are important conditions for ideal photosensitizer in photodynamic therapy application. For this purpose, water soluble pendent groups are attached to the porphyrin monomers before coupling with thiophene monomer to form oligomers and polymer. The presence of sulfur atom in thiophene facilitates intersystem crossing due to spin-orbit coupling and thus will increase singlet oxygen generation. Consequently, the ability of singlet oxygen generation of the polymer is found to be higher than oligomers followed by monomers.

In the second part of the thesis, the effects of cucurbit[n]uril on photophysical, electrochemical and thermal properties of ionic conjugated polymers in water are described.

Conjugated polymers are well known for their interesting optical properties and are used in the area of light emitting diodes. However, their stacking nature reduces their fluorescent quantum yields and thus limits their further applications. If the interactions among the polymers chains are reduced or the polymer backbones are insulated in some means, the emission efficiency of the polymers could be enhanced.

For this purpose, two different green emitting fluorene-thiophene based polymers (**29** and **33**) and their cucurbituril based polyrotaxanes counterparts (**30** and **34**) are synthesized through Suzuki Coupling. In both polyrotaxane **30** and **34**, enhancement in optical properties was

observed showing fluorescent quantum yields of 0.46 and 0.55 in water respectively comparing to polymers **29** and **33** which has only 0.10 and 0.35 in water respectively.

Their optical and electroluminescent properties were further utilized by fabricating devices as multilayer white polymer light emitting diodes (PLEDs).

The synthesized molecules are characterized by ^{1}H-NMR, ^{13}C-NMR, ESI mass spectrometry, UV-VIS, photoluminescence, time resolved fluorescence spectroscopy, FT-IR, elemental analysis gel permeation chromatography, size exclusion chromatography, thermogravimetric analysis and cyclic voltammetry.

Keywords: Photodynamic therapy, Singlet oxygen, Conjugated polymer, Polyrotaxane, Cucurbituril, Polymer light emitting diode.

ÖZET

POLİMER IŞIK YAYAN DİYOTLAR VE FOTO DİNAMİK TERAPİ UYGULAMARA YÖNELİK OLİGOMERLERİN, POLİMERLERİN VE KÜKÜRBİTÜRİL TABANLI POLİROTAKSANLARIN SENTEZİ

MUAZZAM IDRIS

Kimya Bölümü Yüksek Lisans Tezi

Tez Yöneticisi: Assoc. Prof. Dr. Dönüş Tuncel

Haziran 2014

Bu çalışmanın ilk bölümünde, porfirin-tiyofen tabanlı monomerler, oligomerler ve polimerler, foto dinamik terapi uygulaması için sentezlendi. Bir molekülün iyi bir foto uyarıcı olabilmesi için suda çözünürlüğünün iyi olması ve singlet oksijen üretme veriminin yüksek olup, tümörlü hücreye zarar vermesi gibi koşulları sağlaması gerekmektedir. Bu amaçla, oligomer ve polimer elde etmek için, tiyofin ile eşleşme reaksiyonundan önce, suda çözünür yan gruplar porfirin molekülüne takıldı. Porfirin tabanlı oligomer ve polimerin, tiyofende bulunan sülfür atomunun ağır atom etkisi yaratıp, porfirinin singlet elektronik durumundan triplete geçişini kolaylaştıracağı ve dolayısı ile reaktif oksijen radikallerinin oluşum verimini de yükselteceği bilinmektedir. Sonuç olarak, polimerin reaktif oksijen radikallerinin oluşum verimi, oligomer ve monomerin reaktif oksijen radikallerinin oluşumunundan daha fazla olduğu gözlenildi.

Çalışmanın ikinci kısmında ise, kükürbitürilin iyonik konjuge polimerlerin uzerine fotofiziksel, elektrokimyasal ve termal özellikleri etkisi incenlendi.

Konjuge polimerlerin ilginç optik özelliklerinden dolayı, bu polimerler ışık yayıcı diyotların alanında kullanılmaktadır. Fakat, konjuge polimerin üst üste binme yapısından dolayı flüoresans verimi düşer bu da foto uygulamarını sınırlandırır. Eğer polimerler zincirleri

arasında etkileşimler azatılırsa veya polimer omurgaları bazı yollarla izole edilirse, polimerlerin emisyon verimliliği arttırılabilir.

Bu amaçla, iki farklı yeşil ışık yayan fluoren-tiyofen tabanlı polimerler (**29** ve **33**) ve bunların kükürbitüril tabanlı polirotaksanlar (**30** ve **34**) Suzuki eşleşme yoluyla sentezlendi. Hem polirotaksan **30** hem de polirotaksan **34**'te flüoresans verimi artışı gözlendi. Polimer (**29**), polimer (**33**), polirotaksan (**30**) ve polirotaksan (**34**) 0.1, 0.35, 0.46 ve 0.55 sırasıyla flüoresans kuantum verimine sahipler.

Bu malzemelerin optik ve elektrokimyasal özellikleri daha da incelemek için çok tabakalı beyaz polimer ışık yayan diyotlarda (PLEDs) kullanıldı.

Sentezlenen malzemelerin yapılarını tayin etmek için, nükleer manyetik resonans spektrometresi (NMR), kütle spektrometresi, UV-Vis, Flüoresan, zaman ayrımlı floresans spektroskopisi, kızıl ötesi (FT-IR) spektrometresi, elemental analiz, jel geçirgenlik kromatografisi (GPC), termogravimetrik analiz (TGA) ve döngüsel voltametri yöntemlerinden yararlanıldı.

Anahtar kelimeler: Foto dinamik terapi, Singlet oksijen üretimi, Konjuge polimer, Polirotaksan, Kükürbitürilin, Polimer ışık yayan diyotlar.

Acknowledgement

I would like to express my deepest appreciation to Assoc. Prof. Dr. Dönüş Tuncel for her supervision and support throughout my master studies.

I would like to thank Dr. Rehan Khan who helped me throughout the porphyrin work. I would like to also thank Burak Güzeltürk for his help in the fabrication of polymer light emitting diodes.

A special thanks to TÜBİTAK-TBA6 112T058 for supporting this project.

I finally want to thank Sinem Gürbüz, Esra Deniz Soner, Dr. Jousheed Pennakalathil, Hamidou Keita, Alp Özgün and Özlem Ünal for their kind help throughout my master degree.

A special thanks to all my family members who supported and encouraged me throughout my entire education.

Table of Contents

Abbreviations

BBr_3	Boron tribromide
CV	Cyclic voltammetry
CD	Cyclodextrin
CB	Cucurbituril
DMF	Dimethyl formamide
DMSO	Dimethyl sulfoxide
DPBF	1,3-diphenylisobenzofuran
DCM	Dichloromethane
Da	Dalton
EL	Electroluminescence
GPC	Gel Permeation Chromatography
THF	Tetrahydrofuran
ITO	Indium tin oxide
IMWs	Insulated Molecular Wires
MeOH	Methanol
OLED	Organic light emitting diode
PS	Photosensitizer
PL	Photoluminescence
PDT	Photodynamic Therapy
PLED	Polymer light emitting diode
SEC	Size Exclusion Chromatography
TGA	Thermogravimetric Analysis
TLC	Thin Layer Chromatography
TFA	Trifluoroacetic acid
TCBQ	Tetrachloro-*p*-benzoquinone
TEG	Triethylene glycol
$^1O_2$	Singlet oxygen
Φ	Photoluminescence quantum yield
λ	Wavelength

List of Figures

List of Schemes

List of Tables

Chapter 1 Introduction

1.1. Conjugated polymers

Conjugated system is a system having pi electrons connected to one another in a compound having single bonds alternated by multiples bonds. In 1977 Shirakawa and cowers observed the significant increase in conductivity of polyacetylene by doping it with various electron acceptors or electron donors [1]. This finding opens the way for designing different conjugated polymers by varying the nature of the backbone and pendent groups. Some of the common conjugated polymers are given in Table 1.1.

Table 1.1: Some Important Conjugated Polymers

Polymer	Structure	Band gap (eV)
Trans-polyacetylene (PA)	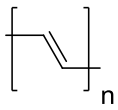	1.5
Poly(*p*-phenylene) (PPP)	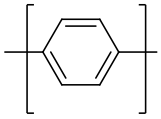	3.3
Poly(*p*-phenylenevinylene) (PPV)	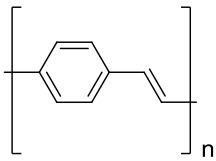	2.5
Polyfluorene (PF)	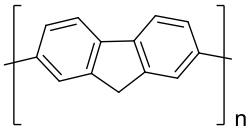	3.2
Polythiophene (PT)	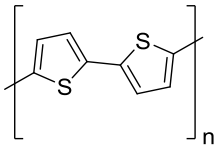	2.0

1.1.1. Structure of Conjugated Polymers

The alternation of multiple and single bonds along the skeleton chain of conjugated polymers results in the π- electron delocalization. Such delocalization results in conducting or semiconducting properties of conjugated polymers. These properties made conjugated polymers to be good candidates for electrochemical insertion electrodes, high-conductivity/low-density metals, materials for non-linear optics and as semiconductors [2-5].

There are two conditions conjugated polymer must satisfy to work as a semiconductor [6, 7]. The first one is that the σ bonds should be much stronger than the π bonds so that they can hold the molecule together even when there are excited states, such as electrons and holes, in the π bonds otherwise the π bonds and the molecule would split apart. The second one is that π-orbitals on neighboring polymer molecules should overlap with each other so that electrons and holes can move in three dimensions between molecules. Fortunately many polymers satisfy these two requirements. Most conjugated polymers have semiconductor band gaps of 1.5-3.0 eV, which means that they are ideal for optoelectronic devices.

1.1.2. Band gap of conjugated polymers

Electrical properties of inorganic materials are determined by the movement of electron from one energy discrete level to another known as energy bands. Considering conductivity in inorganic materials, there are basically three types of materials: Conductors, semiconductors and insulators. Conductors for example metals have high conductivities [8]. In these kinds of materials there is no energy difference between the conduction and the valence band and thus electrons can easily flow from valence band to the conduction band. However, semiconductors have small energy difference between the valence and the conduction band. Thus it is more difficult for the electrons to flow from the valence band to the conduction band. Insulators have very large band gap and thus it is impossible to transfer electrons from the valence bands to the conduction bands.

In contrasts to the inorganic materials the electronic and optical properties of conjugated polymers are mainly determined by their π-electron system. In the ground state of the conjugated polymer, the π-electrons have a sequence of energetic levels that together form the π-bonds. The highest energy π-electron level is referred to as the highest occupied molecular orbital (HOMO). In the excited state, the π-electrons form the π*-electron level which is referred to as the lowest unoccupied molecular orbital (LUMO). The HOMO and

LUMO are known as the frontier orbitals. The energy difference between the HOMO and LUMO (π-π*) is called the energy band gap of the polymer.

The value of HOMO is same as the ionization potential (IP) of the molecule while the value of the LUMO represents the electron affinity (EA). The values of IP and EA are important parameters for an OLED material because they determine the ease of hole and electron injection.

The HOMO level and LUMO level of small molecules can easily be determined using ultraviolet photoelectron spectroscopy (UPS). However for large molecules like polymers, this technique cannot be used because large molecules cannot be thermally deposited. To measure the HOMO and LUMO energy of large molecules, cyclic voltammetry (CV) is usually used [9]. CV is an electrochemical method that gives the values of the oxidation and reduction potentials for a material in solution relative to a reference redox couple. The HOMO and LUMO values obtained from CV may not be equivalent to the true IP or EA.

Generally the band gap of conjugated polymers lies within the range of 1.0-4.0 eV and this value increases when the π-electrons become more highly confined [10, 11]. However, in polymers where the wavefunctions are highly delocalized, the band gap is largely determined by the degree of conjugation or bond alternation and increasing the delocalized π-electrons.

1.1.3. Photoluminescence from conjugated polymers

The conjugated backbones of conjugated polymers allow π-electrons to be delocalized extensively along the chain. Due to this π-electrons delocalization, most conjugated polymers appear colored and show interesting photophysical phenomena, such as photoluminescence (PL) [12], photoconductivity, [13] and nonlinear optical properties (NLO) [2]. Electron is excited from highest occupied molecular orbital (HOMO) (or ground state S_0) to the lowest unoccupied molecular orbital (LUMO) when conjugated polymer is irradiated by light. The excited electron in LUMO is unstable and loses its energy in the following ways: (1) Emission of radiation, such as fluorescence; (2) Radiationless transitions, such as internal conversion or intersystem crossing; (3) Photochemical reactions, such as rearrangements and dissociations. The excess energy of the electron in the excited state is rapidly dissipated and the lowest vibration level of the excited singlet state is attained. This phenomenon is known as internal conversion. If all of this excess energy is not further dissipated by collisions, the electron returns to the ground state with the emission of energy in the form of light. This phenomenon is called fluorescence. Because some of the energy of the electron was lost through vibrational relaxation, the energy of the light emitted ($h\upsilon_e$) by the conjugated

polymer is always less than the energy of the light ($h\upsilon_a$) used to excite the electron. This energy difference between absorbed and emitted light ($h\upsilon_a$-$h\upsilon_e$) is termed as the Stokes shift. Another possibility is that the electron will not return to the ground state, instead it will cross to triplet state (intersystem crossing) and then returns to singlet ground state with the emission of light. This phenomenon is called phosphorescence. Organic molecules usually have very low possibility of emitting light through phosphorescence because their spin-orbit coupling is very small. To increase the possibility of phosphorescence in organic molecules heavy atoms are usually introduced to increase the spin-orbit coupling [90]. Photoluminescence (PL) is the collective name of phosphorescence and fluorescence when light is used as a source of energy for the excitation.

The photoluminescence (PL) property of conjugated polymers makes them suitable for the application as active layers in polymer light-emitting diodes (PLEDs). In PLED light is emitted through electroluminescence (EL). PL and EL are similar concepts but often they are wrongly used. In PL light is converted into visible light using an organic compound as the active material whereas in EL, the organic compound converts an electric current into visible light [14].

Photoluminescence efficiency is an important property of photonic device. In polymers, excimer formation and existence of quenching center determines the photoluminescence efficiency [15]. Excimer formation usually occurs when the backbones of neighboring polymers are very close which will result in a spectral red shift, spectral broadening and inefficiency [16-18]. Although the mechanism of polymer quenching is not fully understood, one type of quenching is the nonradiative recombination through carbonyl defects [19]. Carbonyl defects form when conjugated polymers are excited in the presence of oxygen. This defect reduces the efficiency of a polymer because excitations migrate to find the defects, which have an energy level within the band gap of polymer. To prevent this effect, photonic devices are usually made in an inert atmosphere and sealed in an air tight package.

Another factor that affects the fluorescence of conjugated polymers is the substituents on the conjugated polymer. Large bulky substituent groups weaken intermolecular interaction and mobility and thus increase the PL efficiency [20]. Increasing the intrinsic stiffness of the polymer also increases the PL efficiency [20]. The close relationship between PL and EL implies that increasing the PL efficiency will result in equal improvements in EL efficiency [20]. The electronic and vibrational states and the transition between them are summarized in Jablonski Energy Diagram (Figure 1.1).

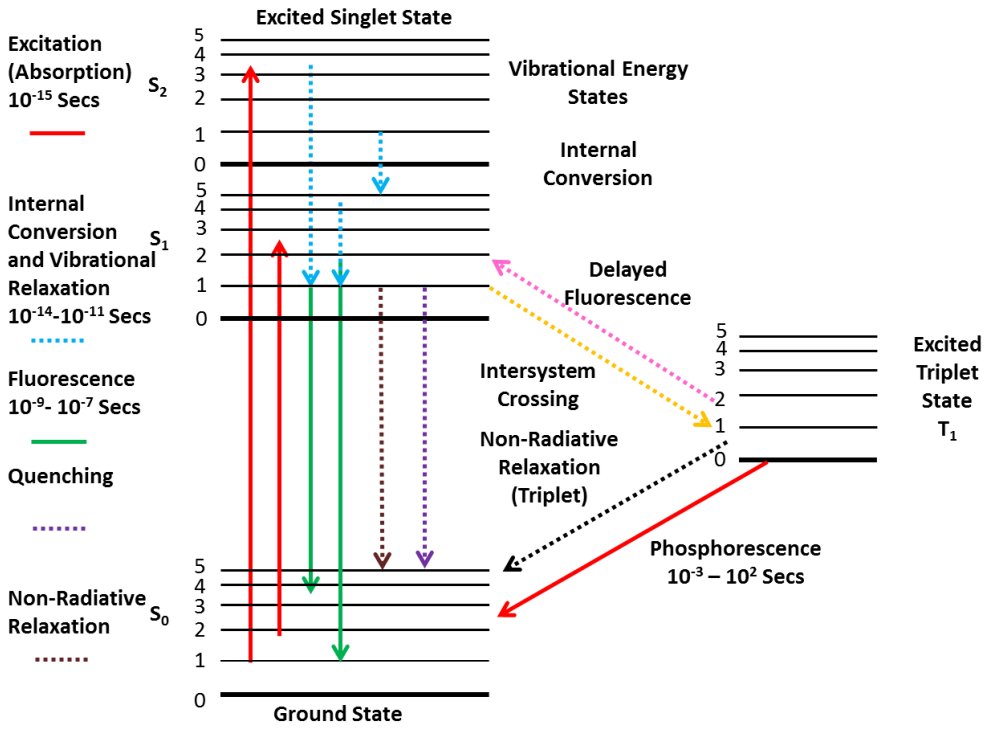

Figure 1.1: Jablonski Energy Diagram

1.1.4. Application of conjugated polymers

The stability, processability, electroactivity and conductivity properties of conjugated polymers allow them to be used for variety of applications. Some applications of conjugated polymers rely on their redox properties (i.e. electroactivity). This means that the electrical and optical properties of conjugated polymers depend on their level of oxidation or reduction. This makes it possible for conjugated polymers with this characteristic to be used as electronic devices [21], rechargeable batteries [22], and drug release system. When these polymers are modified to be water soluble, they can also be used for biomedical application [23, 24].

Conjugated polymers have also been used in the area of sensors. There are many examples where conjugated polymers are used as amperometric sensors, primarily for detection of glucose [25-27], chemosensors [28], biosensors [29] based on a variety of schemes including conductometric [30], potentiometric, colorimetric and fluorescent sensors. Conjugated polymers are potential candidates for electrically conducting textiles [31] and candidates as artificial muscles. [32] Due to their low cost and energy conservation, conjugated polymers

have gained more attention as potential candidates in industry for separation purposes. For example polymers such as polymethylpyrrole and polyaniline are promising materials for industrial gas separation. [161]

The conductive property combined with light-weight, processability and flexibility of conjugated polymers makes them attractive alternatives for certain materials currently used in microelectronics. The conductivity of conjugated polymers can be tuned to a desired value by chemical manipulation of the polymer backbone and by conjugating with other polymers or dopants. Polyaniline [33], polyacetylene [34] and polypyrrole [35] were all reported to be used as conducting resists in the lithographic applications.

Further applications of conducting polymers is their use as active materials in photoelectronic devices, such as light-emitting diodes [36], light-emitting electrochemical cells, [37, 38] photodiodes [39-41], field effect transistors [42-48] and laser diodes [51] etc. The performance of some of these polymer-based devices has surpassed the performance of common inorganic-based devices.

1.1.5. Organic Light Emitting Diodes

Organic Light Emitting Diodes OLEDs are solid-state devices composed of thin films of organic molecules that emit light with the application of electricity. This process is electroluminescence (EL). OLEDs can provide brighter, sharper displays on electronic devices and use less power than conventional light-emitting diodes (LEDs) or liquid crystal displays (LCDs) used today. The structure of OLED is very complicated because of different layers materials needed to construct the device. Thus, fabricating these devices has to be done with careful molecular design and synthesis. [52] The number of layers in an OLED device depends upon the specific application of the device. Some of the important layers are discussed below.

1.1.5.1. Substrate:

The substrate supports the OLED and all the subsequent layers are deposited on it. Normally OLEDs are usually fabricated on a glass substrate just like LED display, but due to the flexible nature of the organic materials used to construct OLED, the glass substrate can be replaced with a flexible plastic such as polyethylene terephthalate (PET). [53] This allows the OLEDs to be bent and stretched without losing their optical properties. Inorganic based devices cannot be fabricated on flexible plastic substrate due to the need for lattice matching and the high temperature fabrication procedure involved. [54] In contrast, flexible

OLED devices can be fabricated by deposition of the organic layer onto the flexible substrate using a method derived from inkjet printing. [55, 56] This allows the production of displays that can be rolled, or displays that can be bent and used for integration into clothes, wallpaper or other curved surfaces. [57-59]

1.1.5.2. Anode:

The anode removes electrons when a current flows through the device. In most cases, Indium Tin Oxide (ITO) glass is used as the anode in OLED. It is widely used because of its high conductivity, high optical transparency and its work function is suitable for hole injection for certain emitting polymers of relatively high HOMO levels. Despite these excellent properties of ITO, it has some drawbacks when used as anode in OLED device. [60, 61] First, the brittle nature of ITO gave it big disadvantage especially in flexible OLED where resistance to mechanical bending is necessary. Furthermore, very high temperature is needed to process ITO making it difficult to form a high quality anode on substrates that can easily be damaged at high temperature such as the commonly used poly(ethylene-terephthalate) (PET). Third, the dwindling supply of indium by ITO and the limited global reserve of indium make ITO very expensive and as a result raise the manufacturing cost of OLED. Another drawback is the difficulty of processing ITO in solution, while solution processable anode material is vital for the development of all solution processed OLEDs [62, 63]. Many alternatives to ITO like metal oxides [63], conductive polymers [64], thin metal films [65, 66], metal grids [67], graphene sheets [68] and carbon nanotubes [69] were reported in literature. Despite the excellent properties of these materials, their properties still do not surpass the properties of ITO making it still one of the leading candidate anodes in OLED.

1.1.5.3. Cathode:

The cathode supplies electrons to the active layer when current flows through the device. Metals are usually used as cathode in OLED. One of the examples is aluminum and calcium.

1.1.5.4. Hole Injection Layer (HIL)/Hole Transport Layer (HTL):

High power efficiency (PE) is achieved in OLEDs when charge injection and transport is effective and balanced. In an OLED device, the hole injection/transporting material is in the middle of anode and emitting layer. It will help the hole transportation and injection into the emitting layer. The HOMO energy level of hole transporting materials should be near the potential of the anode and be higher than the emitting layer. In some devices the same material can serve as both hole injection and transport material and in some different materials are used as hole injection layer and hole transport layer. One of the widely used

hole injection and transport layer is the poly(3,4-ethylenedioxythiophene): poly(styrenesulfonic acid) (PEDOT:PSS). PEDOT:PSS is water soluble and insoluble in commonly used organic solvent (such as toluene, chloroform, etc.) thus eliminating the interface mixing problem. This polymer can both be used as hole injection and transport material [70] due to its relatively high conductivity and transparency in the visible region with good stability and good film-forming properties. The conductivity of PEDOT:PSS thin films can be tuned by varying the ratio between PEDOT and PSS or controlling the film morphology. However, PEDOT:PSS has some drawbacks when used as HTM in OLED devices. First, PEDOT:PSS is very acidic which can cause corrosion of the ITO anode [71]. Another problem is the poor hole injection of PEDOT:PSS for most of the blue- and green-emitting materials due to the mismatched energy levels, and exciton quenching at the interface between PEDOT:PSS and emissive materials [72]. There have been many efforts to find better materials for effective hole transportation from the anode to the emissive layer. One of the approaches was to develop cross-linkable HTL materials to introduce efficient cross-linking functionalities into traditional HTL (triarylamine) molecules, such as N,N'-(3-methyl-phenyl)-1,10-biphenyl- 4,4'-diamine (TPD), 4,4'-bis[N-(1-naphthyl-1)-N-phenylamino]- biphenyl (NPB), tri(N-carbazolyl)-triphenylamine (TCTA), and so forth. The structures of these compounds are given in Figure 1.2.

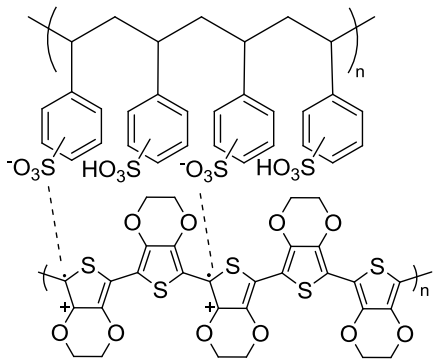

PEDOT:PSS

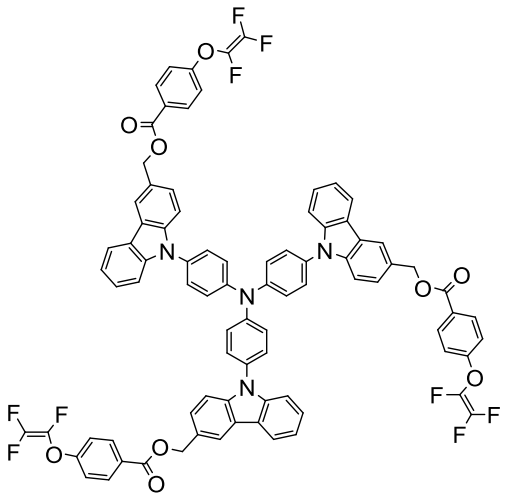

TriTFV-TCTA

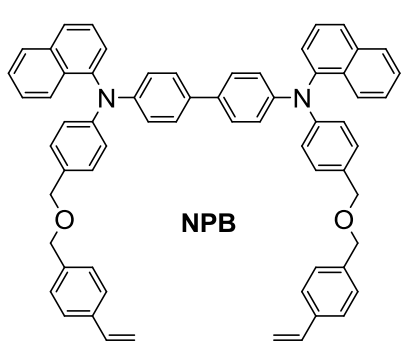

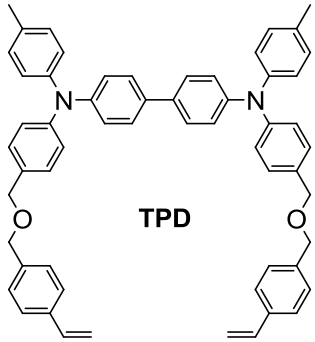

Figure 1.2: Some of the HIL/HTL compounds

1.1.5.5. Electron Transport Layer (ETL):

Electron transporting materials (ETM) usually have low LUMO energy level meaning materials with high electron affinity will serve this purpose. The ETL matches the LUMO level of emitting layer with the potential of cathode, thus increases the efficiency of electron injection. Furthermore, ETL with high ionization energy (low HOMO energy level) will increase the efficiency of the device by limiting the holes in the surface of emitting layer and ETL layer. For this purpose, metal ion or electron-withdrawing groups are usually introduced into the synthesized ETL compounds. There are basically two types of ETL materials. The first category is the ETL based on organometallic compounds. These materials usually contain a central metal coordinated by aromatic moieties. Some of the well-known organometallic HTM are shown in Figure 1.3.

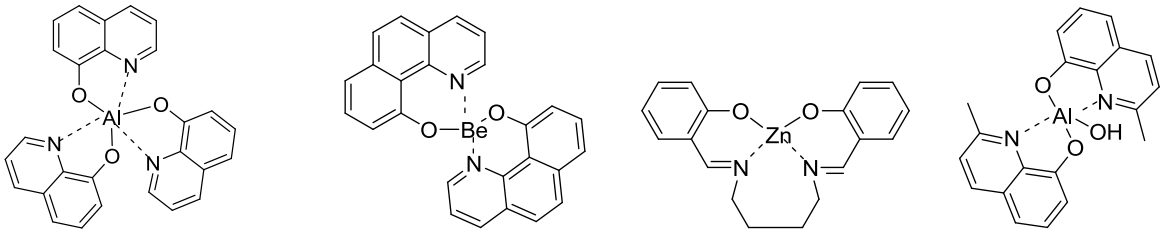

Figure 1.3: Some of the Organometallic ETL compounds

The second category is the ETL based on non-organometallic compounds. Pyrimidine cycle is one of the widely used compounds as ETL due to its high electron affinity. Some of the pyrimidine based ETL compounds are shown in Figure 1.4.

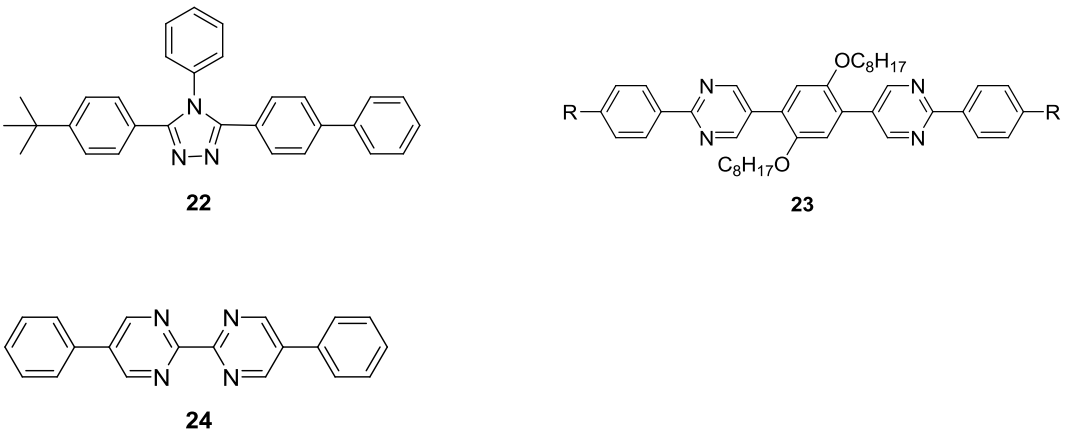

Figure 1.4: Pyrimidine units in ETL materials

Another sets of compounds used as ETL materials are triazene cores due to their good electron transport ability. Some common triazene compounds used as ETL materials are shown in Figure 1.5.

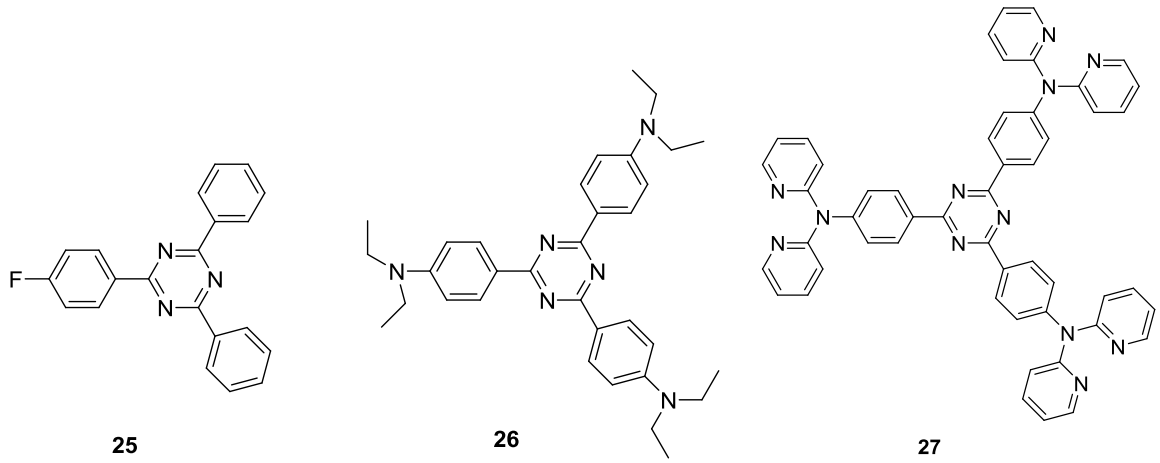

Figure 1.5: Triazene units in ETL materials

The σ^*(Si)-π(C) in silole cycles can lower the LUMO and thus can serve as ETL material.

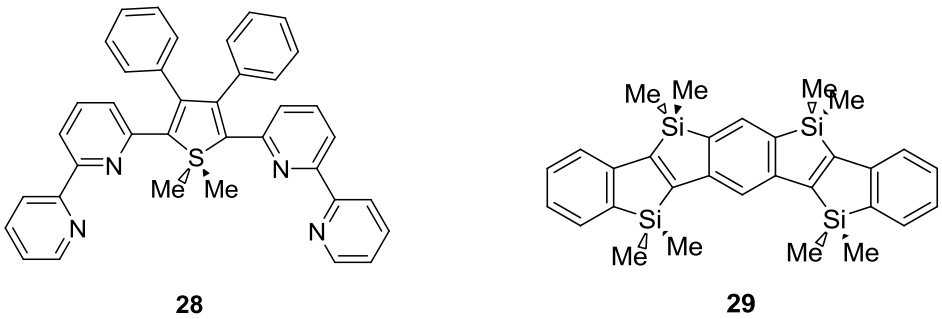

Figure 1.6: Silole Units in ETL materials

One of the strategies to increase withdrawing power of the aromatic moiety is by attaching highly electronegative element like fluorine [73].

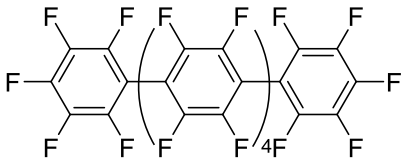

30

Figure 1.7: Per-fluorobenzene units in ETL materials

1.1.5.6. Emissive Layer:

This is the layer where light is emitted. In OLED device, this layer is made of small or large organic molecules. The organic molecules can be deposited on the substrate in different ways:

Vacuum deposition or **vacuum thermal evaporation (VTE):** In this method the organic molecules are gently heated to evaporate in a vacuum chamber. The vapor of the organic molecules is allowed to condense as thin films onto cooled substrates. This method often results in non-uniform film formation on the substrate and thus is considered expensive and inefficient.

Organic vapor phase deposition (OVPD): This process is similar to vacuum deposition except that this process involves the use of a carrier gas. The organic molecule is first evaporated at low temperature in hot wall and then transported by the carrier gas onto cooled substrates, where they condense into thin films. The use of a carrier gas increases the efficiency and reduces the cost of making OLEDs.

Inkjet printing: This process uses the inkjet technology where the organic molecules are sprayed onto substrates just like inks are sprayed onto paper during printing. Inkjet technology greatly reduces the cost of OLED manufacturing and allows OLEDs to be printed onto very large films for large displays like 80-inch TV screens or electronic billboards.

Emissive layer can be small or large organic molecules. The first OLED device designed by Kodak scientists in 1987 used small organic molecules. Although small molecules emitted bright light, their ability to form thin films on substrate is not excellent and thus scientists had to deposit them onto the substrates by vacuum deposition. This led the search for better thin film forming organic molecules. Since 1990, researchers have been using large polymer molecules to emit light. OLEDs can be made less expensive using conjugated polymers and can be made in large sheets which can further be used for large-screen displays. One of the molecules used as emissive layer in OLED device is polyfluorene.

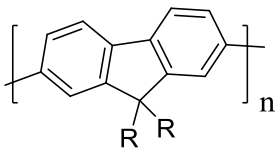

Polyfluorene

Polyfluorenes have high photoluminescence quantum yields due to their rigid structure and can be tuned to emit light throughout the entire visible region. Normally polyfluorene emits blue color, but the color can be tuned by conjugating the fluorene molecule with electron donating or withdrawing substituents such as thiophene and benzothidiazole

Working Principle of OLED

In an OLED device, current is supplied by an external source (e.g. battery). The electrical current (an electrical current is a flow of electrons) flows from the cathode to the anode through the organic layers. The electrons from cathode are transported by ETL materials to the emissive layer of organic molecules. The anode removes electrons from the conductive layer of organic molecule which is equivalent to giving electron holes to the HIL/HTL materials. At the boundary between the emissive and the HIL/HTL (conductive layers), electrons from the cathode find electron holes removed by anode. When an electron finds an electron hole, the electron fills the hole (it falls into an energy level of the atom that's missing an electron). When this happens, the electron gives up energy in the form of a photon of light. Thus the OLED device emits light. The working principle of OLED is summarized in Figure 1.8.

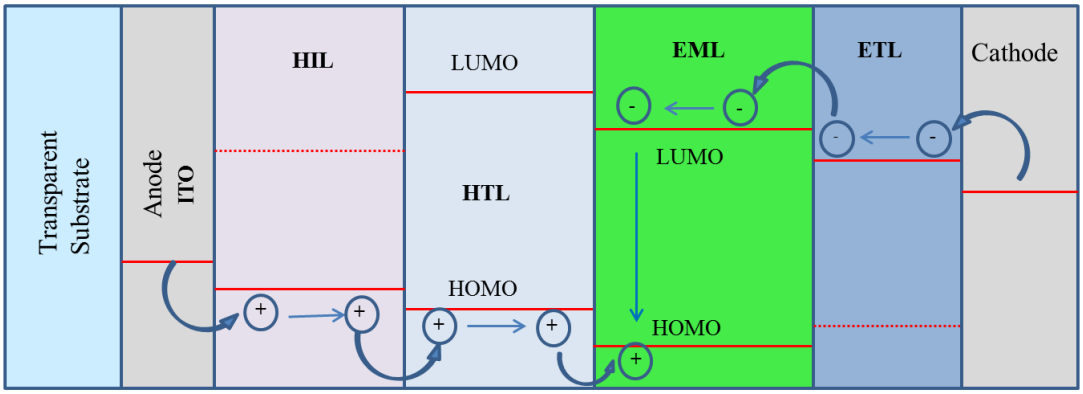

Figure 1.8: Working principle of OLED device: Negative circle = electron, Positive circle = hole

The color of the light emitted by OLED device depends on the type of organic molecule in the emissive layer. Multiple color display is obtained by depositing several types of organic

films on the same OLED device. Furthermore, the intensity or brightness of the light depends on the amount of electrical current applied where higher current produces brighter light.

1.2. Rotaxanes and Polyrotaxanes

Supramolecular chemistry is the field of chemistry that involves the study of systems involving molecules or ions held together by non-covalent interactions such as electrostatic interactions, hydrogen bonding, $\pi - \pi$ interactions, dispersion interactions and hydrophobic or solvophobic effects. The field of supramolecular chemistry dates back to the 1890s where Sir Humphrey Davy discovered the inclusion of chlorine within a solid water lattice. The importance of non-covalent interaction in biological systems and in some chemical processes led the supramolecular chemistry to gain more attention.

Supramolecular chemistry can be divided into two categories; host-guest chemistry and self-assembly. As the name implies host guest chemistry involves two molecules or ions one serving as the host and the other as the guest. These molecules usually have different sizes; the larger molecule serves as the host and the smaller molecule as the guest. In host-guest chemistry the host recognizes the guest through binding site and binds it via non-covalent interaction (Figure 1.9).

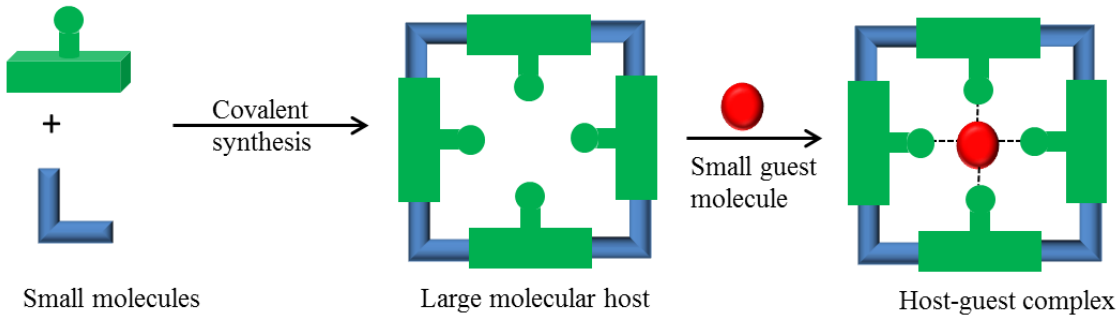

Figure 1.9: Host–guest complexation (Reproduced from [77])

Examples of host-guest molecules are rotaxanes and polyrotaxanes. The name rotaxane is derived from Latin rota (wheel) and axle (axis) describing rotaxane as a molecule consisting of a linear molecule which is threaded through a ring (macrocycle) with the ends of the thread, or axel, capped in such a manner that the ring cannot slip off. Bulky groups like $-CPh_3$ and PPh_3 ligands are normally used as capping groups although recently large aromatic moieties like porphyrins and fullerenes are used. The linear molecules consist of

simple aromatic molecules or long alkyl chains that have affinity to the ring (macrocycle). When the linear segment is polymer, the resulting molecule after threading by the macrocylcle is called polyrotaxane. The intermediates for rotaxanes and polyrotaxanes are pseudorotaxanes. Unlike rotaxanes and polyrotaxanes, pseudorotaxanes do not have terminal groups at the ends of the thread to prevent slipping off of the ring. Rotaxanes are named according to this general notation: [n]-(pseudo)rotaxane where n represents the number of components used to construct the rotaxane. Hence [2]-rotaxane represents a rotaxane constructed from a macrocycle and a linear molecule whereas [3]-rotaxane represents a rotaxane constructed from three components, two macrocycles threaded along with a linear molecule. It should be noted that pseudo or poly has to be added between the ‘’[n]’’ and ‘’rotaxane’’ when the rotaxane is pseudorotaxane or when the linear molecule contains polymer chains.

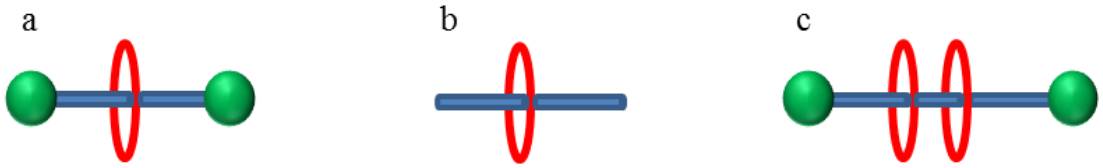

Figure 1.10: Schematic diagrams of (a) a [2]-rotaxane, (b) a [2]-pseudorotaxane and (c) a [3]-rotaxane.

One of the early rotaxanes was reported by Harrison and Harrison [78]. In their work 2-hydroxy-cyclotriacontanone was used as macrocycle to encapsulate decane-1,10-diol bis(triphenylmethyl) ether. Since then rotaxanes and polyrotaxanes have been synthesized and used for different applications. One of the applications is their use as vehicles in biomedical application [79-83]. Polyrotaxanes and rotaxanes are also used as pH- responsive [79, 84], thermo-responsive [85-87] and photo-responsive devices [88]. Threading macromolecule on polymer backbone will change the electronic and photochemical properties of the polymer. In addition, the viscosity, solubility, thermo and chemical stability and melting point of the polymer could be altered when the polymer backbone is encapsulated by a macrocycle. Considering these changes, rotaxanes and polyrotaxanes can be used in optoelectronics applications [89].

1.2.1. Classification of Rotaxanes and Polyrotaxanes

Rotaxanes and polyrotaxanes are classified based on location of macrocycle, synthetic route and type of macrocycle.

1.2.1.1. According to the location of rotaxane units

As discussed above, the location of macrocycle can be on the backbone or side chain of the linear molecule. Accordingly, rotaxanes and polyrotaxanes are classified as ‘’Side chain’’ and ‘’Main chain’’ polyrotaxanes. In side chain rotaxanes/polyrotaxanes the macrocycle is located on the side chain of the molecule (Figure 1.11). Main chain rotaxane/polyrotaxane has the macrocycle located on the backbone of the molecule. Their examples are shown in Figure 1.12.

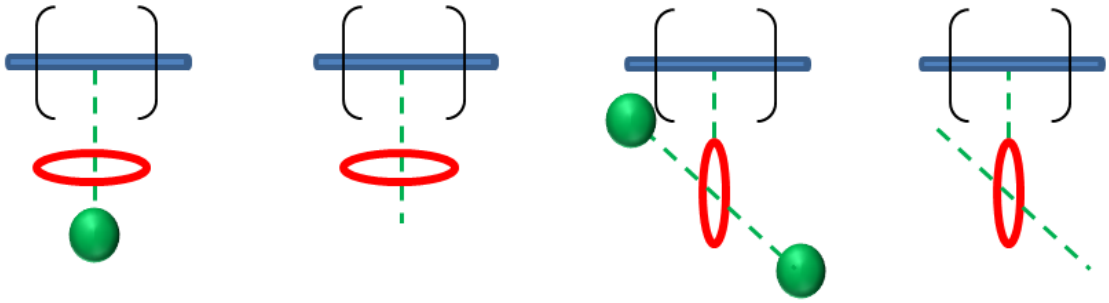

Figure 1.11: Schematic representation of various types of side chain polyrotaxanes (Reproduced from [77])

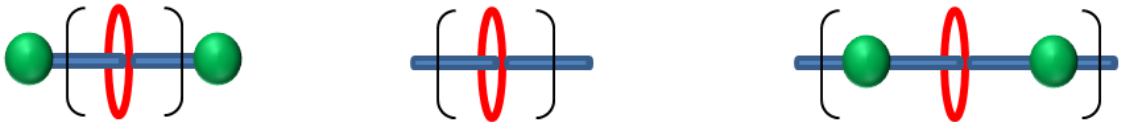

Figure 1.12: Schematic representation of various types of main chain polyrotaxanes (Reproduced from [77])

1.2.1.2. According to synthetic route

There are four different ways in which polyrotaxanes can be synthesized.

- **Threading:** In this method, the macrocycle is first threaded on the linear molecule and then held in place by one or more interactions between the macrocycle and the linear molecule. The linear molecule contains reactive functional groups at the

terminal ends which can be reacted with bulky groups to prevent the macrocycle from slipping off.

- **Trapping**: This method is similar to threading method except that one end of the linear molecule is first capped with bulky groups so that when the linear molecule is threaded by the macrocycle only one end of the linear molecule will be capped. This method has more advantage compared to threading because there is statistically less chance of the macrocycle slipping off at one end of the linear molecule. Also this method can be used to synthesize unsymmetrical rotaxanes and polyrotaxanes.
- **Clipping**. In this method the macrocycle contains two species each having functional groups that can easily react to form covalent bond. The two species are threaded onto fully assembled axel at a suitable template point. The macrocycle is closed by simple covalent reaction and will not slip off because the linear molecule was already capped with bulky terminal groups.
- **Slipping**. At high temperature it is possible for a macrocycle to be forced to slip over the bulky groups and thus will thread on the axel. This method is not very efficient because if the macrocycle can slip over bulky groups at high temperature, it can also slip off at the same conditions giving rise to reversible process. This will decrease the number of threaded macrocycle on the axel.

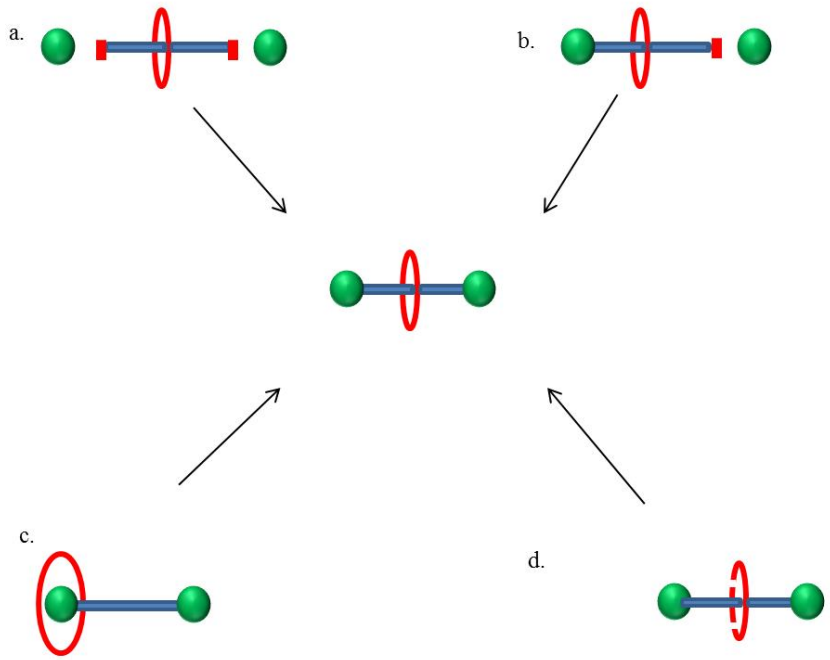

Figure 1.13: The synthesis of rotaxanes can be achieved via (a) threading, (b) clipping, (c) slipping or (d) trapping (Reproduced from [77])

1.2.1.3. According to the type of macromolecule

Another way to classify rotaxanes and polyrotaxanes is according to the type of macrocycle used to build the molecular structure of the rotaxanes. Many rotaxanes are reported based on cyclodextrins, crown ethers, cyclophanes and cucurbituril.

1.2.1.4. Cyclodextrins

Cyclodextrins (CD) are cyclic oligosaccharides consisting glucopyranose units linked by α-(1,4) bonds (Figure 1.14). [91,92] Cyclodextrins can be produced as a result of exposure of starch to an enzyme called cyclomaltodextrin glucanotransferase (CGTase) enzyme, naturally excreted by B. macerans, to yield a mixture of six-, seven- and eight-member rings which corresponds to α-CD, β-CD and γ-CD, respectively. [93]

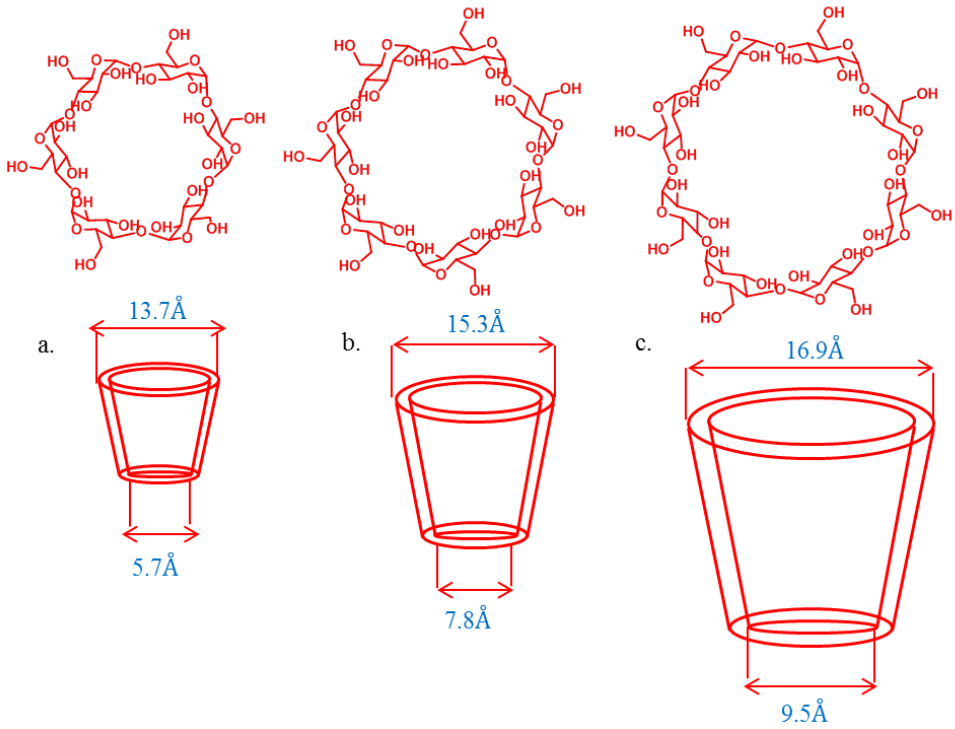

Figure 1.14: Structure of a) α-CD, b) β-CD and c) γ-CD

The hydroxyl groups on the surface of cyclodextrins make their surface hydrophilic and thus water soluble compounds. However due to the ether linkage inside the cavity of CDs, their inner cavity is hydrophobic which provides a hydrophobic environment for hydrophobic guests. [94] As a result of this hydrophobic cavity, cyclodextrins are able to form inclusion complexes with a wide variety of hydrophobic guest molecules in aqueous environment.

1.2.1.4. Crown ethers

Crown ethers are cyclic ethers which are commonly the oligomers of ethylene oxide having repeating unit of ethyleneoxy, i.e., -CH_2CH_2O-. The name crown ether is derived from the

complex between crown ether and cation resembling a crown sitting on person's head. The notation '' n-crown-m'' is used to represent the nomenclature of crown ether where n is the total number of atoms in the cycle (excluding hydrogens), and m refers to the number of oxygen atoms in the cycle. Thus 18-crown-6 represents crown ether having a total of 18 atoms in cycle and 6 oxygen atoms. The structures of some important crown ethers are given in Figure 1.15.

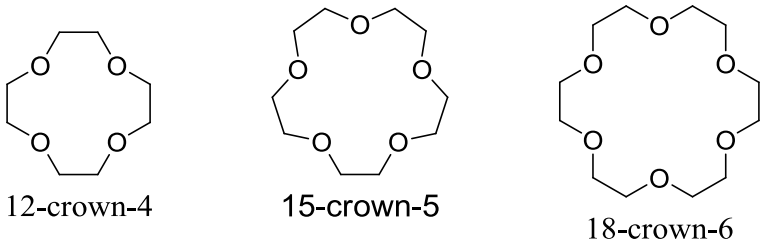

Figure 1.15: Structures of common crown ethers

The ability for crown ethers to form hydrogen bonds through well suited oxygen atoms with acidic protons like –NH and –OH is the driving force for the formation of rotaxanes and polyrotaxanes. [107] The solubility of crown ethers in common solvents makes the synthesis and purification of crown ether based rotaxanes and polyrotaxanes easy. [108]

1.2.1.5. Cyclophanes

A cyclophane is another type of macrocycle consisting of an aromatic unit (typically a benzene ring) and an aliphatic chain that forms a bridge between two non-adjacent positions of the aromatic ring. Compared to cyclodextrins and crown ethers there are fewer examples of cyclophane in literature. Cyclobis(paraquat-p-phenylene) synthesized by Stoddart [112-116] (Figure 1.16) is one of the examples of cyclophanes used to thread polymer backbones.

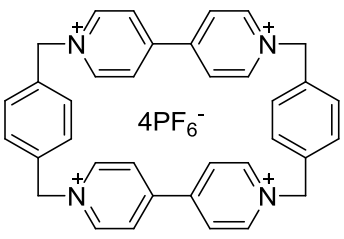

Figure 1.16: Cyclobis(paraquat-*p*-phenylene) as macrocycle

1.2.1.6. Cucurbituril

Cucurbiturils are macrocycles consisting of glycoluril units linked together by methylene groups. The structure of cucurbituril resembles pumpkin and hence the name cucurbituril ‘’cucurbita’’ from Latin. Unlike cyclodextrins, cucurbiturils have very symmetrical structure and thus their openings have the same size.

1.2.1.7. Synthesis, Properties and Recognition

The products of condensation of glycoluril with formaldehyde were first characterized by Behrend and coworkers in 1905 as white amorphous materials. [117] One of the products was found to contain at least three molecules of glycoluril condensed with two equivalents of formaldehyde corresponding to the formula $C_{18}H_{18}N_{12}O_6$. In 1981 Mock and coworkers revised the work of Behrend and reported a macrocycle containing six units of glycoluril. [118] Nowadays it is known as Cucurbit[6]uril abbreviated as CB[6], CB6, Q[6], Q6 or Cuc6, where 6 represents the number of glycoluril units in the macrocycle. The structure of CB[6] was characterized with IR, ^{1}H-NMR, ^{13}C-NMR and X-ray crystallography. The peak at 1730cm^{-1} shows the presence of carbonyl group from glycoluril unit. The two protons on methylene group in ^{1}H-NMR resonate at different chemical shifts [119, 120] because one of protons points towards the carbonyl group resonating at 5.5 ppm as doublet and the other pointing out of the carbonyl groups resonating at 4.5 ppm as doublet. The equatorial proton resonates as singlet at around 5.3 ppm. Although CB[6] has very limited solubility, it can be complexed with cations to improve the water solubility. Since the discovery of CB[6] there was no much study reported on cucurbituril until 1990 where Kim and cowers started to report very elegant work on the cucurbit[6]uril which contributed substantially to the field of CB[6]. It took more than a decade to discover other cucurbituril homologues. In 2000 Day and Kim discovered three new CB homologues; CB[5] CB[7] and CB[8] having 5, 7 and 8 glycoluril units respectively. [121] These homologues were obtained in similar manner with CB[6] except that the reaction conditions such as temperature were adjusted. The discovery of CB[7] excites the supramolecular chemists because of its both large cavity and water solubility which is very important feature for biological applications. [122] In 2002 Day and coworkers reported CB[10] interlocked with CB[5]. [123] However, isolating the CB[10] from CB[5] was not accomplished by direct separation methods due to the high affinity of CB[5] towards CB[10]. In 2005 pure CB[10] was isolated by Isaacs and coworkers by simply introducing a more strongly binding melamine diamine guest that is capable of displacing the CB[5]. [124] Many other oligomers of glycoluril and cucurbit[n]uril were also reported in

recent years. For example the inverted cucurbit-[6]uril and inverted cucurbit[7]uril (*i*CB[6] and *i*CB[7]) [125], the chiral norseco-cucurbituril (±)-bis-ns-CB[6] [126], and the nor-seco-cucurbit[10]uril (ns-CB[10]) [127], were all reported. Miyahara and co-workers have reported a large hemicucurbit[12]uril [128], which does not show typical CB[n] properties. Recently Ni and Tao reported Twisted Cucurbit[14]uril. [129] Unlike other cucurbituril homologues this cucurbituril has two different rings owing to its twisted nature. The structure of Twisted Cucurbit[14]uril was confirmed by X-ray crystallography.

In almost all the CB[n] homologues the peak pattern in both ^{1}H-NMR and ^{13}C-NMR were the same although their chemical shifts differ by very small values. By using X-ray crystallography CB[n] homologues were all characterized and some of their structural parameters like portal diameter and height were determined. Table 1.2 shows structural parameters of CB[n] homologues obtained from X-ray crystallography.

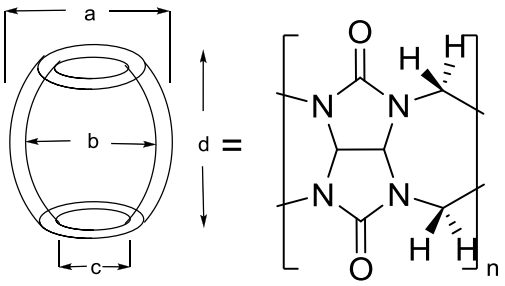

CB[n] : n = 5, 6, 7, 8 and 10

Table 1.2: structural parameters of CB[n] homologues obtained from X-ray crystallography (Reproduced from [130])

		CB[5]	**CB[6]**	**CB[7]**	**CB[8]**	**CB[10]**
Outer diameter/Å	a	13.1	14.4	16.0	17.5	18.7-21.0
Cavity/Å	b	4.4	5.8	7.3	8.8	10.7-12.6
	c	2.4	3.9	5.4	6.9	9.0-11.0
Height/Å	d	9.1	9.1	9.1	9.1	9.1
Cavity Volume/Å^3	-	82	164	279	479	870

Similar to cyclodextrins, cucurbiturils have hydrophilic carbonyl portals and hydrophobic cavity which serves as a host for hydrophobic molecules. However not all the CB[n]s are soluble in water, only the odd numbered CB[n]s are soluble in water that is CB[5] and CB[7]

with the exception of twisted CB[14] due to its unsymmetrical nature. Thus CB[6], CB[8] and CB[10] are not soluble in water.

Cucurbiturils are synthesized based on general procedure developed by Day [131] Kim [121] and Isaacs. [124] This procedure involves condensing a mixture of glycoluril and paraformaldehyde with concentrated hydrochloric or sulfuric acid (concentrated, or diluted to approximately 5 M) at 80–100 ^{0}C for 10–100 h (Scheme 1.1). Upon evaporation and consecutive precipitations in water and methanol, CB[6], CB[7], CB[8], CB[5], CB[10], twisted CB[14], *i*CB[6] and other oligomers are obtained. Purification of CB[n]s is based on their solubility in different solvents (Figure 1.17). Day [123], Halterman [132] and Leventis [133] used 20% hot aqueous solution of glycerol to extract CB[7] from the mixture of CB[n]s with good selectivity. A useful variation to this was proposed by Scherman where CB[5] and CB[7] were separated from the CB[n] mixture by selectively complexing CB[7] with 1-alkyl-3-methylimidazolium bromides and recrystallizing CB[5] from the aqueous solution (Figure 1.18). [134] CB[10] is isolated by introducing more strongly binding melamine diamine guest that is capable of displacing the CB[5]. [124]

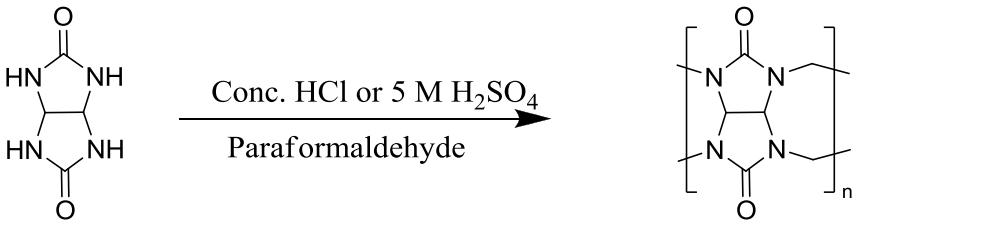

Scheme 1.1: Synthesis of CB[n]

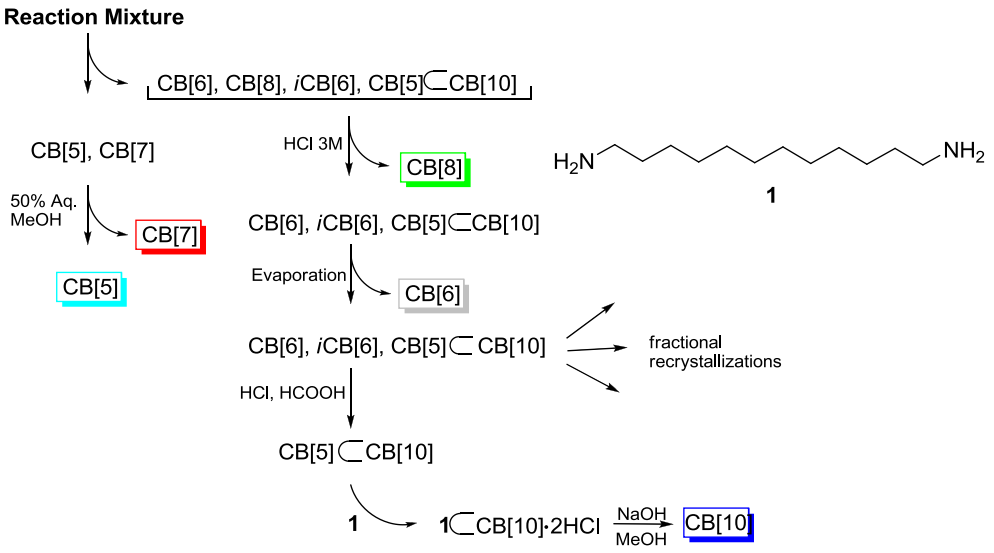

Figure 1.17: Purification of CB[n]s (Reproduced from [135])

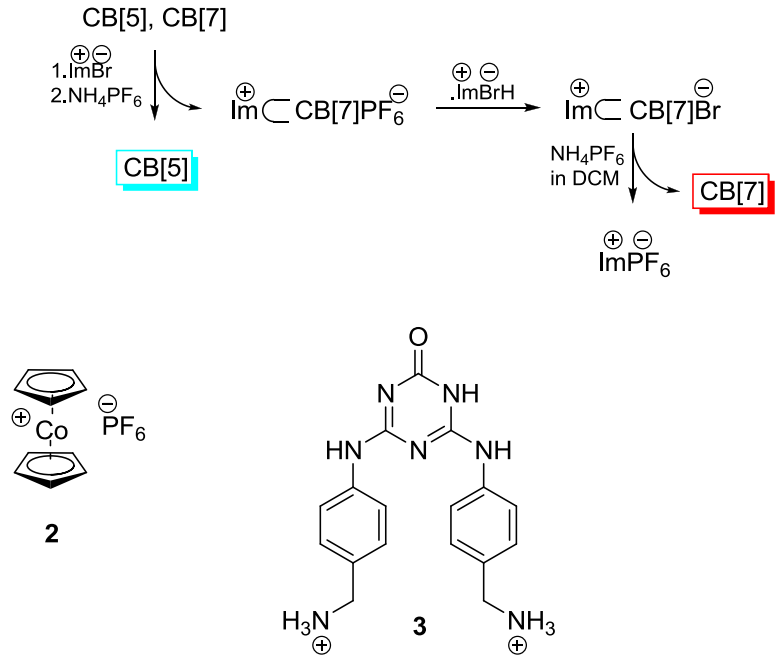

Figure 1.18: Purification of CB[n]s: (b) alternate method for the separation of CB[5] and CB[7]. Curved arrows indicate precipitation. (Reproduced from [135])

CB[n]s form complexes with different guest molecules depending on the size of the guests. The smaller homologues prefer to form complexes with smaller guest molecules and the larger members of the CB[n]s family form complexes with larger guest compounds. Kim and cowers [136] reported some of the inclusion complexes of CB[n] homologues with different guest molecules and are tabulated in Table 1.3.

Table 1.3: Some common guest molecules for CB[n]s

CB[5]	Alkalı metal ions NH_4^+ Pb_2^+:Binds to the carbonyl oxygen
CB[6]	$NH_3^+(CH_2)_n\ NH_3^+$ (n=4-7, $K_a > 10^5$) THF, benzene 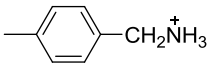 $K_a \sim 3 \times 10^2$ o- and m- isomers are not included
CB[7]	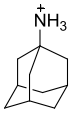 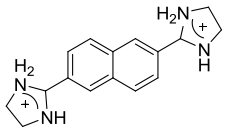 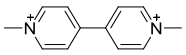  M = Fe M = Co
CB[8]	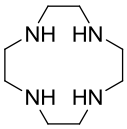 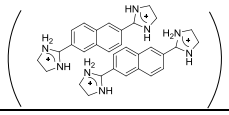 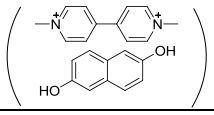
CB[10]	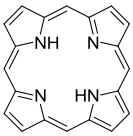 CB[5]
CB[14]	1,12-diaminododecane, 1,ω-alkylenedi-4,4'-bipyridines, 1,ω-alkylenedipydines. Ref [14]

Cucurbituril based rotaxanes and polyrotaxanes are constructed based on the general scheme above (Figure 1.13).

1.2.2. Insulated Molecular Wires

Delocalized molecular structures with low $\pi - \pi^*$ band gap are vulnerable to attack because reactions with electrophiles, nucleophiles, or radicals lead to stable delocalized intermediates. Furthermore, the fluorescence of these molecules can be quenched through aggregation particularly if two or more chromophores come together in a parallel face-to-face

arrangement. The reactivity and instability of organic semiconductors is often regarded as their main drawback for many applications. Encapsulation of the aromatic backbone by macrocycles is one of the ways to block this reactivity. Encapsulation of the aromatic backbone does not only block the reactivity but also increases the fluorescence efficiency by preventing aggregation or by modifying the geometry of the aggregate. These effects of macrocycles on conjugated polymers have been the key motivation for the synthesis of insulated molecular wires (IMWs).

Many polyrotaxane and pseudopolyrotaxane IMWs based on cyclodextrin and cyclophane macrocycles have been reported. The synthesis of IMWs uses noncovalent interactions to drive the threading process. The reactions are carried out in water, so that hydrophobic interactions favor threading.

A series of cyclodextrin based conjugated main-chain polyrotaxane insulated molecular wires were synthesized by Anderson's group. [95] The polyrotaxanes were prepared from diiodostilbene and chain terminators naphthalene and phenyl iodide by aqueous Suzuki Coupling. These polyrotaxanes have conjugated polymer cores, such as poly(para-phenylene), polyfluorene, and poly(para-phenylenevinylene), threaded through cyclodextrins. The presence of cyclodextrin has little effect on the absorption spectra of polyrotaxanes, but causes a blue shift in the emission compared with the corresponding unthreaded conjugated polymers. Furthermore, the fluorescence efficiencies were increased upon the formation of the polyrotaxane structure.

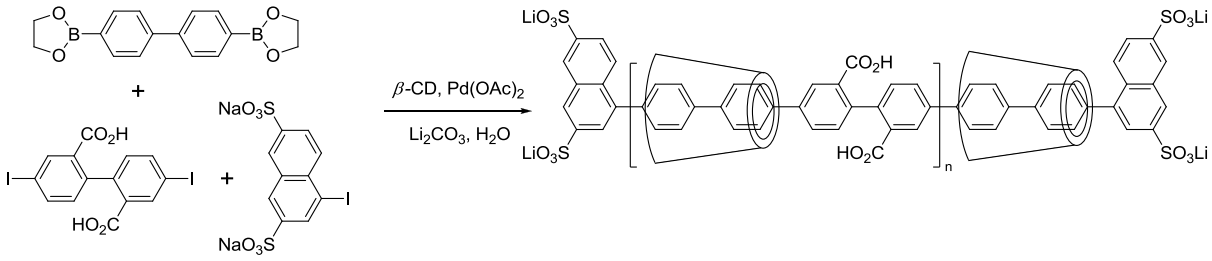

Scheme 1.2: Molecular wire synthesis based on β-Cyclodextrin.

Compared to other macromolecules especially cyclodextrin, there are very few examples of cucurbituril based polyrotaxanes featuring long conjugated threaded $\pi-$ systems. One of the examples of IMW based on polyaniline threaded by CB[6] was reported by Grigoras and Stafie. [96] The polyrotaxane was prepared by two methods. The first method involves chemical oxidative polymerization of aniline in the presence of CB[6] in acidic aqueous

solution using ammonium persulfate as the oxidant. The second method involves threading the preformed polyaniline chain through the inner cavity of CB[6] (Scheme 1.3).

A polymeric pseudorotaxane based on CB[7] and polyaniline has been reported by Liu and coworkers (Scheme 1.4). [97]

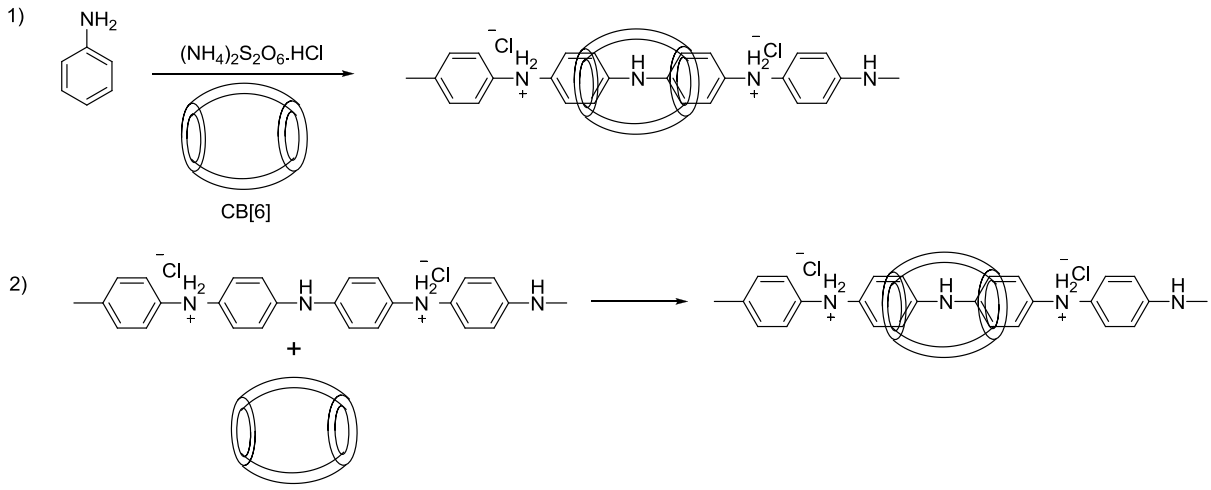

Scheme 1.3: Synthesis of pseudorotaxane polyaniline/CB[6] by (1) chemical polymerisation of aniline/CB[6] inclusion adduct and (2) encapsulation of polyaniline emeraldine salt in CB[6].

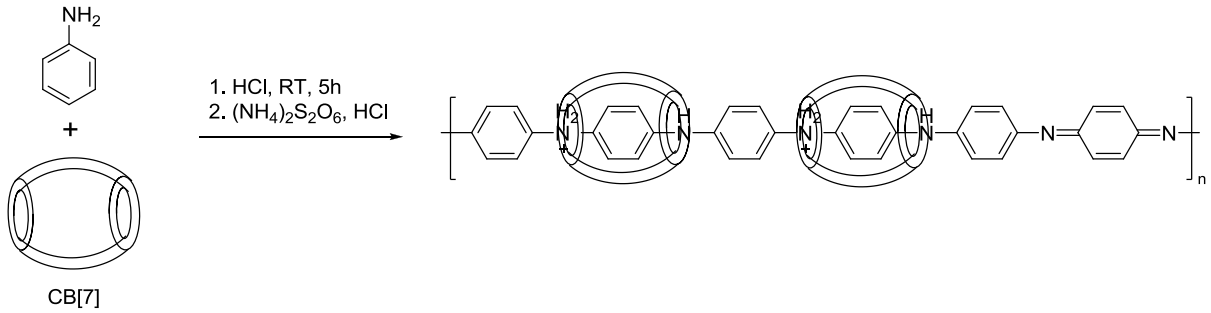

Scheme 1.4: Synthesis of pseudorotaxane polyaniline by polycondensation of aniline in the presence of CB[7].

Normally, encapsulation of a molecular wire is not expected to perturb its electronic structure or change its $\pi - \pi^*$ energy gap, but, in principle, changes in the UV/Vis absorption and fluorescence spectra can arise as a result of three distinct types of effects:

a) Solvatochromism: The electronic structure of the molecular wire can be pertubed by threading with macrocycle when the excited state of the molecular wire is more, or less, polar

than the ground state. Hence, the wavelengths of its absorption and emission bands will be sensitive to the polarity and polarizability of the insulating (just as they are to the polarity and polarizability of the solvent). A change in the polarizability of the environment around the π system can change its extinction coefficients, even if the absorption bands have no charge-transfer character. [98]

b) Conformational effects: Insulation may favor a more twisted geometry, thus leading to a blue shift. In other case, if the encapsulating structure behaves as a long straight tube it may force the molecular wire to adopt linear and/or planar conformations, with the resulting stronger π overlap shifting the absorption and emission to longer wavelengths. Even when encapsulation has no effect on the conformation of the ground state, it can change the fluorescence spectrum by restricting reorganization in the excited state.

c) Aggregation: Long rigid molecules such as conjugated polymers have a strong tendency to aggregate, especially at high concentrations or in poor solvents. In this case exciton coupling between chromophores in these aggregates modifies the absorption and emission spectra. Encapsulation blocks the aggregation of the conjugated cores. Spectral changes are usually attributed to combination of all three of these effects.

The enhanced chemical stabilities and photoluminescence efficiencies of IMWs suggest that they could be used as emissive layer in OLED devices. One example is reported by Anderson's group where cyclodextrin based IMW was used as emissive layer in OLED. The device exhibit enhanced electroluminescence efficiency, compared to the corresponding free polymers. [99]

1.3. Porphyrins

Porphyrins are a class of naturally occurring macrocyclic compounds, which play a very important role in the metabolism of living organisms. [137] Typical porphyrin ring contains four pyrrolic units with the heart of the skeleton a heterocyclic macrocycle, known as porphine. The four pyrrolic sub-units are linked together via methine unit as shown in Figure 1.19a. From the figure α-positions are numbered 1, 4, 6, 9, 11, 14, 16 and 19, the bridges as 5, 10, 15 and 20. Porphyrins have 18π electrons, conjugated and planar which make them aromatic. These electrons are delocalized over the macrocycle and thus typically have very intense absorption bands in the visible region and near infrared region. Porphyrin is the pigment responsible for the red color of red blood cells and green color of chlorophyll. Typical porphyrin have a very strong absorption band at 405 nm (Soret band) and four

relatively low absorption bands (Q bands) near the infrared region (Figure 1.19b). In PDT, the strong absorption of light near infrared is important, but unfortunately porphyrins have low absorption in this region. This creates a great challenge to scientists. Scienstist today have approached this problem by mainly increasing the intensity of the Q-bands without reducing the biocomapatibilty of the porphyrin.

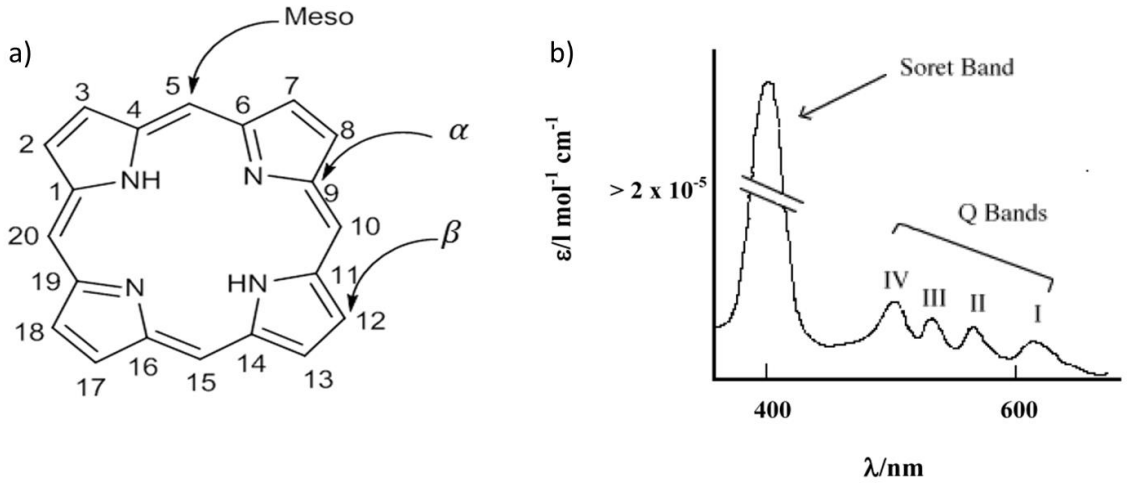

Figure 1.19: a) Porphyrin b) Absorption Spectrum of Porphyrins

1.3.1. Synthesis of Porphyrins

There are two main synthetic routes of porphyrins. In the first method, porphyrins are synthesized by the condensation of benzaldehyde and pyrrole in pyridine at high temperatures. [138] This method is the first method for porphyrin synthesis employed by Rothemund. From Scheme 1.5, it can be seen that this method gives high yield only when one type of aldehyde is used. If more than one aldehyde is used, mixture of products is obtained and the target product will be obtained in extremely low yield. This method was later developed by Adler where propionic acid or acetic acid was used as a solvent. [139] This method gives higher yield but it was later found out that the method fails with aldehydes bearing acid sensitive functional groups. This problem was solved with a new method developed by Lindsey who used trifluoro borane etharate ($BF_3.OEt_2$) as a catalyst in the synthesis of porphyrinogen and oxidized it to porphyrin with DDQ. [140]

The second method was developed by Lindsey where an aldehyde and pyrrole is used in the presence of trifluoroacetic acid as catalyst to synthesize dipyrromethane (Scheme 1.6). The dipyrromethane is then reacted with the second aldehyde, ($BF_3.OEt_2$) as catalyst and then later oxidized using 2,3-Dichloro-5,6-dicyano-1,4-benzoquinone (DDQ) or tetra chlorobenzoquinone (TCBQ) (Scheme 1.7). [141]

This method makes it possible to synthesize trans-porphyrins in high yields. Although one will expect to obtain a single porphyrin product when this synthetic pathway is followed, this is not the case as always mixture of products is obtained. This is because during the second stage of this method, rearrangement or scrambling occurs and thus mixture of products is obtained. [142] The only advantage this method offers is that the targeted product is always obtained in higher yield. In all the synthetic method, column chromatography is used for the purification of the products. Sometimes this purification is extremely difficult especially when trans or cis-porphyrin are targeted. This is because cis- and trans-porphyrin have the same molecular weight and thus their R_f values are very close. [142] The purified porphyrins are modified with different functionalities and coupled with other molecule to obtain a desired property.

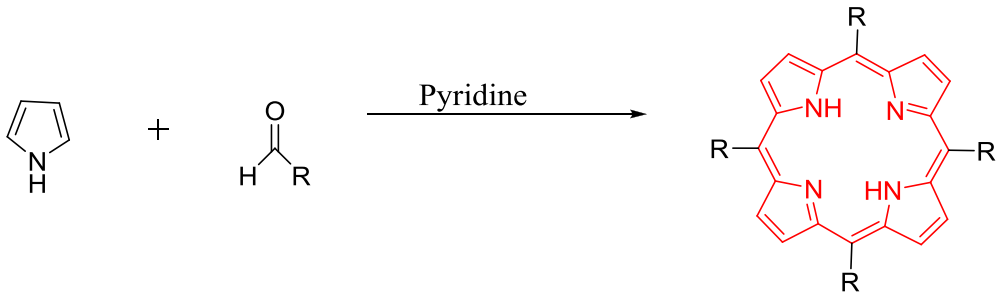

Scheme 1.5: Porphyrin Synthesis (Method 1)

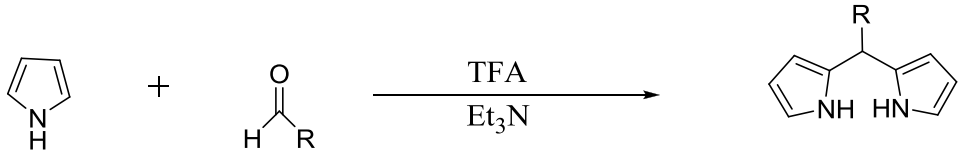

Scheme 1.6: Porphyrin Synthesis (Method 2, Stage 1)

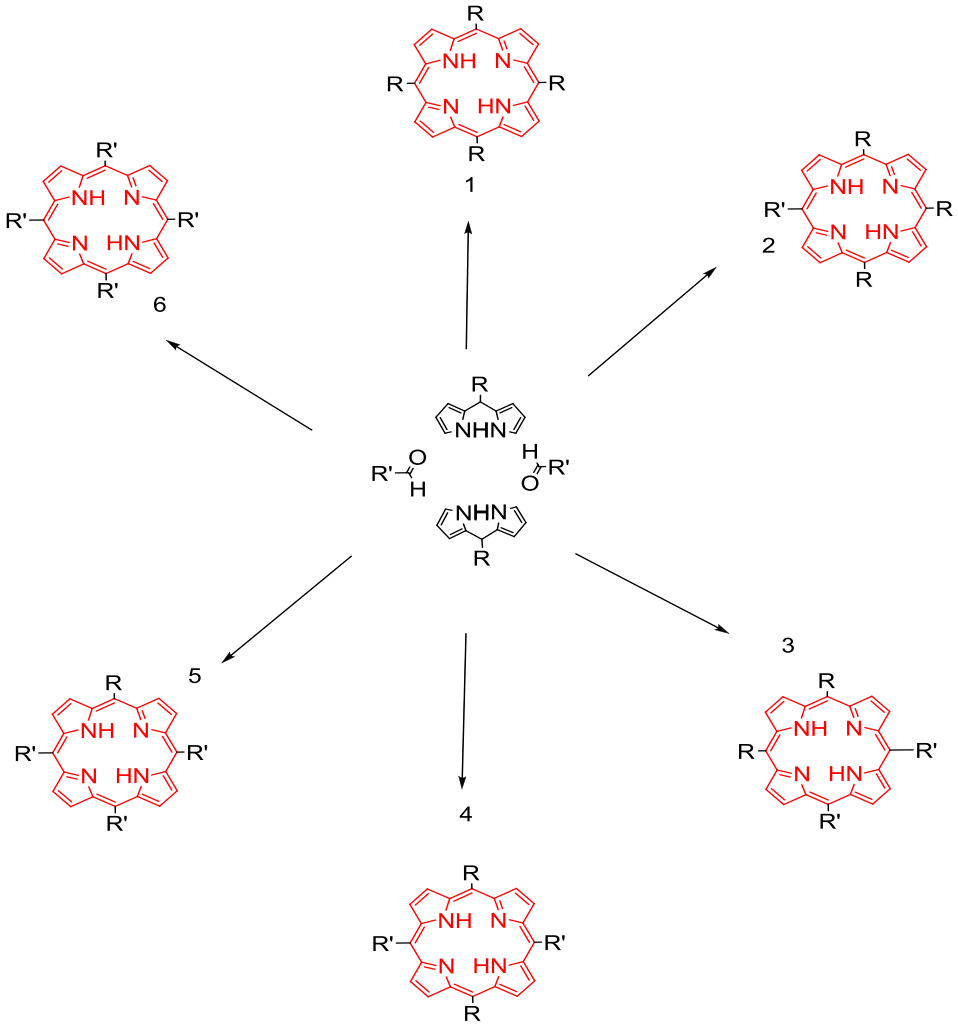

Scheme 1.7: Porphyrin Synthesis (Method 2, Stage 2)

From Scheme 1.7, it can be noted that there are different kinds of products. The targeted product is obtained in higher yield by changing the stoichiometry. For example, if 2 is to be targeted, two equivalence of dipyrromethane and two equivalence of the aldehyde should be used. Porphyrins are modified in various ways in order to function as a perfect photosensitizer in PDT.

1.3.2. Photodynamic Therapy

Photodynamic therapy (PDT) is the use of non-toxic drug to cancer patients to suppress the disease by the help of light. [143] This drug is usually a photosensitizer that can absorb light at near infrared region. The light used is usually white light which is not harmful. The drug is delivered in vivo through various mechanisms. After the drug is delivered to the targeted cells (cancer cells), excitation of the photosensitizer is done with the white light. The photosensitizer in the excited state transfers its energy to the surrounding triplet oxygen. The

triplet oxygen is converted to more reactive singlet oxygen which leads to the death of cells and tissue destruction. [144, 145] (Figure 1.20)

The concept of PDT dates back to twentieth century when eosin was used together with light to treat skin cancer. [146] At the same era Hematoporphyrin (HP) [147] and sporadic [148] were both used and reported to be both selective in localizing in tumor cells. Immediately after this finding, PDT had its modern interest breakthrough when Lipson and Baldes in 1960 [149] discovered hematoporphyrin derivative (HPD) and catalyzed by studies of this PS in both science and clinical application [150—152] by Dougherty and co-workers.

Photofrin® (PF) which is a semi-purified HPD is the first PS that gained regulatory approval for the treatment of different kinds of cancers in many countries. After prolong usage of this PS, it is realized that this compound has many drawbacks. This includes poor light penetration into the tumor due to the relatively short wavelength (630 nm) used [153], avoidance of sunlight for many weeks due to prolonged skin sensitivity [154], sub-optimal tumor selectivity [155], and the fact that it was a complex mixture of uncertain structure. [156] Since that time finding an ideal photosensitizer has been the most challenging part in PDT. Up till date scientists all over the globe have synthetized and modelled various kinds of photosensitizers. Many problems are encountered when these photosensitizers are used as therapeutic agents in PDT. In recent years several researches have been going on in finding an ideal PS. The properties of an ideal sensitizer according to medicinal chemist are: (1) chemically pure and of known composition, (2) have minimal dark toxicity and only be cytotoxic in the presence of light, (3) be preferentially retained by the target tissue, (4) be rapidly excreted from the body to provide low systemic toxicity, (5) have a high quantum yield for the photochemical event, which is often the generation of singlet oxygen ($^1O_2$) or superoxide (O^{2-}), and (6) have strong absorbance with a high extinction coefficient in the 600-800 nm range where tissue penetration of light is at a maximum and where the wavelengths of light are still energetic enough to produce singlet oxygen. [157] Among the synthetic PS, porphyrin emerged to be one of the most successful PS in PDT because of its biocompatibility, strong absorption in the 600-800 nm and relatively higher singlet oxygen quantum yield. [158]

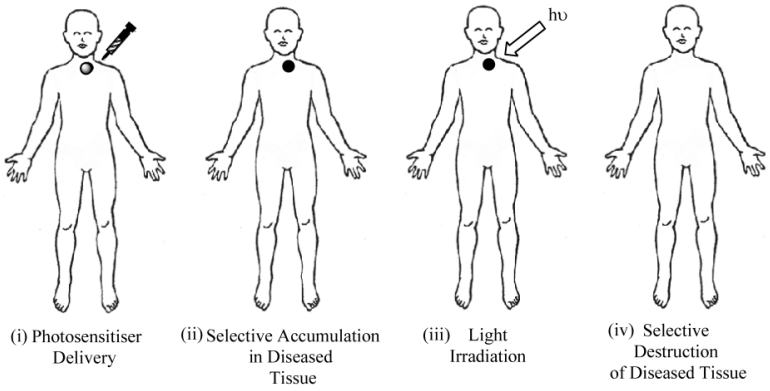

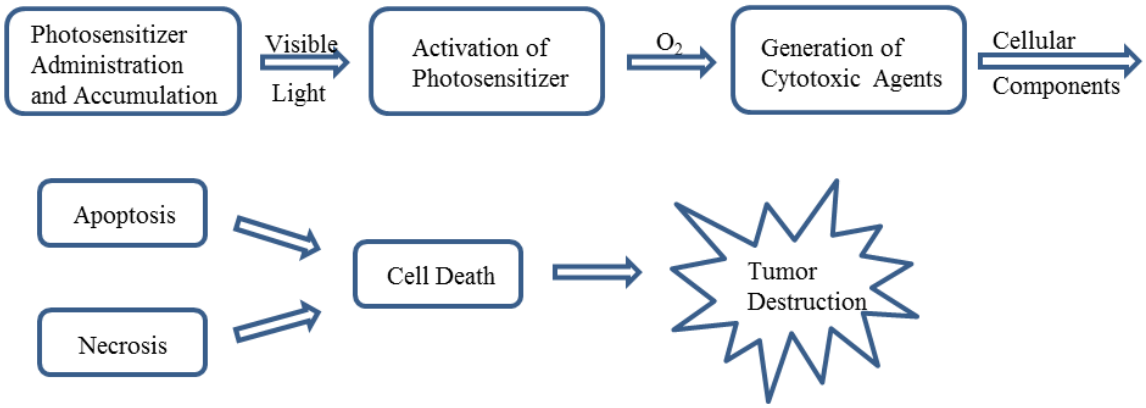

Figure 1.20: Clinical Procedure for PDT and Photosensitizer Initiated Cell Death.

Chapter 2 EXPERIMENTAL

2.1.Materials

In all the experiments commercial grade reagents and solvents were used without further purification unless noted. Silica gel (Kieselgel 60, 0.063-0.0200 mm) was used to carry out column chromatography. Thin layer chromatography was carried out on silica gel plates (Kieselgel 60 F254, 1 mm).

2.2.Instrumentation

2.2.1. FT-IR Spectroscopy

The IR spectrum was recorded with Bruker Tensor 27 model FT-IR spectrometer. High sensitivity DLATGS detector with a resolution of up to1 cm^{-1} was used. All the samples were grinded very well to a fine powder before further grinding with KBr. The samples together with KBr were pressed under high pressure to form solid pellet disks. For hygroscopic samples, the pellets were first dried under oven before taking the measurement. The FT-IR of the samples was recorded in the range 400-4000 cm^{-1} for 64 scans.

2.2.2. UV-VIS Spectroscopy

UV-Vis absorbance Spectrum was recorded with Cary 300 UV-Vis double beam spectrophotometer with spectral bandwidth down to 0.2 nm and Xenon Flash Lamp as the light source. The UV-Vis absorbance of the samples was recorded in solution using quartz cuvettes with 1cm length within the range 200-800 nm.

2.2.3. Photoluminescence Spectroscopy

The photoluminescence spectrum was recorded with Cary Eclipse Varian Spectrophotometer and Xenon lamp as the light source. The photoluminescence of the samples was recorded in solution using quartz cuvettes with 1cm length within the range 200-800 nm. Solid state photoluminescence of the samples was recorded on quartz. Slit width of 2.5 nm was used for fluorene based polymers and 5 nm for porphyrin based monomers, oligomers and polymer. All the samples were excited at their respective excitation wavelength.

2.2.4. Time Resolved Spectroscopy

The photoluminescence decay was measured with (Fluo Time 200, Pico Harp 300, Picoquant GMBH). The photoluminescence decay of all the samples was measured in both solution and solid state (on glass substrate). FluoFit software was used for decay analysis to obtain correlated life times of the samples.

2.2.5. ^{1}H-NMR and ^{13}C-NMR Spectroscopy

Both proton and carbon NMR were recorded with Bruker Avance DPX-400 MHz spectrometer. All the spectra were recorded in solution using different deuterated solvents. The chemical shift values were expressed relative to tetramethylsilane as an internal standard.

2.2.6. Elemental Analysis

The elemental composition of the samples was determined using FLASH 2000 Organic Elemental/ CHNS-O Analyzer. 2,5-(Bis(5-tert-butyl-2-benzo-oxazol-2-yl) thiophene (BBOT) was used as a standard and vanadium (V) pentaoxide (V_2O_5) was used as a catalyst.

2.2.7. Mass Spectroscopy

The mass of the monomers, oligomers and polymers were determined with Agilent 6224 High Resolution Mass Time-of-Flight (TOF) LC/MS with Electrospray Ionization method.

2.2.8. Size Exclusion Chromatography (SEC)

Molecular weight of fluorene based polymers was determined by Agilent 1200 series SEC equipped with refractive index and UV-Vis detectors. Aqueous solution of 0.2-0.8 M $NaNO_3$, 0.01 M NaH_2PO_4 (pH = 2-7) was used as eluent on PL aquagel-OH MIXED-H column calibrated with poly(ethylene oxide) standards. In all the measurements 20 μl of 1 mg/ml polymer solution was injected to the column and flows at a flow rate of 0.6 ml/min.

2.2.9. Thermal Gravimetric Analysis (TGA)

TGA measurement was done on TGA Q500 at a heating rate of 20 ℃/min from 35 ^{o}C to 900 ^{o}C.

2.2.10. Cyclic Voltammetry

The electrochemical behavior of polymers and polyrotaxanes was investigated by the Cyclic Voltammetry (CV). The CV was performed in a solution of tetrabutylammonium perchlorate Bu_4NClO_4 (0.10 M) in acetonitrile at a scan rate of 100 mV/s at room temperature. A platinum electrode was used as the working electrode. A Pt wire was used as the counter electrode and $Ag/AgNO_3$ electrode was used as the reference electrode.

2.3. Synthesis

2.3.1. Synthesis of Cucurbituril[n] [121,123,124,131-133]

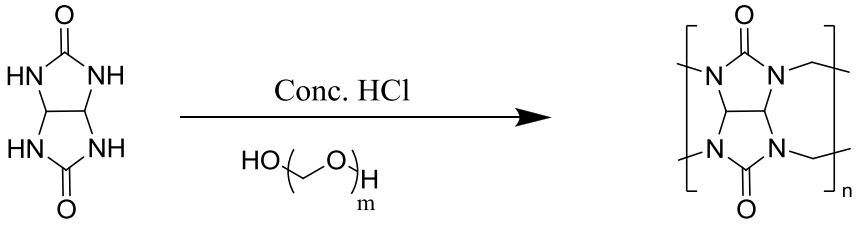

1

2: n = 6
3: n = 7
4: n = 8

Glycoluril **1** (20 g, 141 mmol) and paraformaldehyde (22.5 g, 37.5 mmol) were dissolved in 90 ml concentrated HCl in 250 ml two-neck round bottom flask. The reaction mixture is stirred for 30 minutes at room temperature. The reaction flask was immersed into a pre-warmed oil bath (95 ^{o}C) for overnight. The reaction mixture was left to stay for 2-3 days for crystal growth. The work-up was done according to literature (Figure 1.17 and Figure 1.18) [121, 123, 124, 131-133]. CB[6], CB[7] and CB[8] were obtained as white solid powder in a yield (5.86 g, 25%), (2.01 g, 8.6%) and (1.10 g, 4.7%) respectively.

CB[6]: ^{1}H-NMR (400 MHz, D_2O, 25 ^{o}C) δ: 4.29 (d, 14H, *J* = 15.5 Hz), 5.54 (s, 14H), 5.71 (d, 14 H, J = 15.5 Hz) ppm.

CB[7]: ^{1}H-NMR (400 MHz, D_2O, 25 ^{o}C) δ: 4.29 (d, 14H, *J* = 15.5 Hz), 5.60 (s, 14H), 5.91 (d, 14 H, J = 15.5 Hz) ppm.

FT-IR (KBr, ν_{max}/cm^{-1}): 1733 (C = O)

2.3.2. Synthesis of 2,5-thiophenediboronic ester: (7)

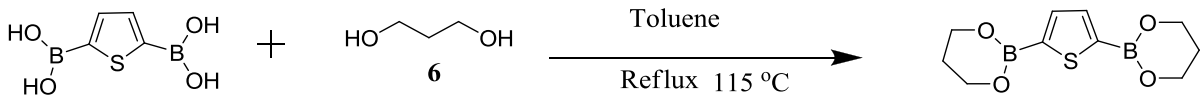

5 **6** **7**

2,5-thiophenediboronic acid **5** (2.00 g, 11.6 mmol) was placed in a 50 ml two-neck round bottom flask. Toluene (25 ml) was added to the flask and the solution was stirred for 10 minutes. To the solution, 1,3-propanediol was added and the mixture was heated to 130 ^{o}C. The reaction mixture was refluxed for overnight. The reaction mixture was transferred into one-neck round bottom flask and the solvent was removed under reduced pressure. A white precipitate was observed in the flask and ethanol was used to wash the product under suction. The product was further purified by washing with N-hexane. A white solid powder was obtained. Yield = 1.89 g, 64%. ^{1}H-NMR (400 MHz, D_2O, 25 ^{o}C) δ: 1.71 (m, 4H), 3.86 (t, 8H), 7.25 (s, 2H) ^{13}C-NMR (100 MHz, $CDCl_3$, 25 ^{o}C) δ: 136.03, 62.09, 27.40 ppm.

2.3.3. Synthesis of Monotosyl triethylene glycol (16)[105]

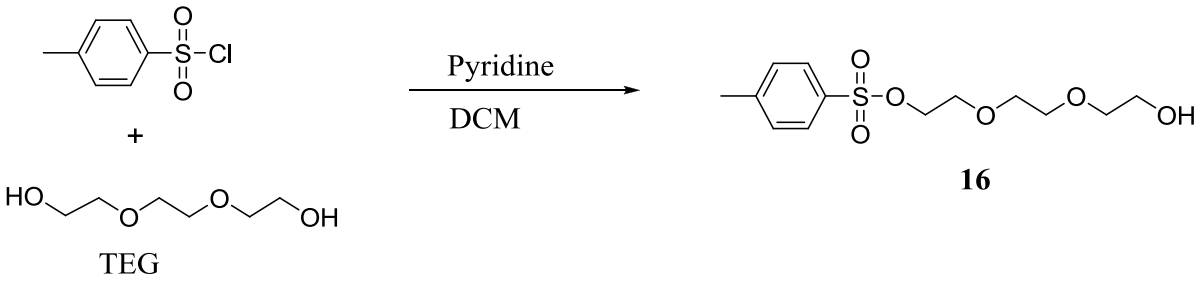

In a 250 ml two-neck round bottom flask, triethylene glycol (TEG) (5.00 g, 33.3 mmol) was dried under vacuum for 30 minutes followed by the addition of 100 ml DCM. 2.7 ml of pyridine (2.63 g, 33.3 mmol) was added and the reaction mixture was stirred for 10 minutes at room temperature. The flask was cooled to 0 ^{o}C and kept at this temperature while tosyl chloride was added under argon to the reaction mixture. After 3-4 hours ice was removed and the flask content was stirred at room temperature for overnight. The reaction mixture was extracted first with 2 M HCl (100 ml) followed by $NaHCO_3$, brine and water consecutively. The product was further purified by column chromatography using DCM/MeOH (1:1) system as eluent. Transparent viscous liquid was obtained. Yield = 5.20 g, 51%

^{1}H-NMR (400 MHz, $CDCl_3$, 25 ^{o}C) δ: 2.42 (s, 3H), 3.37 (m, 2H), 3.59 (s, 4H), 3.67 (t, 4H) 4.11 (br, 1H) 4.13 (t, 2H) 7.49 (d, 4H), 7.79 (d, 4H)

2.3.4. Synthesis of Dipyrromethane (2,2'-((4-bromophenyl)methylene)bis(1H-pyrrole)) (10)[100]

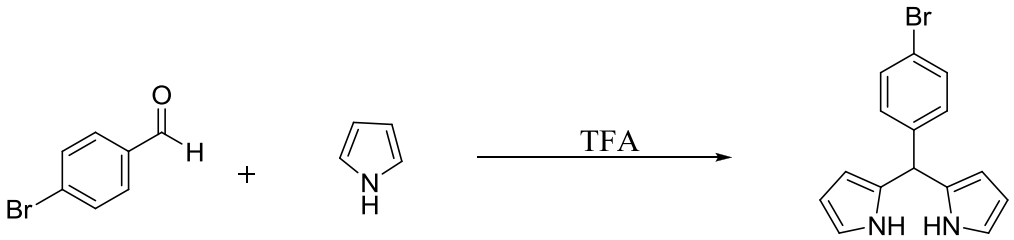

8 **9** **10**

p-bromo benzaldehyde **8** (2.00 g, 10.8 mmol) and 50 ml of freshly distilled pyrrole **9** (48.5 g, 723 mmol) were placed into a two-neck round bottom flask under nitrogen atmosphere. The mixture was heated to 50 ^{o}C. After removing the heat source, trifluoroacetic acid (TFA) 83 μl (0.124 g, 1.08 mmol) was added immediately. After 10 minutes the solution was quenched with 11 ml 0.1 M NaOH. The solvents and the unreacted pyrrole were removed under reduced pressure to yield a light brown oily product. The product was purified by recrystallization in N-hexane. The precipitate was collected under suction filtration to yield a brownish solid substance. Yield = 726 mg, 22%

^{1}H-NMR (400 MHz, $CDCl_3$, 25 ^{o}C) δ: 5.45 (s, 1H), 5.91 (d, 2H), 6.17 (t, 2H), 6.73 (d, 2H), 7.10 (d, 2H), 7.45 (d, 2H), 7.94 (br, 2H, N-H) ppm; ^{13}C-NMR (100 MHz, $CDCl_3$, 25 ^{o}C) δ: 141.20, 132.69, 131.68, 130.13, 117.48, 108.58, 107.44, 43.46 ppm. Elemental analysis: calcd for $C_{15}H_{13}BrN_2$: C 59.82, H 4.35, N 9.30; found: C 58.48, H 4.40, N 9.41.
ESI-MS m/z $[M+H]^{+1}$: for $C_{15}H_{13}BrN_2$: Calcd. 300.03, found m/z 301.01 $[M+H]^{+1}$.

2.3.5. Synthesis of Dipyrromethane (2,2'-((3,5-dimethoxyphenyl)methylene)bis(1H-pyrrole)) (12)[100]

11 **9** **12**

3,5-dimethoxy benzaldehyde **11** (1.00 g, 6.02 mmol) and freshly distilled pyrrole **9** 25 ml (24.3 g, 361 mmol) were placed into a two-necked round bottom flask under nitrogen atmosphere. The mixture was heated to 50 ^{o}C. After removing the heat source, trifluoroacetic acid (TFA) 46 μl (0.0686 g, 0.602 mmol) was added immediately. After 10 minutes the solution was quenched with 6 ml 0.1 M NaOH. The solvents and the unreacted pyrrole were removed under reduced pressure. The product was purified using column chromatography with DCM:Et_3N (20:1) as eluent. The yellow oily product from the column was recrystallized by dissolving the product in hot ethanol followed by addition of water. Water addition stops when the solution becomes cloudy yellow. The precipitate was collected under suction filtration to yield a greyish solid substance. Yield = 945 mg, 56%.

^{1}H-NMR (400 MHz, $CDCl_3$, 25 ^{o}C) δ: 3.76 (s, 6H), 5.43 (s, 1H), 5.98 (d, 2H), 6.17 (t, 2H), 6.38 (s, 1H), 6.39 (s, 2H), 7.29 (d, 2H), 7.95 (br, 2H, N-H) ppm; ^{13}C-NMR (100 MHz,$CDCl_3$, 25 ^{o}C) δ: 161.00, 144.46, 132.10, 117.18, 108.46, 107.21, 106.72, 98.82, 55.31, 44.32.

Elemental analysis: calcd for $C_{17}H_{18}N_2O_2$: C 72.32, H 6.43, N 9.92, O 11.33; found: C 71.79, H 6.32, N 9.84, O 12.05.

ESI-MS m/z $[M+H]^{+1}$: for $C_{17}H_{18}N_2O_2$: Calcd. 282.14, found m/z 281.12 $[M+H]^{+1}$.

2.3.6. One Pot Synthesis of 5-(*p*-brommophenyl)-10,15,20-tri(3,5-dimethoxy phenyl)porphyrin (13) and 5,15-di(*p*-bromophenyl)-10,20-di(3,5-dimethoxyphenyl)porphyrin (14)[140]

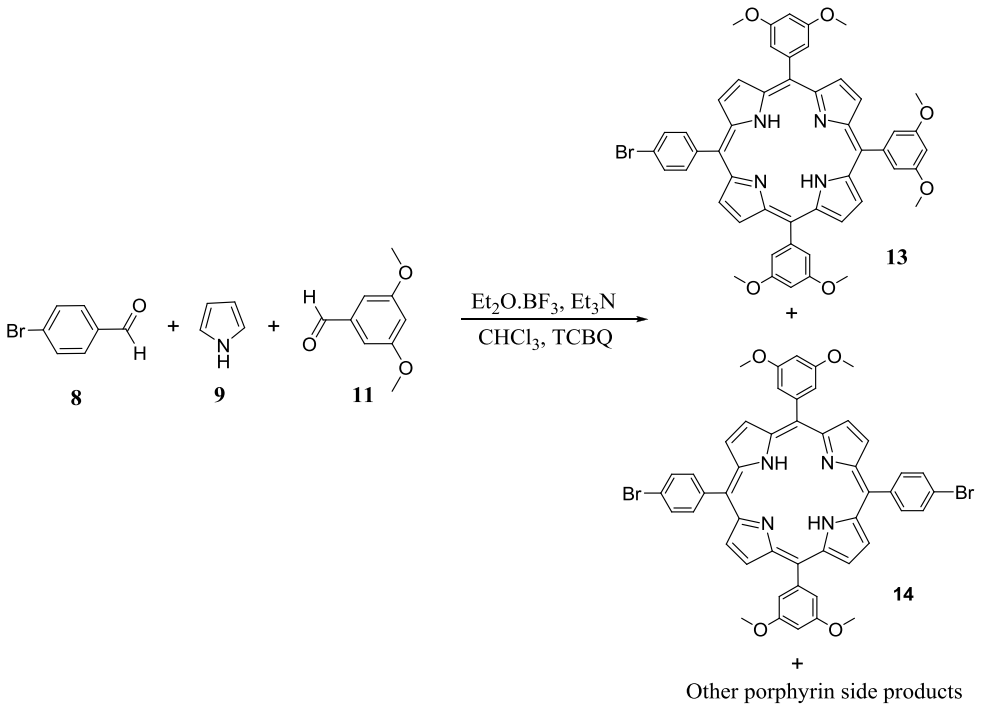

To 1.5 L of chloroform were added (1.00 g, 6.01 mmol) of 3,5-dimethoxybenzeldehyde, (1.13 g, 6.01 mmol) 4-bromobenzaldehyde and (0.80 g, 12.03 mmol) of pyrrole and the reaction flask was kept away from light. During stirring, (0.56 g, 4.00 mmol) of the Lewis acid catalyst ($Et_2O.BF_3$) was added to the reaction mixture under nitrogen atmosphere. The reaction mixture was stirred for 1 hour at room temperature followed by the addition of (0.48 g, 4.81 mmol) of triethylamine and (1.11 g, 4.53mmol) of TCBQ. The reaction mixture was reflux for 1 hour. The solution was cooled to room temperature and the volume of the reaction mixture was reduced to ca. 300 ml, filtered through silica gel, and evaporated to dryness. The purple residues were washed with MeOH. The residues were further purified by column chromatography on silica gel using toluene as eluent. The first fraction was collected and evaporated under reduced pressure and the resultant product was again triturated with MeOH to give compound **13** as shiny purple crystals. Yield: 0.18 g (13%).

^{1}H-NMR (400 MHz, $CDCl_3$, 25 ^{o}C) δ: -2.81 (s, 2H), 3.98 (s, 18H), 6.92 (s, 3H), 7.42 (s, 6H), 7.93 (d, 2H), 8.11 (d, 2H), 8.83 (d, 2H), 8.97 (d, 6H) ppm; ^{13}C-NMR (100 MHz, $CDCl_3$, 25 ^{o}C) δ: 158.88, 143.93, 135.83, 129.91, 113.88, 100.18, 106.72, 55.63 ppm.
Elemental analysis: calcd for $C_{50}H_{41}BrN_4O_6$: C 46.19, H 4.65; found: C 46.90, H 8.20
ESI-MS m/z $[M+H]^{+1}$: for $C_{50}H_{41}BrN_4O_6$: Calcd. 874.22, found m/z 875.22 $[M+H]^{+1}$
UV-VIS ($CHCl_3$): λ_{max} (nm); 421, 512, 547, 585, 638
5,15-di(*p*-bromophenyl)-10,20-di(*m*-dimethoxyphenyl)porphyrin **14** was also collected from the same column. Yield: 0.23 g (26%).
^{1}H-NMR (400 MHz, $CDCl_3$, 25 ^{o}C) δ: -2.82 (s, 2H), 3.99 (s, 12H), 6.92 (s, 2H), 7.41 (s, 4H), 7.93 (d, 4H), 8.11 (d, 4H), 8.82 (d, 4H), 8.84 (d, 4H) ppm; ^{13}C-NMR (100 MHz,$CDCl_3$, 25 ^{o}C) δ: 158.90, 143.83, 141.04, 135.81, 129.93, 122.51, 120.16, 118.60, 100.19, 55.62 ppm.
Elemental analysis: calcd for $C_{48}H_{36}Br_2N_4O_4$: C 46.19, H 4.65; found: C 46.90, H 8.20
ESI-MS m/z $[M+H]^{+1}$: for $C_{48}H_{36}Br_2N_4O_4$: Calcd. 892.11, found m/z 893.11 $[M+H]^{+1}$
UV-VIS ($CHCl_3$): λ_{max} (nm); 421, 512, 547, 585, 638
Note: Four other porphyrin side products were also isolated and identified.

2.3.7. Synthesis of 5-(*p*-brommophenyl)-10,15,20-tri(3,5-dimethoxyphenyl)porphyrin (13) from 12[141]

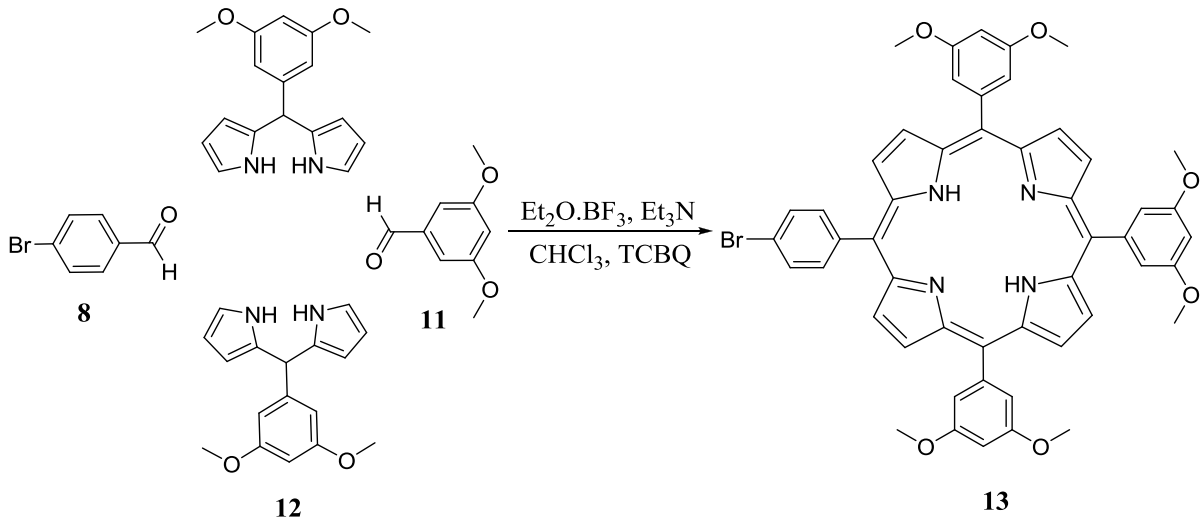

Compound **12** (0.500 g, 1.77 mmol), **8** (0.164 g, 0.886 mmol) and **11** (0.147 g, 0.886 mmol) were dissolved in distilled chloroform (1000 ml) and stirred under nitrogen. Oxygen was removed from the resulting solution by briefly keeping the mixture under vacuum for at least 30 minutes and the reaction flask was kept away from light. During stirring, 37 μl (0.0420 g, 0.296 mmol) of the Lewis acid catalyst ($Et_2O.BF_3$) was added to the reaction mixture under nitrogen atmosphere. The reaction mixture was stirred for 1 hour at room temperature followed by the addition of 50 μl (0.0358 g, 0.354 mmol) of triethylamine and (0.164 g, 0.667 mmol) of TCBQ. The reaction mixture was reflux for 1 hour. The solution was cooled to room temperature and the volume of the reaction mixture was reduced to ca. 300 ml, filtered through silica gel, and evaporated to dryness. The purple residues were washed with MeOH. The residues were further purified by column chromatography on silica gel using toluene as eluent. The first fraction was collected and evaporated under reduced pressure and the resultant product was again triturated with MeOH to give compound **13** as shiny purple crystals. Yield: 0.232 g (15%).

Note: Four other porphyrin side products were also isolated and identified.

2.3.8. Synthesis of 5,15-(*p*-dibromophenyl)-10,20-di(3,5-dimethoxyphenyl)porphyrin (14) from 12[141]

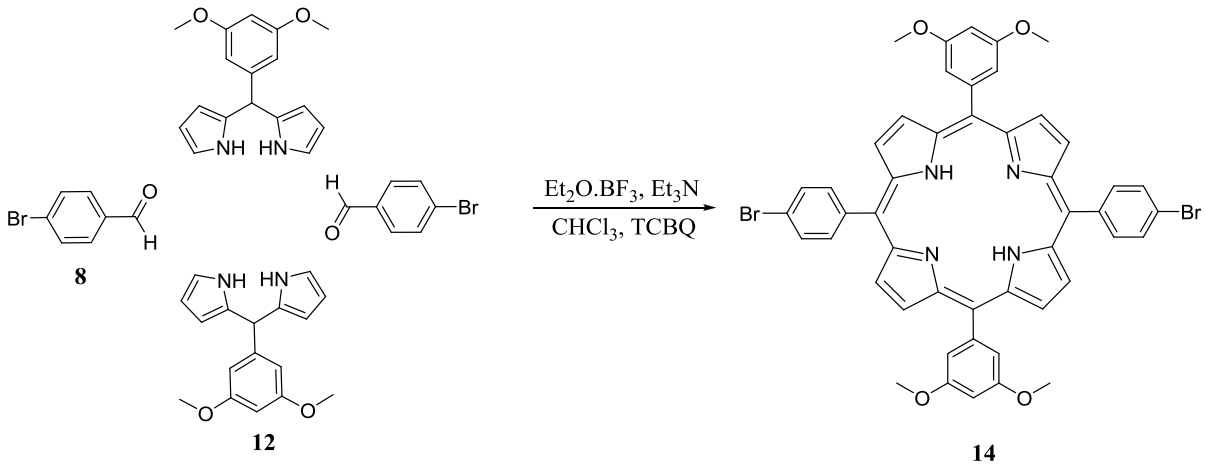

Compound **12** (0.400 g, 1.42 mmol) and **8** (0.262 g, 1.42 mmol) were dissolved in distilled chloroform (1000 ml) and stirred under nitrogen. Oxygen was removed from the resulting solution by briefly keeping the mixture under vacuum for at least 30 minutes and the reaction flask was kept away from light. During stirring, 61 μl (0.0696 g, 0.490 mmol) of the Lewis acid catalyst ($Et_2O.BF_3$) was added to the reaction mixture under nitrogen atmosphere. The reaction mixture was stirred for 1 hour at room temperature followed by the addition of 79 μl (0.0573 g, 0.567 mmol) of triethylamine and (0.2625 g, 1.07 mmol) of TCBQ. The reaction mixture was reflux for 1 hour. The solution was cooled to room temperature and the volume of the reaction mixture was reduced to ca. 300 ml, filtered through silica gel, and evaporated to dryness. The purple residues were washed with MeOH. The residues were further purified by column chromatography on silica gel using toluene as eluent. The product was collected and evaporated under reduced pressure and triturated with MeOH to give compound **14** as shiny purple crystals. Yield: 0.100 g (16%).

2.3.9. Synthesis of 5,15-(*p*-dibromophenyl)-10,20-di(3,5-dimethoxyphenyl)porphyrin (14) from 10[141]

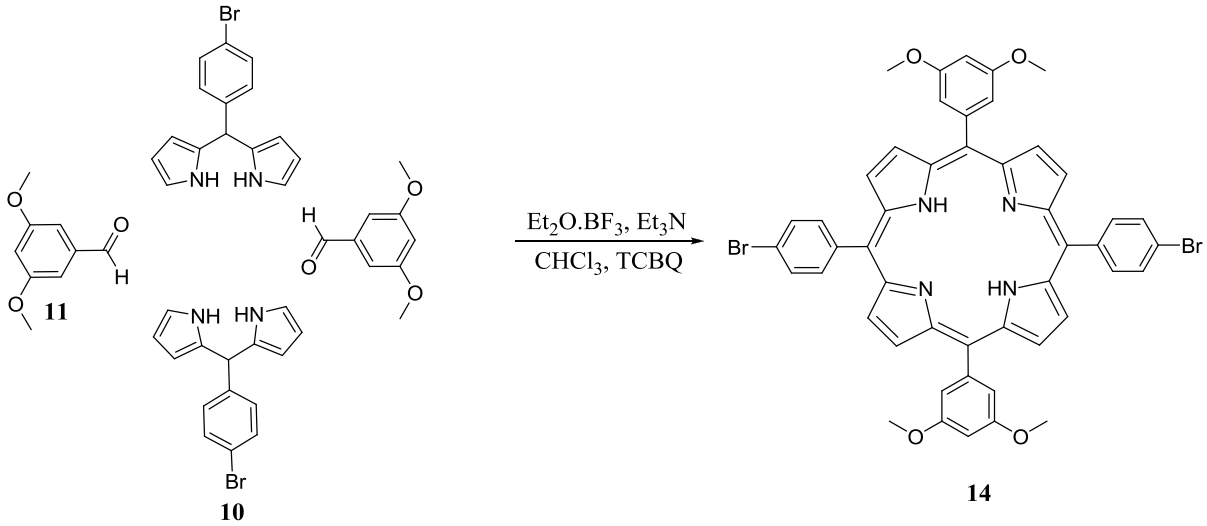

Compound **10** (0.50 g, 1.66 mmol) and **11** (0.276 g, 1.66 mmol) were dissolved in distilled chloroform (1000 ml) and stirred under N_2. Oxygen was removed from the resulting solution by flash-vacuum for at least 30 minutes and the reaction flask was kept away from light. During stirring, 70 μl (0.0787 g, 0.555 mmol) of the Lewis acid catalyst ($Et_2O.BF_3$) was added to the reaction mixture under nitrogen atmosphere. The reaction mixture was stirred for 1 hour stirring at room temperature followed by the addition of 93 μl (0.0672 g, 0.664 mmol) of triethylamine and (0.308 g, 1.25 mmol) of TCBQ. The reaction mixture was reflux for 1 hour. The solution was cooled to room temperature and the volume of the reaction mixture was reduced to ca. 300 ml, filtered through silica gel, and evaporated to dryness. The purple residues were washed with MeOH. The residues were further purified by column chromatography on silica gel using toluene as eluent. The product was collected and evaporated under reduced pressure and triturated with MeOH to give compound **14** as shiny purple crystals. Yield: 0.130 g (18%).

2.3.10. Synthesis of 5-(*p*-brommophenyl)-10,15,20-tri(3,5-dihydroxy phenyl)porphyrin (15)

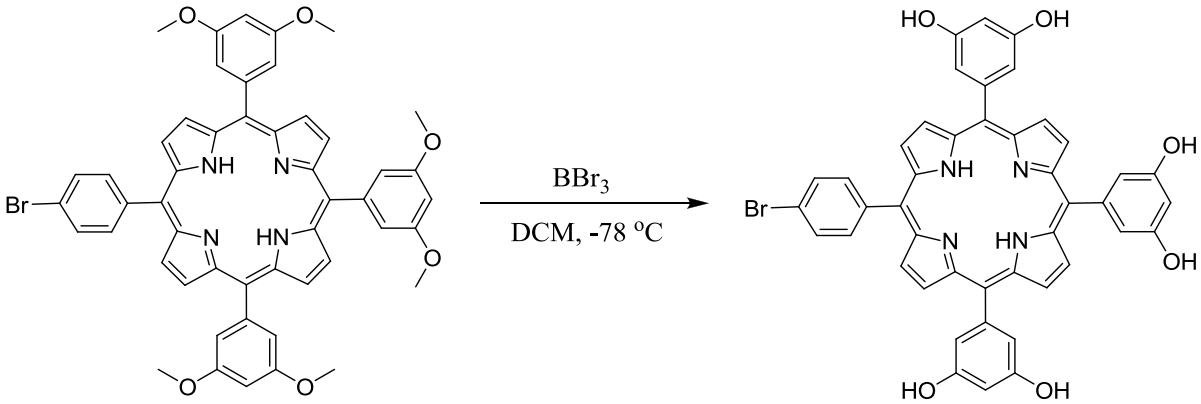

13 15

To a solution of **13** (100 mg, 0.11 mmol) in dry dichloromethane (25 ml) at –78 °C under an argon atmosphere, boron tribromide solution BBr_3 (1M in dichloromethane, 12 ml, 33 mmol) was added. The reaction mixture was stirred at –78 °C for 1 hour, and then allowed to warm to room temperature. After the reaction was stirred at room temperature for overnight, the reaction mixture was cooled to 0 °C followed by the addition of 10 ml of water. The resulting mixture was stirred for 5-10 minutes and the solvents were removed under reduced pressure. The aqueous phase was extracted with ethyl acetate (5 × 20 ml) followed by the removal of the solvents under reduced pressure. The solid residue was further washed with chloroform to give 74 mg as purple crystals in 91% yield. ^{1}H-NMR (400 MHz, DMSO-d6, 25 °C) δ: 9.75 (s, 6H, OH), 8.95-8.83 (m, 4H, bromophenyl-H), 8.03-8.19 (m, 6H, O-phenyl-H), 6.67-7.09 (m, 3H, p-phenyl-H), -3.00 (s, 2H, pyrrole, NH) ppm. ^{13}C-NMR (100 MHz, DMSO-d6, 25 °C) δ: 156.52, 143.53, 135.71, 129.69, 114.37, 101.81 ppm.

ESI-MS m/z $[M+H]^{+1}$: for $C_{44}H_{29}BrN_4O_6$: Calcd. 789.13, found m/z 789.117 $[M+H]^{+1}$.

UV-VIS (MeOH): λ_{max} (nm); 418, 512, 547, 585, 638.

2.3.11. Synthesis of 5-(*p*-brommophenyl)-10,15,20-tri(3,5-di-*O*-TEGphenyl)porphyrin (17)

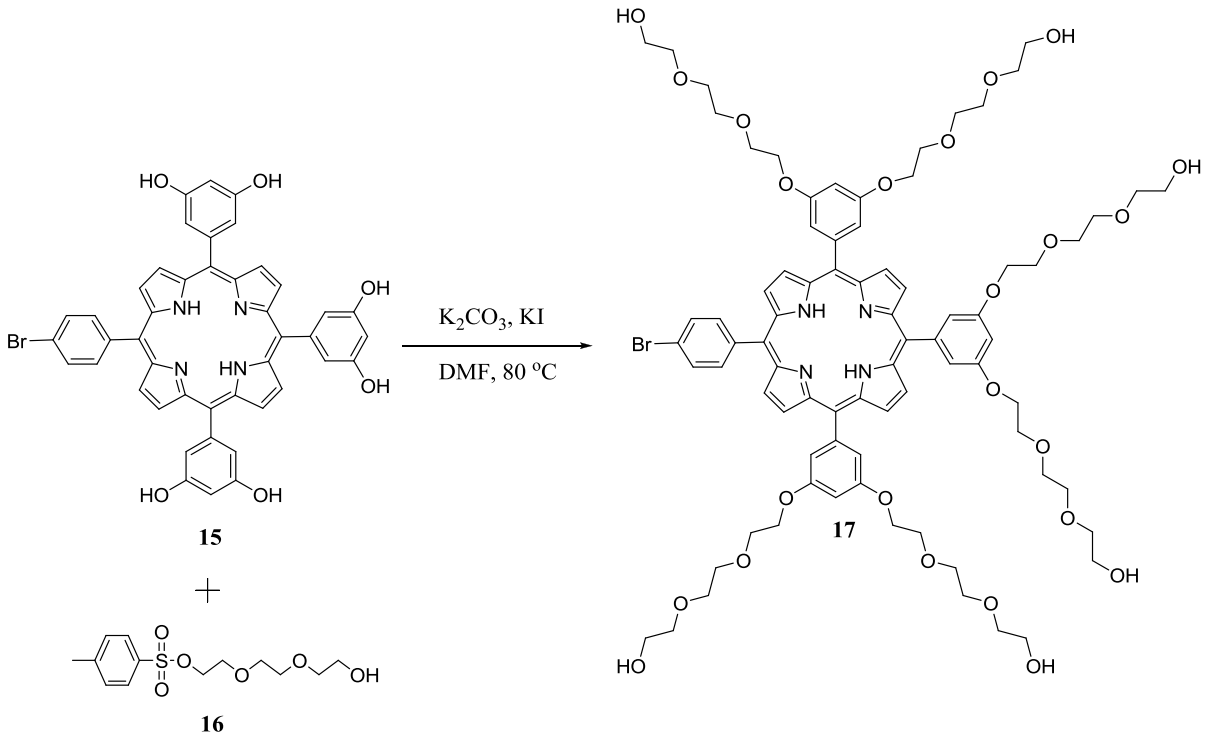

To a solution of **15** (370 mg, 0.46 mmol) in 30 ml anhydrous DMF, was added K_2CO_3 (1.29 g, 9.38 mmol), KI (0.15 g, 0.93 mmol) and tri(ethylene glycol) monotosylate **16** (1.14 g, 3.75 mmol) and refluxed at 80 °C for 12 hours. Thereafter, the reaction mixture was cooled to room temperature and the solvent was removed under reduced pressure to give gummy purple residues. The resulting mixture was washed with chloroform and filtered under suction. The product was further purified by column chromatography using $CHCl_3$/ MeOH (9:1) system as the eluent to obtain purple gum (0.60 g, 84%). ^{1}H-NMR (400 MHz, $CDCl_3$, 25 °C) δ: 8.81-8.99 (m, 4H, bromophenyl-H), 7.91-8.19 (m, 6H, O-phenyl-H), 7.42 (s, 3H, p-phenyl-H), 6.95 (s, 3H, p-phenyl-H), 3.03-4.32 (m, 72H, TEG-C*H*$_2$), -2.90 (s, 2H, pyrrole, NH) ppm. ^{13}C-NMR (100 MHz, $CDCl_3$, 25 °C) δ: 157.95, 143.79, 135.85, 129.95, 114.81, 72.18, 69.86, 67.76, 61.18, 29.70 ppm.

ESI-MS m/z $[M+H]^{+1}$: for $C_{80}H_{101}BrN_4O_{24}$: Calcd. 1580.5989, found 1581.60 $[M+H]^{+1}$.

UV-VIS ($CHCl_3$): λ_{max} (nm); 421, 512, 547, 585, 638.

2.3.12. Synthesis of 5-(*p*-brommophenyl)-10,15,20-tri(3,5-di-*O*-TEGphenyl)porphyrin Zinc (18)

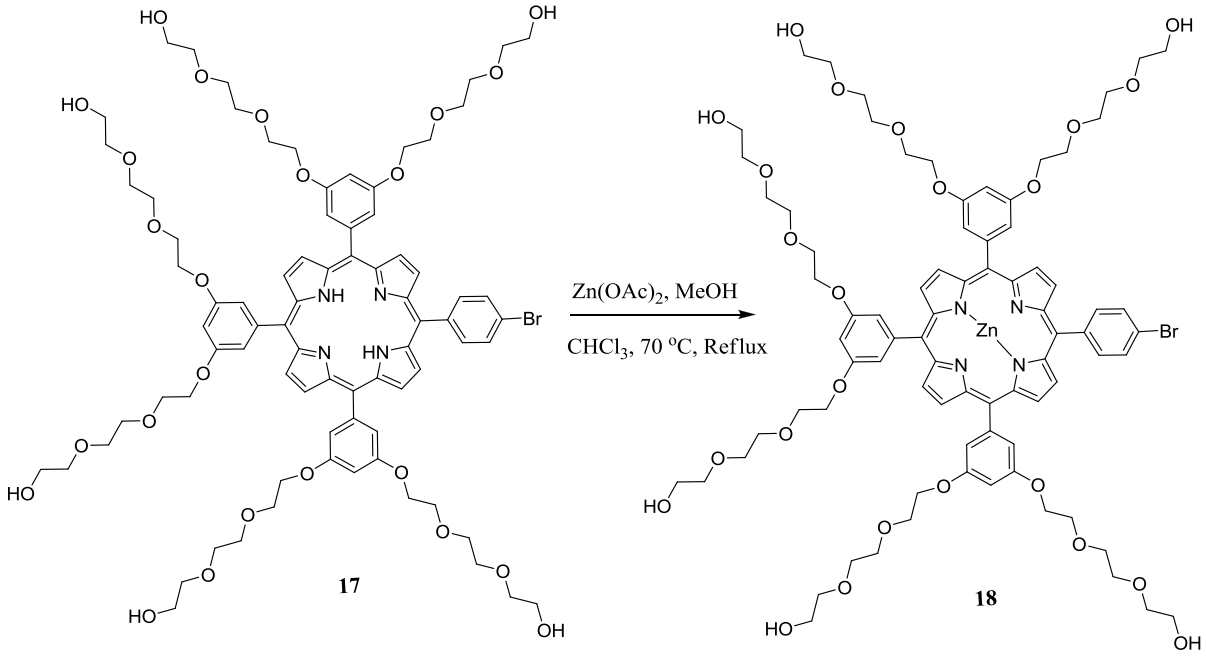

To a 50 ml two-neck round bottom flask containing 30 ml of $CHCl_3$/MeOH mixture (v/v = 9/1) **17** (600 mg, 0.38 mmol) was added and stirred for a while. Then, $Zn(OAc)_2$ (300 mg, 1.63 mmol) was added to the reaction mixture and refluxed at 65-70 °C for 2 hours. Thereafter, the reaction mixture was cooled to room temperature and filtered under suction to remove inorganic salts. The filtrate was evaporated and passed through a small pad of silica gel using DCM/MeOH (1:1) system as the eluent. The product was evaporated under reduced pressure to yield a purple-red gum. Yield: 580 mg, 86%. ^{1}H-NMR (400 MHz, $CDCl_3$, 25 °C) δ: 8.87-9.05 (m, 4H, bromophenyl-H), 7.89-8.03 (m, 6H, O-phenyl-H), 7.45 (s, 3H, p-phenyl-H), 6.90 (s, 3H, p-phenyl-H), 3.05-4.33 (m, 72H, TEG-CH_2) ppm. ^{13}C-NMR (100 MHz, $CDCl_3$, 25 °C) δ: 157.95, 143.79, 135.85, 129.95, 114.81, 72.18, 69.86, 67.76, 61.18, 29.70 ppm. Elemental analysis: calcd for $C_{80}H_{99}BrN_4O_{24}Zn$: C 58.238, H 6.06, N 3.40. found: C 57.29, H 6.38, N 2.93.

ESI-MS m/z $[M+H]^{+1}$: for $C_{80}H_{99}BrN_4O_{24}Zn$: Calcd. 1644.54, found 1645.16 $[M+H]^{+1}$.

UV-VIS ($CHCl_3$): λ_{max} (nm); 426, 557, 604.

2.3.13. Synthesis of 5-phenyl(2,5-thienylene)-10,15,20-tri(3,5-di-*O*-TEGphenyl)oligoporphyrin Zinc (19)[101-103]

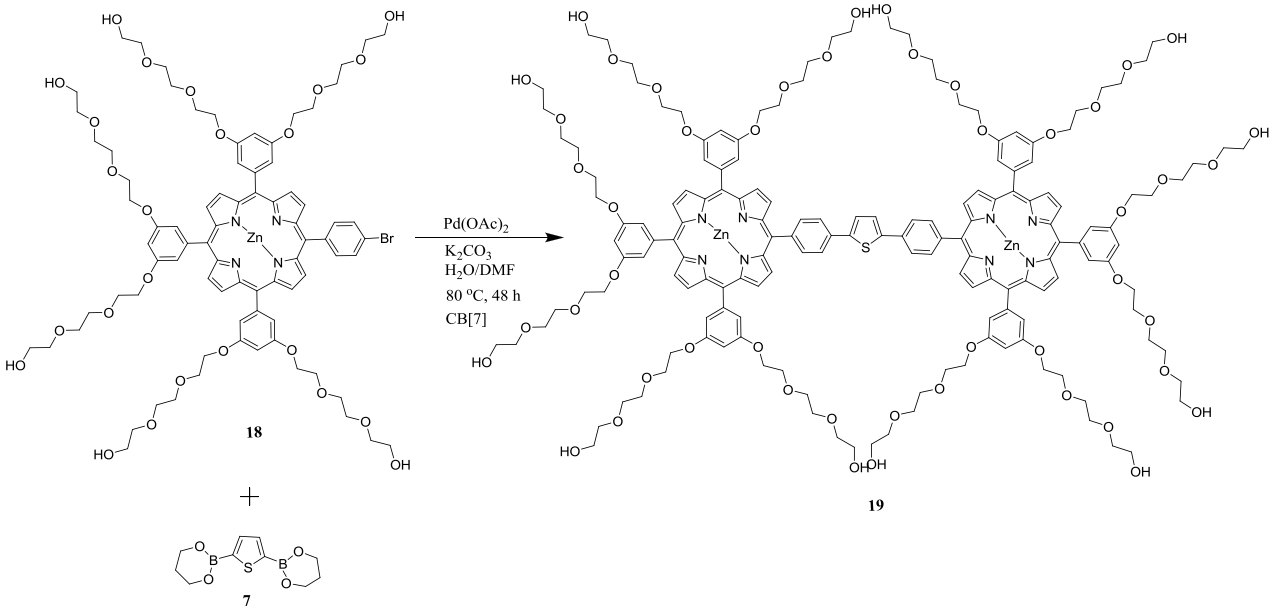

Thiophene diboronic ester **7** (13 mg, 0.051 mmol) and CB[7] (118 mg, 0.101 mmol) were placed in a two-neck round bottom flask, equipped with a condenser. Degassed DMF/water 3:1 (15 ml) was added to dissolve the mixture in the flask and under nitrogen **18** (167 mg, 0.101 mmol) was added. The mixture was stirred under nitrogen while heating at around 50 ^{o}C. Twenty minutes later aqueous K_2CO_3 (140 mg, 1.01 mmol) in degassed water (3 ml) was added to the reaction flask followed by the addition of $Pd(OAc)_2$ (catalytic amount). The reaction mixture was heated to 80 ^{o}C for 48 hours under nitrogen. All the solvents from the reaction mixture were removed under reduced pressure and the resulting solid residue was dissolved in chloroform and filtered under suction. The filtrate was further purified by column chromatography using CH_3Cl/MeOH (1:1) system as the eluent. Solid purple product was obtained. Yield: 100 mg, 61%. ^{1}H-NMR (400 MHz, $CDCl_3$, 25 ^{o}C) δ: 8.97-8.88 (m, pyrrolic-H), 8.22-7.75 (m, Ar-H), 7.50-6.95 (m, Ph-H), 4.33-3.15 (m, TEG-CH_2) ppm. ^{13}C-NMR (100 MHz, $CDCl_3$, 25 ^{o}C) δ: 157.67, 150.02, 149.72, 145.00, 143.18, 134.48, 132.45, 131.11, 128.08, 126.43, 120.83, 114.85, 71.93, 70.66, 70.14, 69.85, 67.80, 61.05, 61.02 ppm. Elemental analysis for $C_{164}H_{200}N_8O_{48}SZn_2$ Calcd: S, 1.00; H, 6.27; N, 3.49. found: S, 0.41; H, 6.34; N, 3.20. ESI-MS m/z $[M+H]^{+2}$: for $C_{164}H_{200}N_8O_{48}SZn_2$: Calcd. 3209.1759, found 1605.5490 $[M+H]^{+2}$.

UV-VIS ($CHCl_3$): λ_{max} (nm); 426, 557, 604.

2.3.14. Synthesis of 5-phenyl(2,5'-bithienylene)-10,15,20-tri(3,5-di-*O*-TEGphenyl)oligoporphyrin Zinc (20)[104]

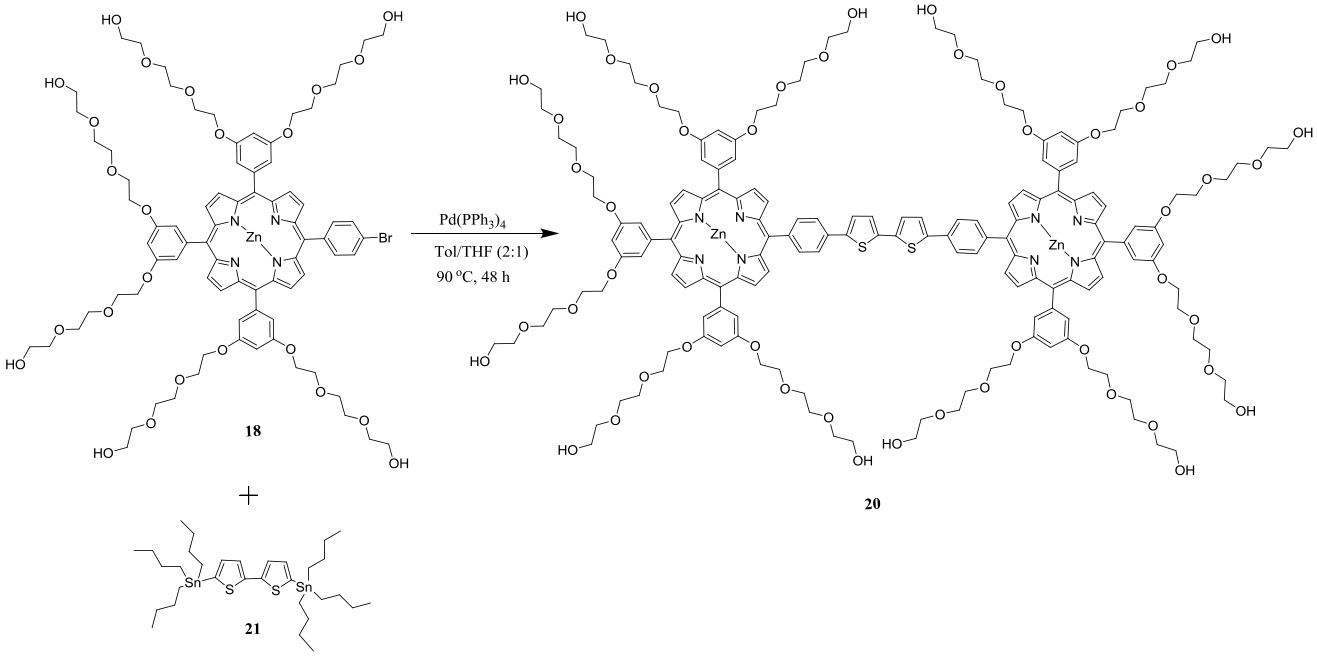

In a 30 ml two-neck round bottom flask **18** (0.53 g, 0.65 mmol) and 5,5′-Bis(tributylstannyl)-2,2′-bithiophene **21** (0.26 g, 0.35 mmol) were added. Anhydrous Toluene/THF mixture (2:1, 30 ml) was added to the flask and the resulting solution was degassed using freeze-pump thaw method three consecutive times. Catalytic amount of $Pd(PPh_3)_4$ was added to the reaction flask under argon atmosphere. The temperature of the reaction was raised to 80-90 ºC and stirred for 48 hours. The solvent of the reaction mixture was removed under reduced pressure to give a purple solid residue. The solid residue was further washed with cold 1M aqueous NaOH followed by diethyl ether (Et_2O). The resulting product was dissolved in chloroform and passed through a pad of silica. The solvent was removed and dried under vacuum to obtain a purple residue. Yield: 250 mg, 21 %. ^{1}H-NMR (400 MHz, $CDCl_3$, 25 ^{o}C) δ: 8.71-8.49 (m, pyrrolic-H), 8.18-8.28 (m, Ar-H), 7.19-7.79 (m, Ph-H), 3.61-4.50 (m, TEG CH_2) ppm. ^{13}C-NMR (100 MHz, $CDCl_3$, 25 ^{o}C) δ: 159.21, 146.07, 141.64, 128.28, 118.50, 103.73, 72.59, 2.59, 70.98, 70.45, 69.83, 68.26, 61.71, 61.68 ppm.

Elemental analysis for $C_{168}H_{202}N_8O_{48}S_2Zn_2$ Calcd: S, 1.95 ; H, 6.18 ; N, 3.40. Found: S, 1.32; H, 6.57 ; N, 3.11. ESI-MS m/z $[M+2H]^{+2}$: for $C_{168}H_{202}N_8O_{48}S_2Zn_2$: Calcd. 3291.1636, found 1645.5221 $[M+2H]^{+2}$.

UV-VIS ($CHCl_3$): λ_{max} (nm); 426, 557, 604.

2.3.15. Synthesis of 5,15-di(*p*-bromophenyl)-10,20-di(3,5-dihydroxyphenyl)porphyrin (22)

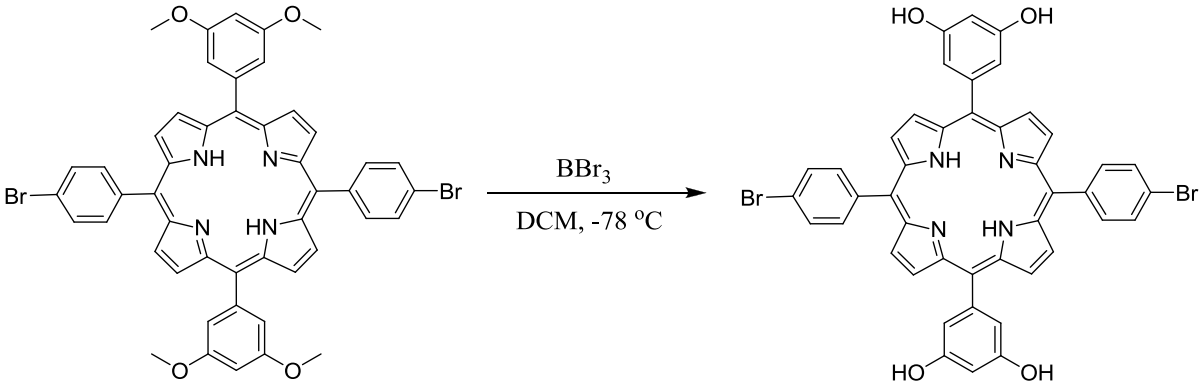

14 **22**

To a solution of **14** (625 mg, 0.700 mmol) in dry dichloromethane (30 ml) at –78 °C under an argon atmosphere, boron tribromide solution BBr_3 solution (1 M in dichloromethane, 8 ml, 8.06 mmol) was added. The reaction mixture was stirred at –78 °C for 1 hour, and then allowed to warm to room temperature. After the reaction was stirred at room temperature for overnight, the reaction mixture was cooled to 0 °C followed by addition of 10 ml of water. The resulting mixture was stirred for 5-10 minutes and the solvents were removed under reduced pressure. The aqueous phase was extracted with ethyl acetate (5 × 20 ml) followed by the removal of the solvents under reduced pressure. The solid residue was further washed with cold chloroform to give 585 mg as purple crystals in 98 % yield. ^{1}H-NMR (400 MHz, DMSO-d6, 25 ^{o}C) δ: 9.72 (s, 4H, OH), 8.85-8.98 (m, 8H, bromophenyl-H), 8.03-8.17 (m, 4H, Ophenyl-H), 6.78-7.15 (m, 2H, p-phenyl-H), -3.05 (s, 2H, pyrrole, NH) ppm.^{13}C-NMR (100 MHz, DMSO-d6, 25 ^{o}C) δ: 157.02, 143.13, 140.92, 136.48, 130.48, 122.50, 120.95, 118.72, 114.67, 102.78 ppm.

ESI-MS m/z $[M+H]^{+1}$: for $C_{44}H_2Br_2N_4O_4$: Calcd. 836.05, found m/z 837.06 $[M+H]^{+1}$.

UV-VIS (MeOH): λ_{max} (nm); 418, 512, 547, 585, 638.

2.3.16. Synthesis of 5,15-(*p*-dibromophenyl)-10,20-di(3,5-di-*O*-TEGphenyl)porphyrin (23)

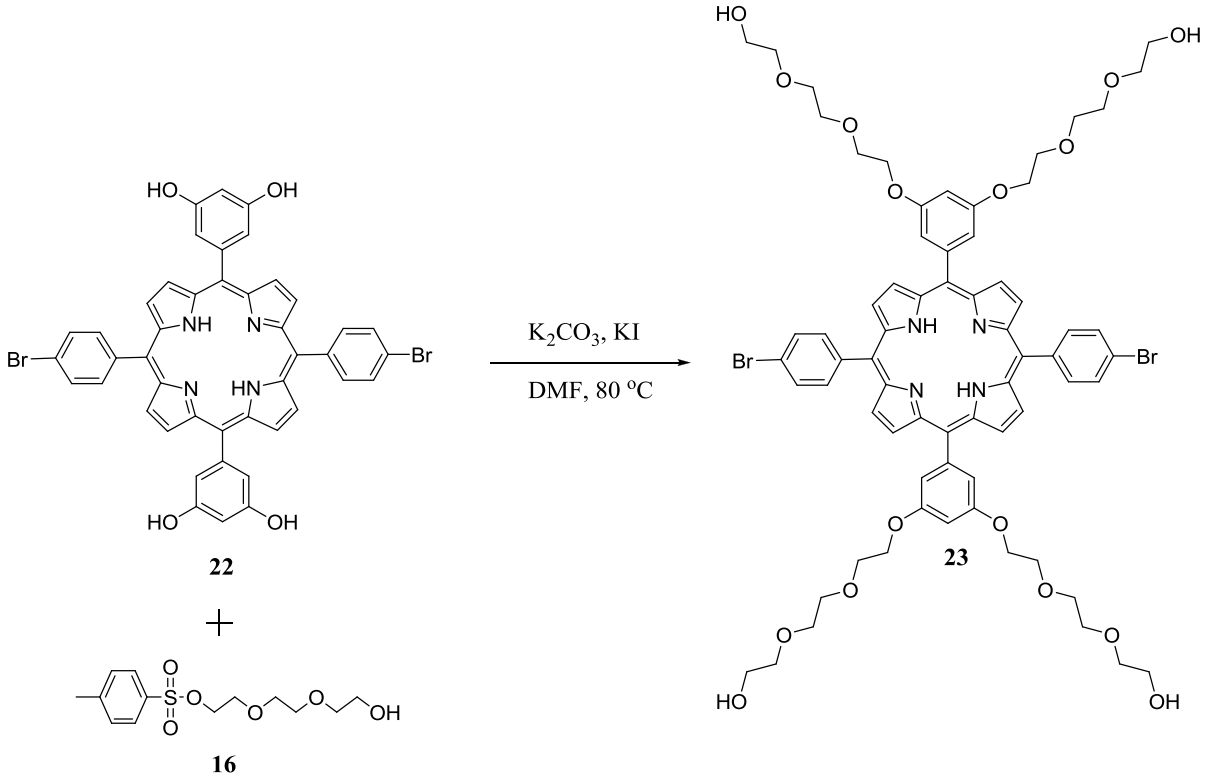

To a solution of **22** (500 mg, 0.598 mmol) in 30 ml anhydrous DMF, was added K_2CO_3 (1.24 g, 9.00 mmol), KI (0.200 g, 1.20 mmol) and tri(ethylene glycol)monotosylate **16** (1.09 g, 3.60 mmol) and refluxed at 80 °C for 12 hours. Thereafter, the reaction mixture was cooled to room temperature and the solvent was removed under reduced pressure to give gummy purple residues. The resulting mixture was washed with chloroform and filtered under suction. The product was further purified by passing through a pad of silica using chloroform as the eluent to obtain purple gum (645 mg, 79%).

^{1}H-NMR (400 MHz, $CDCl_3$, 25 °C) δ: 8.87-9.05 (m, 8H, bromophenyl-H), 7.87-8.09 (m, 4H, O-phenyl-H), 7.46 (s, 2H, p-phenyl-H), 6.89 (s, 2H, p-phenyl-H), 2.88-4.27 (m, 48H, TEG-C*H*$_2$). -2.90 (s, 2H, pyrrole, NH).

ESI-MS m/z $[M+H]^{+1}$: for $C_{68}H_{76}Br_2N_4O_{16}$: Calcd. 1364.36, found 1366.16 $[M+H]^{+1}$.

UV-VIS ($CHCl_3$): λ_{max} (nm); 421, 512, 547, 585, 638.

2.3.17. Synthesis of 5,15-di(*p*-bromophenyl)-10,20-di(3,5-di-*O*-TEGphenyl)porphyrin Zinc (24)

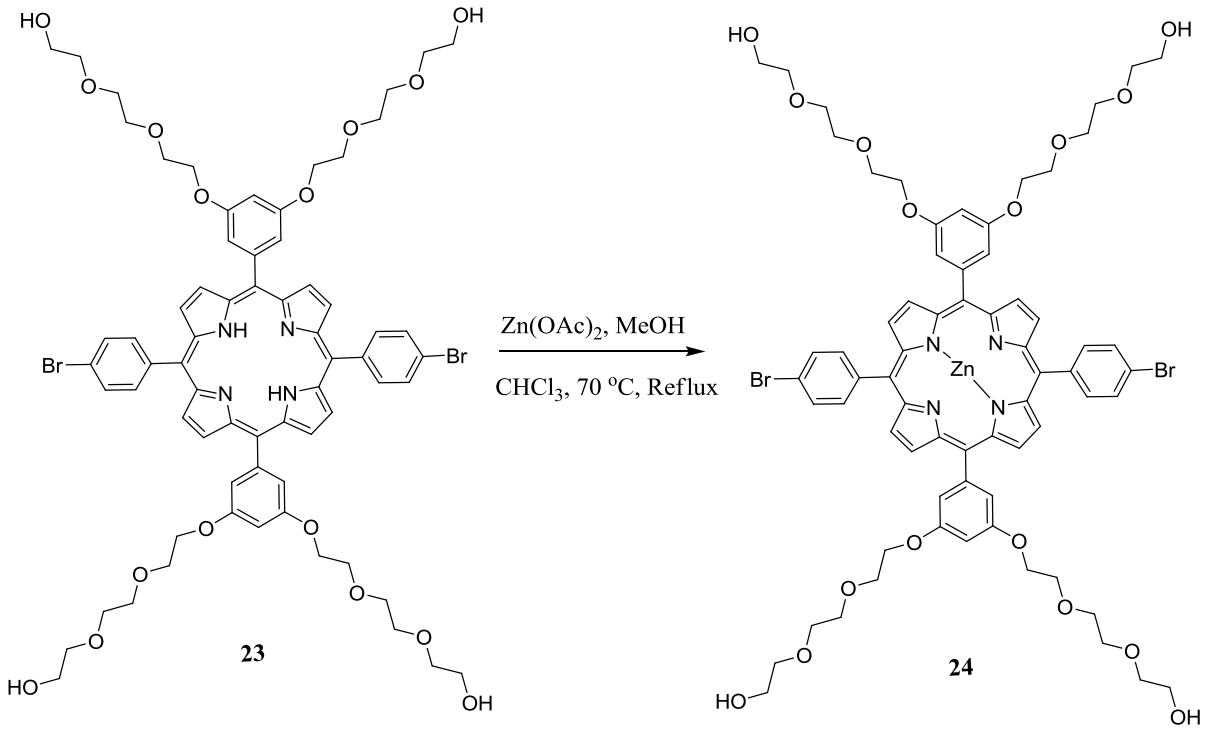

To a 50 ml two-necked round bottom flask containing 30 ml of $CHCl_3$/MeOH mixture (9:1) **23** (600 mg, 0.440mmol) was added and stirred for a while. Then, $Zn(OAc)_2$ (347 mg, 1.89 mmol) was added to the reaction mixture and refluxed at 65-70 ^oC for 2 hours. Thereafter, the reaction mixture was cooled to room temperature and filtered under suction to remove inorganic salts. The filtrate was evaporated and passed through a small pad of silica gel using DCM/MeOH (1:1) system as the eluent. The product was evaporated under reduced pressure to yield a purple-red gum. Yield: 578 mg, 92%.

^{1}H-NMR (400 MHz, $CDCl_3$, 25 ^oC) δ: 8.87-9.05 (m, 8H, bromophenyl-H), 7.87-8.09 (m, 4H, O-phenyl-H), 7.46 (s, 2H, p-phenyl-H), 6.89 (s, 2H, p-phenyl-H), 2.88-4.27 (m, 48H, TEG-C*H*$_2$) ppm. ^{13}C-NMR (100 MHz, $CDCl_3$, 25 ^oC) δ: 165.71, 152.92, 145.22, 144.89, 139.97, 7237.31, 131.05, 127.05, 126.16, 124.10, 117.29, 115.97, 110.12, 96.84, 77.34, 72.59, 70.11, 67.05, 65.35, 63.04, 61.67, 56.12 ppm. Elemental analysis: calcd for $C_{68}H_{74}Br_2N_4O_{16}Zn$: C 57.17, H 5.22, N 3.92. found: C 57.24, H 5.42, N 3.28

ESI-MS m/z $[M+H]^+$: for $C_{68}H_{74}Br_2N_4O_{16}Zn$: Calcd. 1426.2738, found 1426.2842 $[M+H]^{+1}$.
UV-VIS ($CHCl_3$): λ_{max} (nm); 426, 557, 604.

2.3.18. Synthesis of 5,15-diphenyl(2,5'-dithienylene)-10,20-di(3,5-di-*O*-TEGphenyl) polyporphyrin Zinc (25)[104]

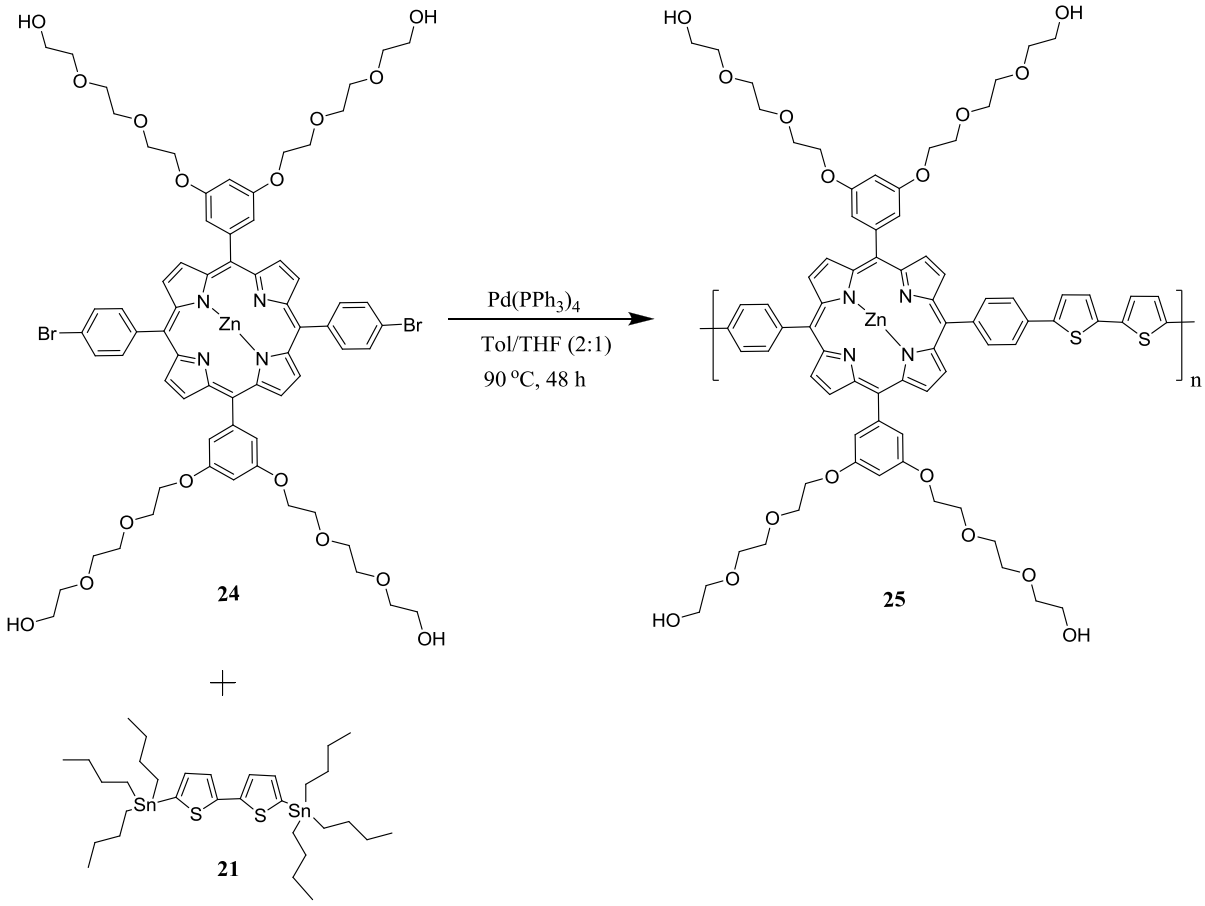

In a 50 ml two-neck round bottom flask **24** (350 mg, 0.245mmol) and **21** (180 mg, 245mmol) were dissolved in anhydrous and degassed (via; freeze-pump-thaw) Toluene:DMF mixture (2:1, 30 ml). After stirring for some time, catalytic amount of $Pd(PPh_3)_4$ was added and the resulting reaction mixture was refluxed under argon at 90 ºC for 48 hours. The reaction mixture was directly precipitated in cold MeOH, filtered and further washed with MeOH (3-4 times) followed by *n*-hexane. The polymer was obtained as purple solid in 57 % yield. ^{1}H-NMR (400 MHz, $CDCl_3$, 25 ^{o}C) δ: 9.05-8.95 (m, pyrrolic-H), 7.75-8.02 (m, Ar-H), 7.56-6.85 (m, Ph-H), 4.35-2.10 (m, TEG-CH_2) ppm. ^{13}C-NMR (100 MHz $CDCl_3$, 25 ^{o}C) δ: 158.67, 150.03, 144.03, 135.77, 135.03, 132.13, 131.66, 130.90, 129.71, 128.83, 125.60, 124.78, 124.59, 124.23, 123.64, 113.86, 69.37, 55.55, 53.55 ppm. Mn = 3109, Mw/Mn = 1.21.
UV-VIS ($CHCl_3$): λ_{max} (nm); 431, 557, 604.

2.3.19. Synthesis of 2,7-Dibromo-9,9-bis(6-bromo-hexyl)-9H-fluorene (27)

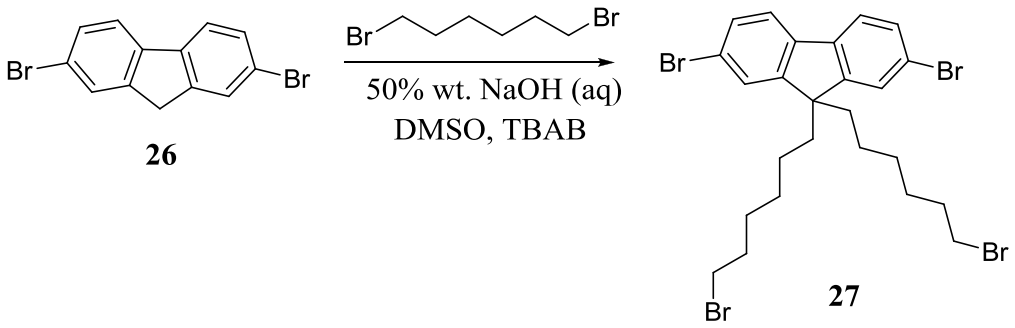

2,7-dibromo fluorene **26** (3.00 g, 9.25 mmol) and Tetra-*n*-butylammonium bromide (TBAB) (0.600 g, 1.85 mmol) were placed in a 100 ml two-neck round bottom flask. The mixture was placed under vacuum for 30 minutes. DMSO (15 ml) was added to the solution under nitrogen and subsequently 50 wt% NaOH solution (15 ml) was added to the reaction mixture. The mixture was stirred under ice bath to keep the temperature at 25 ^{o}C. 1,6-dibromohexane (25.6 g, 129 mmol) was added to the reaction flask and stirred for 2 hours at room temperature. The color changed to purple and then yellow with time. The reaction mixture was extracted with water and diethyl ether. The organic layer was further washed with 2M HCl, brine solution and then excess water. The organic layer was dried over $CaCl_2$ and the solvent was removed under rotary evaporator to yield a viscous yellow liquid. The product was further purified by column chromatography on silica gel using cyclohexane as eluent to yield a yellow viscous liquid. The product was crystallize with cold methanol to yield a white solid powder (1.00 g, 47%); ^{1}H-NMR (400 MHz, $CDCl_3$, 25 ^{o}C) δ: 0.62 (m, 2H), 1.08 (m, 4H), 1.26 (m, 2H), 1.95 (m, 2H), 1.09 (m, 8H), 7.47-7.59 (m, 3H) ppm; ^{13}C-NMR (100 MHz,$CDCl_3$, 25 ^{o}C) δ: 152.17, 139.05, 130.31, 126.10, 121.55, 55.53, 40.00, 33.81, 32.58, 28.92, 27.72, 23.44 ppm.

Elemental analysis: calcd for $C_{25}H_{30}Br_4$: C 46.19, H 4.65; found: C 46.90, H 8.20.

2.3.20. Synthesis of {6-[2,7-Dibromo-9-(6-trimethylamino-hexyl)-9H-fluoren-9-yl]-hexyl}-trimethyl-amine (28)

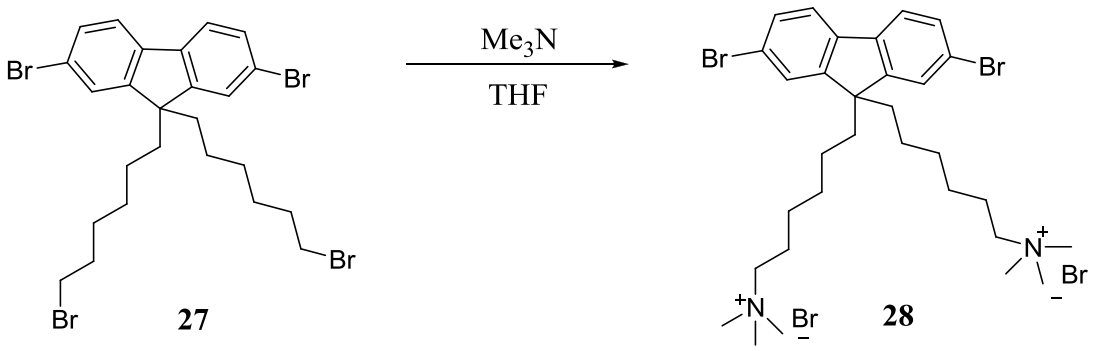

2,7-Dibromo-9,9-bis(6-bromo-hexyl)-9H-fluorene **27** (1.00 g, 1.54 mmol) was dissolved in dry THF (5 ml) and flushed with nitrogen. 25 wt% solution of trimethylamine in THF (10 ml, 20 mmol) was added under nitrogen. The mixture was stirred at room temperature for 24 hours. The reaction mixture was extracted with water and chloroform. The aqueous layer was precipitated with analytical cold acetone and the solvent was removed under suction. White solid powder was obtained (0.99 g, 84%). ^{1}H-NMR (400 MHz, D_2O, 25 ^{o}C) δ: 0.43 (m, 4H), 0.99 (m, 4H), 1.00 (m, 4H), 1.47 (m, 4H), 1.98 (m, 4H), 2.90 (s, 18H), 3.19 (m, 4H), 7.47-7.59 (m, 6H) ppm; ^{13}C-NMR (100 MHz, D_2O, 25 ^{o}C) δ: 152.86, 139.21, 130.30, 126.10, 121.42, 121.22, 67.84, 55.72, 52.68, 48.89, 38.69, 27.58, 24.39, 22.38, 21.40 ppm.

Elemental analysis: calcd for $C_{31}H_{48}Br_4N_2$: C 48.46, H 6.30, N 3.65; found: C 47.75, H 10.66, N 3.73.

ESI-MS m/z $[M-2Br]^{+}$: for $C_{31}H_{48}Br_4N_2$: Calcd. 608.22, found 609.23 $[M-2Br]^{+2}$.

2.3.21. Poly[9,9-bis{6(N,N,N-trimethylamino)hexyl}fluorene-co-2,5-thienylene (29)[101-103]

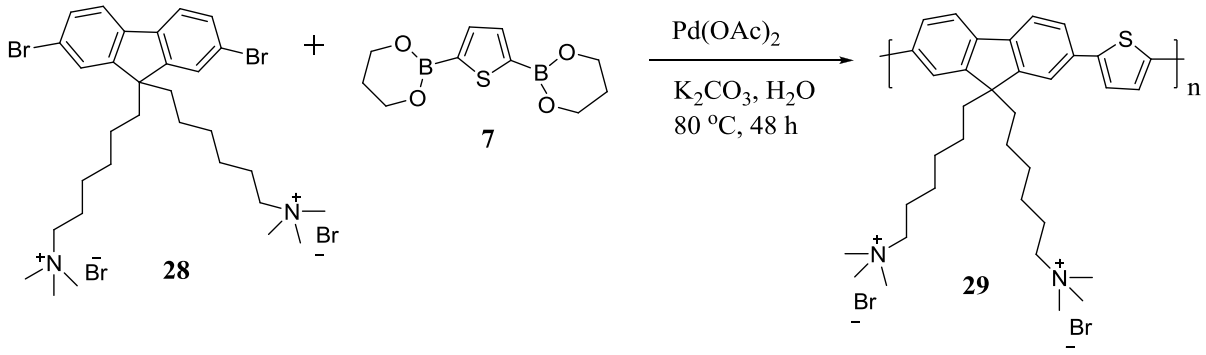

28 (300 mg, 0.691 mmol), 2,5-thiophenediboronic ester **7** (119 mg, 0.692 mmol), $Pd(OAc)_2$ (10 mg, 0.01 mmol), and potassium carbonate (500 mg, 3.61 mmol) were placed in a 25-ml round-bottom flask. Water (10 ml) was added to the flask and the reaction vessel was degassed. The mixture was stirred at 80 ^oC for 48 hours under nitrogen. Water was added to the reaction mixture and filtered under suction. The filtrate was concentrated to 120 ml and placed under ultrafiltration with 5000 Da cut-off filter at 5 bar and 1 ml/min flow rate. The filtration was stopped after 2 L of water was collected. The residue was precipitated with analytical cold acetone and the solvent was removed under suction. Shiny dark greenish solid flake was obtained (247 mg). ^1H-NMR (400 MHz, D_2O, 25 ^oC) δ: 0.4-1.5 (br, 20 H), 2.5-3.2 (br, 22H), 7.0-8.5 (br, 8H) ppm.

UV-VIS (H_2O): λ_{max} (nm); 427

PL (H_2O): λ_{max} (nm); 501

2.3.22. Poly[9,9-bis{6(N,N,N-trimethylamino)hexyl}fluorene-co-2,5-thienylene with Cucurbit[7]uril (30)[101-103]

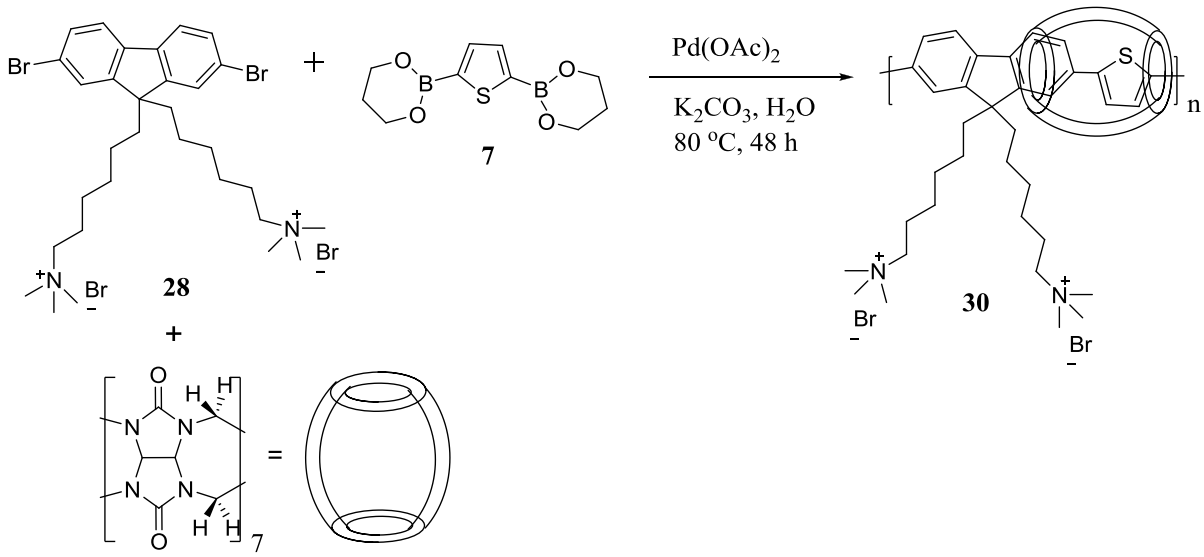

Cucurbit[7]uril (287 mg, 0.247mmol) and 2,5-thiophenediboronic ester **7** (62mg, 0.247 mmol) were placed in a 25-ml two-neck round bottom flask. Water (10 ml) was added to the flask and the reaction vessel was degassed. The mixture was stirred for 2 hours at 50 ^oC. **28** (150 mg, 0.195 mmol), $Pd(OAc)_2$ (10 mg, 0.01mmol), and potassium carbonate (500 mg, 3.61 mmol) were added to the reaction mixture. The mixture was stirred at 80 ^oC for 48 hours under nitrogen. Water was added to the reaction mixture and filtered under suction. The filtrate was concentrated to 120 ml and placed under ultrafiltration with 5000 Da cut-off filter

at 5 bar and 1 ml/min flow rate. The filtration was stopped after 2 L of water was collected. The residue was precipitated with analytical cold acetone and the solvent was removed under suction. Brownish yellow solid powder was obtained (187 mg). ^{1}H-NMR (400 MHz, D_2O, 25 ^{o}C) δ: 0.4-1.5 (br, 20 H), 2.5-3.2 (br, 22H), 4.07 (br, 14H), 5.34 (br, 14H), 4.07 (br, 14H), 6.24 (br, 1H), 6.54 (br, 1H), 7.0-8.5 (br, 8H) ppm.

FT-IR (KBr, ν_{max}/cm^{-1}): 1735 (C = O)

UV-VIS (H_2O): λ_{max} (nm); 407

PL (H_2O): λ_{max} (nm); 574

2.3.23. Synthesis of 2,7-Dibromo-9,9-bis(3-bromo-propyl)-9H-fluorene (31)

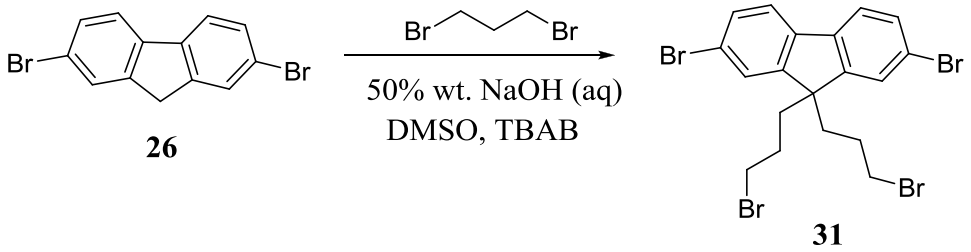

26 **31**

2,7-dibromo fluorene **26** (3.00 g, 9.25 mmol) and Tetra-*n*-butylammonium bromide (TBAB) (0.600 g, 1.85 mmol) were placed in a 100 ml two necked round bottom flask. The mixture was placed under vacuum for 30 minutes. DMSO (15 ml) was added to the solution under nitrogen and subsequently 50 wt% NaOH solution (15 ml) was added to the reaction mixture. The mixture was stirred under ice bath to keep the temperature at 25 ^{o}C. 1,3-dibromopropane (25.6 g, 129 mmol) was added to the reaction flask and stirred for 2 hours at room temperature. The color changed to purple and then yellow with time. The reaction mixture was extracted with water and diethyl ether. The organic layer was further washed with 2 M HCl, brine solution and then excess water. The organic layer was dried over $CaCl_2$ and the solvent was removed under reduced pressure to yield a viscous yellow liquid. The product was further purified by column chromatography on silica gel using cyclohexane as eluent to yield a yellow viscous liquid. The product was crystallized with cold methanol to yield a white solid powder (1.00 g). ^{1}H-NMR (400 MHz, $CDCl_3$, 25 ^{o}C) δ: 1.154 (m, 4H), 2.16 (m, 4H), 3.17 (m, 4H), 7.47-7.59 (m, 6H) ppm; ^{13}C-NMR (100 MHz, $CDCl_3$, 25 ^{o}C) δ: 150.71, 138.98, 130.99, 126.20, 121.99, 121.47, 38.51, 33.59, 26.98 ppm.

ESI-MS m/z [M-Br]$^{-1}$: for $C_{19}H_{18}Br_4$: Calcd. 561.81, found 565.82 [M-Br]$^{-1}$.

2.3.24. Synthesis of {3-[2,7-Dibromo-9-(3-trimethylamino-propyl)-9H-fluoren-9-yl]-propyl}-trimethyl-amine (32)

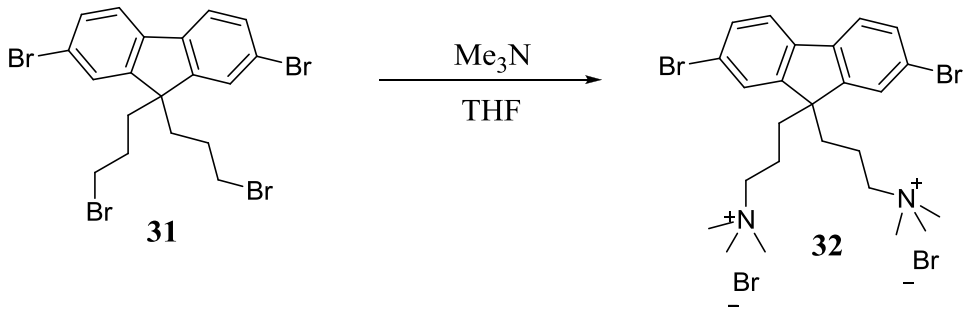

2,7-Dibromo-9,9-bis(3-bromo-propyl)-9H-fluorene **31** (1.00 g, 1.77 mmol) was dissolved in dry THF (5 ml) and flushed with nitrogen. 25 wt% solution of trimethylamine in THF (10 ml, 20 mmol) was added under nitrogen. The mixture was stirred at room temperature for 24 hours. The reaction mixture was extracted with water and chloroform. The aqueous layer was precipitated with analytical cold acetone and the solvent was removed under suction. White solid powder was obtained (1.05 g, 87%). ^{1}H-NMR (400 MHz, D_2O, 25 ^{o}C) δ: 0.90 (m, 4H), 2.06 (m, 4H), 2.71 (s, 18), 2.96 (m, 4H), 7.47-7.59 (m, 6H) ppm; ^{13}C-NMR (100 MHz, D_2O, 25 ^{o}C) δ: 160.84, 150.04, 139.27, 131.43, 126.68, 122.06, 66.13, 52.59, 35.05, 17.37 ppm.

ESI-MS m/z $[M\text{-}Br]^{+1}$: for $C_{25}H_{36}Br_4N_2$: Calcd. 603.04, found 603.04 $[M\text{-}Br]^{+1}$.

2.3.25. Poly[9,9-bis{3(N,N,N-trimethylamino)propyl}fluorene-co-2,5-thienylene (33)[101-103]

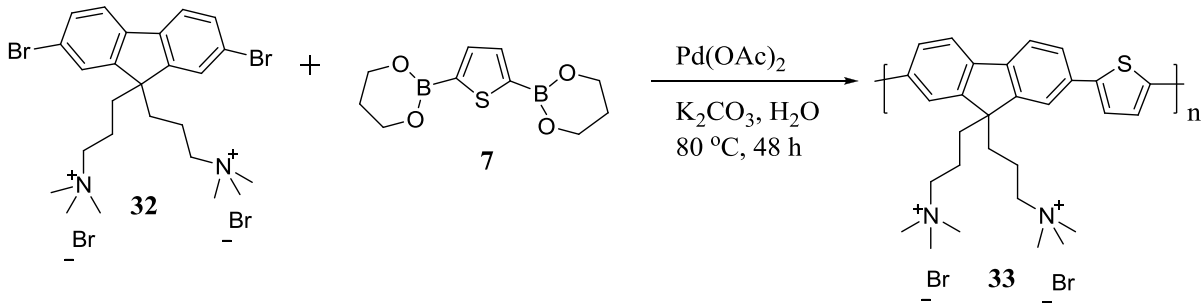

32 (300 mg, 0.691 mmol), 2,5-thiophenediboronic ester **7** (119 mg, 0.692 mmol), $Pd(OAc)_2$ (10 mg, 0.01 mmol), and potassium carbonate (500 mg, 3.61 mmol) were placed in a 25 ml two-neck round bottom flask. Water (10 ml) was added to the flask and the reaction vessel was degassed. The mixture was stirred at 80 ^{o}C for 48 hours under nitrogen. Water was added to the reaction mixture and filtered under suction. The filtrate was concentrated to 120 ml and placed under ultrafiltration with 5000 Da cut-off filter at 5 bar and 1 ml/min flow rate. The

filtration was stopped after 5 L of water was collected. The residue was precipitated with analytical cold acetone and the solvent was removed under suction. Dark greenish solid powder was obtained (205 mg). ^{1}H-NMR (400 MHz, D_2O, 25 ^oC) δ: 0.96 (m, 4H), 2.21 (m, 4H), 2.68 (s, 18), 2.91 (m, 4H), 7.12-7.89 (m, 8H) ppm.

UV-VIS (H_2O): λ_{max} (nm); 413

PL (H_2O): λ_{max} (nm); 465

2.3.26. Poly[9,9-bis{3(N,N,N-trimethylamino)propyl}fluorene-co-2,5-thienylene with Cucurbitu[6]uril (34)[101-103]

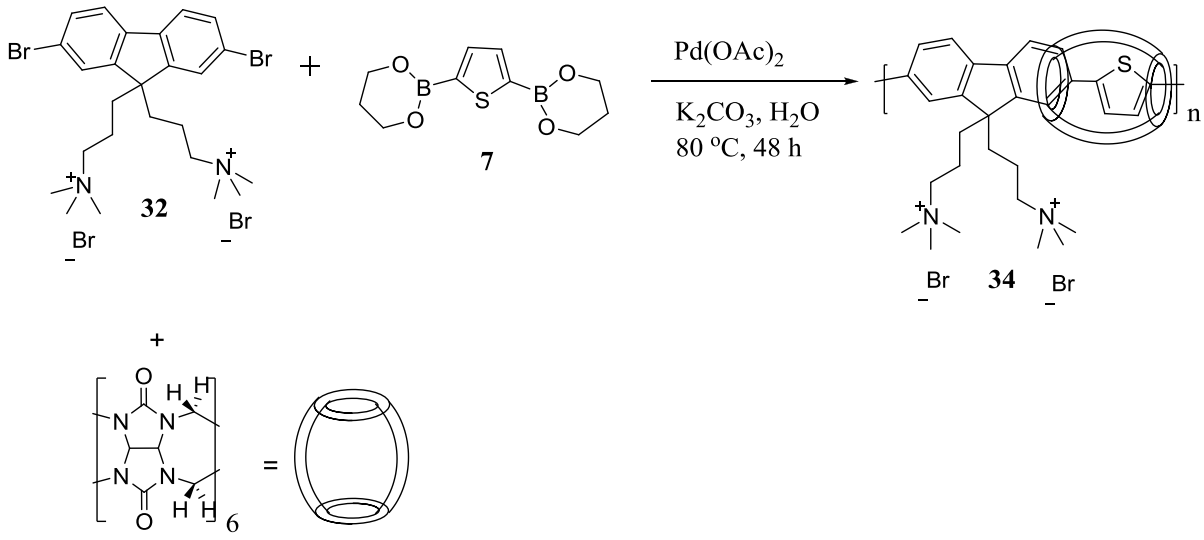

Cucurbit[6]uril (1.38 g, 1.38 mmol) and 2,5-thiophenediboronic ester **7** (119 mg, 0.692 mmol) were placed in a 25 ml two-neck round bottom flask. Water (10 ml) was added to the flask and the reaction vessel was degassed. The mixture was stirred for 2 hours at 50 ^oC. **32** (150 mg, 0.691 mmol), $Pd(OAc)_2$(10 mg, 0.01mmol), and potassium carbonate(500 mg, 3.61 mmol) were added to the reaction mixture. The mixture was stirred at 80 ^oC for 48 hours under nitrogen. Water was added to the reaction mixture and filtered under suction. The filtrate was concentrated to 120 ml and placed under ultrafiltration with 5000 Da cut-off filter at 5 bar and 1 ml/min flow rate. The filtration was stopped after 5 L of water was collected. The residue was precipitated with analytical cold acetone and the solvent was removed under suction. Brownish yellow solid powder was obtained (50 mg).

^{1}H-NMR (400 MHz, D_2O, 25 ^oC) δ: 1.03 (m, 4H), 2.23 (m, 4H), 2.69 (s, 18), 2.96 (m, 4H), 4.17 (br, 12H), 5.44 (br, 12H), 5.85 (br, 12H), 7.17-7.91 (m, 8H) ppm.

FT-IR (KBr, ν_{max}/cm^{-1}): 1735 (C = O)

UV-VIS (H_2O): λ_{max} (nm); 400

PL (H_2O): λ_{max} (nm); 463

2.4. Singlet Oxygen Generation

The absorbance of an aerated solution of the photosensitizer of known concentration (10^{-6}M) in DMF (25 ml) was first recorded. Thereafter, 1,3-diphenylisobenzofuran (DPBF) (5×10^{-5}M) was added to the solution and the absorbance without irradiation with light is recorded for at least five times. The solution was then irradiated with white light (home-made source) at 25 ^{o}C for 1 minute intervals. Reaction of DPBF with singlet oxygen ($^1O_2$) was monitored by the decrease in the intensity of the absorption band of DPBF at 414 nm over time. Irradiation of aerated DPBF solution without photosensitizer gave no reduction in intensity of the 414 nm absorption band.

2.5. Quantum Yield and Molar Absorptivity Measurement

The photoluminescence quantum yields (Φ_A) of the fluorene based polymers and polyrotaxanes were determined relative to fluorescence quantum yield (Φ_B) of quinine sulfate 0.1 M H_2SO_4 (Φ_f= 55%) and quantum yields (Φ_A) of porphyrin based monomers, oligomers and polymer were determined relative to tetraphenyl porphyrin ($\Phi_f = 0.11$). In a typical experiment, the absorbance and fluorescence intensity of the sample and the standard were measured at five different concentrations at low optical density (A < 0.2). The slope of the graph (fluorescence area versus absorption maxima) gives the quantum yield according to the formula $\Phi_A = [(m_A n_A^2 \Phi_B)/(m_B n_B^2)]$ where m_A and m_B are the slopes obtained from the plot for the sample and the standard respectively. $n_A$and n_B are refractive indexes of the solvents used to dissolve the sample and the standard respectively.

Molar absorptivity was obtained from the slope of the graph (absorption maxima versus concentration).

2.6. PLED Fabrication

ITO coated (15 Ohm/Sq) glass substrates were partially etched and cleaned by solvent cleaning (water, acetone, and isopropyl alcohol). Then, UV-Ozone treatment was performed. PEDOT:PSS (Clevios PVP AI 4083) was spin coated at 4000 rpm for 1 minute and annealed at 150 °C for 30 minutes. Poly-TPD (American Dye Source, ADS 254BE) was dissolved in chlorobenzene (10 mg/ml) and spin coated on the film at 2000 rpm for 1 minute and annealed

at 120 °C for 30 minutes. Polymers and polyrotaxanes (**29**, **30**, **33** and **34**) dissolved in methanol were spin coated on the poly-TPD layer at 1500 rpm for 1 minute. Subsequently, our own synthesized ZnO nanoparticles (2-4 nm in size) were spin coated at 2000 rpm for 1 minute and annealed at 80 °C. Finally, the samples were loaded into a thermal evaporator with a hard-mask defining the device area as 2 by 2 mm. 100 nm thick Aluminum was deposited at the base pressure of $2x10^{-6}$ Torr. The devices were tested using Agilent B1500A parameter analyzer and electroluminescence spectra were collected via fiber connected spectrometer (Ocean Optics, Maya2000).

Chapter 3 RESULTS AND DISCUSSIONS

3.1. Introduction

This section contains two main parts. The first part involves the results and discussion of the works on porphyrin-based monomers, oligomers and polymers. This section also includes the studies on the singlet oxygen generation ability of porphyrin-based oligomers and polymers. The second part discusses the synthesis and characterization of fluorene-based monomers, polymers and polyrotaxanes including the application of polymers and polyrotaxanes in the fabrication of polymer light emitting diode.

3.2. SECTION 1: Porphyrin-Based Monomers, Oligomers and Polymers

Aim of the Study

Porphyrin-based photosensitizers (monomers, oligomers and polymer) for photodynamic therapy application will be synthesized according to the Scheme 3.1. The porphyrin-based photosensitizers are designed to meet the conditions for ideal photosensitizer in photodynamic therapy application explained in the literature review. Triethylene glycol will be attached to the parent porphyrin monomers to increase water solubility. The porphyrin monomers will be coupled with thiophene monomers to yield oligomers and polymer. The sulfur atom on thiophene molecule eases the intersystem crossing through heavy atom effect and hence will increase the singlet oxygen generation. Moreover, the increased molecular weight of the oligomers and polymer will enhance the effective permeation retention.

The structure of the monomers, oligomers and polymers will be characterized by ^{1}H-NMR, ^{13}C-NMR, FT-IR, ESI mass spectroscopy, Elemental Analysis and Gel Permeation Chromatography. The photophysical properties of the porphyrin based monomers, oligomers, polymer will be studied with UV-VIS Spectroscopy.

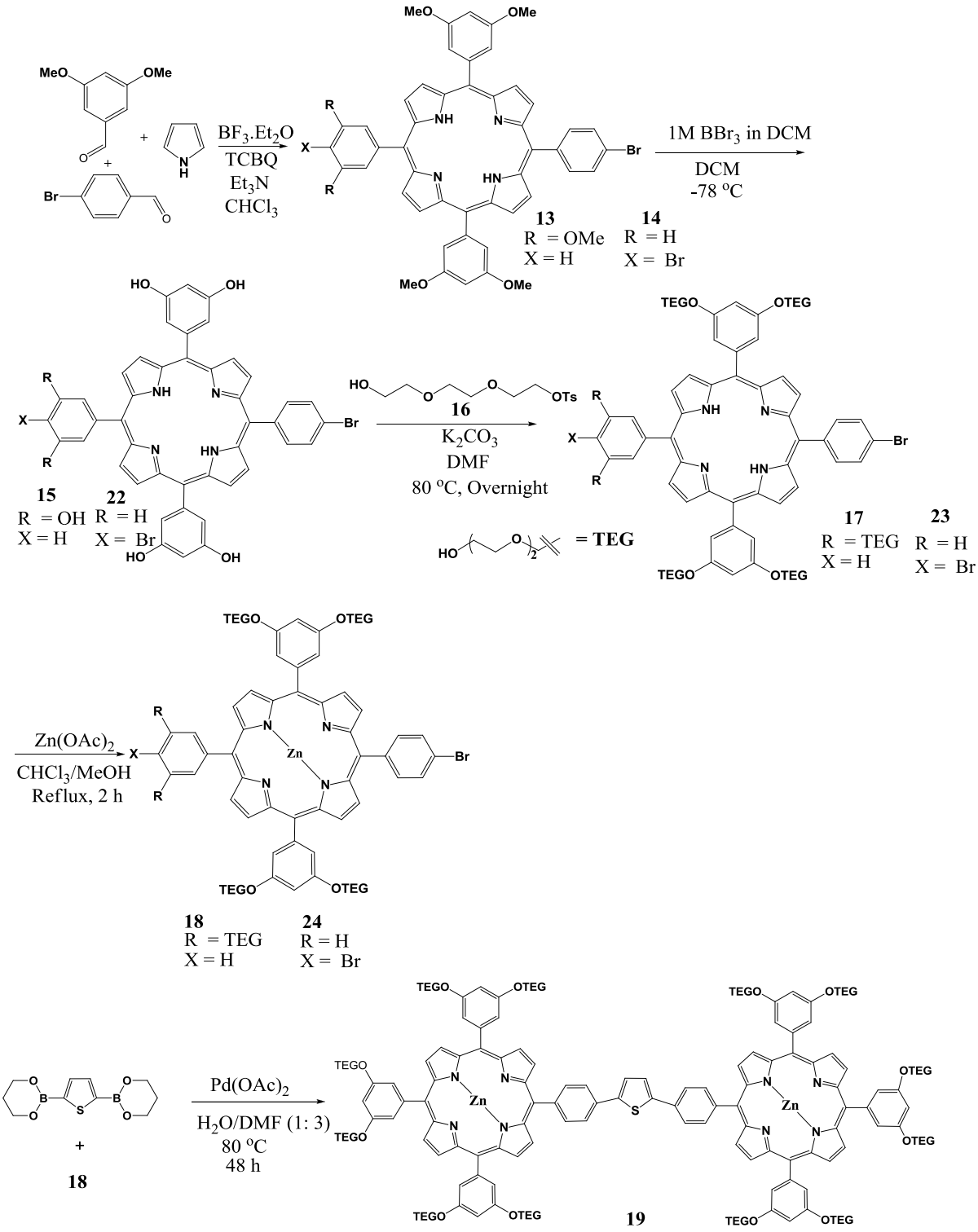

Scheme 3.1: Synthetic pathway of porphyrin monomers, oligomers and polymer.

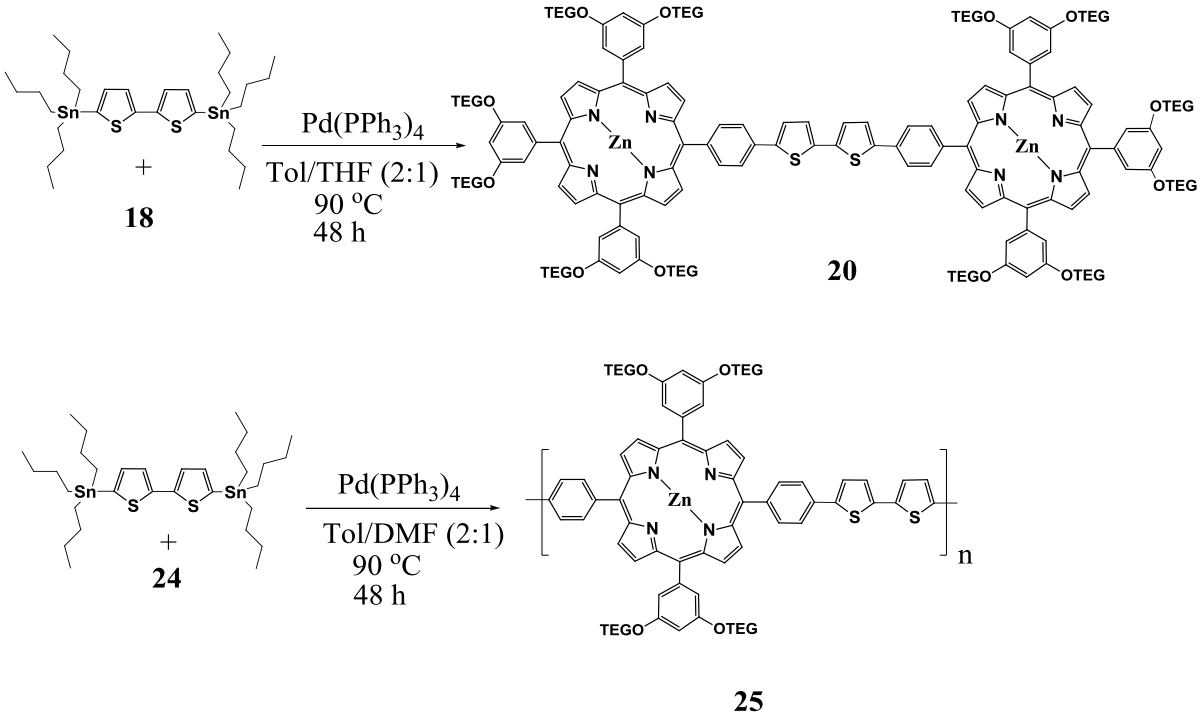

Scheme 3.1: Synthetic pathway of porphyrin monomers, oligomers and polymer.

3.3. Synthesis and Characterization of Cucurbituril[n][121,123,131-133]

CB[n]s were synthesized and purified according to literature as described in section 1.2.1.3.4.1 and section 2.3.1. Ordinary formaldehyde is very reactive and thus can decompose easily even during storage. To make sure fresh formaldehyde is used, paraformaldehyde is used in the synthesis of CB[n]s because it depolymerizes to form fresh formaldehyde upon heating.

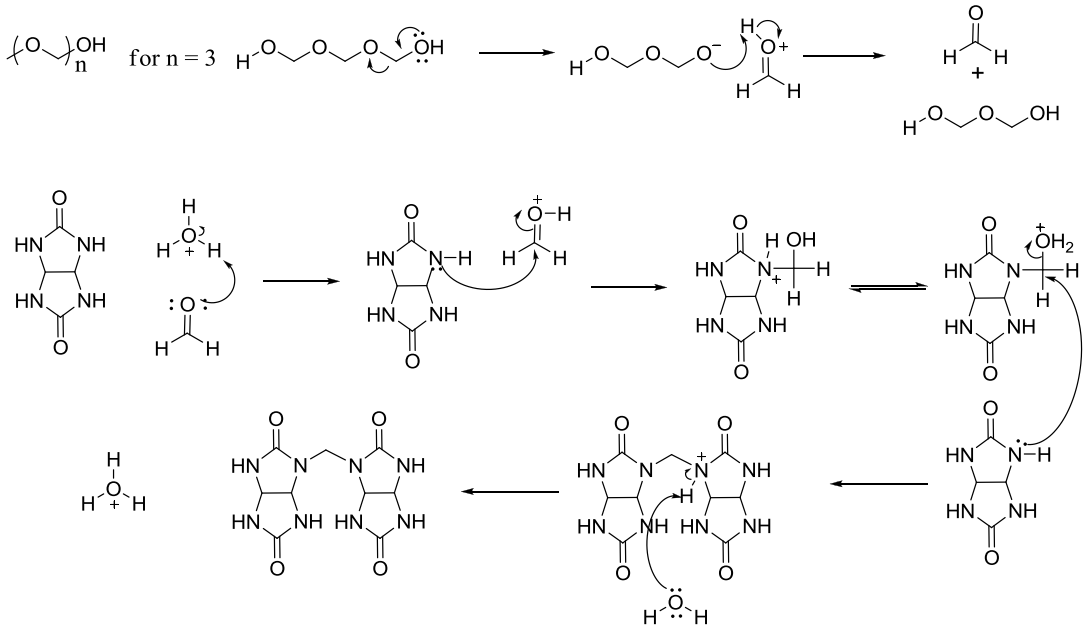

Scheme 3.2: Mechanism of CB[n] formation

IR spectra of CB[6] and CB[7] give similar peak pattern. In the spectra (Figure 3.1), the most significant peak is the carbonyl peak resonating at 1733 cm^{-1}. Peaks at 2854 and 2924 cm^{-1} show antisymmetric and symmetric stretching of C-H bonds respectively. The broad peak at 3450 cm^{-1} can be assigned to both N-H stretching and O-H stretching coming from moisture. Despite all the effort to completely dry the CB[n]s, moisture was still observed due to hydroscopic nature of CB[n]s. The amount of water molecules present in CB[6] and CB[7] was determined from elemental analysis results. In both CB[6] and CB[7] nearly six molecules of water and traces amount of methanol was calculated.

^{1}H-NMR of both CB[6] and CB[7] show the typical CB[n] NMR pattern as explained in Section 1.2.1.3.4.1. The integration values of the peaks in ^{1}H-NMR suggests equal number of protons as expected (Figure 3.2 and Figure 3.3). Due to the water insolubility of CB[6] , very small amount of sodium sulfate was added to the NMR tube to solubilize CB[6] by complexing the Na^{+} ion with the carbonyl oxygen of the CB[6].

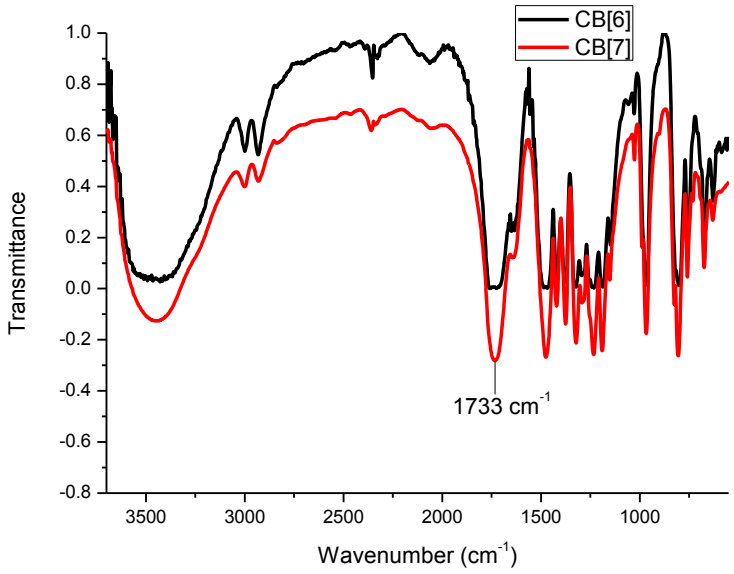

Figure 3.1: FT-IR spectra of CB[6] and CB[7]

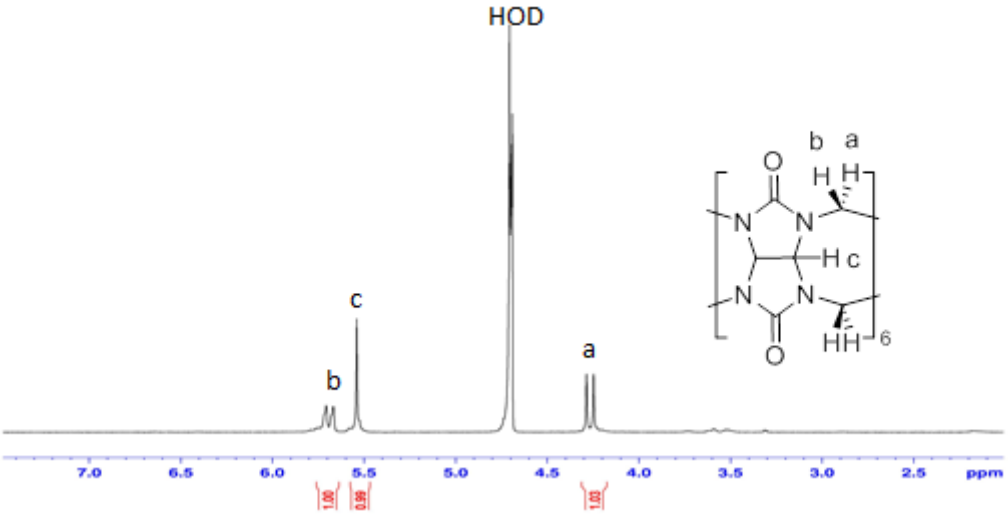

Figure 3.2: ^{1}H-NMR (400 MHz, D_2O, Na_2SO_4, 25 ^{o}C) spectrum of CB[6]

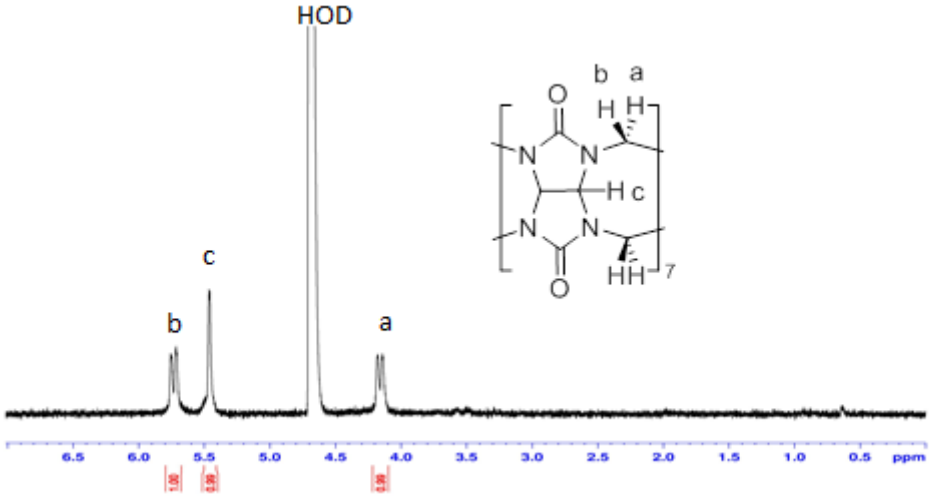

Figure 3.3: ^{1}H-NMR (400 MHz, D_2O, 25 ^{o}C) spectrum of CB[7]

3.4. Synthesis and Characterization of 2,5-thiophenediboronic ester (7)

In Suzuki coupling, either boronic acid or boronic ester can be used for coupling with aryl halides. 2,5-thiophenediboronic acid **5** was available in hand, but synthesis of 2,5-thiophenediboronic ester was necessary because the OH groups in 2,5-thiophenediboronic acid can form hydrogen bond with carbonyl oxygen atoms of CB[n]s, which will prevent the CB[n] from encapsulating the thiophene molecule. So 1,3-propane diol was used to protect the OH groups of the 2,5-thiophenediboronic acid.

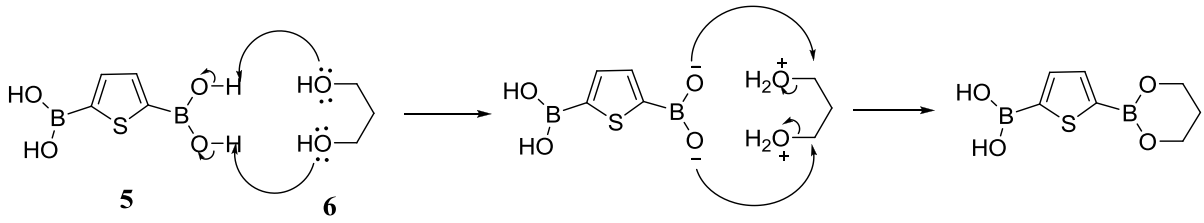

Scheme 3.3: Mechanism of boronic ester formation

Excess amount of **6** was used to make sure all the acid groups in **5** were protected. The excess diol was easily removed by washing the product with ethanol and *n*-hexane. The product was first characterized by ^{1}H-NMR. The triplet peak at 3.62 ppm confirms the presence of –OCH_2 protons connected to –CH_2 which resonates at 1.78 ppm as multiplet. A singlet peak is observed at the aromatic region confirming the thiophene proton. Absence of –OH protons confirms that all boronic acid is converted to the product and all the excess 1,3-propanediol is removed.

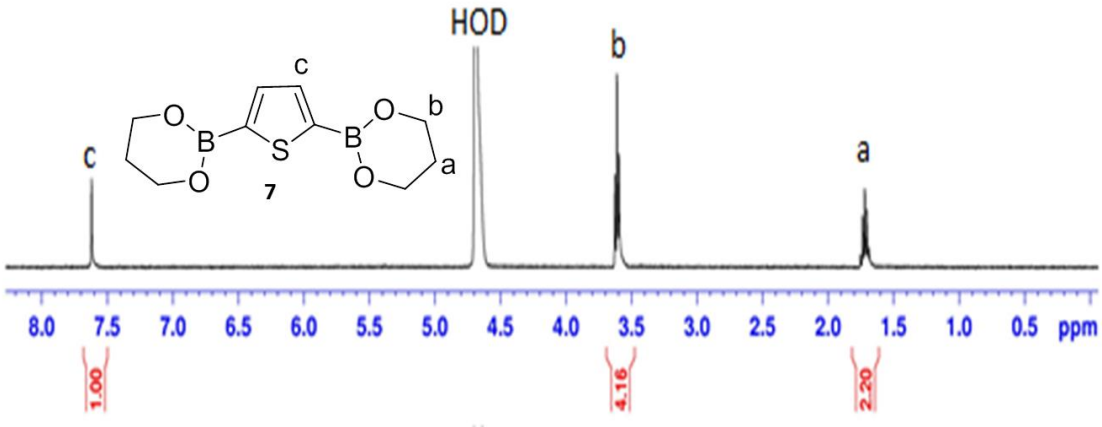

Figure 3.4: ^{1}H-NMR (400 MHz, D_2O, ^{o}C) spectrum of 2,5-thiophenediboronic ester

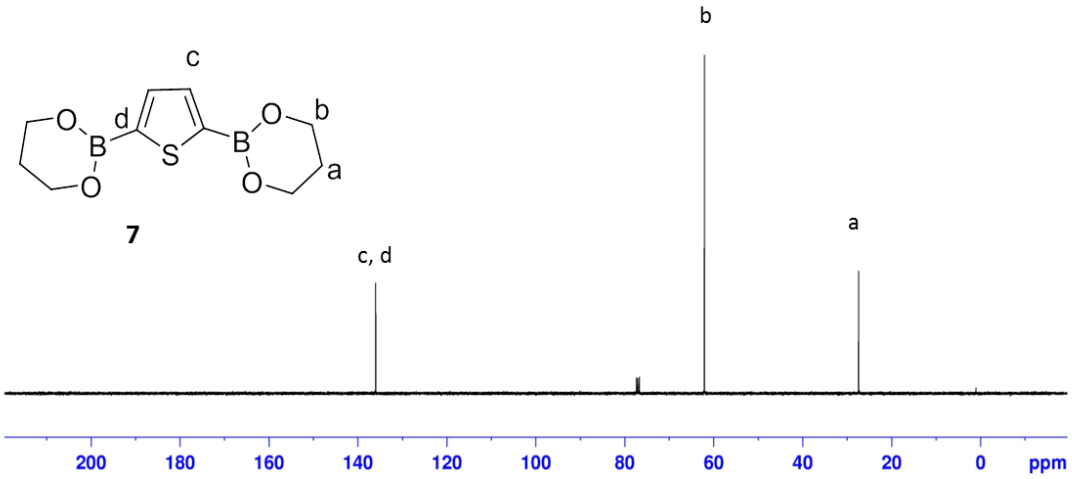

Figure 3.5: ^{13}C-NMR (100 MHz, $CDCl_3$, ^{o}C) spectrum of 2,5-thiophenediboronic ester

3.5. Synthesis and Characterization of Porphyrin and its Precursors

3.5.1. Synthesis and Characterization of Monotosyl triethylene glycol (16)[105]

This compound is synthesized to improve water solubility of the porphyrins when attached to phenolic groups. In the synthesis, tosyl chloride is used to functionalize one of the terminal hydroxyl groups of triethylene glycol (TEG). Functionalization of one hydroxyl group is crucial because porphyrin dimer formation will result if both hydroxyl groups are functionalized with tosyl groups. To assure mono-functionalization of triethylene glycol, limited amount of tosyl chloride was used (half of TEG amount). In addition, TEG was added slowly to the reaction mixture and the reaction was carried out at low temperature to slow down the reaction rate. This made it possible to selectively functionalize one hydroxyl group. Despite all these precautions, di-substituted TEG was formed in small amount. The formation of di-substituted TEG and unreacted TEG resulted in low yield of mono-substituted TEG. The product was obtained as very viscous liquid that dissolves in most of common organic solvents and water.

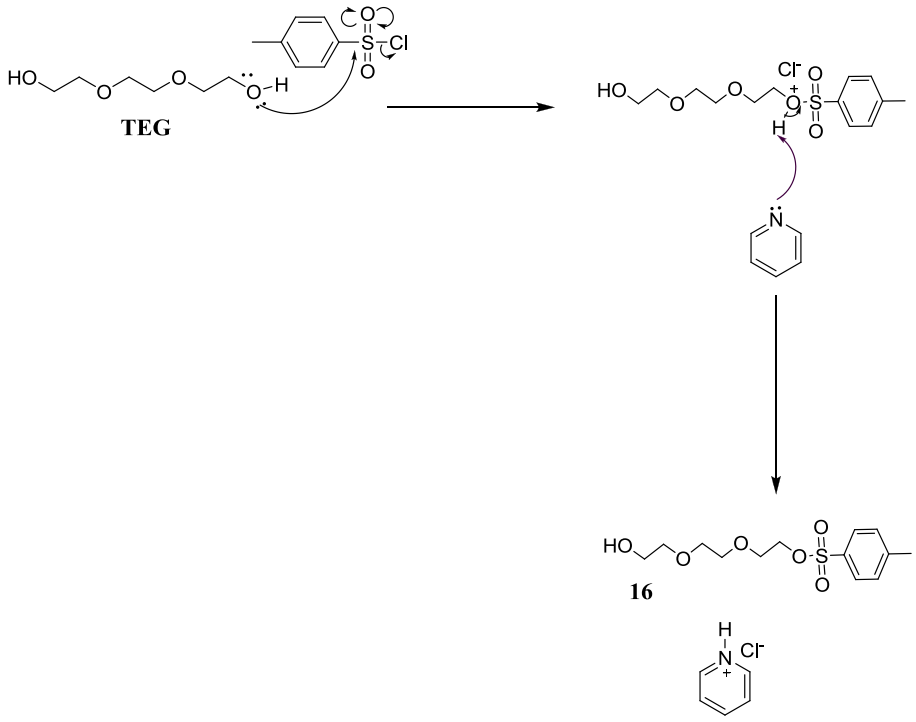

Scheme 3.4: Mechanism of mono-substituted TEG formation

^{1}H-NMR was used to characterize the product. Both mono-substituted and di-substituted TEG have similar ^{1}H-NMR peak pattern, however the integration of their peaks differs. The presence of two doublet aromatic peaks at 7.8 and 7.5 ppm, singlet $–CH_3$ peak at 2.4 ppm and downfield shift of $–OCH_2$ to 4.1 ppm confirms the presence of tosyl group attached to TEG. Integration of aromatic protons (c or b) is similar to $–OCH_2$ (d) suggesting the same number of protons. However, for di-substituted TEG, integration of aromatic protons (c or b) is twice the integration of $–OCH_2$ peaks (d). These observations confirm the structure of mono-substituted TEG and di-substituted TEG.

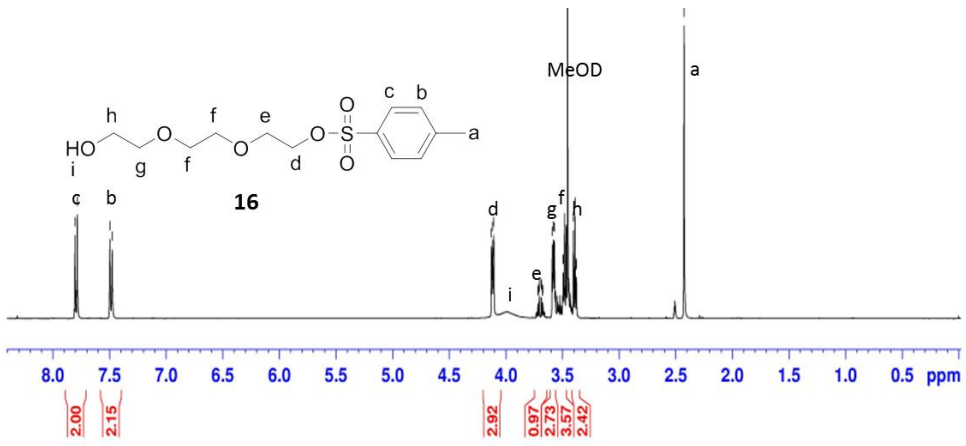

Figure 3.6: ^{1}H-NMR (400 MHz, MeOD, 25 ^{o}C) spectrum of Mono-Substituted TEG

3.5.2. Synthesis and Characterization of Dipyrromethane 10 and 12[100]

Synthesis of porphyrin using one pot synthesis method results in undesired side products and thus the desired product is obtained in low yield [138-140]. One alternative to this method was to first synthesize dipyrromethane as a porphyrin precursor which improves the yield of the desired product [141]. Synthesis of dipyrromethane involves [2 + 2] condensation reaction between a pyrrole and an aldehyde in the presence of catalytic amount of acid. To obtain high yield in this reaction, there are important precautions that have to be taken. First, the choice of acid is very important. Boron trifluoride diethyl etherate ($BF_3 \cdot Et_2O$) and trifluoro acetic acid (TFA) are the two main acid catalysts used in the synthesis of dipyrromethane. Although $BF_3 \cdot Et_2O$ was reported to give higher yield [159], the amount of side products (N-confused dipyrromethane) is much lower with TFA. Secondly, the sequence of addition of the reactants determines the amount ratio between the dipyrromethane and the higher pyrrolic oligomers [160]. Dipyrromethane is obtained as major product if the acid is added after stirring pyrrole and aldehyde for some time. Third, pyrrole was used in excess to suppress the polymerization of the product. Lindsey reported that 25 equiv. of pyrrole and 0.1 equiv. of the acid relative to the aldehyde give the optimum yield [159].

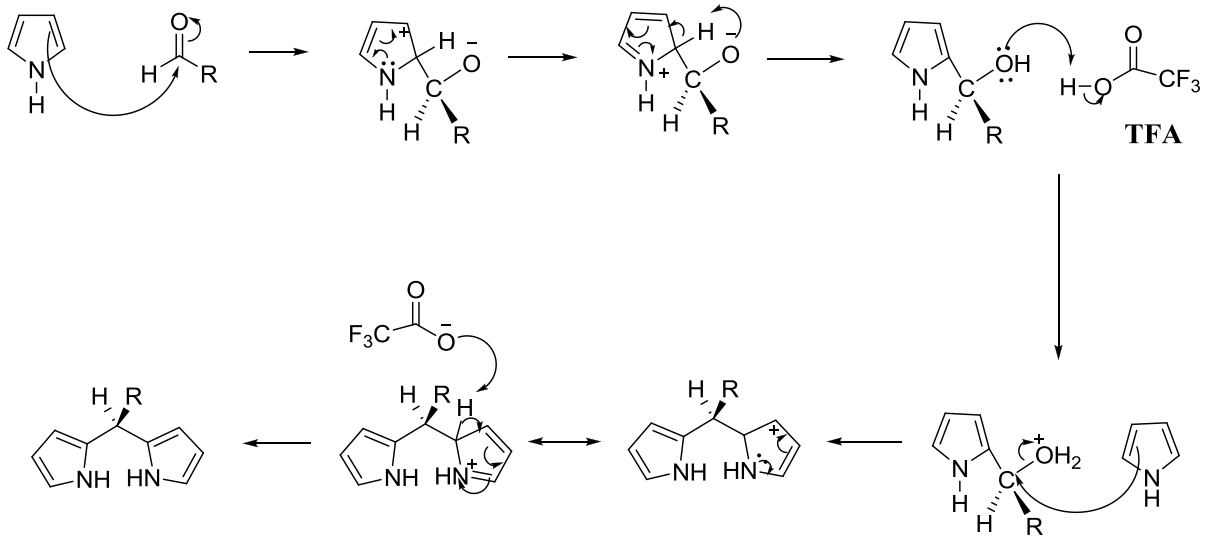

Scheme 3.5: Mechanism of dipyrromethane formation

Considering all these precautions dipyrromethane **10** and **12** were synthesized in good yield. In addition to all these precautions, freshly distilled pyrrole was used because pyrrole decomposes with time. In both syntheses, a sharp color change from colorless to dark brown was observed when the acid was added indicating the condensation of the aldehyde. After removing excess pyrrole under reduced pressure, column chromatography was used to further purify **12** using DCM:Et_3N (20:0.1). Triethyl amine was added to the column to provide basic

conditions because dipyrromethane can easily convert to other pyrrolic compounds under silica. The yellow oily product from the column was recrystallized by dissolving the product in hot ethanol followed by addition of water. Attempt to purify **10** with column chromatography failed because the R_f values of **10** and other pyrrolic compounds were very close. We were fortunate to find out that **10** crystallizes out with cold *n*-hexane. The pure product was obtained after several washing with *n*-hexane.

In both ^{1}H-NMR of **10** and **12** characteristic –NH pyrrolic peak at around 8 ppm was observed. In addition, the singlet peak at 5.4 ppm shows the methine proton and thus confirms the formation of dipyrromethane. Singlet peak at 3.7 ppm in compound **12** ^{1}H-NMR confirms the presence of methoxy (–OCH_3) groups and this can be used to distinguish **12** from **10**. The peaks at the aromatic region represent the protons from pyrrole and benzene rings as labelled in the ^{1}H-NMR (Figure 3.7, Figure 3.8). The integration values suggest the exact number of protons in **10** and **12**.

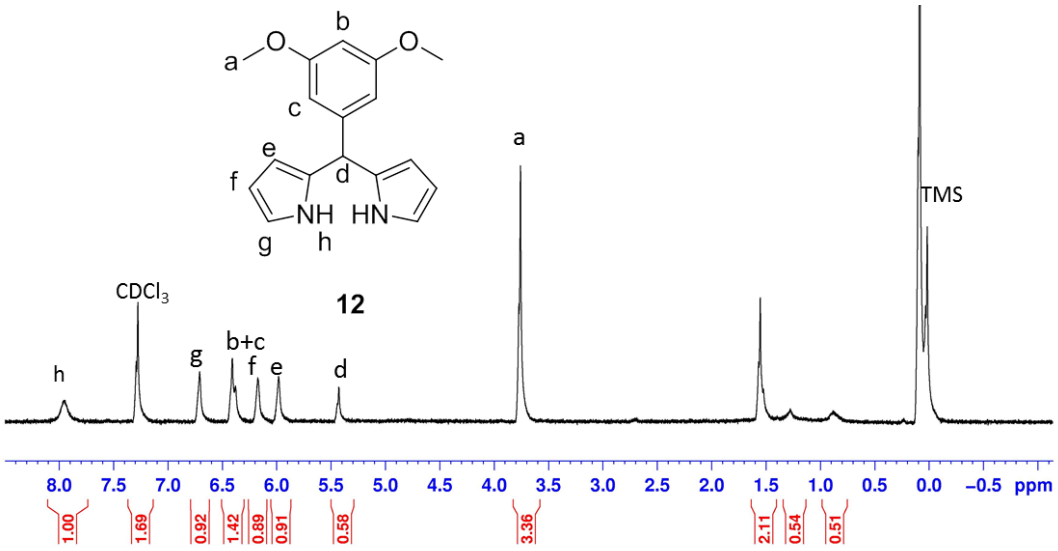

Figure 3.7: ^{1}H-NMR (400 MHz, $CDCl_3$, 25 ^oC) spectrum of **12**

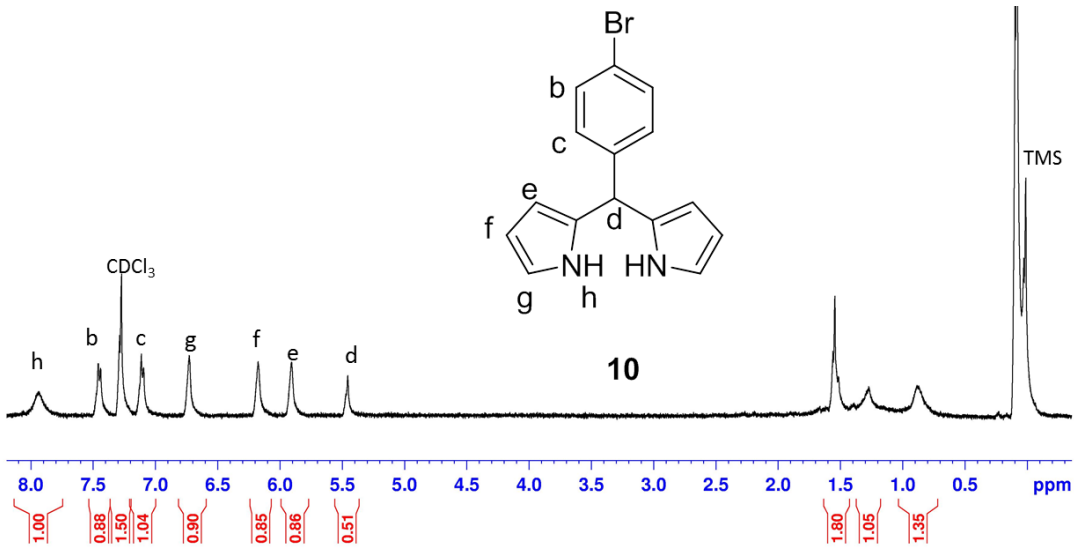

Figure 3.8: ^{1}H-NMR (400 MHz, $CDCl_3$, 25 ^{o}C) spectrum of **10**

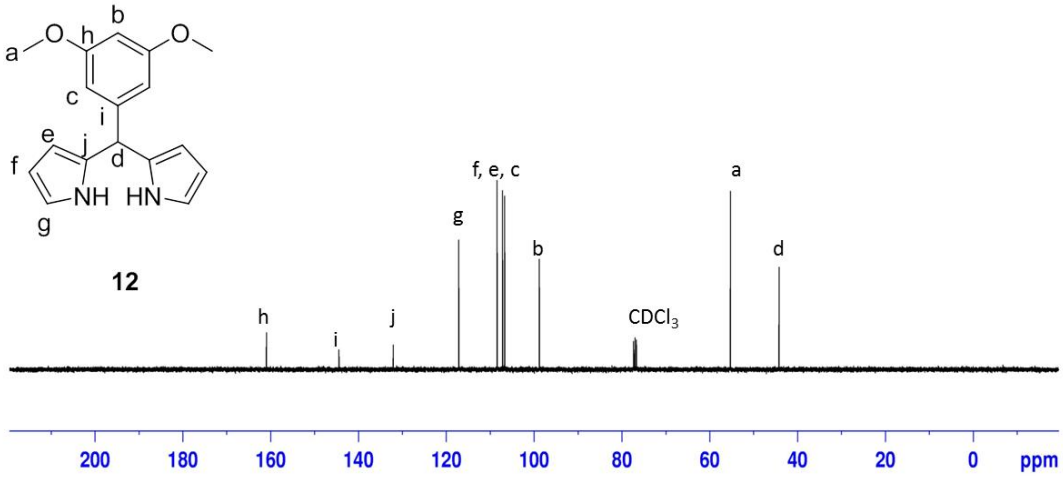

Figure 3.9: ^{13}C-NMR (100 MHz, $CDCl_3$, 25 ^{o}C) spectrum of **12**

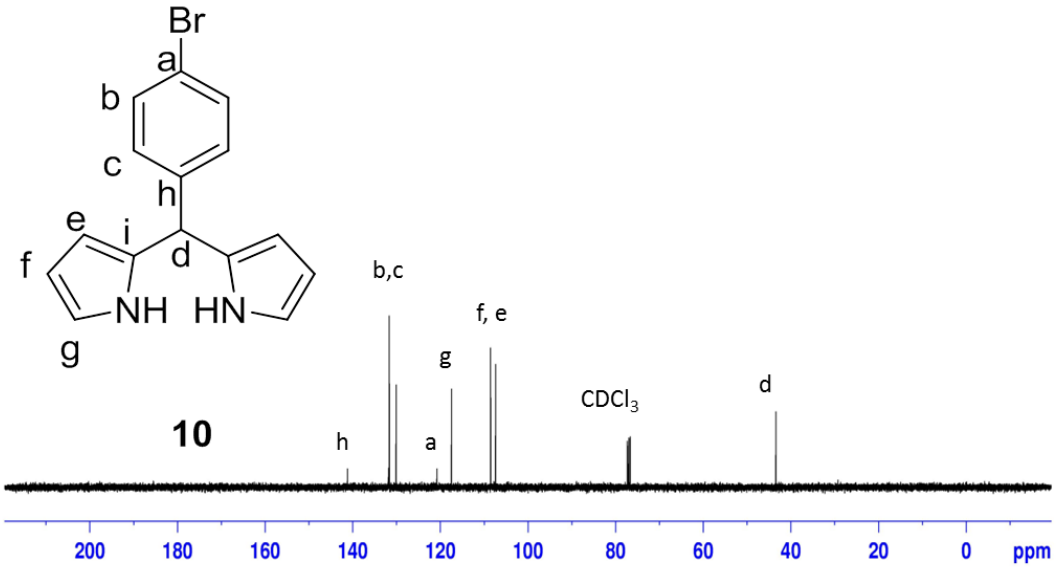

Figure 3.10: ^{13}C-NMR (100 MHz, $CDCl_3$, 25 ^{o}C) spectrum of **10**

Compound **10** and **12** were further characterized with ESI positive mode to give their mass to charge ratio as 301 and 282 which agree with the theoretical values. The molecules were ionized by addition of proton to one of the pyrrolic nitrogen atoms.

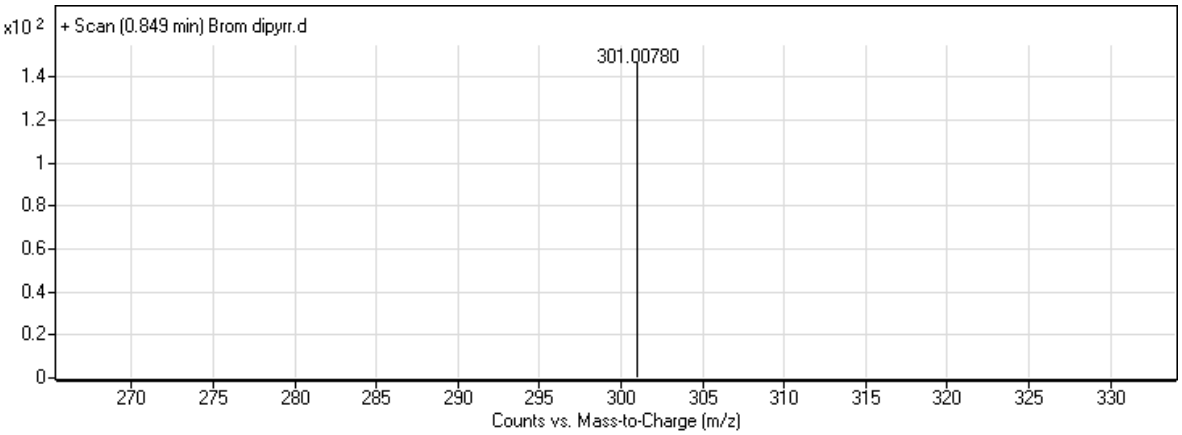

Figure 3.11: ESI spectrum of **12**

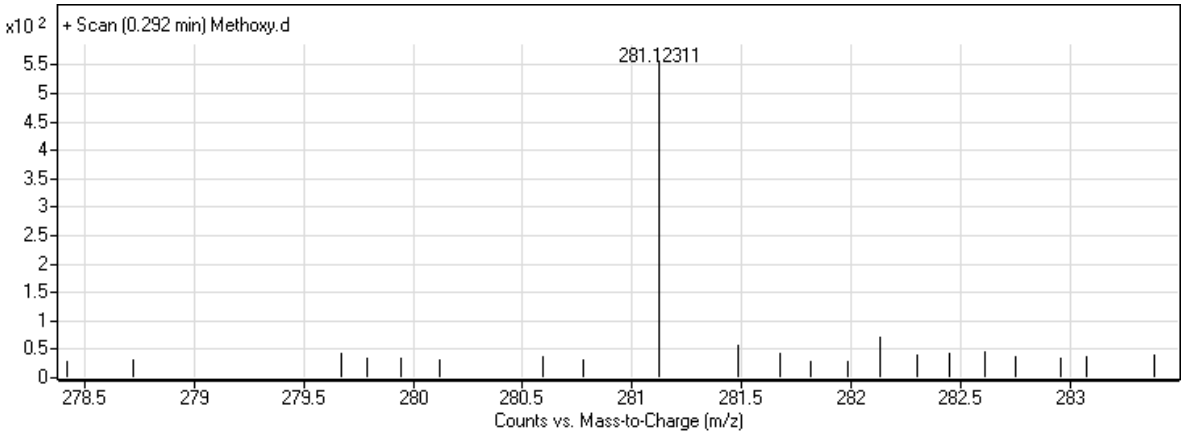

Figure 3.12: ESI spectrum of **10**

Elemental analysis data from the experimental section of **10** and **12** agree with the theoretical data confirming the structure of **10** and **12**.

3.5.3. Synthesis and Characterization of Porphyrin 13 and 14[140,141]

Porphyrins are generally synthesized according to the general procedures described in section 1.3.1. Because porphyrin synthesis starting from dipyrromethane is reported to give higher yield, we started the synthesis of **13** and **14** from the previously synthesized dipyrromethanes **10** and **12**. The reaction was carried out at very low concentration of the reactants (high dilution method) to facilitate the ring formation and to prevent polymerization of the dipyrromethane. We were expecting three different porphyrin products from this reaction **13**, **14** and **36**. However, other porphyrin side products (**37**, **38** and **39)** were also observed. The formation of these unexpected porphyrins can be attributed to the scrambling of the reactants during the porphyrin ring formation when strong acid is used as catalyst [142]. We later tried a much weaker acid catalyst (TFA) to obtain the desired product selectively but the yield was extremely low. The separation of porphyrin products with column chromatography was extremely tedious especially the Cis and Trans isomers (**14** and **39**) because their R_f values are very close even in the best solvent system (toluene). The separation of porphyrin products could only be achieved with very long and wide diameter columns. During the column chromatography, very small amount of triethyl amine was added to the silica to prevent tailing of porphyrin products because of interaction of porphyrin with silica. Although mixture of products was obtained, compound **13** was obtained in highest yield.

To synthesize compound **14**, we came up with another strategy i.e. by using equal equivalents of dipyrromethane **10** and 3,5-dimethoxy benzaldehyde or by using equal equivalents of dipyrromethane **12** and *p*-bromo benzaldehyde in order to increase the yield and minimize the

formation of side products. By following this strategy we were able to decrease the amount of other porphyrin side products although all the porphyrin side products were formed due to scrambling.

Since low yield was obtained for **13** and **14** and all porphyrin side products formed when we started with dipyrromethanes, we changed our synthetic strategy to one pot synthesis i.e. by mixing freshly distilled pyrrole, *p*-bromo benzaldehyde and 3,5-dimethoxy benzaldehyde to obtain all porphryrin products in similar yields. By doing this we get rid of dipyrromethane synthetic step. In this synthesis we tried to adjust the amount of the reactants to target a specific product. However due to rearrangement, the desired product was not always obtained in highest yield. When this method was employed, another red colored product in solution and blue on TLC plate was observed. This product was confirmed to be the six-membered porphyrin isomer called porphycenes.

After column chromatography, the porphyrin products were further washed with cold methanol to obtain shiny purple solid products.

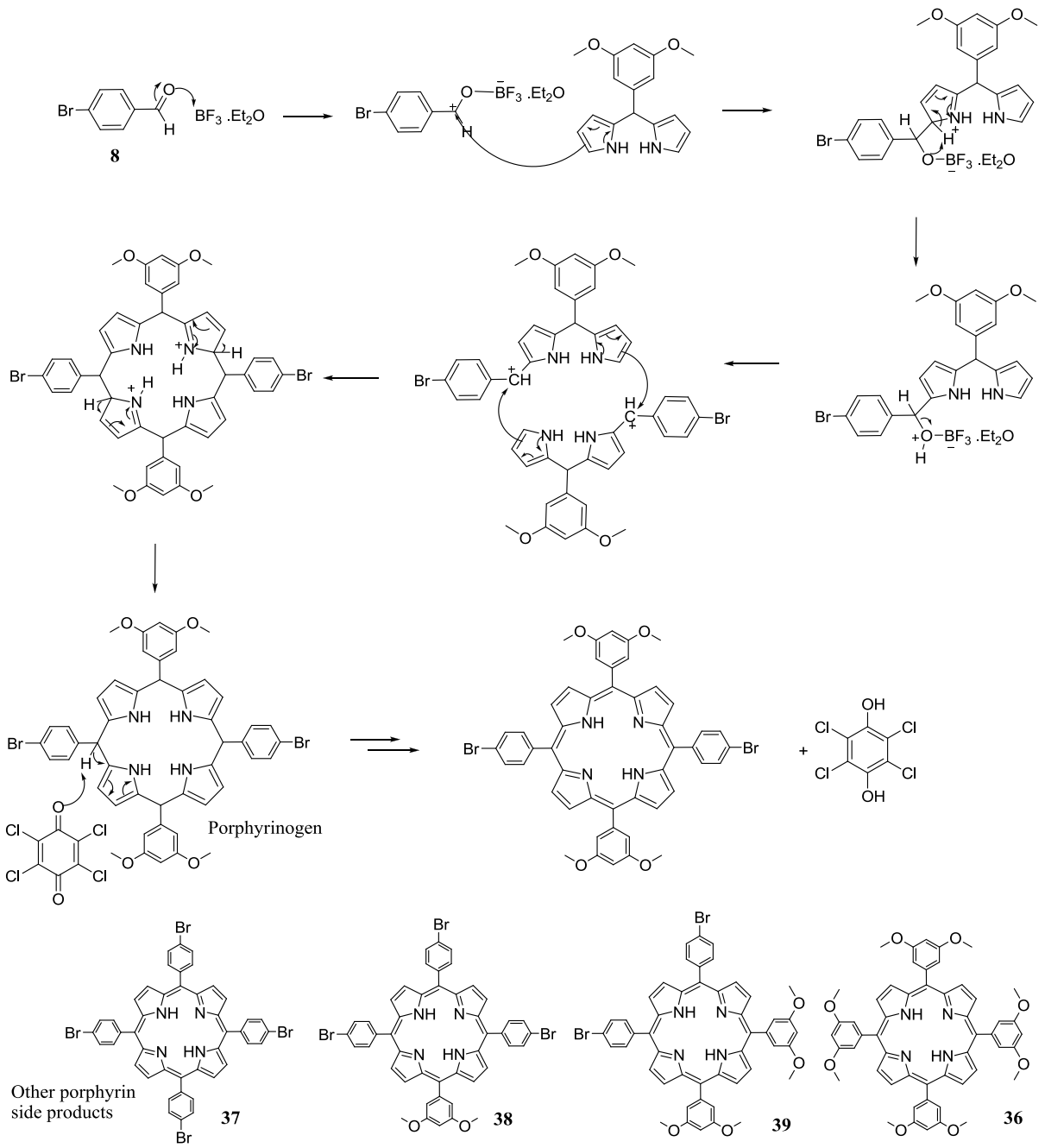

Scheme 3.6: Mechanism of porphyrin formation.

Both compounds **13** and **14** have the same ^{1}H-NMR peak pattern. These compounds were distinguished based on their differences in peak integration values. The total integration value for pyrrolic protons at 8.7 and 9.0 ppm is the same as the total integration values for bromo phenylic protons at 7.9 and 8.1 ppm for compound **14**. However these values are different in the ^{1}H-NMR of compound **13** where the total integration value of pyrrolic protons is twice the total integration value of the bromo phenylic protons suggesting the structure of **13**. The peak observed at –2.8 ppm in the ^{1}H-NMR spectrum of both **13** and **14** is a characteristic –NH peak of porphyrin ring. This peak shifted upfield because of shielding effect created by

the porphyrin ring commonly known as ring current effect. The singlet peak at 4.0 ppm also shows the presence of methoxy (–OCH_3) group. The peaks at 56 and 159 ppm in ^{13}C-NMR of **13** and **14** show the CH_3 and the aromatic carbon connected to oxygen –CO respectively.

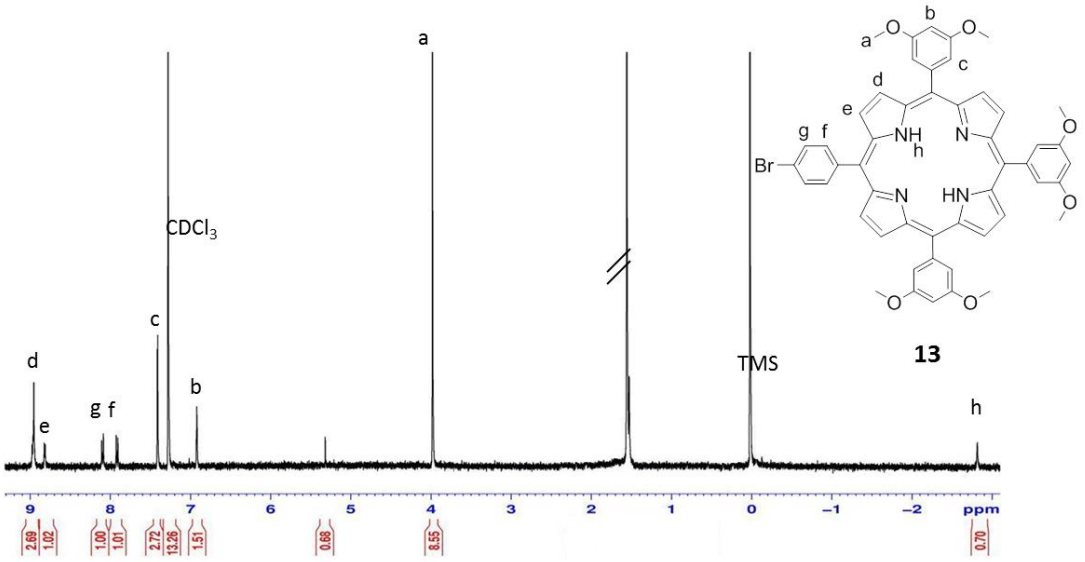

Figure 3.13: ^{1}H-NMR (400 MHz, $CDCl_3$, 25 ^{o}C) spectrum of **13**

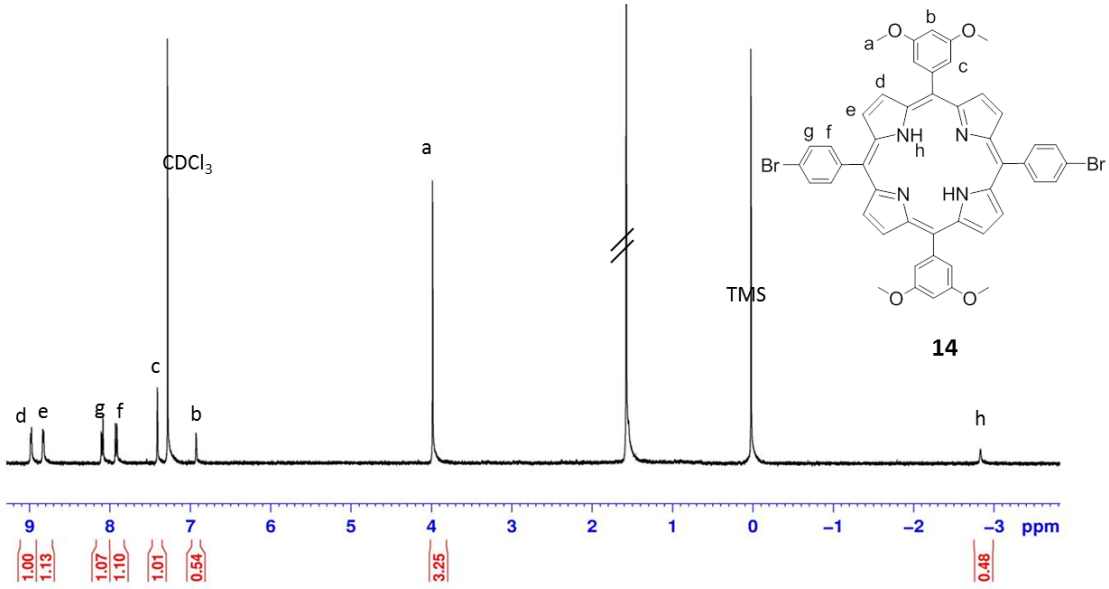

Figure 3.14: ^{1}H-NMR (400 MHz, $CDCl_3$, 25 ^{o}C) spectrum of **14**

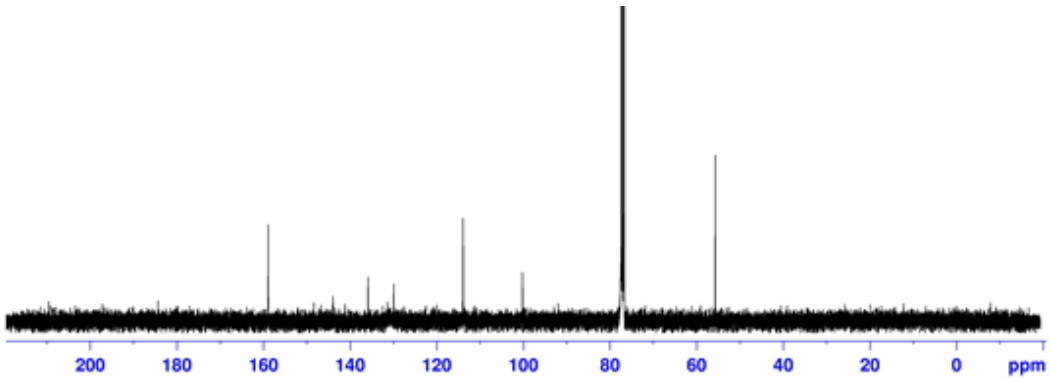

Figure 3.15: ^{13}C-NMR (100 MHz, $CDCl_3$, 25 ^{o}C) spectrum of **13**

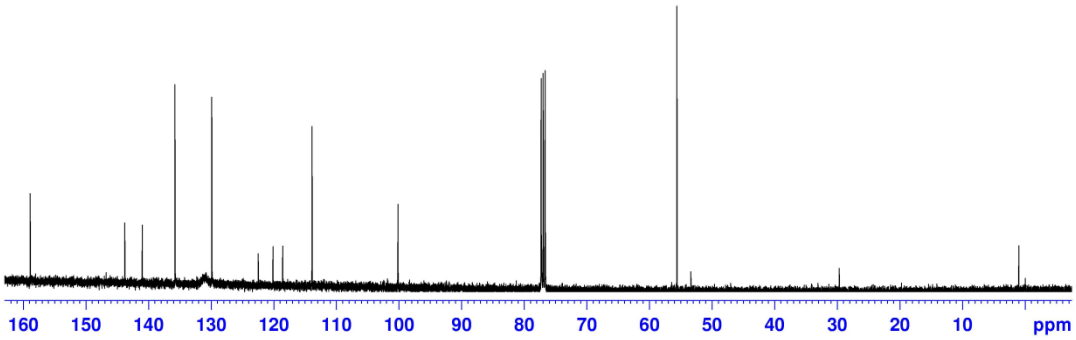

Figure 3.16: ^{13}C-NMR (100 MHz, $CDCl_3$, 25 ^{o}C) spectrum of **14**

Compound **13** and **14** were further characterized with ESI positive mode to give their mass to charge ratio as 874 and 892 which agree with the theoretical values. The molecules were ionized by addition of proton to one of the pyrrolic nitrogen atoms.

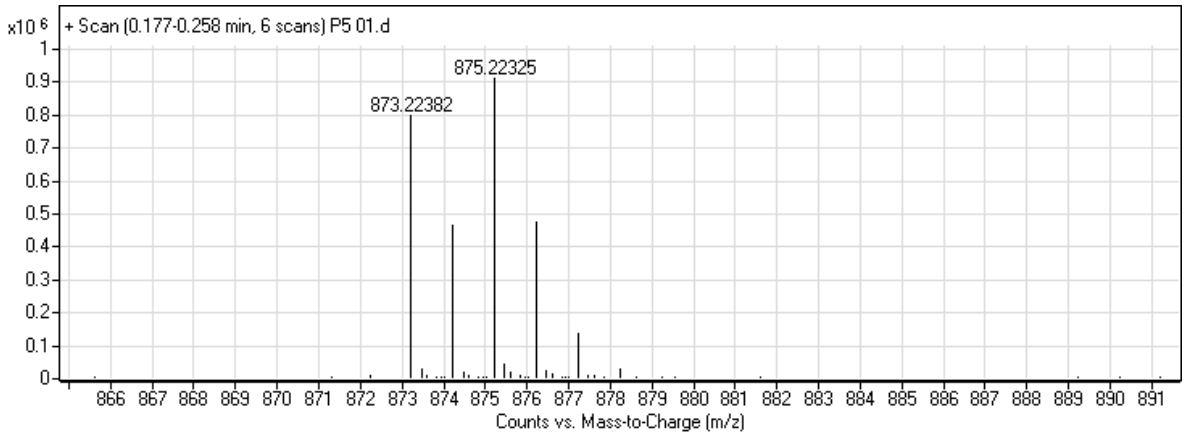

Figure 3.17: ESI spectrum of **13**

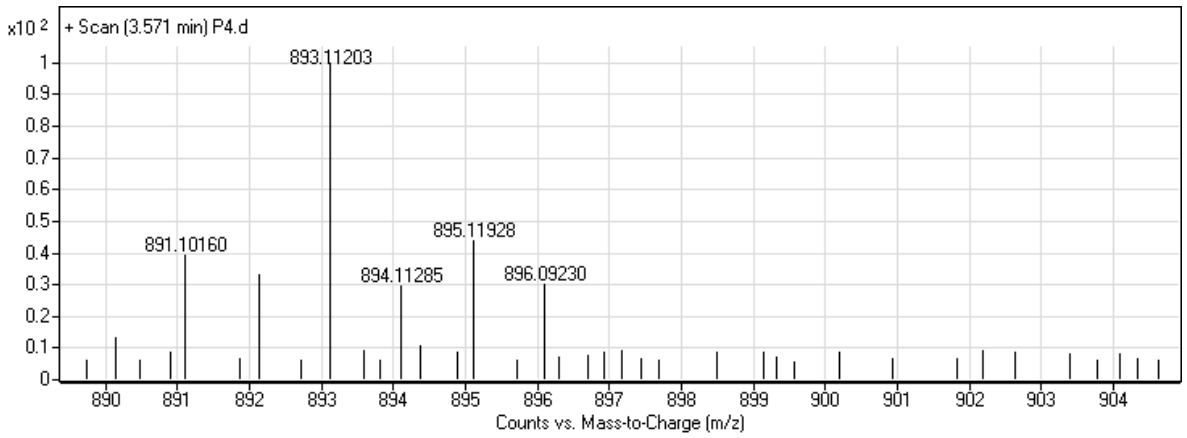

Figure 3.18: ESI spectrum of **14**

Elemental analysis results also agreed with the theoretical value confirming the structure of **13** and **14**. One of the difficulties encountered was distinguishing the trans (**14**) and cis (**39**) isomers by common characterization techniques. We were fortunate to grow single crystals of **14** and **39** and we were able to characterize them by Single Crystal X-ray Diffraction shown in Figure 3.19 and Figure 3.20. The single crystals were grown in air-tight desiccator by slow diffusion of methanol into the solution of **14** and **39** in chloroform. Compound **39** has higher R_f value than compound **14**, so it was collected first from the column chromatography.

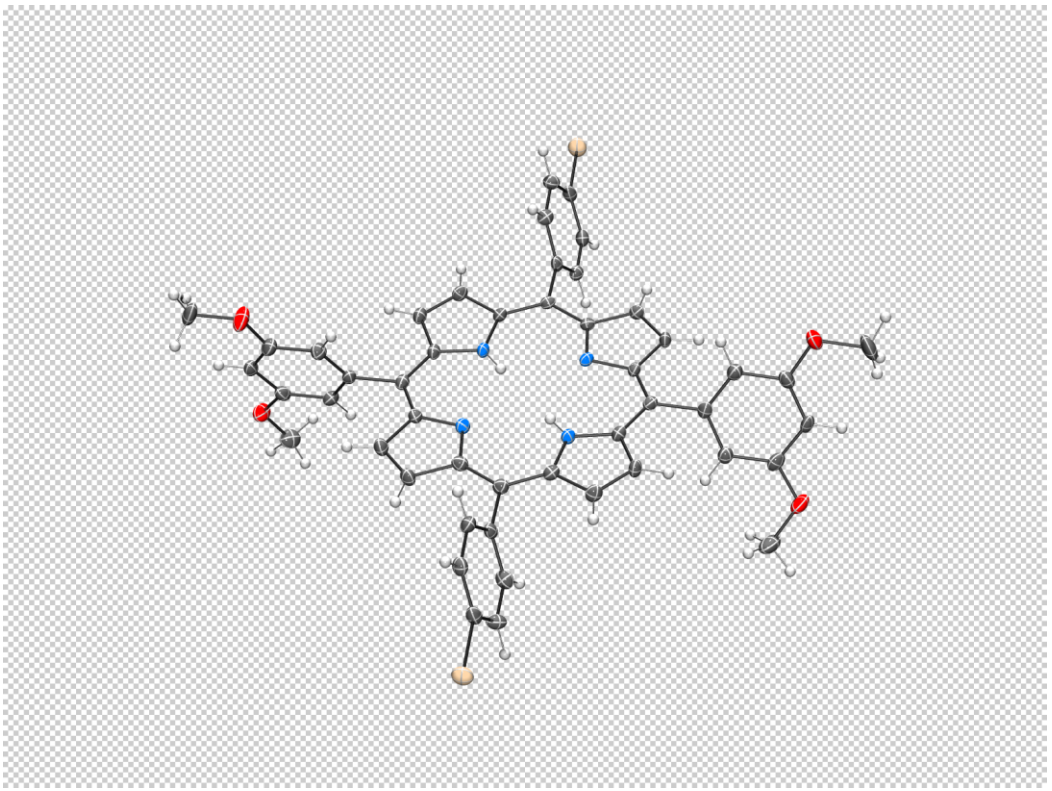

Figure 3.19: Structure of compound **14** by Single Crystal XRD (Determined by Dr. Kitchen, University of Southampton, United Kingdom)

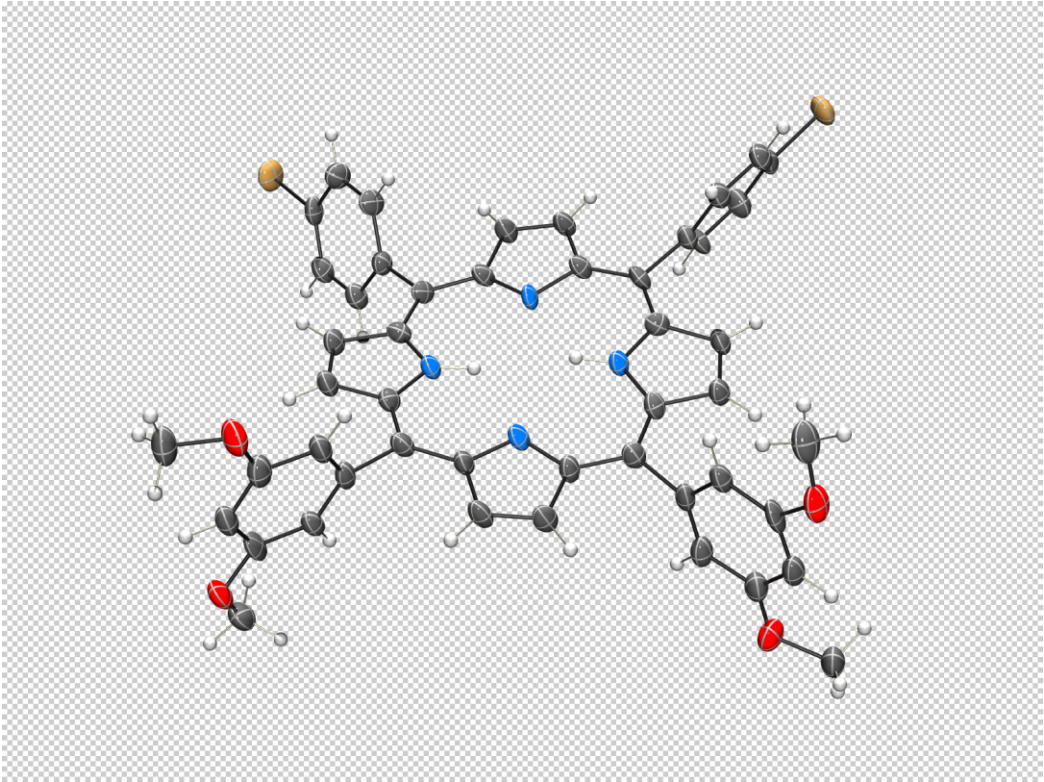

Figure 3.20: Structure of compound **39** by Single Crystal XRD(Determined by Dr. Kitchen, University of Southampton, United Kingdom)

3.5.4. Synthesis and Characterization of Porphyrin 15 and 22

To hydrolyze the methoxy groups on phenyl ring, very strong lewis acid is needed. For this purpose, tribromo borane (BBr_3) was used. The key point in the synthesis is the addition of BBr_3 at very low temperature to prevent effervescent reaction. To keep the reaction temperature at -78 ^oC, a cooling bath of acetone and liquid nitrogen (-94 ^oC) was prepared and placed under the reaction flask for some time making sure DCM (-96 ^oC) did not freeze. Upon addition of BBr_3 the red color of porphyrin changed to green indicating complex formation of BBr_3 with the pyrrolic nitrogen atoms. Compound **15** is insoluble in chloroform, but compound **22** is sparingly soluble in chloroform, so cold chloroform was used to wash compound **22**. Also compound **15** is more soluble in methanol than compound **22** because of the less TEG groups attached to compound **22**.

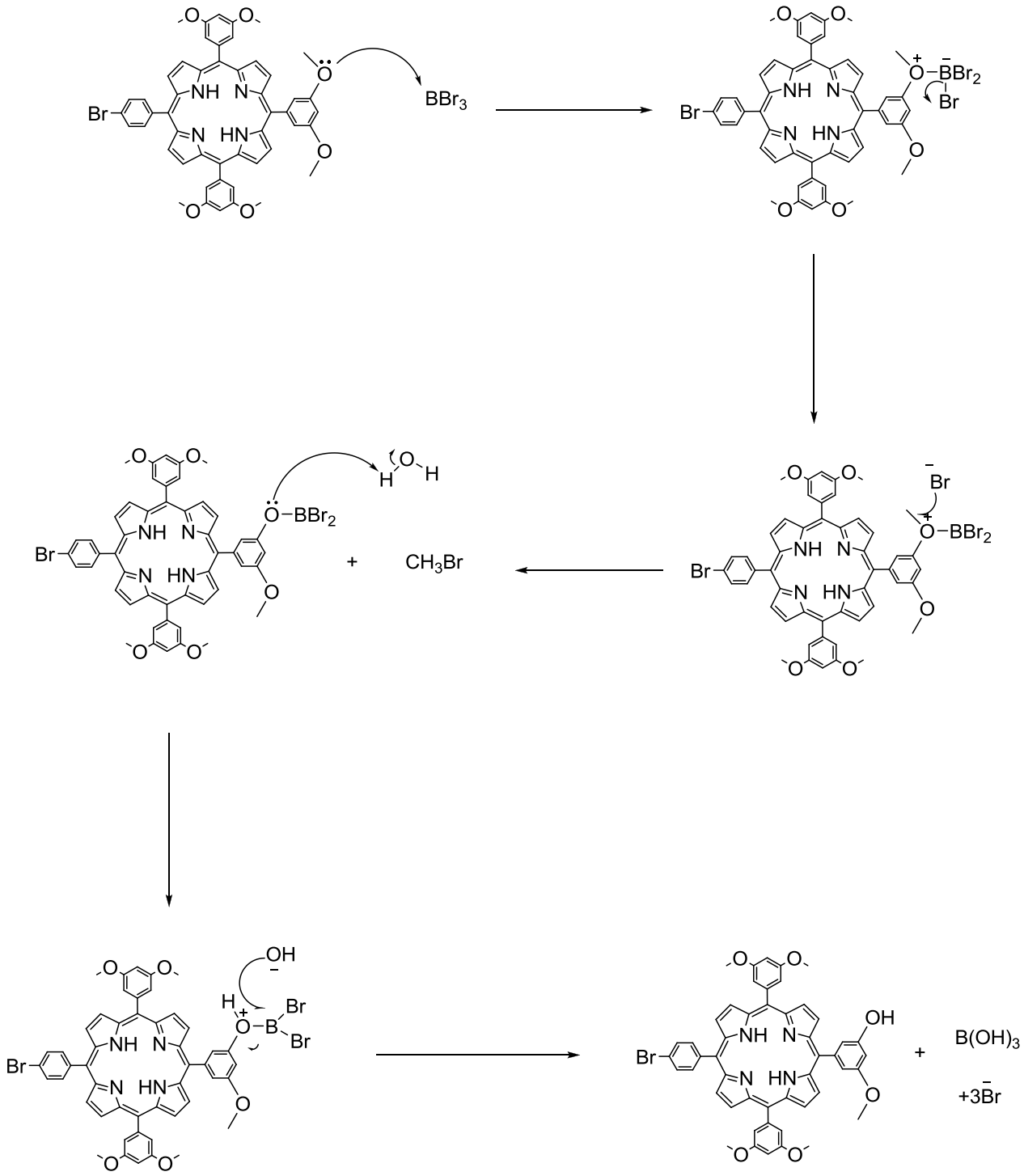

Scheme 3.7: Mechanism of porphyrin hydrolysis.

The disappearance of methoxy singlet peaks at 4.0 ppm and the appearance of hydroxyl protons at 9 ppm in ^{1}H-NMR of both compound **15** and **22** confirmed complete hydrolysis of methoxy groups. Similarly the peak at 55 ppm due methoxy carbons disappeared in the ^{13}C-NMR of these compounds.

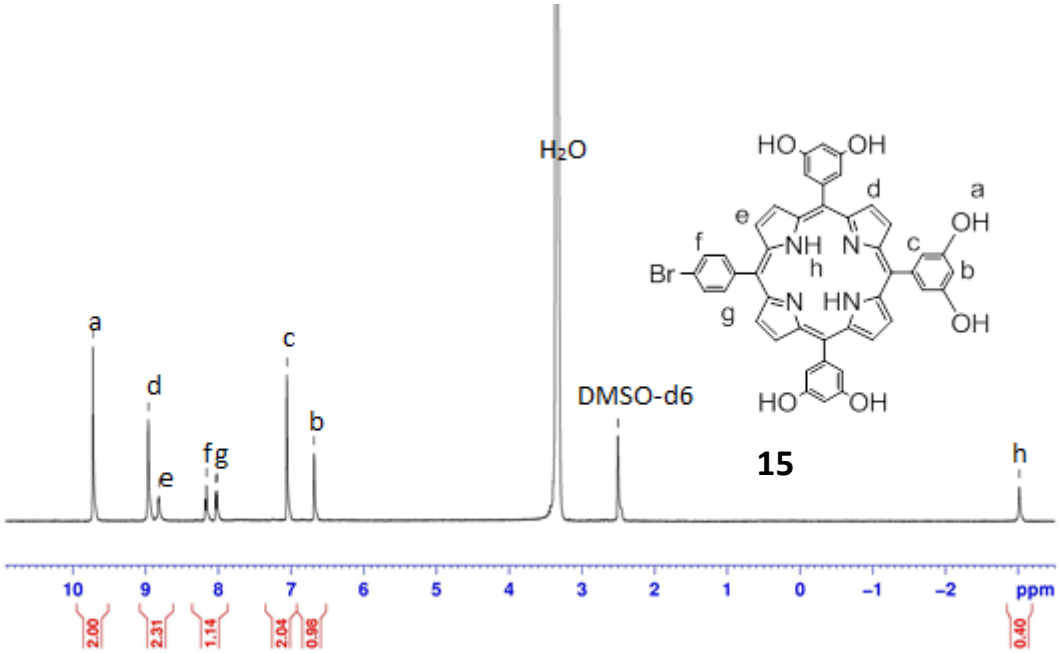

Figure 3.21: ^{1}H-NMR (400 MHz, DMSO-d6, 25 ^{o}C) spectra of **15**

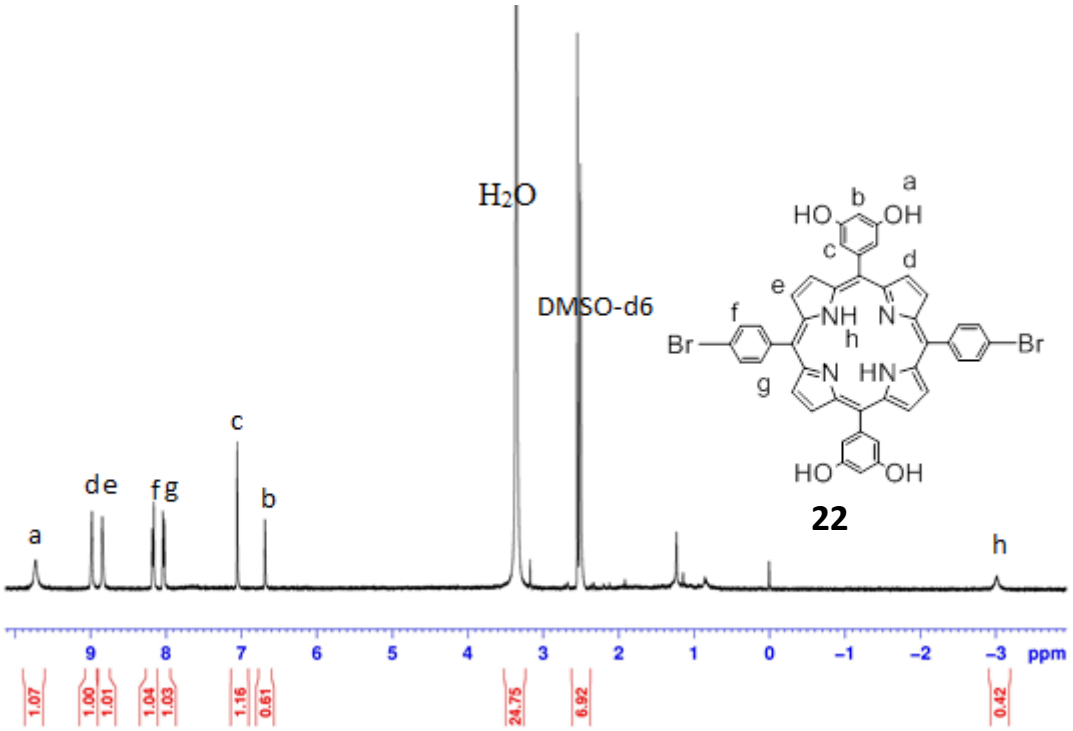

Figure 3.22: ^{1}H-NMR (400 MHz, DMSO-d6, 25 ^{o}C) spectrum of **22**

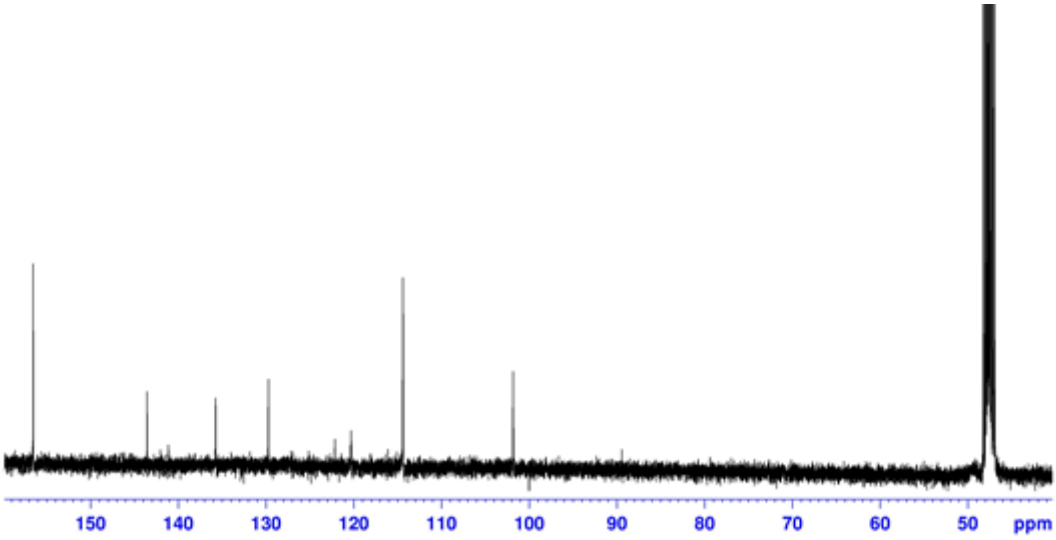

Figure 3.23: ^{13}C-NMR (100 MHz, DMSO-d6, 25 ^{o}C) spectrum of **15**

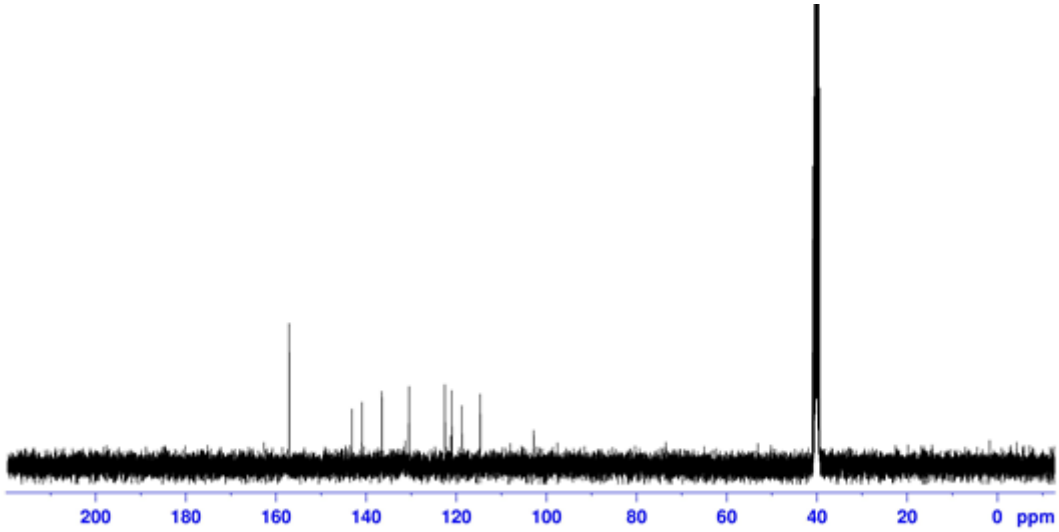

Figure 3.24: ^{13}C-NMR (100 MHz, DMSO-d6, 25 ^{o}C) spectrum of **22**

Compounds **15** and **22** were further characterized by ESI positive mode shown in Figure 3.25 and Figure 3.26.

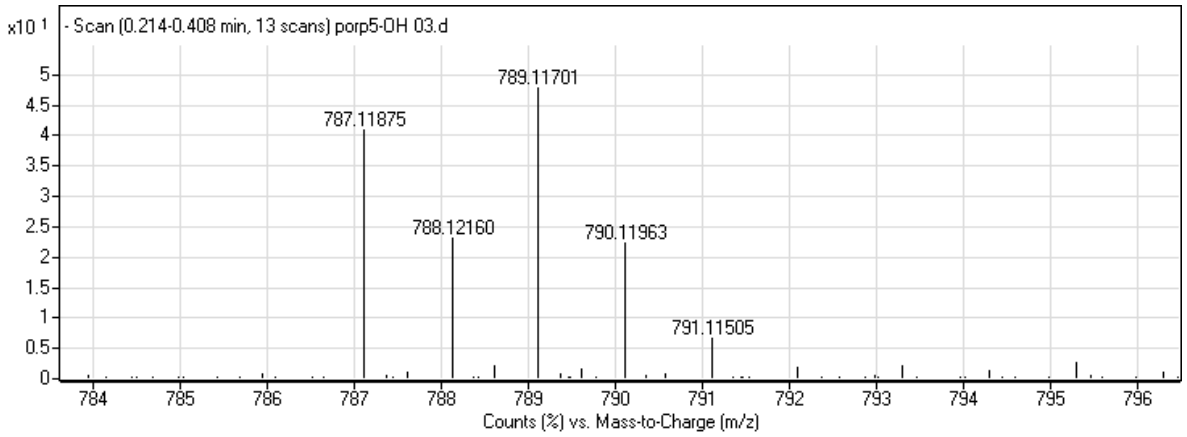

Figure 3.25: ESI spectrum of **15**

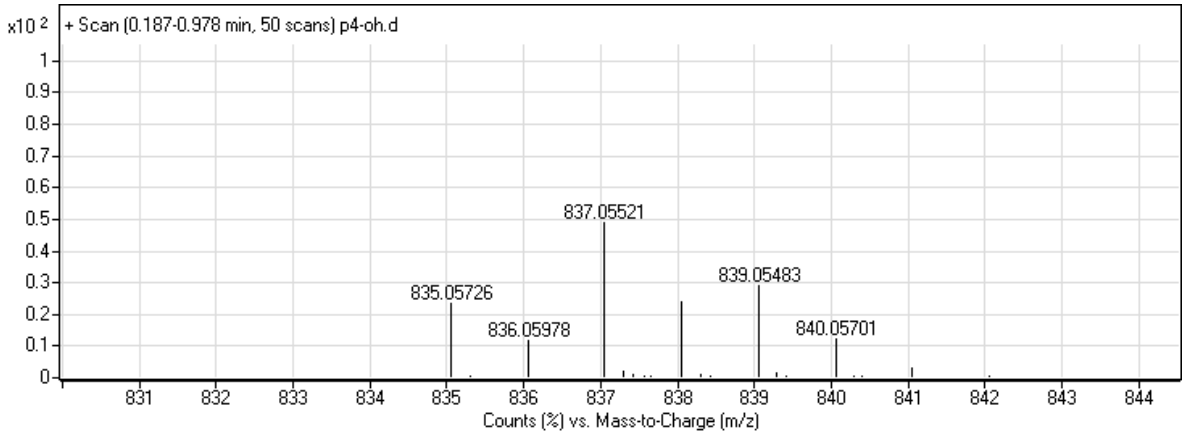

Figure 3.26: ESI spectrum of **22**

3.5.5. Synthesis and Characterization of Porphyrin 17 and 23

Compound **17** and **23** were synthesized from their precursors **15**, **22** and monotosyl triethylene glycol. In this reaction, weak base was used because the phenolic protons are quite acidic compared to aliphatic hydroxyl protons. After removing all the solvents, gummy solid product was obtained due to attachment of TEG groups. Both compound **17** and **23** were expected to be water soluble due to the TEG groups attached. However, none of these compounds were soluble in water.

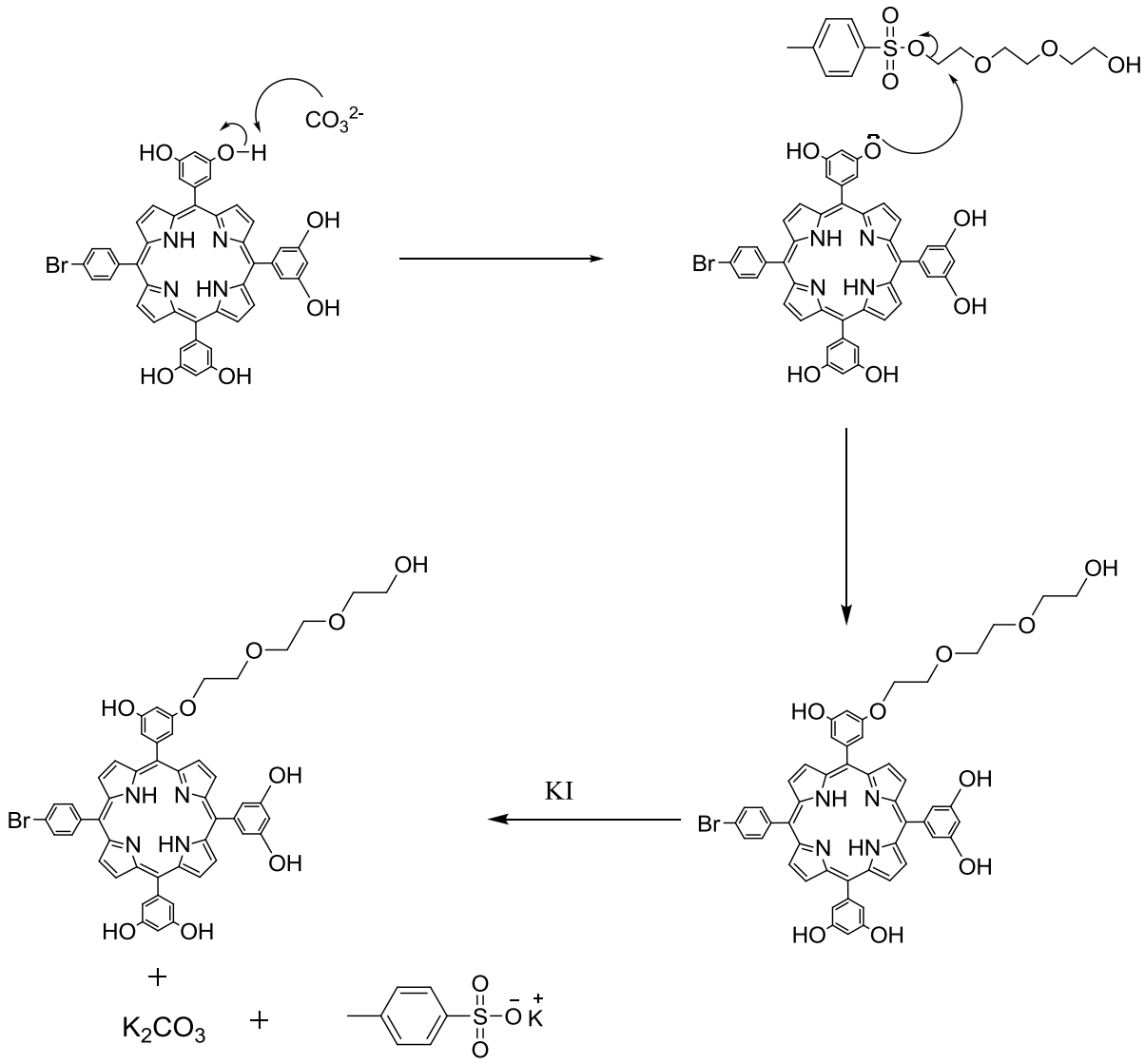

Scheme 3.8: Mechanism of reaction of porphyrin and mono substituted TEG

In ^{1}H-NMR of both compound **17** and **23**, the disappearance of the peak at 9 ppm due to phenolic protons and the appearance of new peaks at 3-4 ppm due to $–OCH_2$ protons confirmed the attachment of TEG groups. Also the appearance of peaks at 150-160 ppm in ^{13}C-NMR of both compound **17** and **23** further confirmed the attachment of TEG groups.

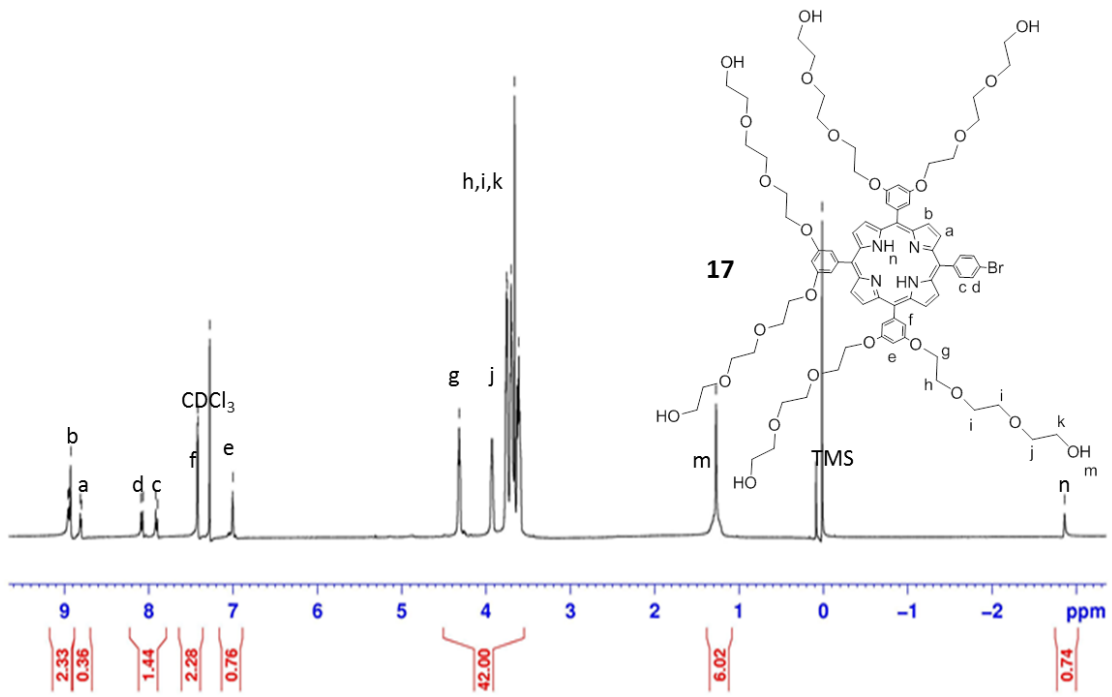

Figure 3.27: ^{1}H-NMR (400 MHz, $CDCl_3$, 25 ^{o}C) spectrum of **17**

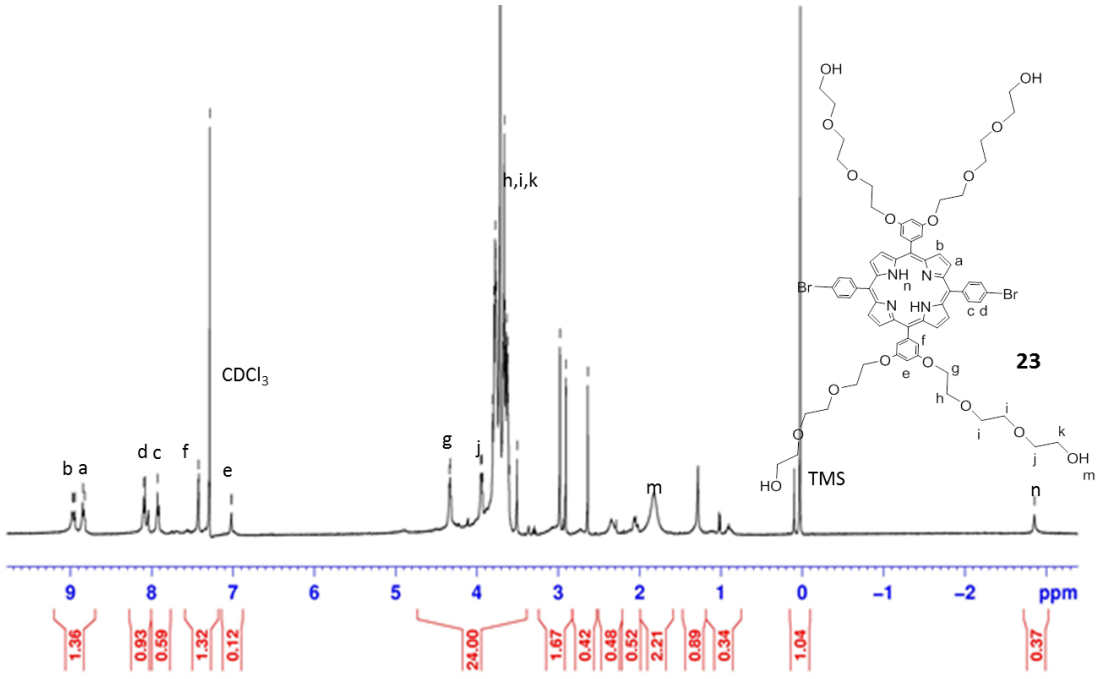

Figure 3.28: ^{1}H-NMR (400 MHz, $CDCl_3$, 25 ^{o}C) spectrum of **23**

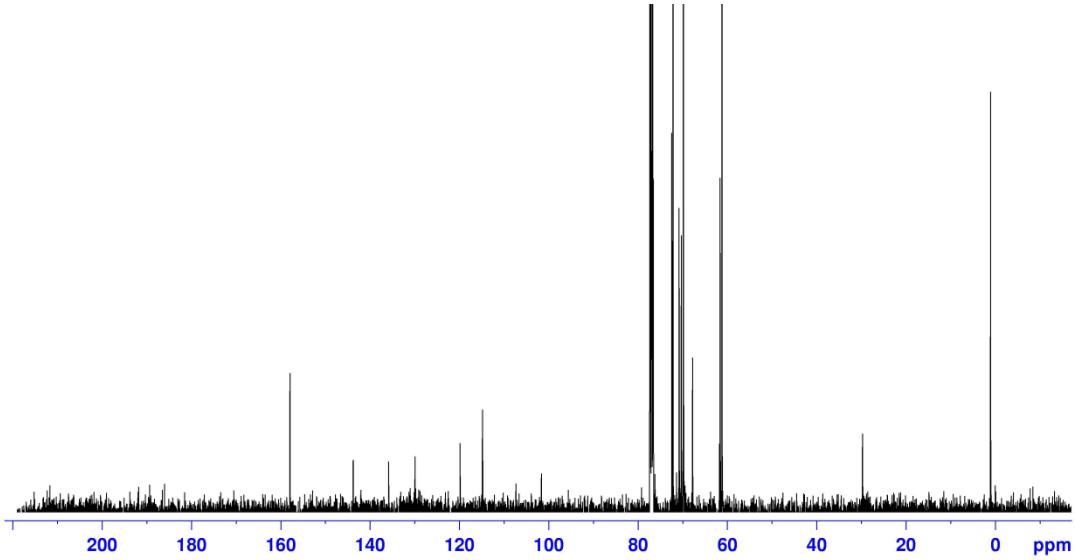

Figure 3.29: ^{13}C-NMR (100 MHz, $CDCl_3$, 25 ^{o}C) spectrum of **17**

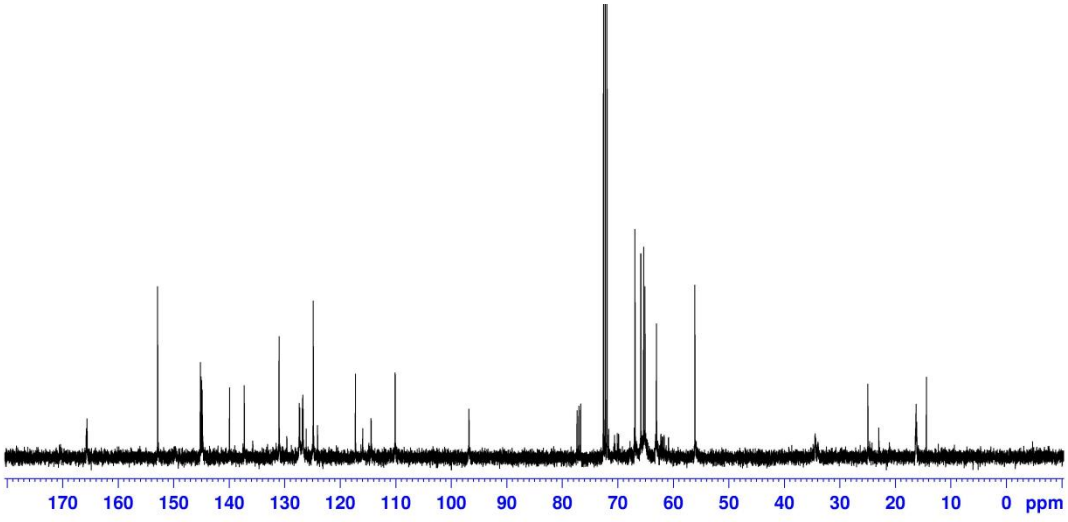

Figure 3.30: ^{13}C-NMR (100 MHz, $CDCl_3$, 25 ^{o}C) spectrum of **23**

Mass to charge ratio of compound **17** and **23** were found to be 1582 and 1362 respectively.

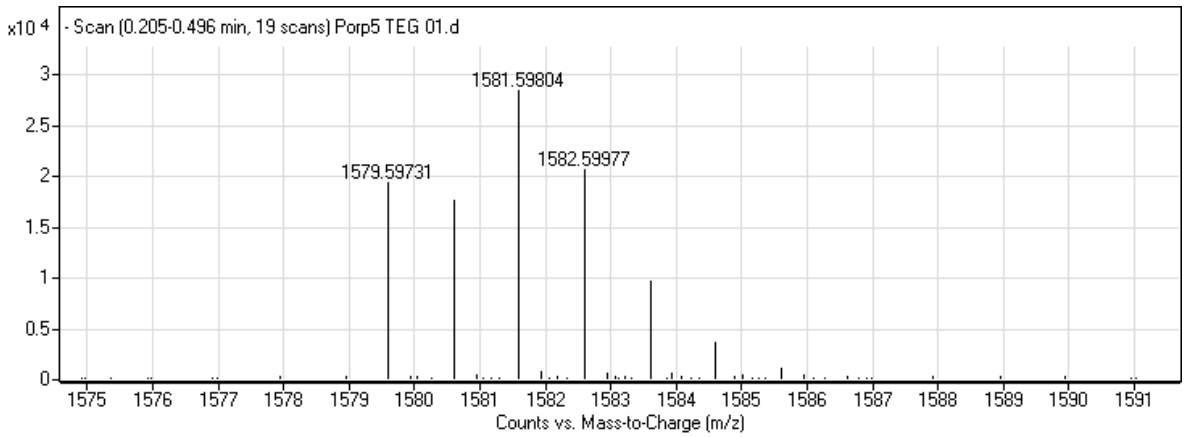

Figure 3.31: ESI spectrum of **17**

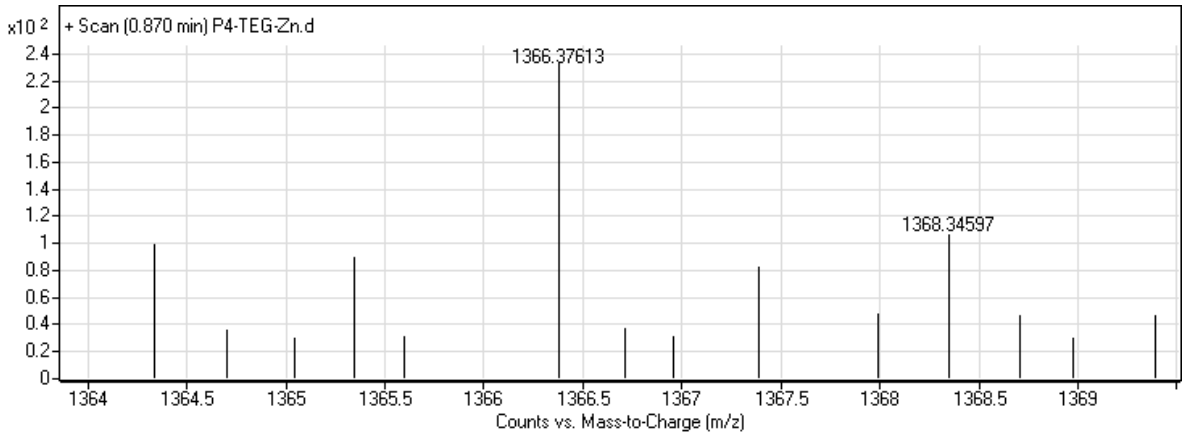

Figure 3.32: ESI spectrum of **23**

3.5.6. Synthesis and Characterization of Porphyrins 18 and 24

The porphyrin core is protected with transition metal so that transition metal catalyst in the next step will not be inserted in the porphyrin core and thus will inhibit the performance of the catalyst. Metallation of compound **18** or **24** was done by refluxing the solution of compound **17** or **23** with zinc (II) acetate overnight. The zinc was inserted into the four-fold (tetradendate) binding site of porphyrin.

The disappearance of peak at -2.8 ppm in the ^{1}H-NMR of both of compound **18** and **24** confirmed the metallation of these compounds.

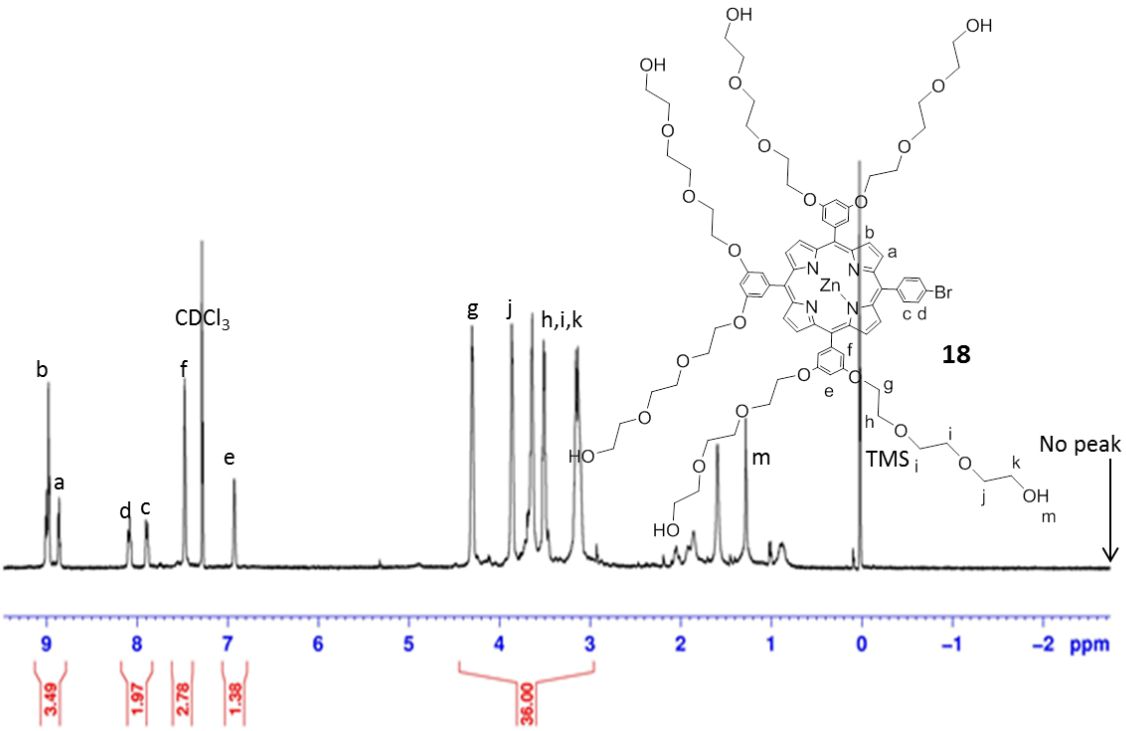

Figure 3.33: ^{1}H-NMR (400 MHz, $CDCl_3$, 25 ^{o}C) spectrum of **18**

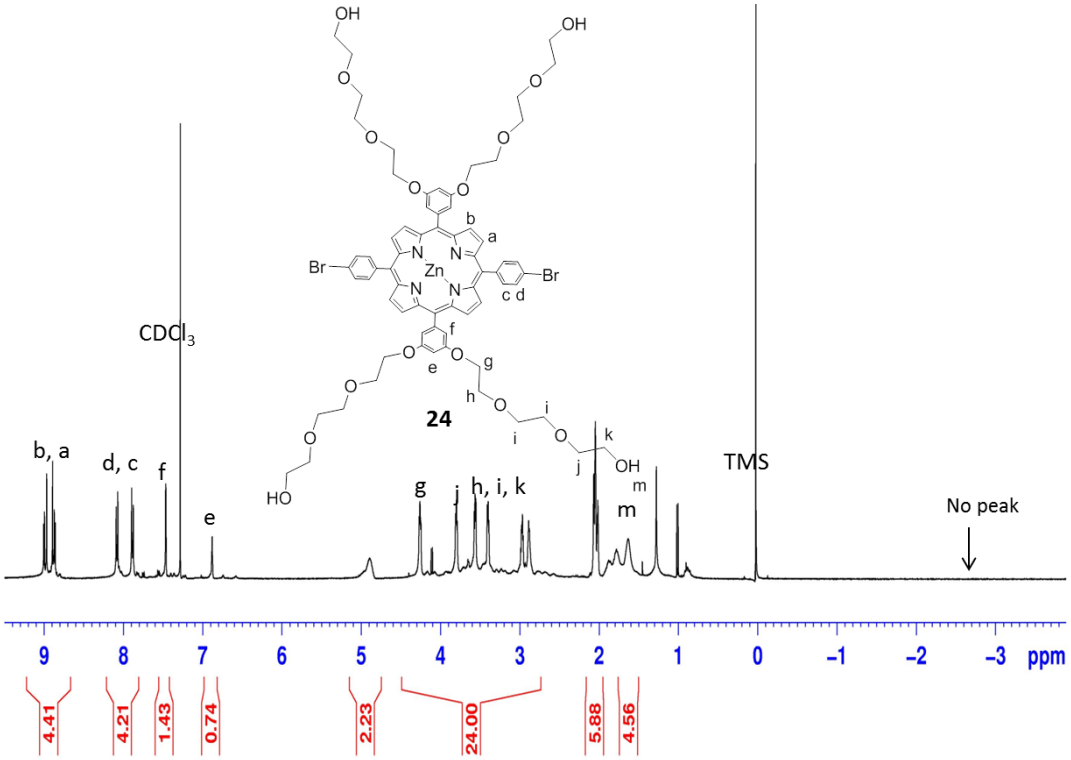

Figure 3.34: ^{1}H-NMR (400 MHz, $CDCl_3$, 25 ^{o}C) spectrum of **24**

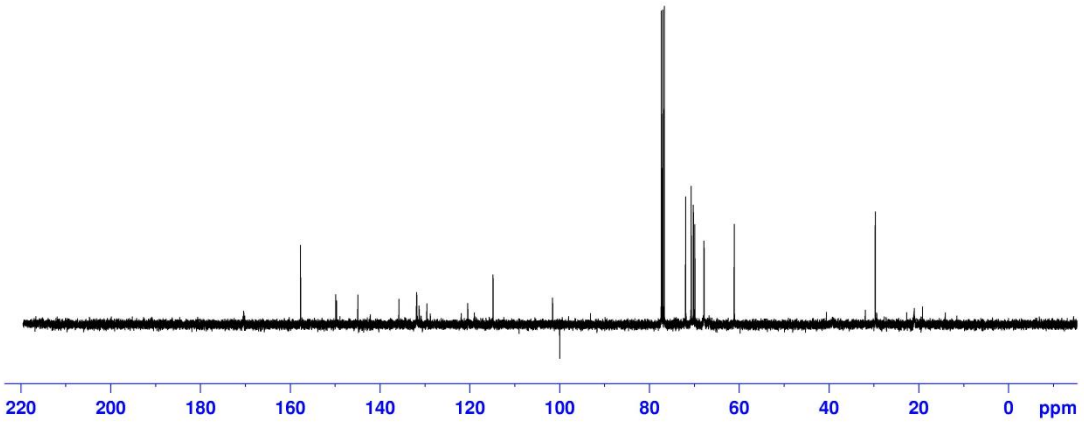

Figure 3.35: ^{13}C-NMR (100 MHz, $CDCl_3$, 25 ^{o}C) spectrum of **18**

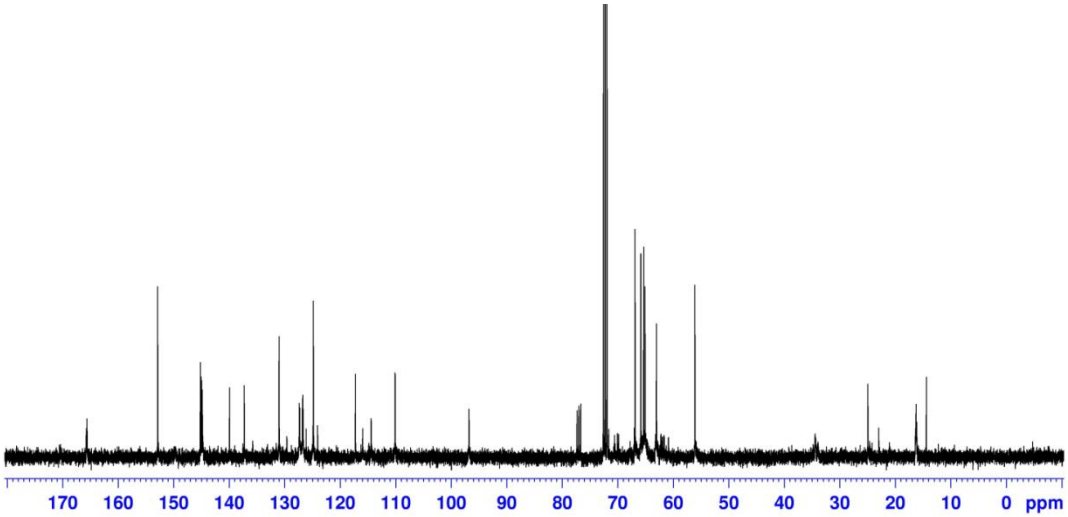

Figure 3.36: ^{13}C-NMR (100 MHz, $CDCl_3$, 25 ^{o}C) spectrum of **24**

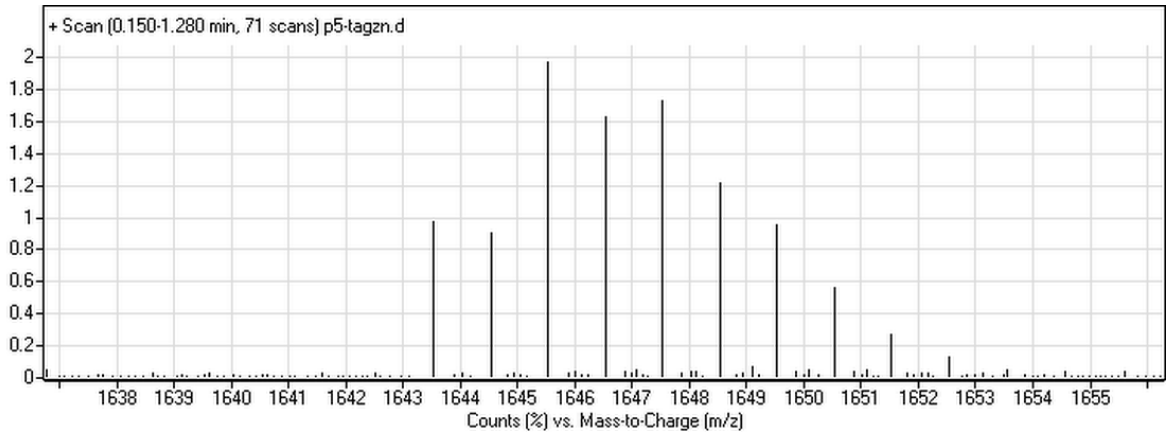

Figure 3.37: ESI spectrum of **18**

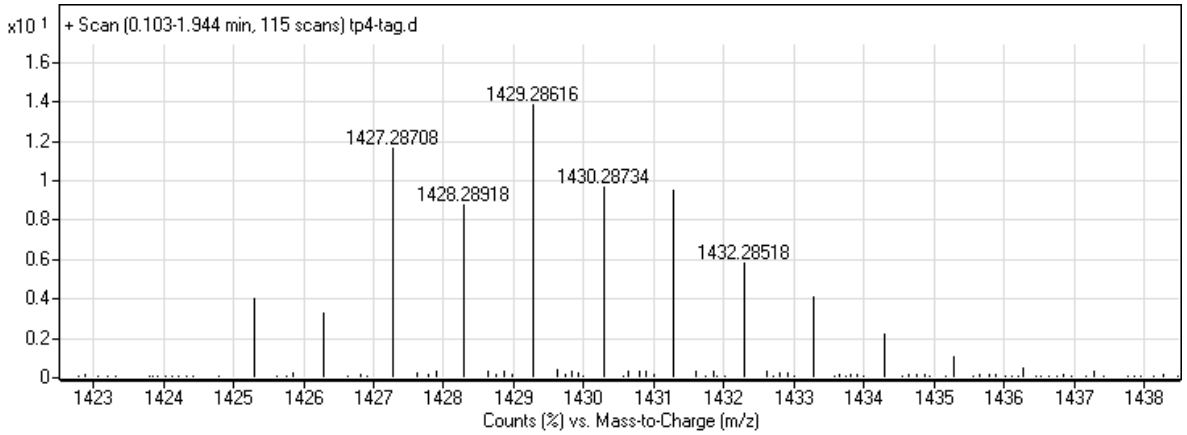

Figure 3.38: ESI spectrum of **24**

3.5.7. Synthesis and Characterization of Oligo-porphyrin 19 and 20[101-104]

In our attempt to synthesize CB[7] based rotaxane containing porphyrin stopper groups using Suzuki Coupling, we ended up synthesizing oligo-porphyrin **19**. In the reaction, excess CB[7] and 2,5-thiophenediboronic ester **7** were dissolved in water and stirred for two hours at 50 ^{o}C. Despite high reaction temperature, compound **18** did not dissolve in water, instead water and DMF layers separated to form two layers. Thiophene boronic ester **7** must have slipped off from CB[7] cavity and passed to DMF layer leaving CB[7] in the aqueous layer. This could be the reason why rotaxane was not formed. The reaction mechanism proceeds by addition of bromide and porphyrin ligands to palladium to increase the oxidation number of palladium by two. This phenomenon is called oxidative addition. The next step involves ligand exchange between the complex and the base. The resulting product reacts with the previously formed trialkyl borate to form palladium complex with both porphyrin and thiophene ligands. This step is known as transmetallation step. Removal of the two ligands and their combination restores the original state of palladium and forms the desired product. This step is known as reductive elimination. The mechanism of this reaction is shown in Scheme 3.9a.

To avoid using salts, compound **20** was synthesized via Stille Coupling. This reaction is similar to Suzuki Coupling except organic tin compound is used instead of aryl boronic acid/ester and salts are not used. Since salts are not involved in this reaction only organic solvents were used. The mechanism of this reaction is shown in Scheme 3.9b.

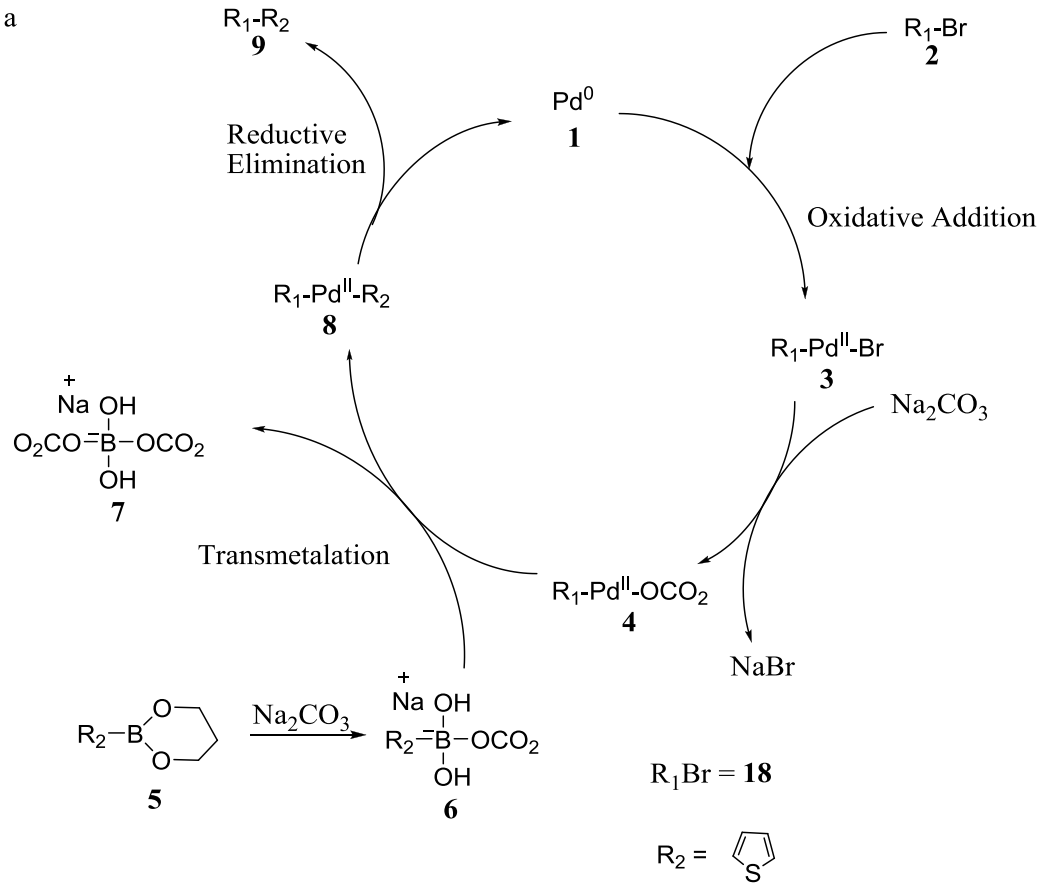

Scheme 3.9: (a) Suzuki coupling reaction

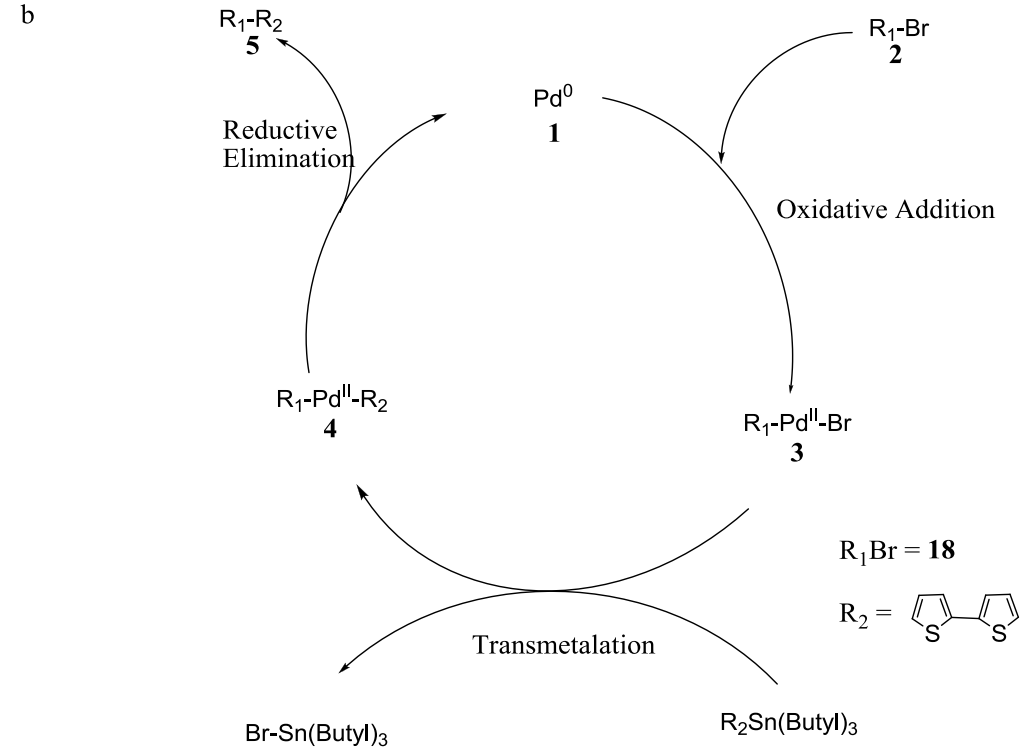

Scheme 3.9: (b) Stille coupling reaction

Both compound **19** and **20** were characterized by ^{1}H-NMR and ^{13}C-NMR. One of the major differences in the ^{1}H-NMR of **19** and its precursor is the bromo phenyl protons. The peaks at 7.9 ppm and 8.1 ppm shifted to 7.7 ppm and 8.3 ppm respectively. However, very small shift was observed in the dimethoxy phenyl protons. Similarly, downfield shift was observed for both bromo phenyl protons and dimethoxy phenyl protons in ^{1}H-NMR of **20** suggesting the coupling reaction took place. Compared to ^{13}C-NMR of compound **19** and **20** precursors, new peaks were observed in the ^{13}C-NMR of compound **19** and **20**. The mass to charge ratio of compound **19** and **20** were observed as 1605 and 1645 suggesting the structure of this compounds with double charge. The presence of sulfur in the elemental analysis results of these compounds clearly shows the presence of thiophene in these molecules. These values agree with the calculated values shown in the experimental section.

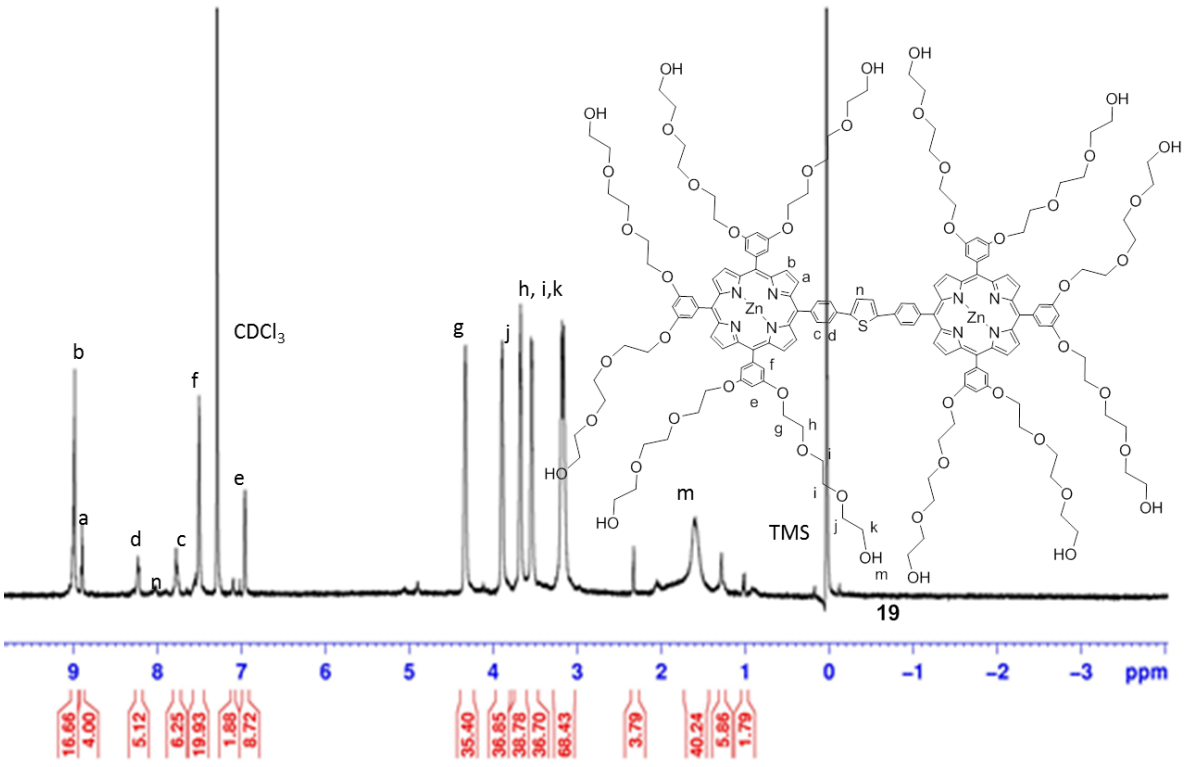

Figure 3.39: ^{1}H-NMR (400 MHz, $CDCl_3$, 25 ^{o}C) spectrum of **19**

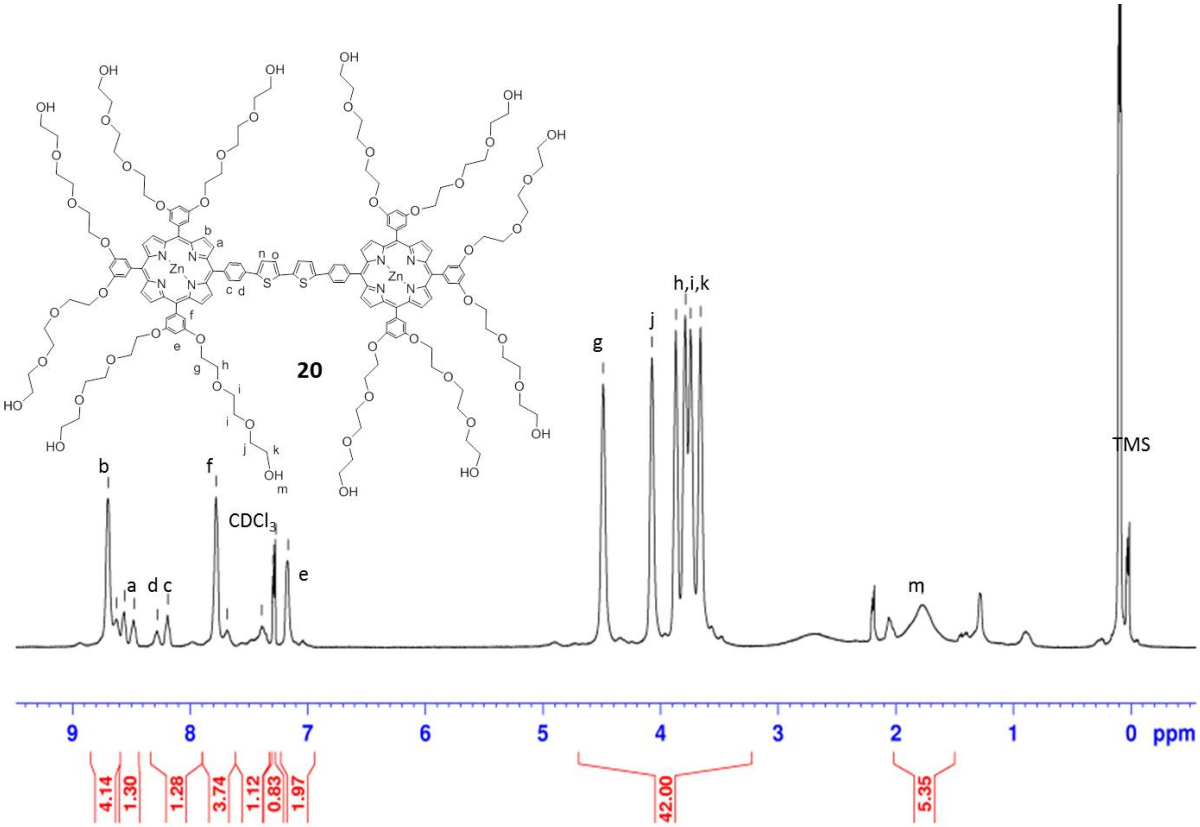

Figure 3.40: ^{1}H-NMR (400 MHz, $CDCl_3$, 25 ^{o}C) spectrum of **20**

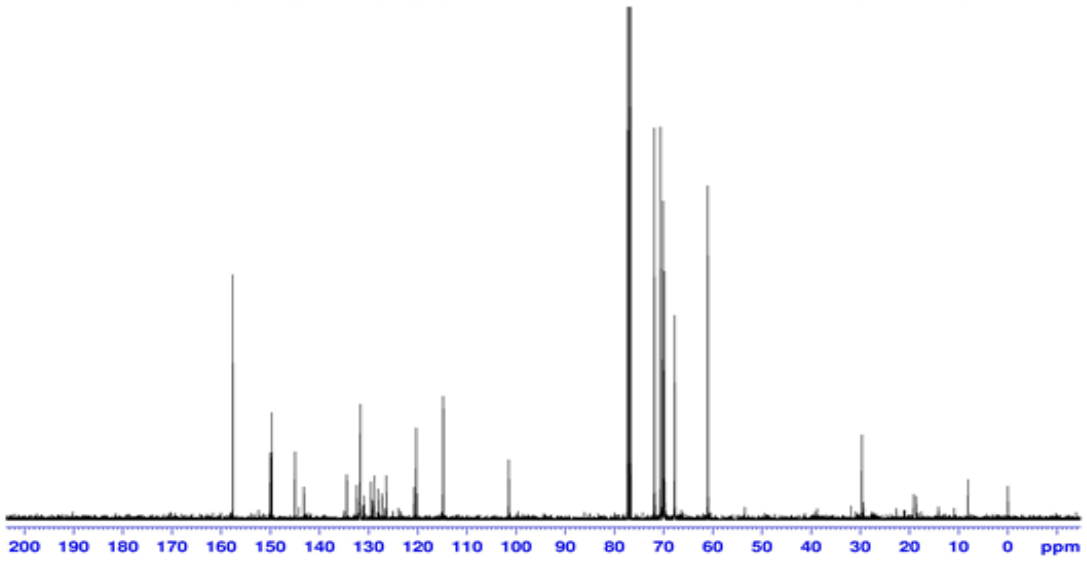

Figure 3.41: ^{13}C-NMR (100 MHz, $CDCl_3$, 25 ^{o}C) spectrum of **19**

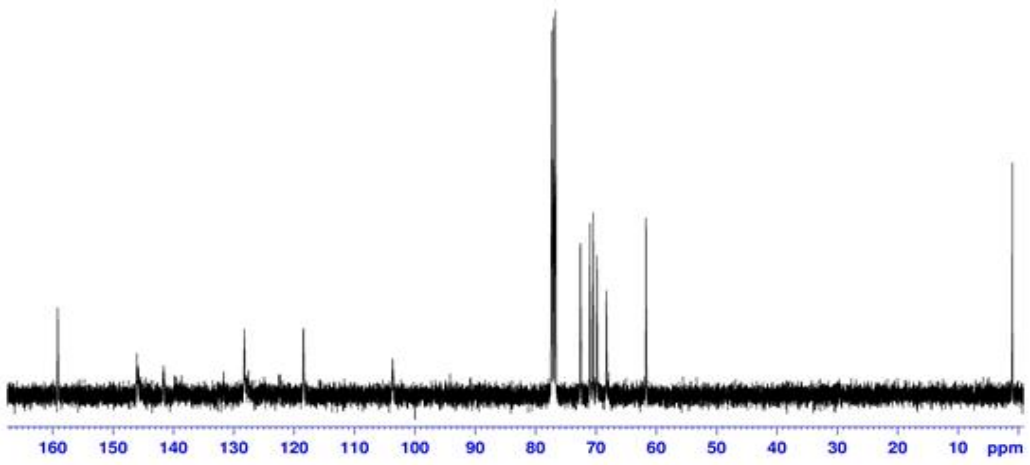

Figure 3.42: ^{13}C-NMR (100 MHz, $CDCl_3$, 25 ^{o}C) spectrum of **20**

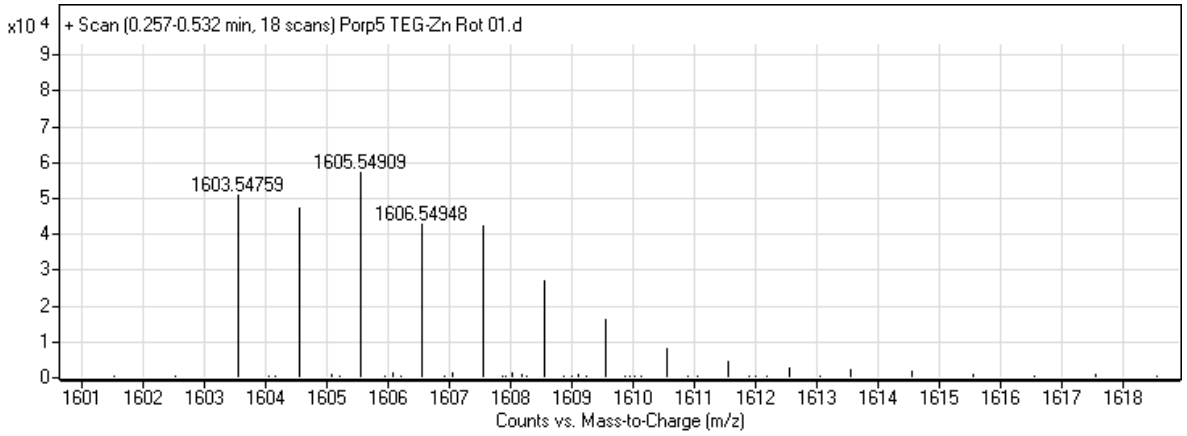

Figure 3.43: ESI spectrum of **19**

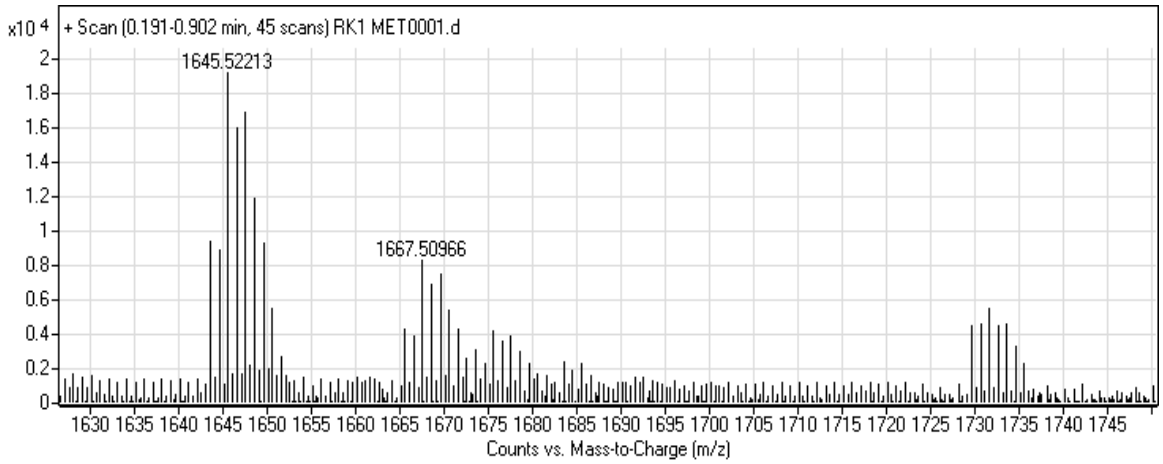

Figure 3.44: ESI spectrum of **20**

3.5.8. Synthesis and Characterization of Poly-porphyrin 25[104]

Poly-porphyrin was synthesized by Stille Coupling discussed above. In this reaction, equal equivalents of boronic ester **7** and porphyrin **24** were used. Despite the TEG groups on the polymer, it was not soluble in both methanol and water. However this polymer is soluble in common organic solvents like chloroform, DCM, THF, DMF and DMSO.

Many peaks appeared in the aromatic region of ^{1}H-NMR of the polymer. These peaks can be assigned to the bithiophene peaks and end group peaks. Downfield shift was observed for both bromo phenyl peaks and dimethoxy phenyl peaks due to introduction of bithiophene. The increase in number of peaks in 130-150 ppm region in ^{13}C-NMR of this polymer proves the coupling between the bithiophene and the porphyrin molecule.

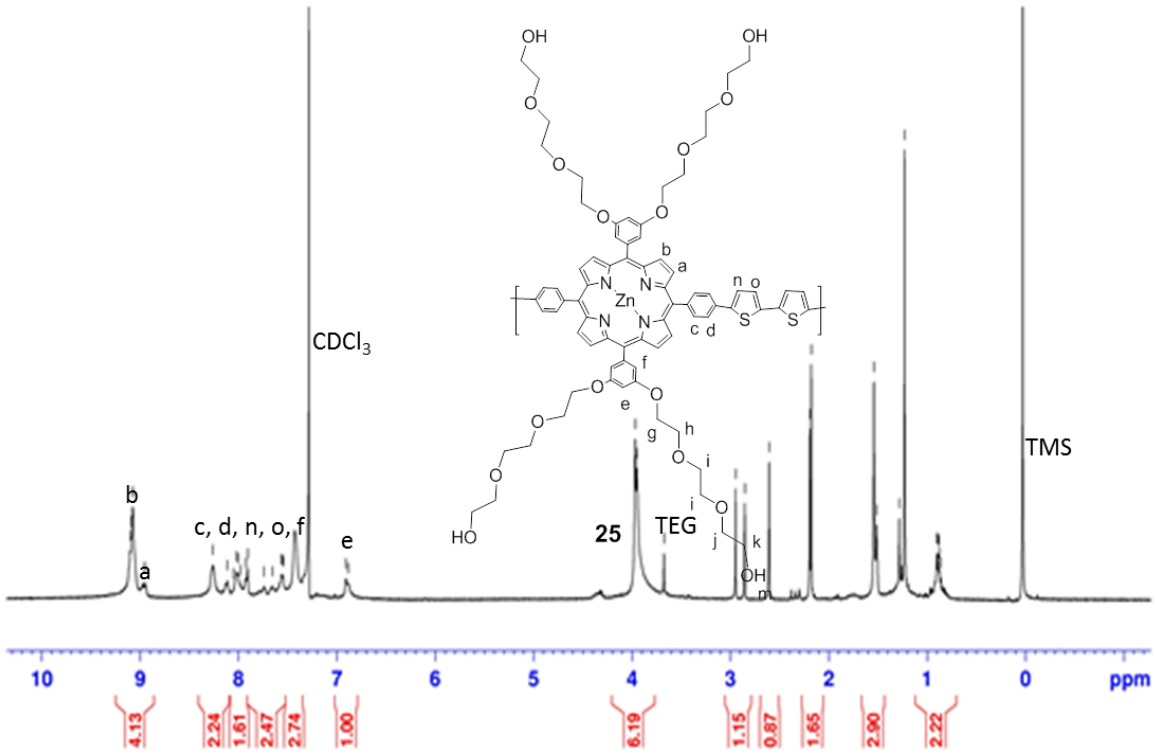

Figure 3.45: ^{1}H-NMR (400 MHz, $CDCl_3$, 25 ^{o}C) spectrum of **25**

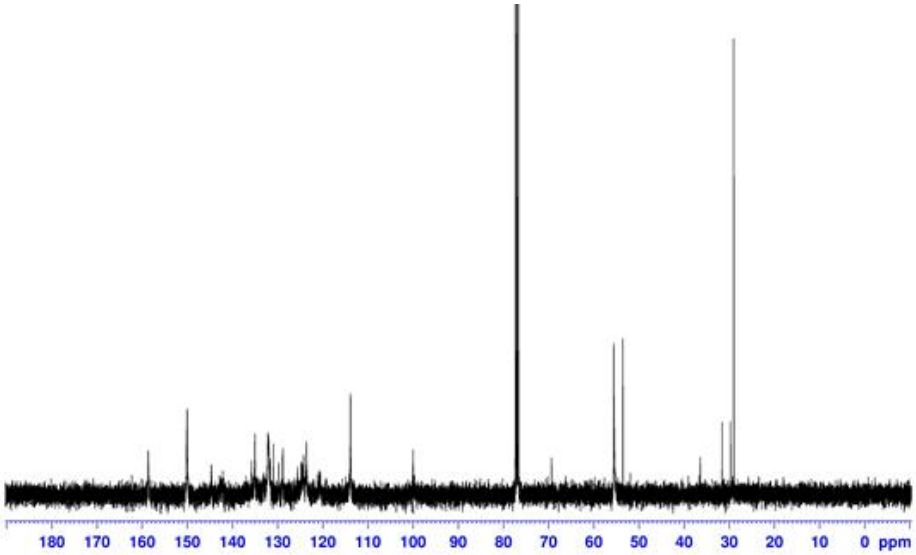

Figure 3.46: ^{13}C-NMR (100 MHz, $CDCl_3$, 25 ^{o}C) spectrum of **20**

The GPC result of this polymer was determined in relative to polystyrene standards in THF. The number average (M_n), weight average (M_w), and viscosity average (M_z) molecular weight of the polymer was found to be 3109, 3549 and 4089 Da respectively and polydispersity index (PDI) of 1.21 corresponding to three repeating units.

3.5.9. Photophysical Properties of Porphyrin Monomers, Oligomers and Polymer

Metal free porphyrins exhibited four Q-bands and one Soret band whereas metalated porphyrins exhibited two Q-bands and one Soret bands. Thus compound **13**, **14**, **15**, **17**, **22**, and **23** showed the same UV-Vis spectrum pattern (Figure 3.47). Similarly, compound **19**, **20**, **18**, **24**, and **25** showed the same UV-Vis spectrum pattern (Figure 3.48). The photophysical properties of final form of the monomers, oligomers and polymer are compared. All the monomers and oligomers have the same peak maxima whereas the polymer **25** has 4 nm red shift (Soret band). This result is expected since coupling reaction doesn't extend the conjugation of porphyrin because the phenyl groups are orthogonal to porphyrin rings.

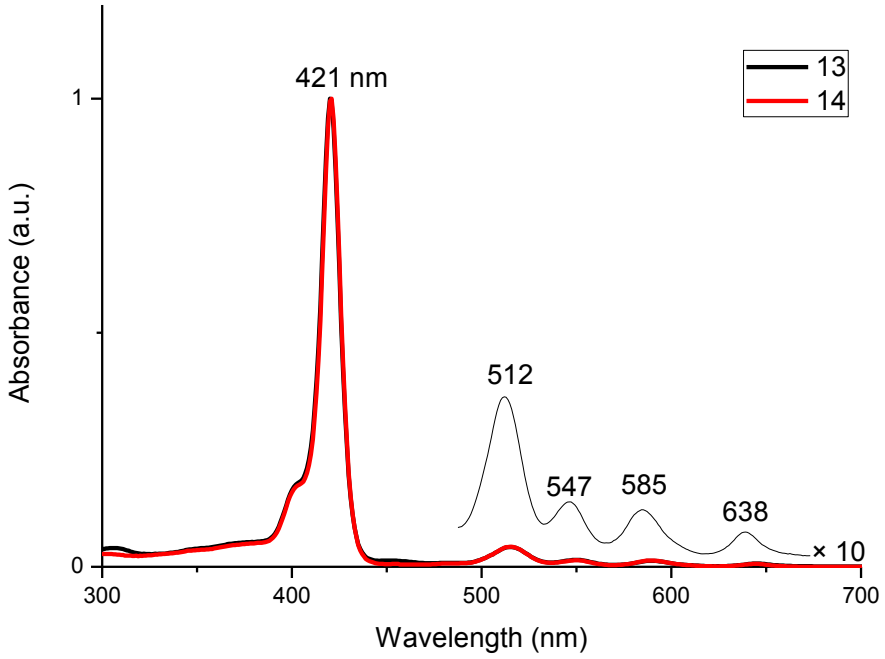

Figure 3.47: Normalized absorbance spectra of **13** and **14** recorded in chloroform

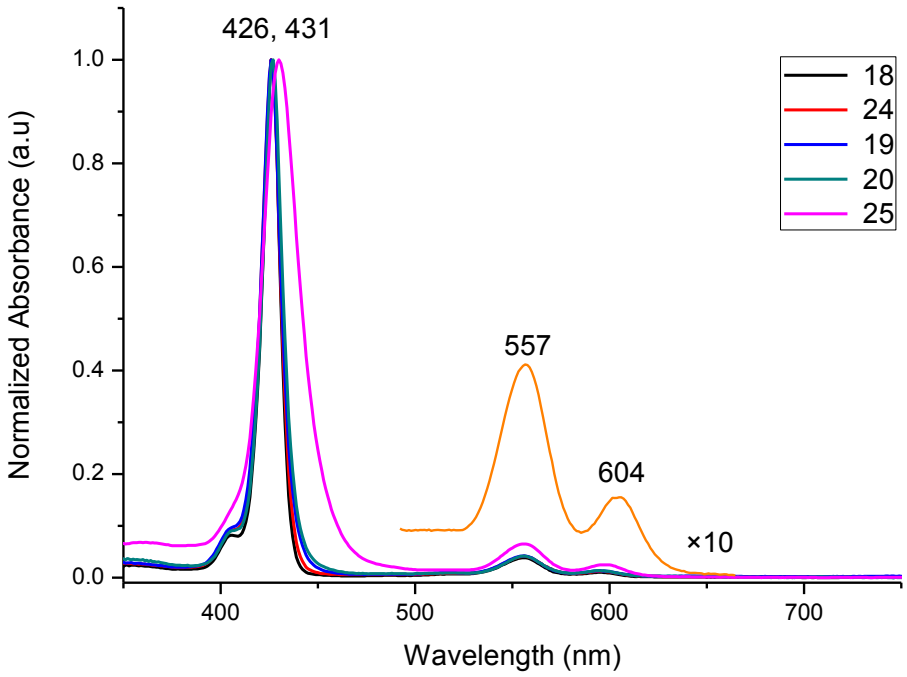

Figure 3.48: Normalized absorbance spectra of **18**, **19**, **20**, **24** and **25** recorded in chloroform.

Using Beer–Lambert law molar absorptivity of Soret bands of these compounds were calculated in both methanol and chloroform. The low molar absorptivity of **18** in chloroform can be attributed to its low solubility in chloroform. Similarly, low molar absorptivity of **24** in methanol is due to its low solubility in methanol. Oligomers **19** and **20** have comparable molar absorptivity in both methanol and chloroform. The molar absorptivity of the oligomers is higher than the molar absorptivity of the monomers because there are two absorbing porphyrin rings per one molecule of the oligomer. Molar absorptivity of the polymer was found to be as high as 5.1×10^5 $cm^{-1}M^{-1}$ per repeat unit which is higher than both oligomers and monomers.

Photoluminescence quantum yield of these compounds in methanol and chloroform was also determined according to the procedure explained in the experimental section. The photoluminescence quantum yields of these compounds were very low. However, compound **19** showed quantum yield greater than tetraphenyl porphyrin standard. The high quantum yield of compound **19** can be attributed to its high rigidity compared to oligomer **20** and polymer **25**. The molar absorptivity and quantum yield data are summarized in Table 3.1.

Table 3.1: Photophysical Data of Porphyrin Monomers, Oligomers and Polymer

	$\boldsymbol{\varepsilon^a}$**($cm^{-1}M^{-1}$)**	$\boldsymbol{\varepsilon^b}$**($cm^{-1}M^{-1}$)**	Φ_f^a	Φ_f^b
18	6.3×10^5	2.7×10^5	9.6	7.1
24	3.5×10^5	6.4×10^5	5.4	5.4
19	1.3×10^6	1.0×10^5	15.4	14.9
20	9.4×10^5	1.0×10^5	6.8	5.7
25	-	5.1×10^{5c}	-	9.7

*a = Methanol (*Quantum yields were measured relative to *Tetraphenyl Porphyrin* Φ_f *=11% in toluene)*

*b = Chloroform (*Quantum yields were measured relative to *Tetraphenyl Porphyrin* Φ_f *=11% in toluene)*

c= Per repeat unit

3.5.10. Singlet Oxygen Generation.

One of the most important properties of sensitizers in photodynamic therapy is their ability to generate singlet oxygen ($^1O_2$) or superoxide (O^{2-}). Generation of singlet oxygen is very crucial because the more singlet oxygen generated the more tumor destruction. To compare the singlet generation ability of the monomers, oligomers and polymer, singlet oxygen generation experiment was conducted. The singlet oxygen generation was measured according to the procedure explained in the experimental section. In a typical experiment, porphyrin in ground state is excited by homemade light source to excited singlet state and then intercrosses to triplet state. The photosensitizer at triplet state transfers its energy to triplet oxygen to form singlet oxygen species. The formation of singlet oxygen species was monitored by the decrease in the absorbance intensity of 1,3-diphenylisobenzofuran (DPBF) over time. The reaction between singlet oxygen and DPBF is a typical Diels-Alder Reaction shown below.

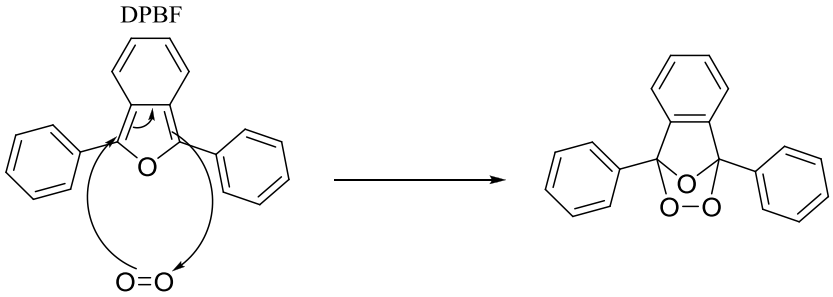

Scheme 3.10: Diels Alder Reaction of DPBF and singlet oxygen

The decrease in absorbance intensity of DPBF with time is shown in Figure 3.49. At the same molar concentration, the decrease in absorbance intensity of DPBF is fastest in the case of the polymer **25** suggesting the polymer is generating more singlet oxygen.

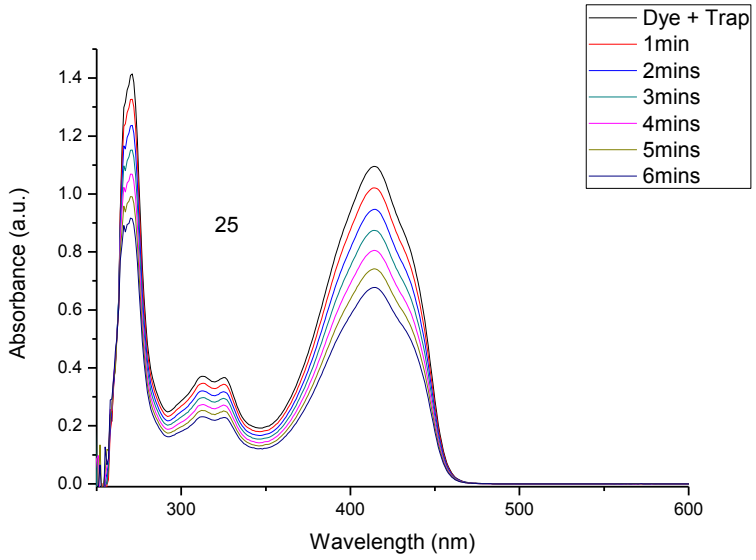

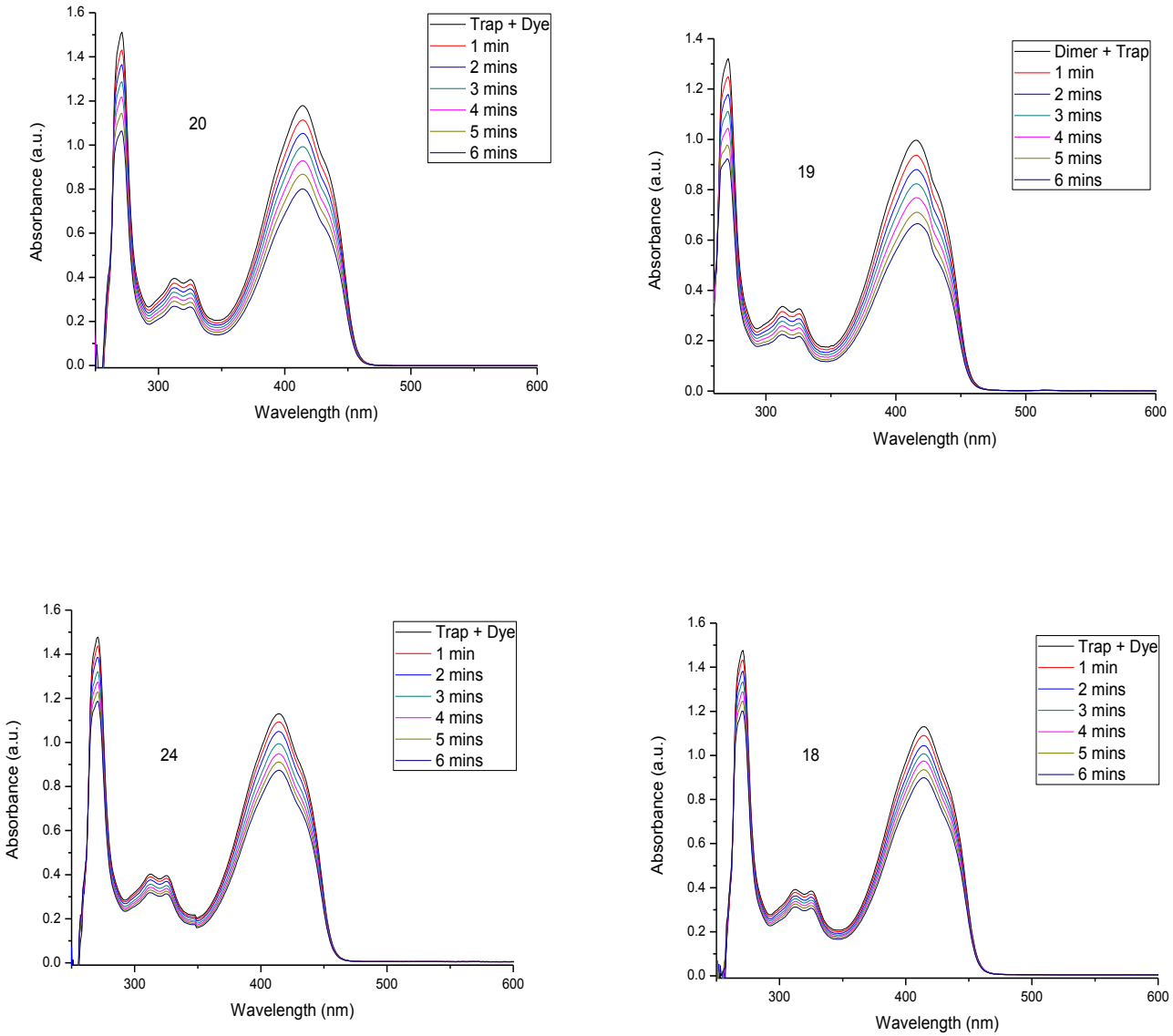

Figure 3.49: Decrease in absorbance intensity of DPBF with time.

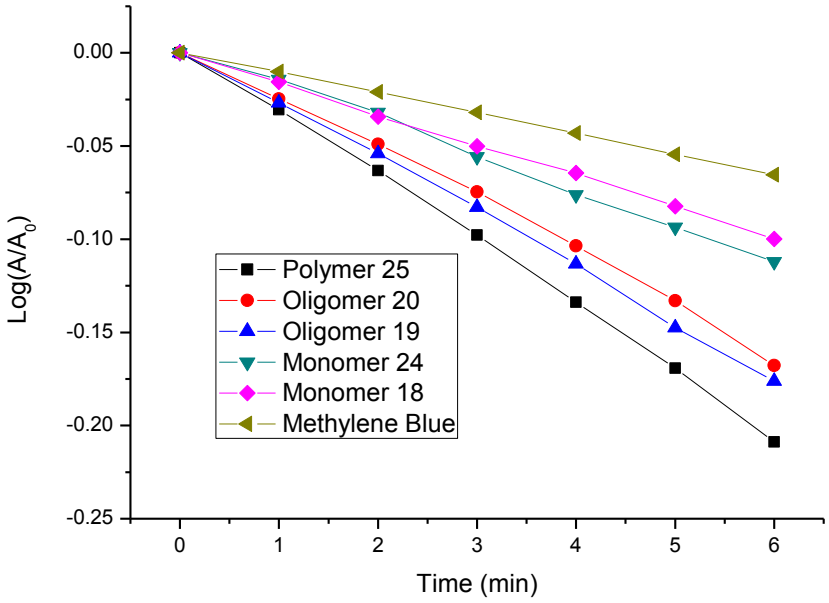

Figure 3.50: Log plot of decrease in absorbance intensity of DPBF with time

To further have a better sight in the singlet oxygen generation of the porphyrin compounds, log vs time plot was driven (Figure 3.50). In this plot, methylene blue, one of the known sensitizers was used as comparison to these compounds. In the above figure, the singlet oxygen generation constant is determined by the slope of the curve. The steepest curve of the polymer suggests its highest singlet oxygen generation constant. The highest singlet oxygen generation of the polymer can be attributed to its highest molar absorptivity. To characterize this data quantitatively, the slopes of the curve are divided with relative to the slope of monomer **18**. The values are tabulated in Table 3.2. All the porphyrin monomers, oligomers and polymer showed higher singlet oxygen generation compared to methylene blue.

Table 3.2: Relative singlet oxygen generation constant

Dye	Methylene Blue	Monomer **18**	Monomer **24**	Oligomer **20**	Oligomer **19**	Polymer **25**
$k_{rel.}$	0.56	1.0	1.17	1.68	1.80	2.11

3.6. SECTION 2: Synthesis and Characterization of Fluorene Monomers, Polymers and Polyrotaxanes

Aim of the Study

The aim of this study is to synthesized fluorene-thiophene based polymers and polyrotaxanes that can have potential application in optoelectronic and biological applications. The fluorene monomers will be functionalized with water soluble ionic pendent groups to solubilize the monomers. The resulting monomers will be coupled with thiophene monomer to obtain water soluble polymers. Finally, thiophene monomer will be encapsulated by cucurbit[7]uril and cucurbit[6]uril before coupling with fluorene monomers as stopper groups. The resulting polyrotaxanes are expected to have better photophysical properties and thermal stability.

The structure of the monomers, oligomers and polyrotaxanes will be characterized by ^{1}H-NMR, ^{13}C-NMR, FT-IR, ESI mass spectroscopy, Elemental Analysis and Size Exclusion Chromatography. The thermal properties of the polymers and polyrotaxanes will be studied by Thermogravimetric Analysis. Electrochemical properties of the polymers and polyrotaxanes will be studied by Cyclic Voltammetry. The photophysical properties of the fluorene-based polymers and polyrotaxanes will be studied with UV-VIS Spectroscopy, Photoluminescence Spectroscopy and Time Resolved Fluorescence Spectroscopy.

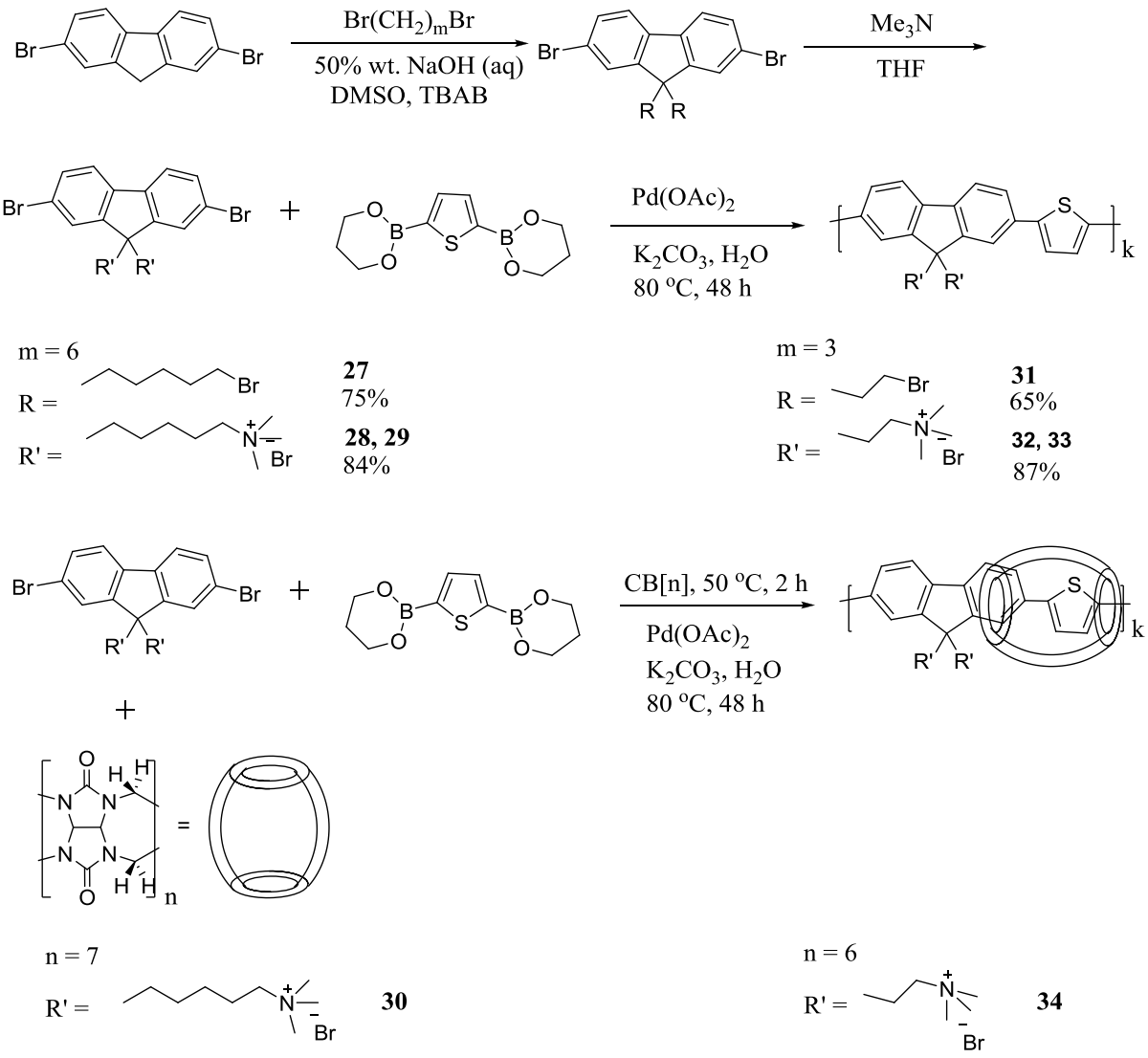

Scheme 3.11: Synthetic pathway of fluorene monomers, polymers and polyrotaxanes.

3.6.1. Synthesis and Characterization of 27 and 31

In the synthesis of **27** and **31**, 1,6-dibromohexane and 1,3-dibromopropane were added in excess respectively to prevent dimer formation and ring formation. The temperature was kept as 25 ^{o}C to prevent elimination reaction. Sodium hydroxide was used as a base to abstract the acidic protons of fluorene monomer. Tetra butyl ammonium bromide was used as phase transfer catalyst to transfer ionic salts into the organic phase. The change in color during the reaction indicated the anion formation and attachment of the alkyl group.

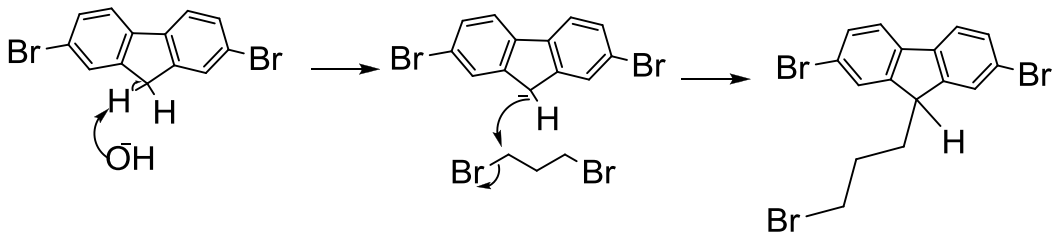

Scheme 3.12: Alkylation of Fluorene monomer

Compound **27** has six different peaks in the aliphatic region of ^{1}H-NMR corresponding to the six different protons on bromo hexyl chain. Similarly there are three different peaks in the aliphatic region of compound **31** ^{1}H-NMR corresponding to the three different protons on bromo propyl chain. Three peaks were observed in aromatic region (two overlapping) of **27** and **31** ^{1}H-NMR corresponding to the three different protons on the aromatic backbone. In ^{13}C-NMR, thirteen different peaks were observed for compound **27** and ten for compound **31**. These results confirmed the structure of both **27** and **31**.

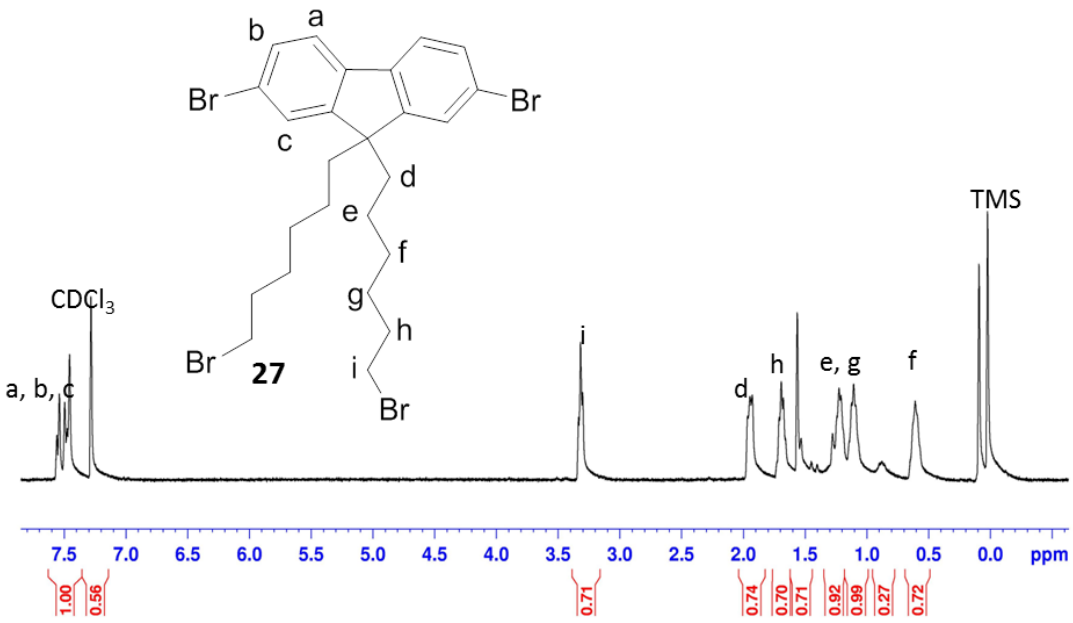

Figure 3.51: ^{1}H-NMR (400 MHz, $CDCl_3$, 25 ^{o}C) spectrum of **27**

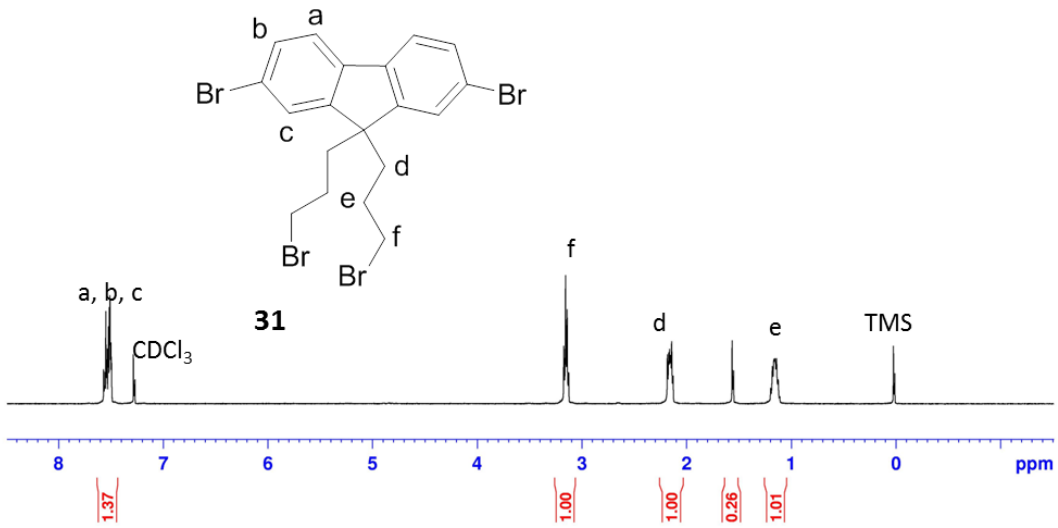

Figure 3.52: ^{1}H-NMR (400 MHz, $CDCl_3$, 25 ^{o}C) spectrum of **31**

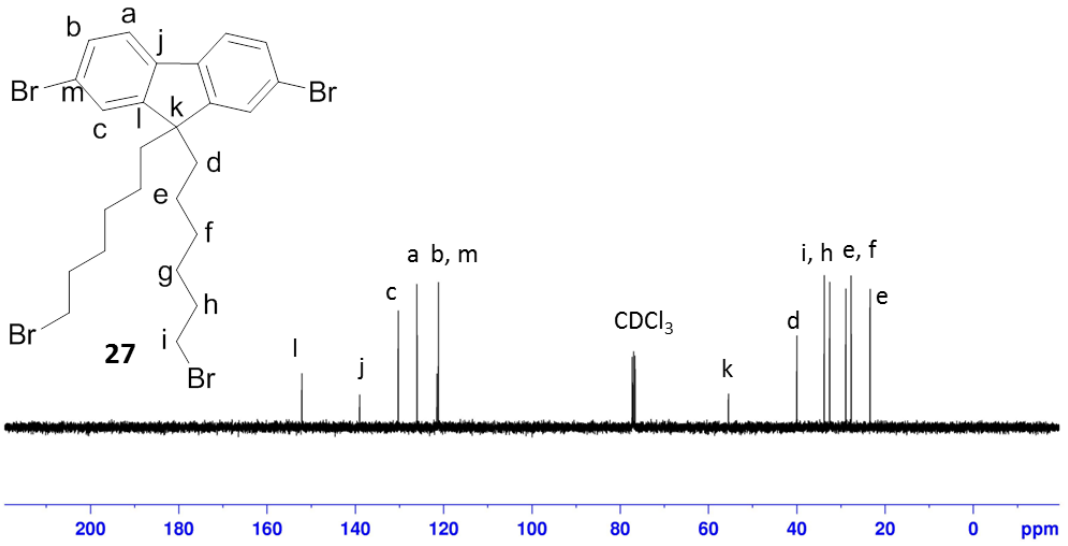

Figure 3.53: ^{13}C-NMR (100 MHz, $CDCl_3$, 25 ^{o}C) spectrum of **27**

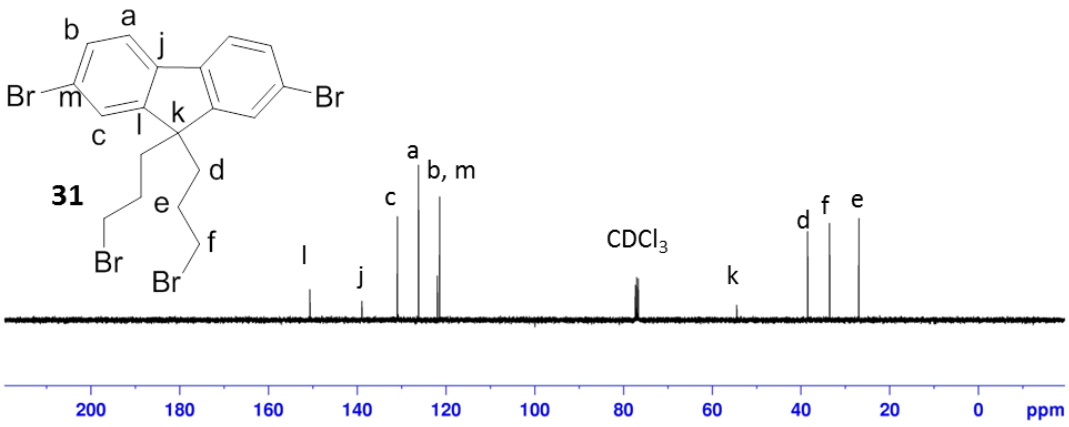

Figure 3.54: ^{13}C-NMR (100 MHz, $CDCl_3$, 25 ^{o}C) spectrum of **31**

Despite our effort to ionize compound **27**, the exact mass to charge ratio was not obtained and elemental analysis had to be used to further characterize this molecule. The mass to charge ratio of compound **31** matches the theoretical value and the elemental analysis result is also in agreement with the calculated value.

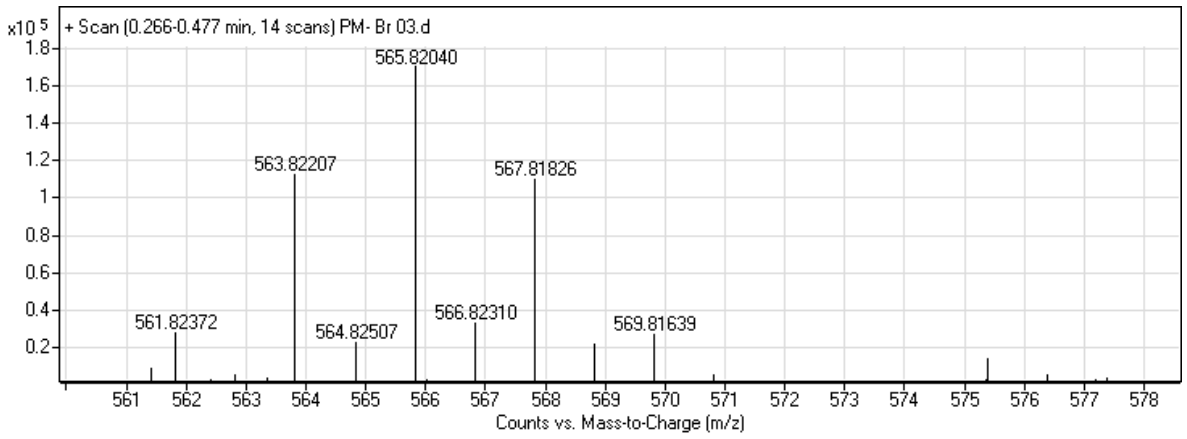

Figure 3.55: ESI spectrum of **31**

3.6.2. Synthesis and Characterization of 28 and 32

To make compound **27** and **31** water soluble, the bromine groups at the alkyl chain terminal were substituted with quaternary amine groups. The reaction involves nucleophilic attack by trimethyl amine group to displace bromide leaving group. Excess trimethyl amine was used to functionalize all the alkyl chains. The reaction was carried out at room temperature and monitored by TLC. The appearance of the dark spot at the baseline and disappearance of the

starting material indicated the completion of the reaction. Both compounds **28** and **32** are water, methanol and ethanol soluble and insoluble in common organic solvents like DCM, THF and chloroform.

The singlet peaks at 2.9 and 2.7 ppm in the ^{1}H-NMR of compound **28** and **32** indicate the presence of trimethyl amine protons. The peaks at 52.5 ppm in the ^{13}C-NMR of compound **28** and **32** further confirmed the trimethyl amine carbons. The $-CH_2$ protons attached to quaternary amine group shifted to 3.0 ppm from 3.4 ppm indicating complete substitution of more electronegative bromine by less electronegative triethyl amine. The integration of all the peaks in ^{1}H-NMR of these compounds also confirmed the exact number of protons.

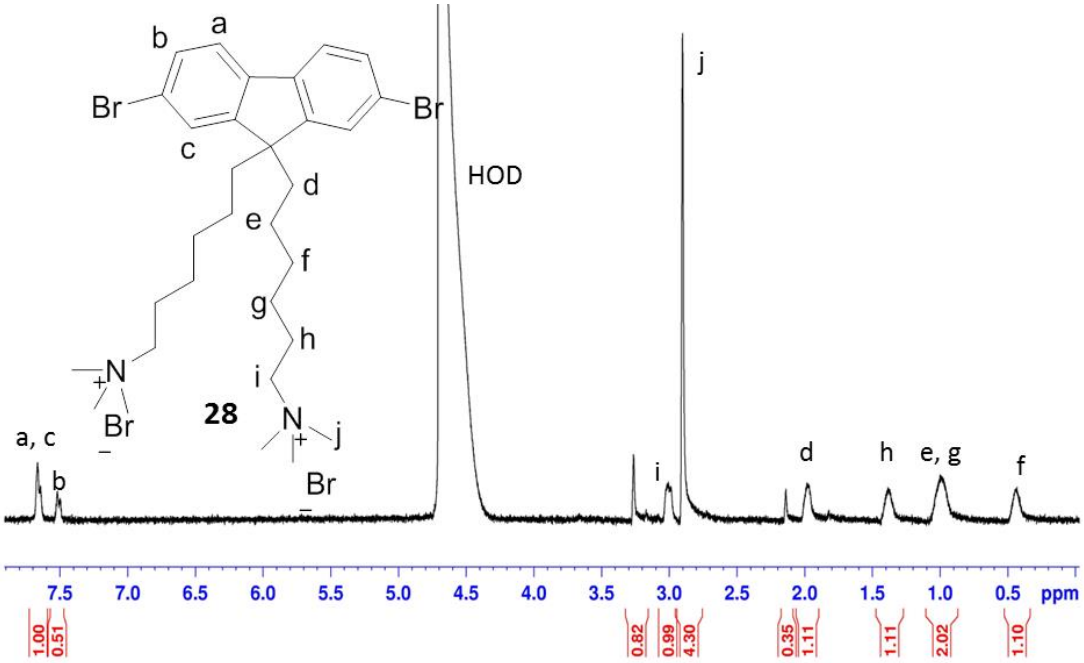

Figure 3.56: ^{1}H-NMR (400 MHz, D_2O, 25 ^{o}C) spectrum of **28**

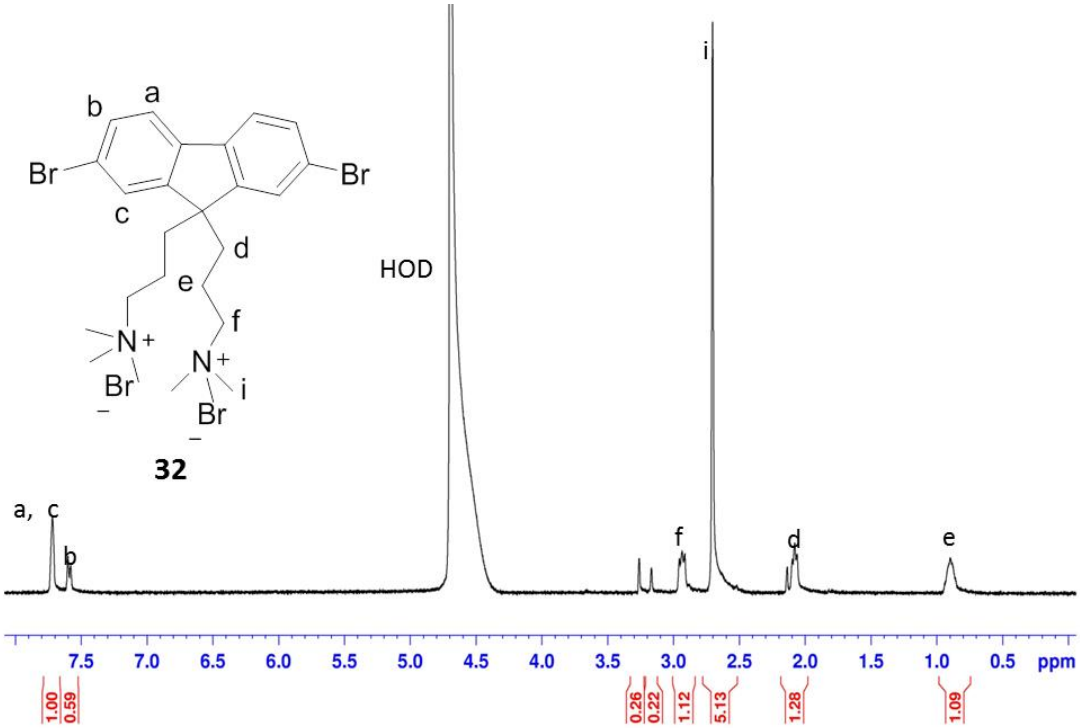

Figure 3.57: ^{1}H-NMR (400 MHz, D_2O, 25 ^{o}C) spectrum of **32**

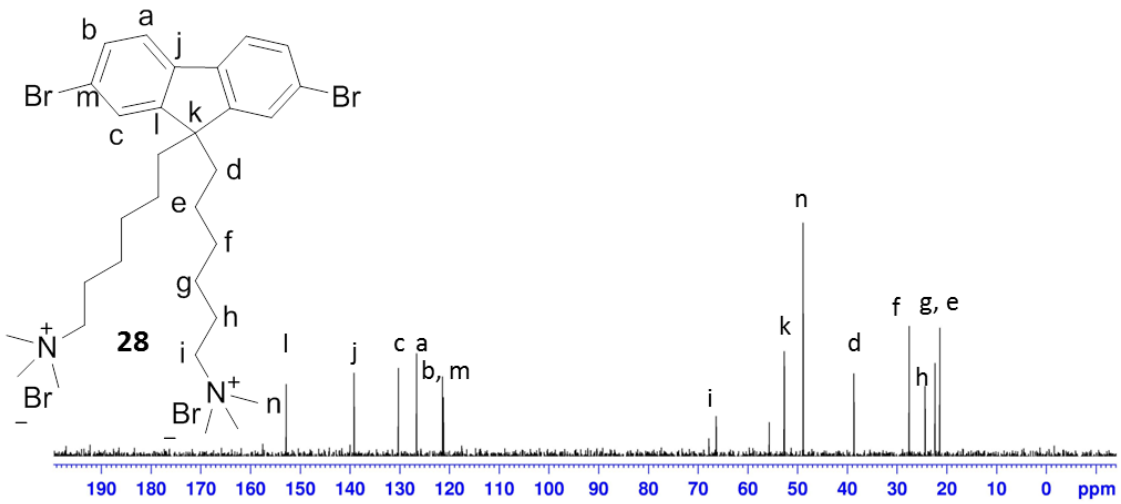

Figure 3.58: ^{13}C-NMR (100 MHz, D_2O, 25 ^{o}C) spectrum of **28**

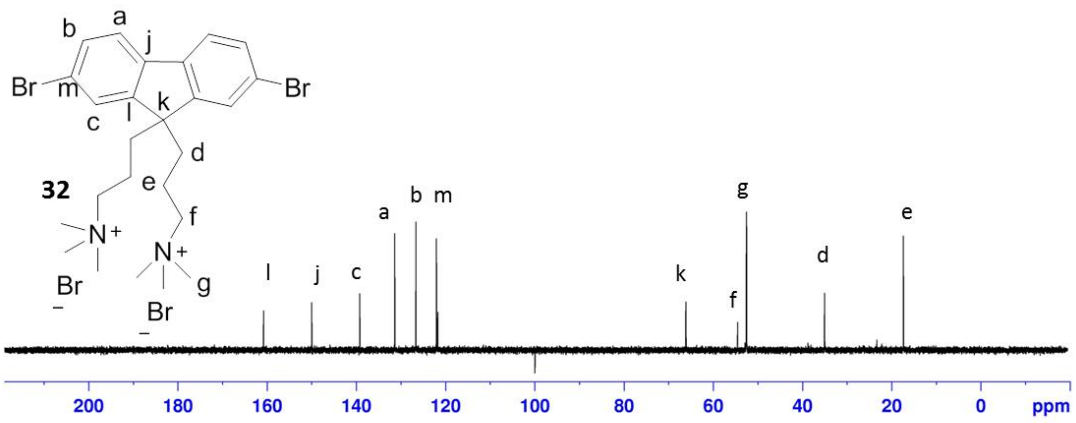

Figure 3.59: ^{13}C-NMR (100 MHz, D_2O, 25 ^oC) spectrum of **32**

The mass to charge ratio of compound **28** and **32** were found as 609 indicating two bromide ions are removed and 603 indicating one bromide ion is removed respectively.

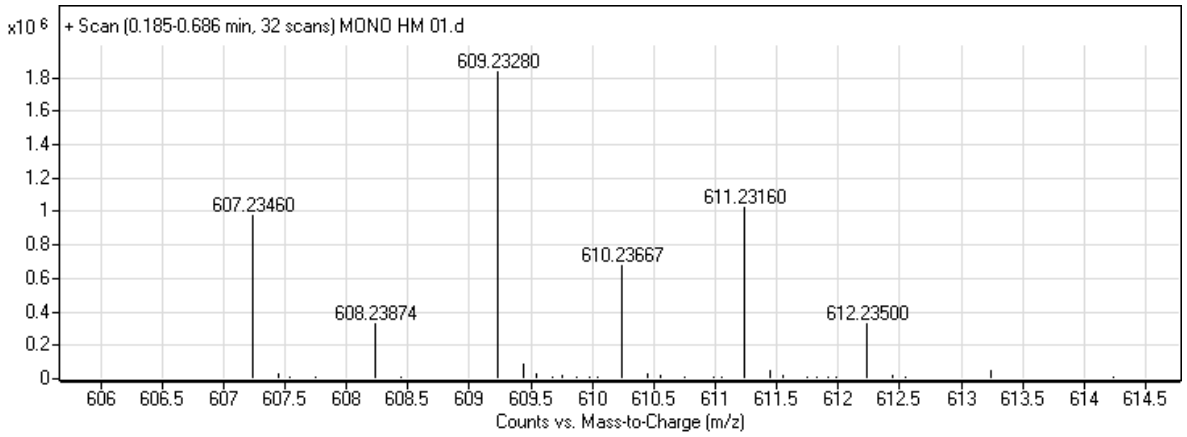

Figure 3.60: ESI spectrum of **28**

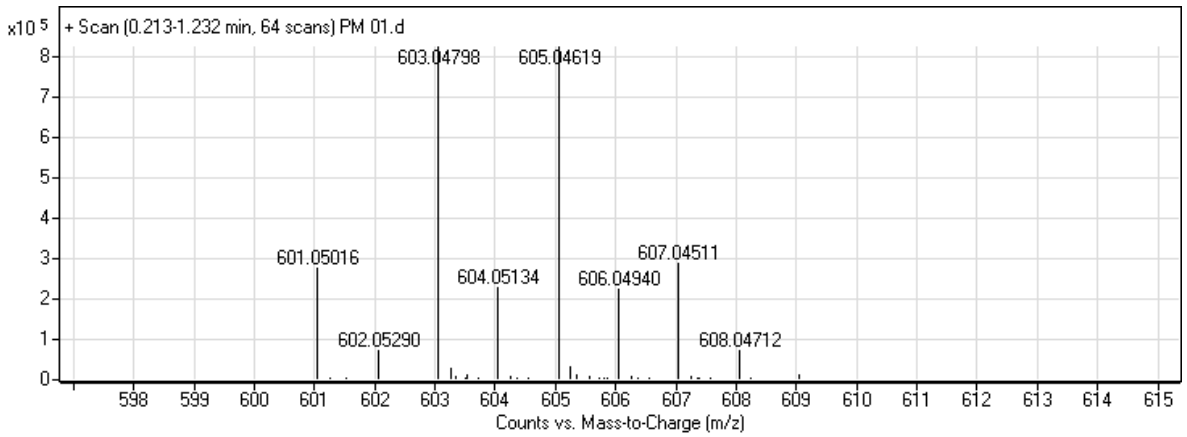

Figure 3.61: ESI spectrum of **32**

3.6.3. Synthesis and Characterization of Polymers 29, 33 and Polyrotaxanes 30, 34[101-103]

The polymers and polyrotaxanes were synthesized using Suzuki Coupling Reaction. Water was used as solvent because all the starting materials are soluble in water. In polymer synthesis, fluorene monomers, 2,5-thiophenediboronic ester **7**, potassium carbonate and Palladium (II) acetate were dissolved in water and the temperature was raised to 80 ^{o}C for 48 hours. In the synthesis of the polyrotaxanes, 2,5-thiophenediboronic ester **7** was first stirred with CB[6] or CB[7] at 50 ^{o}C for two hours to facilitate complexation. Due to hydrophobic effect, the boronic ester **7** will be forced to go inside the hydrophobic cavity of CB[6] or CB[7]. Later on, aqueous solution of potassium carbonate and one equivalent of fluorene monomers were added to the reaction mixture. All the polymers and polyrotaxanes were purified using ultrafiltration with a cut-off filter of 5000 Da. Ultrafiltration is a type of membrane filtration in which pressure is applied to separate high molecular weight molecules from low molecular weight molecules through a semipermeable membrane. The pressure is supplied from a gas cylinder containing inert gas to a vessel containing distilled water. The process can be operated in two modes; gas can be allowed to pass through a cell containing the sample solution to concentrate the solution or by pressurizing the water from the vessel to the cell allowing fresh water to remove low molecular weight molecules. Suspended solids and solutes of high molecular weight are retained in the cell, while water and low molecular weight solutes pass through the membrane (Figure 3.62). The purity of the polymers and polyrotaxanes were monitored by checking the ^{1}H-NMR and ^{13}C-NMR of the filtrate. In the first few hours, CB[n], unreacted monomer and oligomer peaks were observed in ^{1}H-NMR of the polyrotaxanes and polymers. Additionally, the filtrate has absorption maxima at 345 nm showing the presence of oligomers. In the case of polymer **29** and polyrotaxane **30**, no peak was observed in ^{1}H-NMR and no absorbance of the filtrate was observed after two liters of filtrate was collected. However, in the case of polymer **33** and polyrotaxane **34**, five liters of the filtrate had to be collected to get rid of the excess CB[6], unreacted monomer and oligomer. This observation suggests that very less amount of CB[6]

encapsulated thiophene and very short chain polymers were produced.

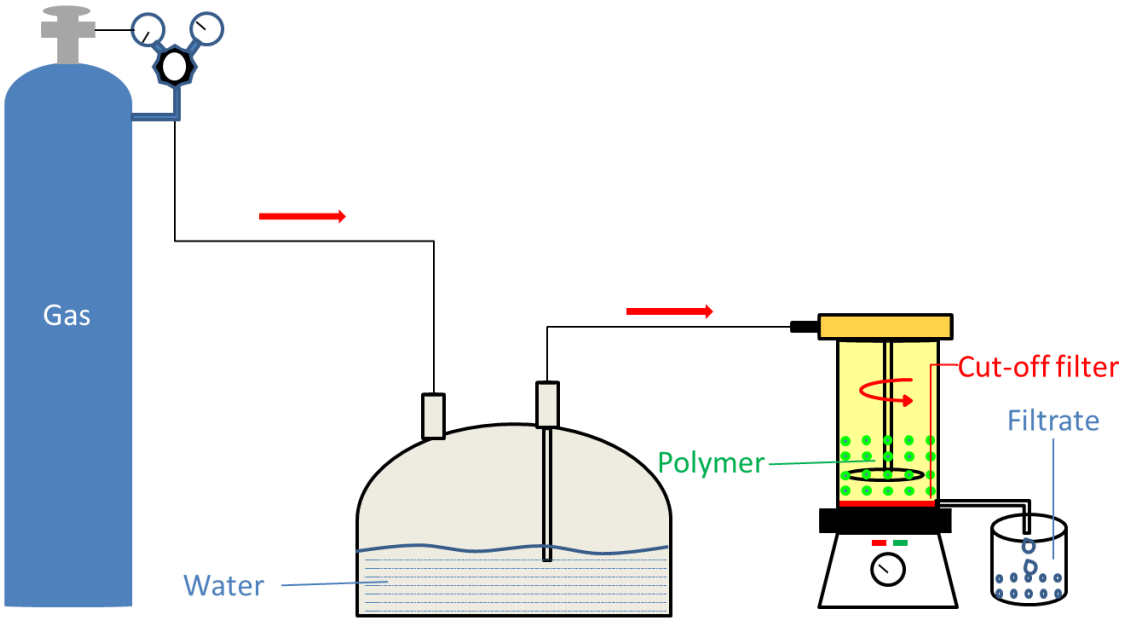

Figure 3.62: Ultrafiltration Set-up

The ^{1}H-NMR of both polymer **29** and polyrotaxane **30** couldn't be resolved because of the aggregation of polymer chains in aqueous media. The ^{1}H-NMR of polyrotaxane **30** is more resolved compared to the parent polymer suggesting less aggregation in the polyrotaxane. This can be attributed to the encapsulation of the aromatic backbone by CB[7]. The broad CB[7] peaks combined with the upfield shift of thiophene peaks in the ^{1}H-NMR of polyrotaxane **30** indicate that the CB[7] is on the backbone of the polymer. The integration value of the thiophene and CB[7] peaks suggest that there is one CB[7] molecule per two repeating unit of the polyrotaxane. In the case of polymer **33** and polyrotaxane **34**, the ^{1}H-NMR is more resolved suggesting less aggregation and low molecular weight polymers. Similarly broad CB[6] peaks were observed in ^{1}H-NMR of polyrotaxane **34**. The integration value of CB[6] peaks was very low and thus no upfield shift of thiophene peak was observed. The low threading efficiency of CB[6] can be attributed to its insolubility in water. The peak at 1735 cm^{-1} in IR spectra of polyrotaxane **30** and **34** confirmed the presence of carbonyl group from CB[7] and CB[6] respectively.

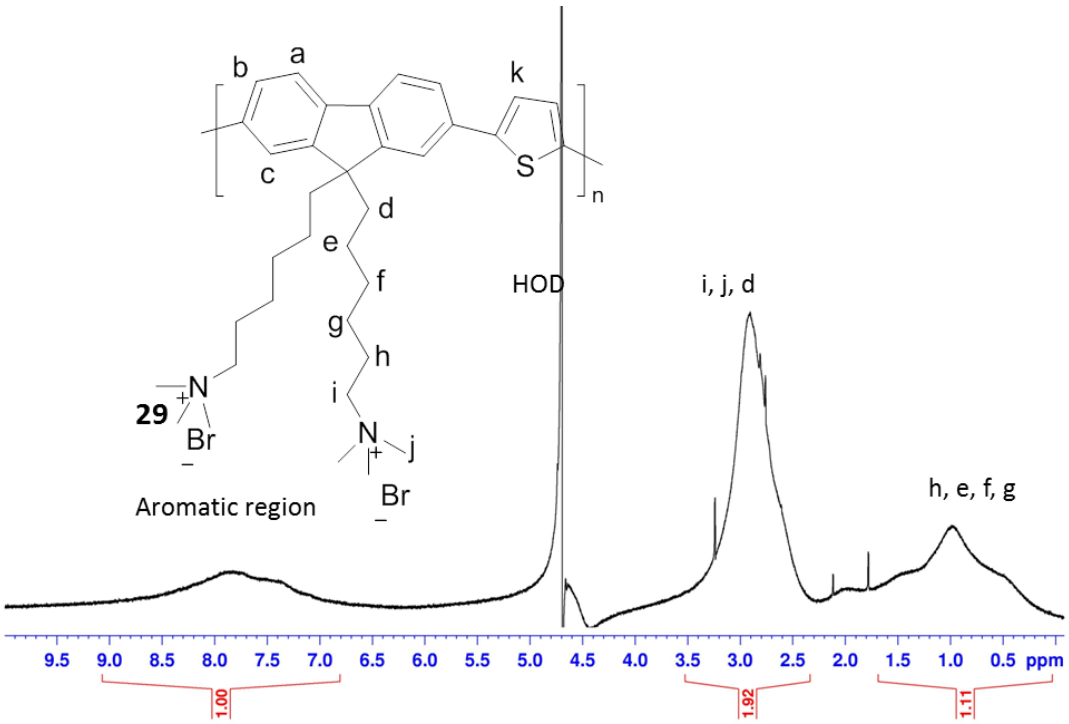

Figure 3.63: ^{1}H-NMR (400 MHz, D_2O, 25 ^{o}C) spectrum of **29**

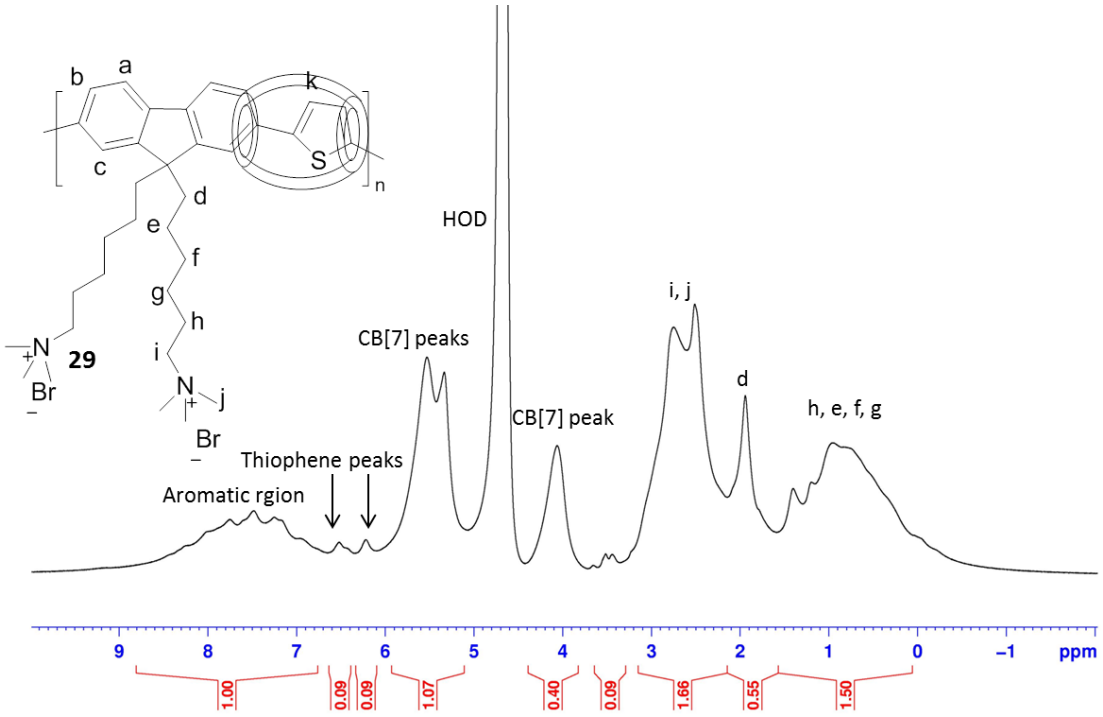

Figure 3.64: ^{1}H-NMR (400 MHz, D_2O, 25 ^{o}C) spectrum of **30**

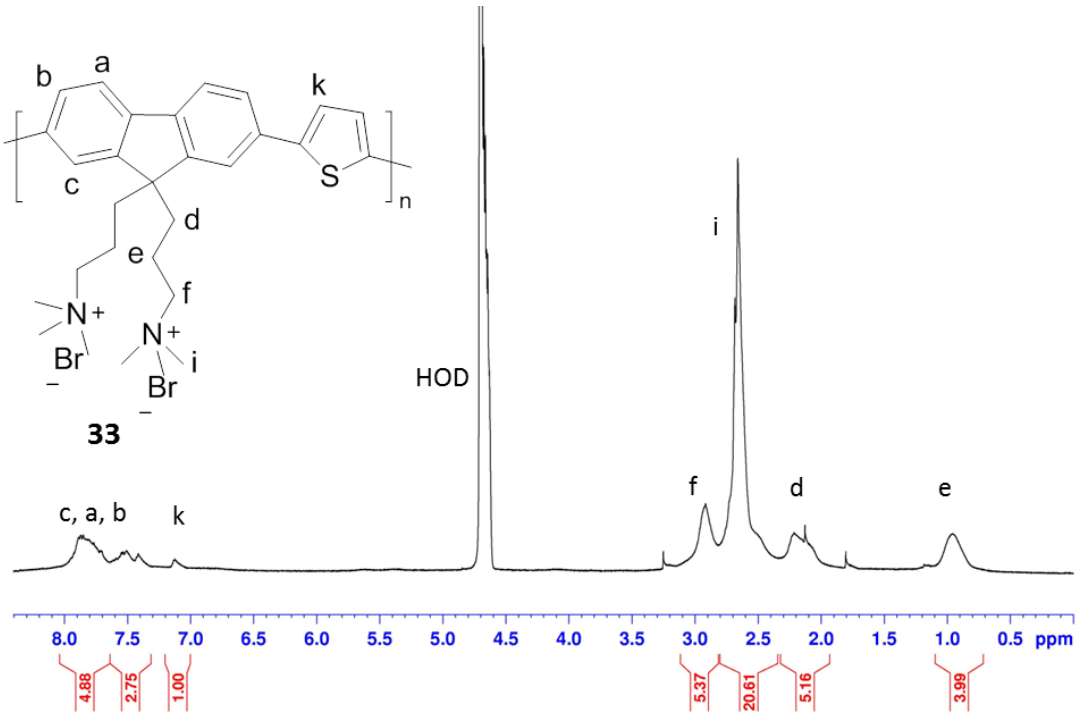

Figure 3.65: ^{1}H-NMR (400 MHz, D_2O, 25 ^{o}C) spectrum of **33**

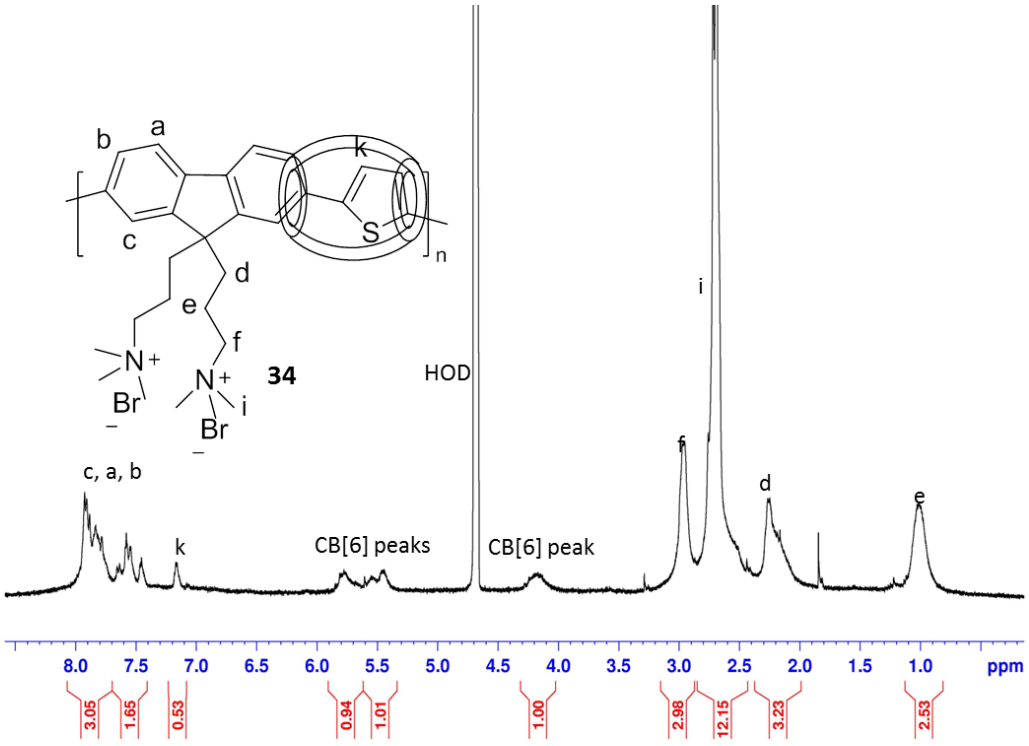

Figure 3.66: ^{1}H-NMR (400 MHz, D_2O, 25 ^{o}C) spectrum of **34**

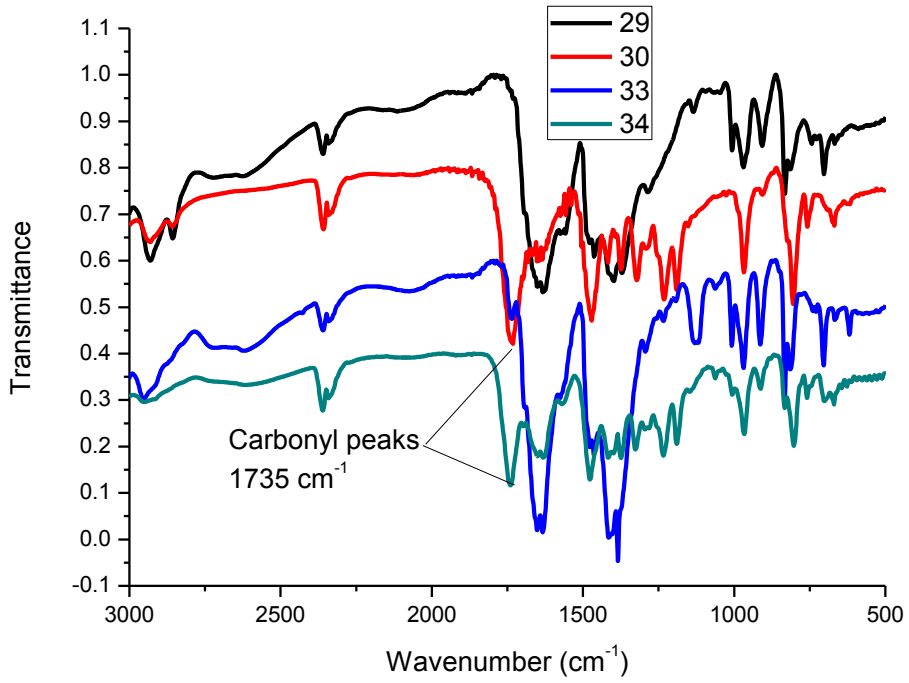

Figure 3.67: FT-IR spectra of **29**, **30**, **33** and **34**

3.6.4. Thermal Properties of polymers and polyrotaxanes

The thermal stability of the polymers and polyrotaxanes in nitrogen was evaluated by thermogravimetric analysis (TGA). About 60% weight loss was observed at 450 ^{o}C for polyrotaxane **30** and about 75% weight loss for polymer **29** at the same temperature. This is at least in part due to the protection provided by the rigid cucurbituril on the aromatic backbone of the polymer. In contrast, the thermal stability of polymer **33** is higher than polyrotaxane **34**. There is about 50% weight loss at 450 ^{o}C for polymer **33** and about 70% weight loss for polyrotaxane **34** at the same temperature. This can be attributed to the low threading efficiency of CB[6]. The TGA data are shown in Figure 3.68 and Figure 3.69.

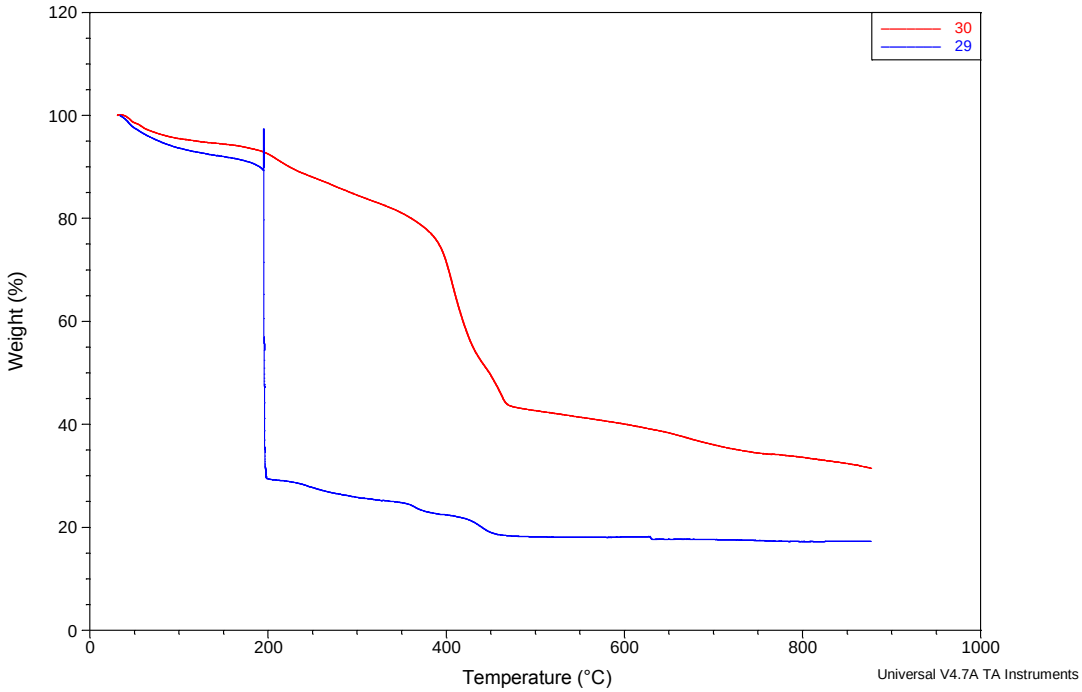

Figure 3.68: Thermogravimetric analysis of **29** and **30**

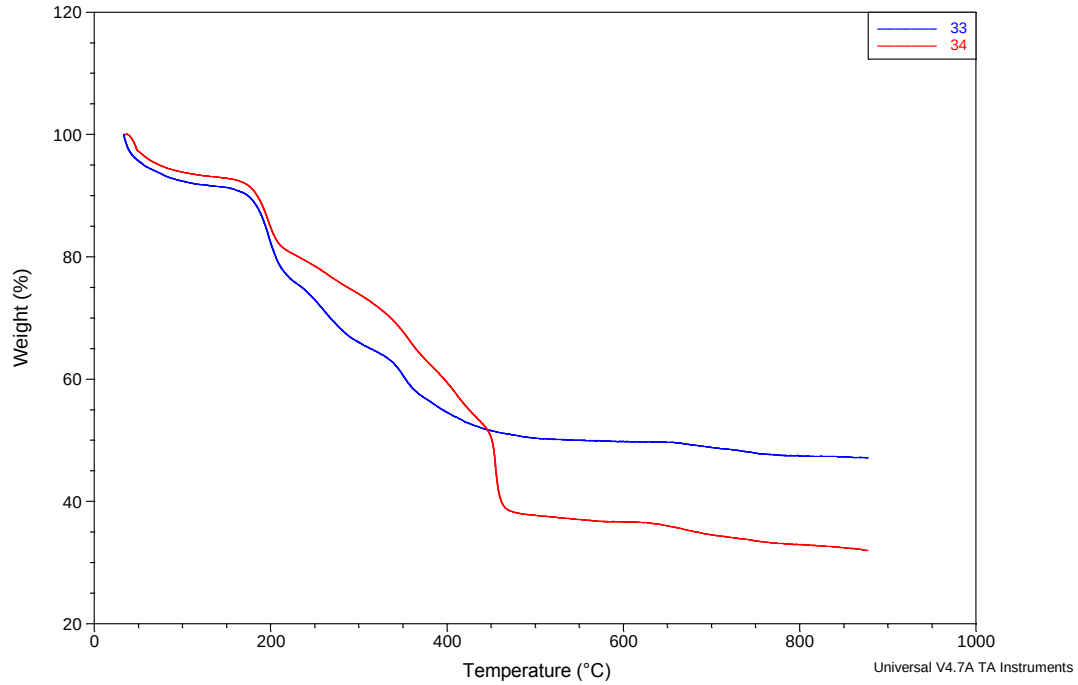

Figure 3.69: Thermogravimetric analysis of **33** and **34**

3.6.5. Electrochemical Properties of Polymers and Polyrotaxanes

Electrochemical properties of the polymers and polyrotaxanes were studied with cyclic voltammetry. Polymer **29** and polyrotaxane **30** have almost the same HOMO energy level (-5.25 and -5.28eV) but differ with 0.07ev in LUMO energy level (-2.77 vs -2.70 eV) respectively. This suggests that **29** can better be used as hole transporting materials and **30** as emission layer materials. Polymer **33** showed lower HOMO energy level (-5.15eV) and LUMO level of (-2.63eV). This also suggests that **33** can be the better used as emission layer materials. Despite all our effort we couldn't form film of **34** on the Pt electrode and thus we couldn't obtain the electrochemical data of **34**.

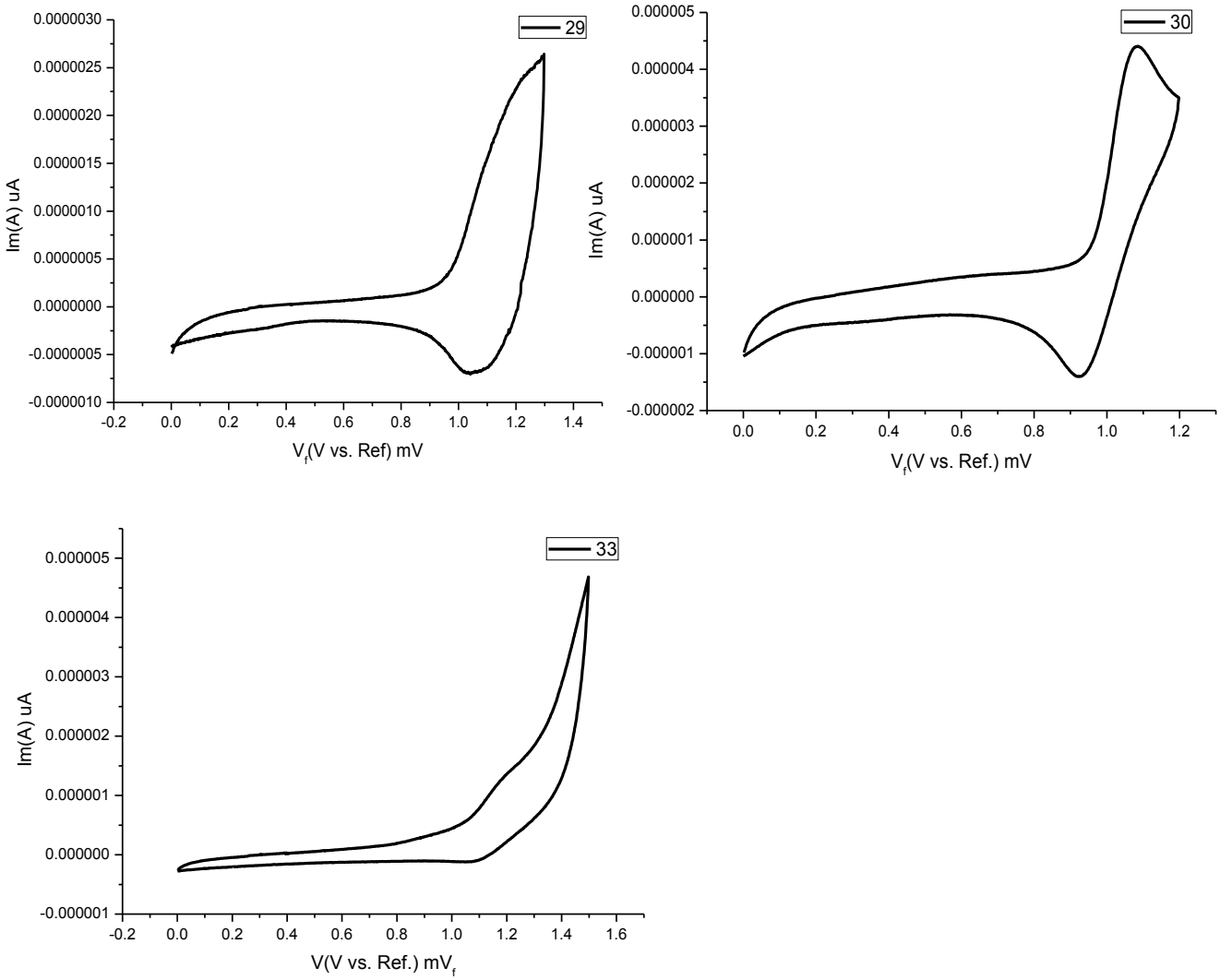

Figure 3.70: Cyclic voltammetry curve **29**, **30**, and **33**

Sample calculation:

The wavelength of polymers is determined from their absorption spectra as shown below.

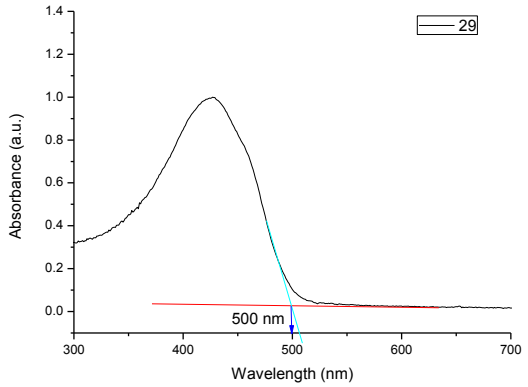

The wavelength is used to calculate the bandgap of the polymers as shown below.

$$E = \frac{hc}{\lambda} = \frac{4.135\times10^{-15}\ \text{eV.s}\times2.998\times10^{17}\ \text{nm}s^{-1}}{500\ \text{nm}} = 2.48\text{eV}$$

E = Bandgap, h = Planck constant, c= speed of light, λ = wavelength.

The HOMO level is determined relative to Ferrocene HOMO level (0.40 V, 4.80eV). The onset oxidation of the polymers is determined from the voltammogram of the polymers shown below.

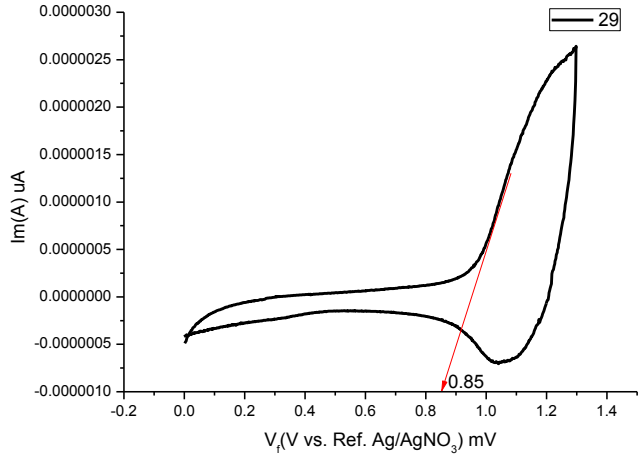

HOMO (V) = 0.85 – 0.40 = 0.45 V

HOMO (eV) = 4.80 + 0.45 = 5.25 eV

E_g = HOMO – LUMO, LUMO = HOMO- E_g, LUMO = 5.25 – 2.48 = 2.77 eV.

Table 3.3: Summary of the electrochemical data of **29**, **30**, **33** and **34**

	Eg	HOMO	LUMO
29	2.48eV	-5.25eV	-2.77eV
30	2.58eV	-5.28eV	-2.70eV
33	2.52eV	-5.15eV	-2.63eV
34	2.60eV		

3.6.6. Photophysical Properties of Polymers and Polyrotaxanes

The polymers are dark greenish solid materials and polyrotaxanes are brownish solid materials. Both polymers and polyrotaxanes are green emitting materials as shown in Figure 3.71.

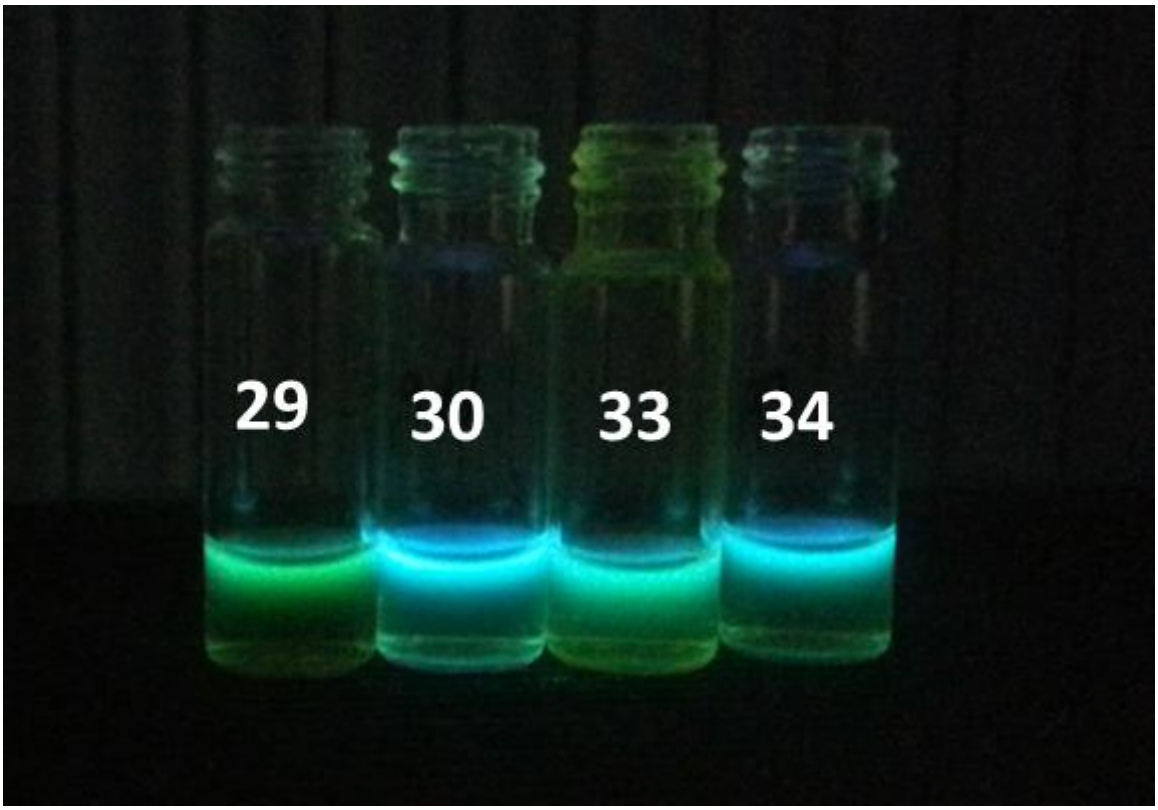

Figure 3.71: Polymers and polyrotaxanes in aqueous solution under UV light

The absorbance and photoluminescence spectra for these compounds were measured in aqueous media. Blue shift was observed in the absorption and fluorescence maxima of **30** and **34** with respect to **29** and **33** respectively (Figure 3.72). Fluorescence was observed in solid state of these compounds revealing that these compounds can be used for organic light

emitting diodes. Similar to solution state fluorescence spectra, blue shift was also observed in the solid state fluorescence maxima of **30** and **34** with respect to **29** and **33** respectively (Figure 3.73). In both **30** and **34**, great enhancement in both quantum yield efficiency and molar absorptivity was observed compared to **29** and **33**, respectively. The quantum yield efficiency and molar absorptivity of **30** in water was found to be 0.46 and 86500 $M^{-1}cm^{-1}$ compared to 0.10 and 6300$M^{-1}cm^{-1}$ for **29**. Similarly the quantum yield efficiency and molar absorptivity of **34** in water was found to be 0.55 and 23500 $M^{-1}cm^{-1}$ compared to 0.35 and 1300$M^{-1}cm^{-1}$ for **33**. This enhancement could be attributed to the reduction of $\pi - \pi$ interaction between the polymer chains. The enhancement of quantum yield and molar absorptivity of **34** is less compared to **30** because less thiophene was encapsulated by CB[6] in **34**.

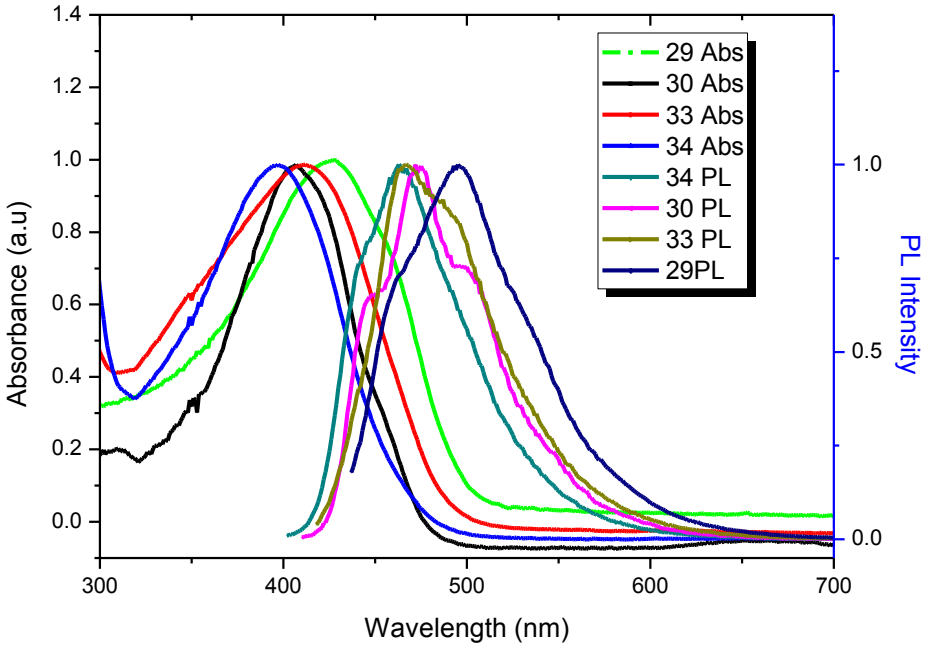

Figure 3.72: Absorbance and Photoluminescence spectra of **29**, **30**, **33** and **34** recorded in water.

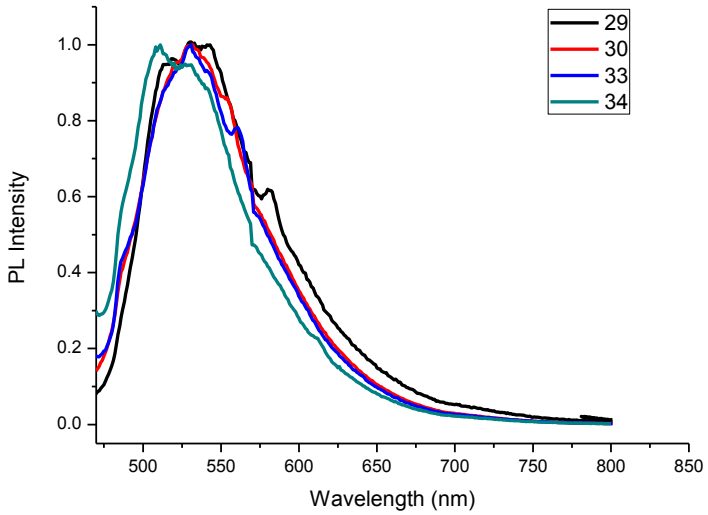

Figure 3.73: Fluorescence spectra of **29**, **30**, **33** and **34** recorded on quartz.

We checked the fluorescence kinetics of the polymers via time resolved fluorescence spectroscopy. Fluorescence lifetime of **29** and **33** are 0.86 and 1.385 ns in solution phase. When these are drop casted on quartz substrates, the fluorescence lifetimes decrease down to 36 and 161 ps for **29** and **33**, respectively. On the other hand, polyrotaxanes **30** and **34** show much longer fluorescence lifetime in their solid films (559 and 681 ps) as compared to their solutions (1.112 and 1.145 ns). This makes them interesting for various applications including organic light emitting diodes (OLEDs). From Figure 3.74, Figure 3.75 and Table 3.4, **30** showed increased of the fluorescence lifetime in both aqueous media and solid state compared to **29**. However, there is no much difference in life time of **34** and **33**. This can be explained by the previous argument that the number of encapsulated thiophene is very less.

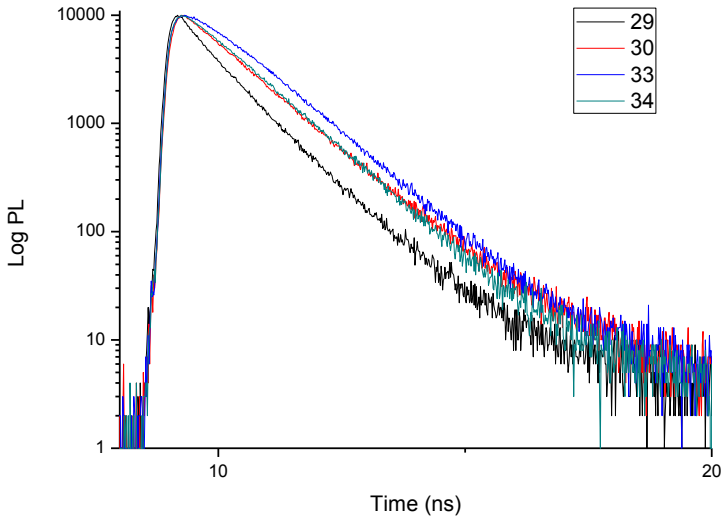

Figure 3.74: Fluorescence life time of **29**, **30**, **33** and **34** in aqueous media.

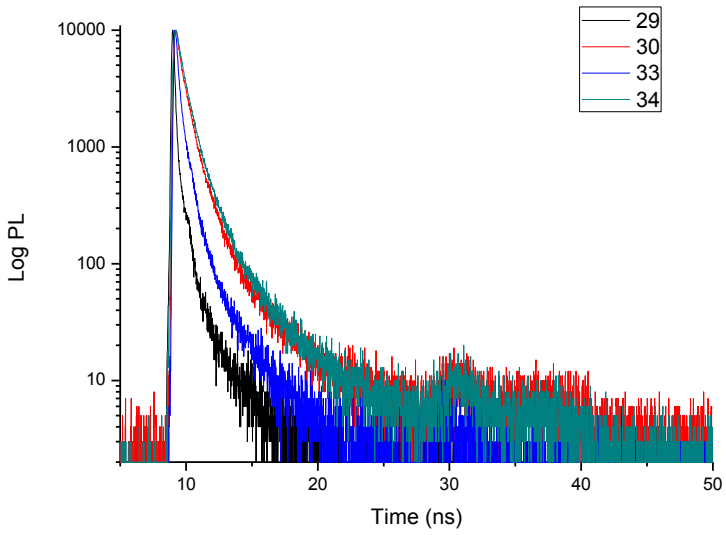

Figure 3.75: Fluorescence life time of **29**, **30**, **33** and **34** in solid state

Table 3.4: Photophysical properties of **29**, **30**, **33** and **34**

	$\lambda^{a}_{max,solution}(nm)$		$\lambda^{b}_{max,film}(nm)$	Φ^{c}_{f}	$\varepsilon^{d}(cmM)^{-1}$	$\mu(cmM)^{-1}$	$\tau^{a}_{solution}(ns)$	$\tau^{b}_{film}(ns)$
	UV	PL	PL					
29	427	501	541	0.11	6563	656.3	0.860	0.036
30	407	474	532	0.46	86294	39696	1.112	0.559
33	413	465	528	0.35	28376	9932	1.385	0.161
34	400	463	510	0.55	42611	23436	1.145	0.681

a = Recorded in aqueous media
b = Recorded on quartz
c = Quantum yields were measured relative to quinine sulfate 0.1 M H_2SO_4 (Φ_f = 55%).
d = Per repeat unit
Φ = Fluorescence quantum yield
ε = Molar absorptivity
μ = Brightness = $\Phi \times \varepsilon$
τ = Fluorescence life time

3.7. Fabrication and Characterization of PLED

All solution processed OLEDs are fabricated as described by the experimental section. The devices emitted white light owing to the emission of the polymers in the green-yellow spectral range. Poly-TPD, which is employed as the hole transport layer, facilitates the blue emission from the devices; therefore, we achieve white light. Figure 3.77 shows the electroluminescence spectra of the OLEDs that employ **29**, **30** and **33**. One of the problems encountered in fabricating these devices was depositing the polymers and polyrotaxanes on glass substrate. Despite all our effort we couldn't form smooth thin film layer of the polymers and polyrotaxanes and thus we couldn't compare the device efficiency based on polymers and their polyrotaxane counterparts. The brightness and stability of the devices fabricated by **33** is higher as compared to those fabricated by using **29** and **30**. In addition, the turn on voltage of the device based on **33** is much lower than those of the device based on **29** and **30**. The electroluminescence spectrum of **34** couldn't be collected due to poor film forming of **34**.

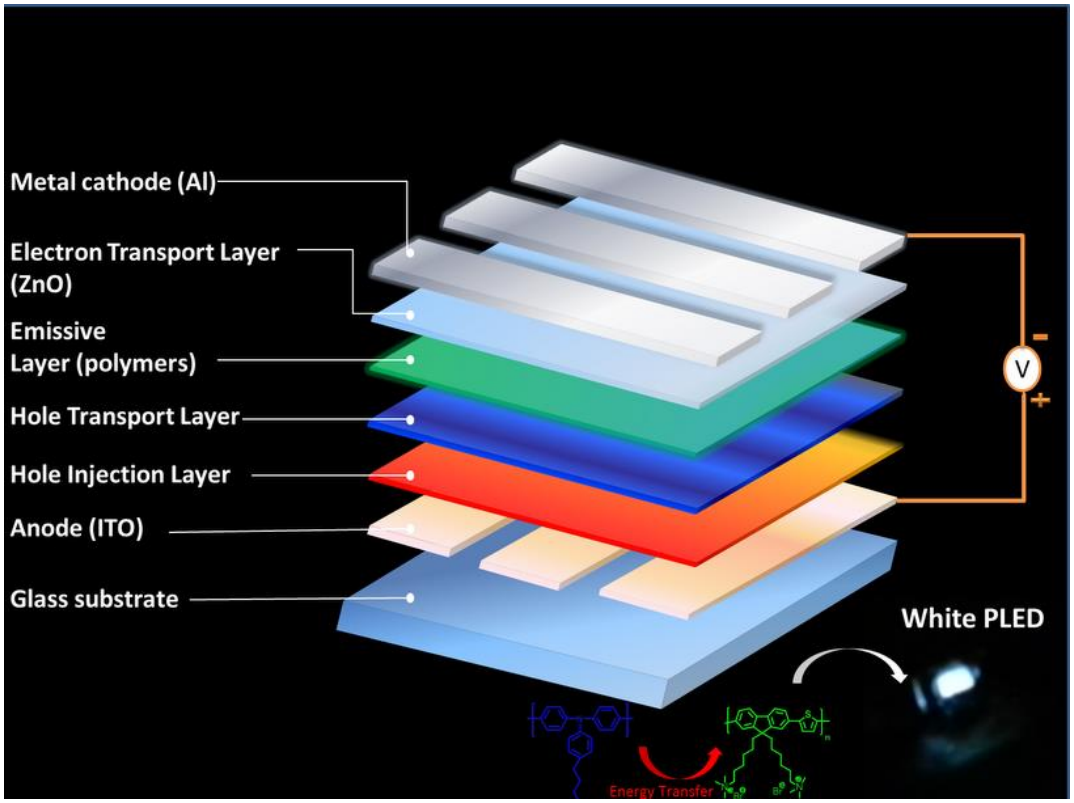

Figure 3.76: Design of PLED fabrication based on **29**, **30**, **33** and **34**

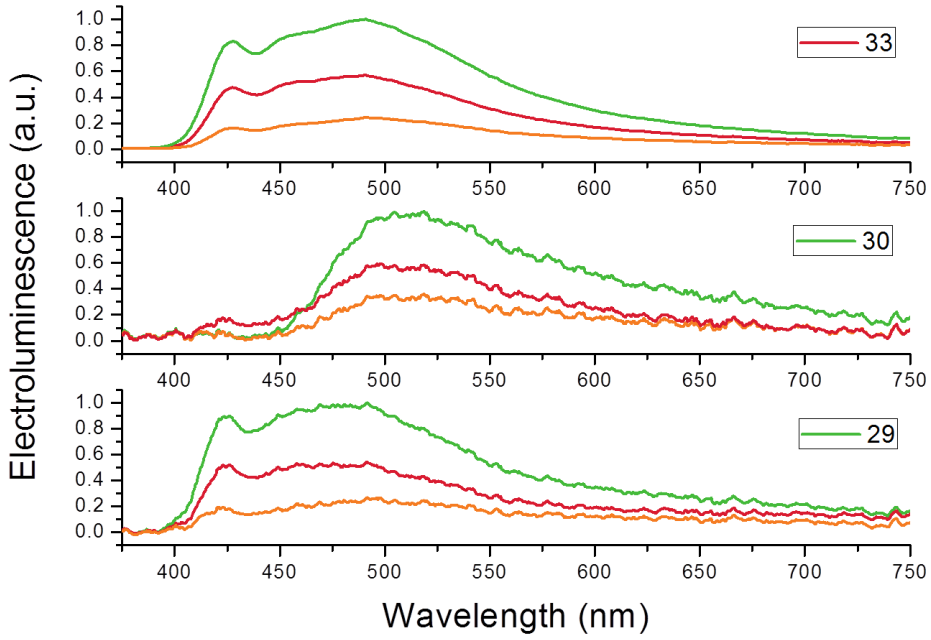

Figure 3.77: Electroluminescence spectra of **29**, **30** and **33** based PLED

Chapter 4 CONCLUSION

Porphyrin and fluorene based monomers, oligomers, polymers and polyrotaxanes that have potential applications in the fields of photodynamic therapy and polymer light emitting diode have been successfully synthesized and characterized.

Porphyrin monomers were first synthesized and functionalized with water soluble groups to improve their water solubility. The functionalized monomers were coupled with thiophene monomer to obtain porphyrin oligomers and polymer. The sulfur atom on thiophene enhanced the singlet oxygen generation through heavy atom effect. There is no significant shift observed in the absorbance spectra between the monomers, oligomers and polymer because the phenyl group on porphyrin ring is orthogonal to the ring. Molar absorptivity of the polymer (Soret band) in chloroform was found to be higher than that of monomers and oligomers. However, the photoluminescence quantum yield of the polymer was found to be lower than that of oligomer **19**. At the same molar concentration, the singlet oxygen generation of porphyrin polymer was found to be higher than that of monomers and oligomers. Although these compounds are not soluble in water, which is one of the conditions for photodynamic application, they give idea about their ability to generate singlet oxygen.

In the second part, fluorene monomer was functionalized with 1,3-dibromo propane and 1,6-dibromo hexane. Later, trimethyl amine was used to substitute the terminal bromide groups to solubilize the fluorene monomers. Then these monomers were coupled with thiophene monomer to obtain fluorene based polymers. The polymer based on hexyl amine pendent was found to have higher molecular weight compared to the one with propyl amine pendent groups. The solubility of these polymers in aqueous media is comparable. Polyrotaxane versions of these polymers were also synthesized. The monomer based on hexyl amine pendent group was used to synthesize polyrotaxane based on CB[7] and the monomer based on propyl amine pendent group was used to synthesize polyrotaxane based on CB[6]. These polyrotaxanes especially polyrotaxane based on CB[7] showed different properties compared to the parent polymer. For example, the solid state color of the polyrotaxanes is brownish yellow while the color of the polymers is dark greenish. Blue shift was observed in the absorbance, solution state fluorescence and solid state fluorescence of the polyrotaxanes compered to their parent polymers. Molar absorptivity, fluorescence quantum yield, life time and thermal stability of the polyrotaxanes were all increased compared to their parent polymers. From the electroluminescence data, these materials showed potential application in

polymer light emitting diodes. Due to the poor film forming properties of these materials, their performance in polymer light emitting diodes could not be compared.

Chapter 5 FUTURE WORKS

One of the problems encountered in this study was the solubility of porphyrin based monomer, oligomers and polymers in water. We selected the polymer because it generates the highest singlet oxygen and further functionalized it with glucose. The solubility of the polymer in water was not enhanced significantly, thus we converted the polymer solution into nanoparticles. We were excited to see no aggregation of these nanoparticles which is commonly encountered in porphyrin nanoparticles. Additionally, these nanoparticles are stable for long period. Singlet oxygen generation in aqueous media will be measured and later cytotoxicity and phototoxicity of these nanoparticles will be checked.

A new method to form smooth thin film of the fluorene based polymers and polyrotaxanes is still under study. As soon as we form thin films of these compounds, we will fabricate other PLED devices employing the polymers and polyrotaxanes to compare their device performance.

Chapter 6 REFERENCES

[1] Cram, D. J.; Abeall, J. *J. Am. Chem. Soc.* **1955,** *77*, 1179. 1.

[2] Feast, W. J.; Tsibouklis, J.; Pouwer, K. L.; Groenendaal, L.; Meijer, E. W. *Polymer* **1996,** *37*, 5017.

[3] Salafsky, J. S.; Laberhuizen, W. H.; Schropp, R. E. I. *Chem.Phys. Lett.* **1998**, 290, 297

[4] Bradley, D.D.C. *Chem. Ber.* **1991**, 21, 719.

[5] Bradley, D.D.C.; Brown, A. R.; Burn, P.L.; Burroughes, J.H.; Friend, R.H.; Greeham, N.C.; Gymer, R. W.; Holmes. A. B.; Kraft, A. M.; Marks, R.N. *Photochem. and Polymeric Syst.* **1993**, 120.

[6] May, *Physics world* **1995**, 52.

[7] Friend, R. H.; Burroughes, J. H.; Shimoda, T. *Physics world* **1999**, 35.

[8] Kanatzldis, M. G. *C&E News* **1990**, 36.

[9] Shaheen, S. E. *Devices Physics of Organic Light-emitting Diodes* Ph. D. dissertation, University of Arizona, **1999**.

[10] Yang, Y.; Pei, Q.; Heeger, A. J. *J. Appl. Phys.* **1996**, *79*, 934.

[11] Wudl, F.; Kobayashi, M.; Heeger, A. J. *J. Org. Chem.* **1984**, *49*, 3382.

[12] Yu, G.; Heeger, A. J. *Synth. Met.* **1997**, *85*, 1183.

[13] Halls, J. J. M.; Walsh, C. A.; Greeham, N. C.; Marseglia, E. A.; Friend, R. H.; Moratti, S. C.; Holmes, A. B. *Nature* **1995**, *376*, 498.

[14] Salbeck, J. *Ber. Bunsenges. Phys. Chem.* **1996**, *100*, 1667.

[15] Greeham, N. C.; Samuel, I. D. W.; Hayes, G. R.; Philips, R. T.; Kessener, Y. A. R. R.; Moratti, S. C.; Holmes, A. B.; Friend, R. H. *Chem. Phys. Lett.* **1995**, 241, 89

[16] Jenekhe, S. A.; Osaheni, J. A. *Science.* **1994**, *265*, 765.

[17] Samuel, I. D. W.; Rumbles, G.; Collison, C. J. *Phys. Rev. B* **1995**, *52*, 573.

[18] Samuel, I. D. W.; Rumbles, G.; Collison, C. J.; Friend, R. H.; Moratti, S. C.; Holmes, A. B. *Synth. Met.* **1997**, *84*, 497.

[19] Yan, M.; Rothberg, L. J.; Papadimitrakopoulos, F.; G *Phys. Rev. Lett.* **1994**, *73*, 744.

[20] Wudl, F.; Allemand, P. M.; Srdanov, G.; Ni, Z.; Mcbranch, D. *ACS Symp. Serv.* **1991**, *455*, 683.

[21] Potember, R. S.; Hoffmann, R. C.; Hu, H., S.; Cocchiaro, J. E.; Viands, C. V.; Murphy, R. A.; Poehler, T. O. *Polymer* **1987**, *28*, 574.

[22] Bond, S. F.; Howie, A.; Friend, R., H. *Sur. Sci* **1995**, *333*, 196.

[23] Couves, L.D.; Porter, S. J. *Synth. Met.* **1989**, 28, C761.

[24] Zinger, B.; Miller, L. L. *J. Am. Chem. Soc.* **1984**, *106*, 6861.

[25] Umana, M.; Weller, J. *Anal. Chem.* **1986**, *58*, 2979.

[26]Barlett, P. N.; Whitaker, R. G. *J. Electroanal. Chem.* **1987**, 37, 224

[27] Caglar, P.; Wnek, G. E. *J. Macromol. Sci. Pure. Appl. Chem.* **1995**, *32*, 349.

[28] Jung, K. S.; Wilson, G. S. *Anal. Chem.* **1996**, *68*, 591.

[29] Swager, T. M. *Acc. Chem. Res.* **1998**, *31*, 201.

[30] Paul, E. W.; Ricco, A. J.; Wrighton, M. S. *J. Phys. Chem.* **1985**, 89, 1441.

[31] Okoniewski, M. *Anderen Eigenschaften*. **1990**, 71, 94.

[32] Kuhn, W.; Hargitay, B.; Katchalsky, A.; Eisenberg, H. *Nature.* **1950**, *165*, 514.

[33]Angelopoulos, M.; Shaw, J. M.; Kaplan, R. D.; Perreault, S. *J. Vac. Sci. Technol B.* **1989**, *7*, 1519.

[34] Clarke, T. C.; Krounbi, M. T.; Lee, V. Y.; Street, G. B. *J. Chem. Soc., Chem Commun.* **1981**, *8*, 384.

[35] Pitchumani, S.; Willig, F. *J. Chem. Soc., Chem. Commun.* **1983**, 13, 809.

[36] Gustafsson, G.; Cao, Y.; Tracy, G. M.; Klavetter, F.; Colaneri, N.; Heeger, A. J. *Nature* **1992**, *357*, 1789.

[37] Pei, Q.; Yu, G.; Zhang, C.; Yang, Y.; Heeger, A. J. *Science* **1995**, 269, 1086

[38] Pei, Q.; Yang, Y.; Yu, G.; Zhang, C.; Heeger, A. J. *J. Am. Chem. Soc.* **1996**, 118, 3922.

[39] Yu, G.; Heeger, A. J. *J. Appl. Phys.* **1995**, *78*, 4510.

[40] Hals, J. J. M.; Walsh, C. A.; Marseglia, E. A.; Friend, R., H.; Moratti, S. C.; Holmes, A. B. *Nature* **1995**, *396*, 498.

[41] Yu, G.; Cao, Y.; Hummelen, J. C.; Wudl, F.; Heeger, A. J. *Science* **1995**, *270*

1789.

[42] Burroghes, J. H.; Jones, C. A.; Friend, R., H. *Nature* **1998**, 335, 137.

[43] Garnier, F.; Hajlaoui, R.; Yasser, A.; Srivastava, P. *Science* **1994**, *265*, 1684.

[44] Brown, A. R.; Pomp, A.; Hart, C. M.; de Leeuw, D. M. *Science* **1995**, *270*, 972.

[45]Torsi, L.; Dodabalapur, A.; Rothberg, L. J.; Fung, A. W. P.; **1996**, *272*, 1462.

[46] Sirringhaus, H.; Tessler, N.; Friend, R., H. *Science* **1998**, *280*, 1741.

[47] Horowitz, G. *Adv. Mater.* **1998**, 10, 365.

[48] Drury, C. J.; Mutsaers, C. M. J.; Hart, C. M.; Matters, M.; de Leeuw, D. M. *Appl. Phys. Lett.* **1998**, *73*, 108.

[49] Yang, Y.; Heeger, A. J. *Nature* **1994**, *372*, 344.

[50] Yu, G.; Pakbaz, K.; Heeger, A. J. *J. Electron. Mater.* **1994**, *23*, 925.

[51] Hide, F.; Diaz-Garcia, M. A.; Schwartz, B. J.; Heeger, A.J. *Acc. Chem. Res.* **1997**, 30, 430.

[52] Wong, K., T.; Leung, M., K.; Luh, T. Y. In *Progress of Advanced Organic Synthesis Chemistry*; Chemical Industry Press Beijing, **2005**, 313.

[53] Gustafsson, G.; Cao, Y.; Treacy, G. M.; Klavetter, F.; Colaneri, N.; Heeger, A. J. *Nature* **1992**, 357, 6378.

[54] Burrows, P. E.; Gu, G.; Bulovic, V.; Shen, Z.; Forrest, S. R.; Thompson, M. E. *Transactions on Electron Devices* **1997**, 44, 1188–1203.

[55] Hebner, T. R.; Wu, C. C.; Marcy, D.; Lu, M. H.; Sturm, J. C. *Applied Physics Letters* **1998**, 72, 519.

[56] Yang, Yang *Applied Physics Letters* **1998**, 72, 2660.

[57] Brandon Bailey (31 January 2011). "Flexible electronic display will get Army field test". Los Angeles Times. Retrieved 14 June 2014.

[58] ‘'Light emitting wallpaper' could replace bulbs". BBC News. 30 December 2009. Retrieved 14 June 2014.

[59] Michael Fitzpatrick (5 July 2010). "Haptics brings a personal touch to technology". BBC News. Retrieved 14 June 2014.

[60] Paetzold, R.; Heuser, K.; Henseler, D.; Roeger, S.; Wittmann, G.;Winnacker, *A. Appl. Phys. Lett.* **2003**, 82, 3342–3344.

[61] Huh, J. W.; Kim, Y. M.; Park, Y. W.; Choi, J. H.; Lee, J. W.; Yang, J. W.; Ju, S. H.; Paek, K. K.; Ju, B. K. J. *Appl. Phys.* **2008,** 103, 044502

[62] R.R. Søndergaard, M. Hösel, and F. C. Krebs, *J. Polym. Sci. Part B Polym. Phys.* **2013,** 51, 16–34.

[63] H. Jin, C. Tao, M. Velusamy, M. Aljada, Y. L. Zhang, M. Hambsch, P. L. Burn, and P. Meredith, *Adv.Mater*. **2012**, 24, 2572–2577.

[64] S. I. Na, S. S. Kim, J. Jo, and D. Y. Kim, *Adv. Mater*. **2008**, 20, 4061–4067.

[65] S. D. Yambem, K. S. Liao, N. J. Alley, and S. A. Curran, *J. Mater. Chem.* **2012**, 22, 6894–6898.

[66] X. Chu, M. Guan, Y. Zhang, Y. Li, X. Liu, and Y. Zeng, *RSC Adv.* **2013**, 3, 9509–9513.

[67] K. Tvingstedt and O. Inganäs, *Adv. Mater.* **2007**, 19, 2893–2897.

[68] T. H. Han, Y. Lee, M. R. Choi, S. H. Woo, S. H. Bae, B. H. Hong, J. H. Ahn, and T. W. Lee, *Nature Photon.* **2012**, 6,105–110.

[69] R. C. Tenent, T. M. Barnes, J. D. Bergeson, A. J. Ferguson, B. To, L. M. Gedvilas, M. J. Heben, and J. L. Blackburn, *Adv. Mater.* **2009**, 21, 3210–3216.

[70] Groenendaal, L. B.; Jonas, F.; Freitag, D.; Pielartzik, H.; Reynolds, J. R. *Adv. Mater.* **2000**, 12, 481–494.

[71] de Jong, M. P.; IJzendoorn, L. J.; de Voigt, M. J. A. *Appl. Phys. Lett.* **2000**, 77, 2255–2257.

[72] Kim, J. S.; Friend, R. H.; Grizzi, I.; Burroughes, J. H. *Appl. Phys. Lett.*

2005, 87, 023506.

[73] Heidenhain, S. B.; Sakamoto, Y.; Suzuki, T.; Miura, A.; Fujikawa, H.; Mori, T.; Tokito, S.; Taga, Y. *J. Am. Chem. Soc.* **2000,** *122*, 10240.

[74] Moo-Jin, Park; Ji-Hoon Lee, Do-Hoon Hwang *Current Applied Physics.* **2006,** 6, 752–755.

[75] Lee, Jeong-Ik; Klaerner, Gerrit; Davey, Mark H.; Miller, Robert D. *Synthetic Metals.* **1999**. 102: 1087–1088.

[76] Hou, Qiong; Xu, Xin; Guo, Ting; Zeng, Xianghua; Luo, Suilian; Yang, Liting *European Polymer Journal* **2010**, 46, 2365–2371.

[77] (**2007**). D. R. Jonathan W. Steed, *Core Concepts in Supramolecular Chemistry and Nanochemistry* (s. 11).

[78] I.T Harrison, S. Harrison. *J. Am. Chem. Soc.* **1967**, 89, 5723-5724.

[79] Ooya, T.; Yui, N. *ACS Symp.* Ser. **2000**, *752*, 375.

[80] Watanabe, J.; Ooya, T.; Park, K.D.; Kim, Y.H.: Yui, N. *J.Biomater. Sci., Polym. Ed.* **2000**, 11, 1333.

[81] Ooya, T.; Yui, N. *Controlled Release* **1999**, *58*, 251.

[82] Ooya, T.; Yui, N.; Eguchi, M.; Ozaki, A. *Int. J. Pharm.* **2002**, *242*, 47 [11] Ooya, T.; Yui, N. *Macromol. Chem. Phys.* **1998**, *199*, 2311.

[83] Ooya, T.; Yui, N. *Crit. Rev. Ther. Drug Carrier Syst.* Ser. **1999**, *16*, 289.

[84] Ooya, T.; Yui, N.; Tomita, H.; Lee, W. K.; Huh, K. M. *Macromol. Rapid Commun.* **2002**, 23, 179.

[85] Fujita, H.; Ooya, T.; Yui, N. *Macromol. Chem. Phys.* **1999**, 200, 706.

[86] Fujita, H.; Ooya, T.; Yui, N. *Macromolecules* **1999**, 32, 2534.

[87] Ikeda, T.; Watabe, N.; Yui, N.; *Macromol. Chem. Phys.* **2001**, 202, 1338.

[88] Ikeda, T.; Ooya, T.; N.; Yui, N. *Polymer J.* **1999**, 31, 658.

[89] Caciali, F.; Wilson, J.S.; Michels, J.J.; Daniel, C.; Silva, C.; Friend, R.H. *Nat Mater.* **2002**, 1, 160.

[90] Koziar, J.; Cowan, D. *ACS.* **1977**, 0001-4842

[91] Villiers A. *Compt Rendu* **1891**, 112, 536.

[92] Eastburn SD, Tao BY. *Biotechnol Adv* **1994**, 12, 325–39.

[93] Szetjli J. *Chem Rev* **1998**, 98, 1743–53.

[94] Szetjli J. Downstream processing using cyclodextrins. *TIBTRCH* **1989**, 7, 171–4.

[95] Taylor, P.N.; O'Connell, M.J.; McNeill, L.A.; Hall, M.J.; Aplin, R.T.; Anderson, H.L. *Angew Chem Int Ed* **2000**, 39, 3456–60.

[96] Grigoras, M.; Conduruta, D.G. *Rev. Roum. Chim*. **2006**, 51, 987–992.

[97] Liu, Y.; Shi, J.; Chen, Y.; Ke, C.F. *Angew. Chem. Int. Ed*. **2008**, 47, 1–5.

[98] C. Marquez, W. M. Nau, *Angew. Chem.* **2001**, 113, 4515 – 4518; *Angew. Chem*. Int. Ed. **2001**, 40, 4387 – 4390.

[99] F. Cacialli, J.S.; Wilson, J.J.; Michels, Daniel, C.; Silva, C.; Friend, R. H.; Severin, N.; Samor, P.; Rabe, J. P.; M. Connell, J. O, Taylor, P. N.; Anderson, H. L.; *Nat. Mater.* **2002**, 1, 160 – 164.

[100] Lindsey, J. S., Littler, B. J. & Wagner, R. W. *J. Org. Chem.* **1999**, 64, 1391.

[101] Miyaura, N.; Yamada, K.; Suzuki, A. *Tetrahedron Letters*, **1979**, 36, 3437–3440.

[102] Miyaura, N.; Suzuki, A. *Chem. Comm.* **1979**, 19, 866–867.

[103] Miyaura, N.; Suzuki, A. *Chemical Reviews* **1995**, 7, 2457–2483.

[104] Stille, J. K.; *Angew. Chem. Int. Ed. Engl.* **1986**, *25*, 508–524.

[105] Arthur, W.S.; Edward, E.F.; Melissa, M. C.; Glen, G.J.; Mario, G.A. *Analyst.* **2009**, 134, 1790-1801.

[106] Harada, A.; Li, J.; Suzuki, S.; Kamachi, M. *Macromolecules* **1993**, 26, 5267.

[107] Izatt, R. M.; Pawlak, K.; Bradshaw, J.S. *Chem. Rev.* **1991**, 91, 1721.

[108] Gibson, H.; Marand, H. *Adv. Mater.* **1993**, 5, 11.

[109] Agam, G.; Graiver, D.; Zilkha, A. *J. Am. Chem. Soc.* **1976**, 98, 5206.

[110] Agam, G.; Graiver, D.; Zilkha, A. *J. Am. Chem. Soc.* **1976**, 98, 5214.

[111] Shen, Y. X.; Xie, D.; Gibson, H. W. *J. Am. Chem. Soc.* **1994**, 116, 537.

[112] Pasini, D.; Raymo, F.M.; Stoddart, J.F. *Gazz. Chim. Ital*. **1995**, 125, 431-435.

[113] Langford, S.J.; Stoddart, J.F. *Pure Appl. Chem.* **1996**, 68, 1255-1260.

[114] Amabilino, D.B.; Raymo, F.M.; Stoddart, J.F. *Comprehensive Supramolecular Chemistry*; Hosseini, M. W.; Sauvage, J. P.; Pergamon. Oxford, **1996**, 9, 85-130.

[115] Raymo, F. M.; Stoddart, J.F. *Pure Appl. Chem.* **1997**, 69, 1987-1997.

[116] Gillard, R. E.; Stoddart, J.F. *Chemtracs* **1998**, 11, 491-511.

[117] R. Behrend, E. Meyer and F. Rusche, Justus Liebigs *Ann. Chem*., **1905**, 339, 1.

[118] W. A. Freeman, W. L. Mock and N.-Y. Shih, *J. Am. Chem. Soc*., **1981**, 103, 7367.

[119] J. Kim, I.-S. Jung, S.-Y. Kim, E. Lee, J.-K. Kang, S. Sakamoto, K. Yamaguchi and K. Kim, *J. Am. Chem. Soc*., **2000**, 122, 540.

[120] W.-H. Huang, S. Liu and L. Isaacs, *Cucurbit[n]urils, in Modern Supramolecular Chemistry: Strategies for Macrocycle Synthesis*, ed. F. Diederich, P. J. Stang and R. R. Tykwinski, **2008**, 113.

[121] J. Kim, I.;S. Jung, S.;Y. Kim, E. Lee, J.;K. Kang, S. Sakamoto, K. Yamaguchi and K. Kim, *J. Am. Chem. Soc*., **2000**, 122, 540.

[122] a) W. S. Jeon, K. Moon, S. H. Park, H. Chun, Y. H. Ko, J. Y. Lee, E. S. Lee, S. Samal, N. Selvapalam, M. V. Rekharsky, V. Sindelar, D. Sobransingh, Y. Inoue, A. E. Kaifer, K. Kim, *J. Am. Chem. Soc.* **2005**, 127, 12984; b) M. V. Rekharsky, T. Mori, C. Yang, Y. H. Ko, N. Selvapalam, H. Kim, D. Sobransingh, A. E. Kaifer, S. Liu, L. Isaacs, W. Chen, S. Moghaddam, M. K. Gilson, K. Kim, Y. Inoue, Proc. Natl. *Acad. Sci. USA* **2007**, 104, 20737.

[123] A. I. Day, R. J. Blanch, A. P. Arnold, S. Lorenzo, G. R. Lewis and I. Dance, *Angew. Chem., Int. Ed*., **2002**, 41, 275.

[124] Simin Liu, Peter Y. Zavalij, and Lyle Isaacs *J. Am. Chem. Soc.*; **2005**, 48, 16798 – 16799.

[125] W. H. Huang, P. Y. Zavalij, L. Isaacs, *J. Am. Chem. Soc.* **2005**, 127, 18000 – 18001.

[126] W. H. Huang, P. Y. Zavalij, L. Isaacs, *Angew. Chem.* **2007,** 119, 7569 – 7571; *Angew. Chem. Int. Ed.* **2007**, 46, 7425 – 7427.

[127] W. H. Huang, S. M. Liu, P. Y. Zavalij, L. Isaacs, *J. Am. Chem. Soc.* **2006**, 128, 14744 – 14745.

[128] Y. Miyahara, K. Goto, M. Oka, T. Inazu, *Angew. Chem.* **2004**, 116, 5129 – 5132; *Angew. Chem. Int. Ed.* **2004**, 43, 5019 – 5022.

[129] X. J. Cheng, L. L. Liang, K. Chen, N. N. Ji, X. Xiao, J. X. Zhang, Y.Q. Zhang, S. F. Xue, Q. J. Zhu, X. L. Ni, and Z. Tao. *Angew. Chem.* **2013**, 125, 7393 –7396.

[130] (**2009**). Cucurbituril. In J. W. Steed, & J. L. Atwood, *Supramolecular Chemistry.* Wiley.

[131] A. Day, A. P. Arnold, R. J. Blanch and B. Snushall, *J. Org. Chem*., **2001**, 66, 8094.

[132] R. L. Halterman, J. L. Moore and L. M. Mannel, *J. Org. Chem*., **2008**, 73, 3266.

[133] A. Thangavel, A. M. M. Rawashdeh, C. Sotiriou-Leventis and N. Leventis, *Org. Lett*., **2009**, 11, 1595.

[134] D. Jiao, N. Zhao and O. A. Scherman, *Chem. Commun*., **2010**, 46, 2007.

[135] E. Masson, X. Ling, R. Joseph, L. K. Mensah, X. Lu. *RSC Advances,* **2012**, 2, 1213–1247.

[136] Kim, K.; Selvapalam, N.; Oh, D.H. *J. Incl. Phenom*., **2004**, 50, 31-36.

[137] a) Baris Temelli, C. U. *Tetrahedron*. **2009**, 2. ; b)Dolphin, D. Academic: New York, NY, **1978**, 1–6; c)Milgrom, L. R. Oxford University Press: Oxford, **1997**.

[138] Rothemund, P. J. *Handbook of Porphyrin Science: With Applications to Chemistry, Physics, Materials Science, Engineering, Biology and Medicine.* **1936**.

[139] Adler, A. D., Longo, F. R., Finarelli, J. D., Goldmacher, J., Assour, J., & Korsakoff, L. *Journal of Organic Chemistry*, **1967**, 32, 476.

[140] Jonathan S. Lindsey, R. W. *The Journal of Organic Chemistry*. **1989**, 54, 828-836.

[141] Fan, D., Taniguchi, M., Yao, Z., Dhanalekshmi, S., & Lindsey. *Tetrahedron*. **2005**, 61, 10291, 10302.

[142] Benjamin J. Littler, Y. C. *The Journal of Organic Chemistry*, **1999**, 1-2.

[143] J.G. Levy, M. Obochi, *Photochem. Photobiol*. **1996**, 64, 737–739.

[144] Svanberg K, Wang I, Colleen S, Idvall I, Ingvar C, Rydell R, Jocham D, Diddens H, Brown S, Gregory G, Montan S, Anderson-Engels S, Svanberg S. *Acta Radiol.* **1998**, 39, 2-9.

[145] Bonnett R, Martinez G. *Tetrahedron*. **2001**, 57, 9513-9547.

[146] Jesionek A, von Tappenier H. *Muench Med Wochneshr* **1903**, 47, 2042.

[147] Hausman W. Die. *Biochem Z.* **1911**, 30, 276.

[148] Figge FH, Weiland GS, Manganiello LO. *Proc Soc Exp Biol Med* **1948**, 68, 640.

[149] Lipson RL, Baldes EJ. *Arch Dermatol.* **1960**, 82, 508.

[150] Dougherty TJ. *J Natl Cancer Inst.* **1974**, 52, 1333—6.

[151] Dougherty TJ, Kaufman JE, Goldfarb A, Weishaupt KR, Boyle D, Mittleman A.

Cancer Res **1978**, 38, 2628—35.

[152] Dougherty TJ, Lawrence G, Kaufman JH, Boyle D, Weishaupt KR, Goldfarb A. *J Natl Cancer Inst.* **1979**, 62, 231—7.

[153] Spikes JD. *J Photochem Photobiol B.* **1990**, 6, 259—74.

[154] Baas P, van Mansom I, van Tinteren H, Stewart FA, van Zandwijk N. *Lasers Surg Med* .**1995**, 16, 359—67.

[155] Orenstein A, Kostenich G, Roitman L. *Br J Cancer* **1996**, 73, 937—44.

[156] Kessel D, Thompson P. *Photochem Photobiol.* **1987**, 46, 1023—5.

[157] Sharman, W. M.; Allen, C. M.; van Lier, J. E. *Drug Discovery Today.* **1999**, *4*, 507-517.

[158] X. L. Liang, X. D. Li, X. L. Yue, Z. F. Dai, *Angew. Chem.* **2011**, 123, 11826; *Angew. Chem. Int. Ed.* **2011**, 50, 11622.

[159] Litter, B.J; Miller, M.A.; Hung, C. H.; Wagner, R.W.; O' Shea, D.F.; Boyle, P.D.; Lindsey, J.S. *J. Org. Chem.* **1999**, 64, 1391.

[160] Ka, J. W.; Lee, C. H. *Tetrahedron Lett*., **2000**, 41, 4609.

[161] Kuwabata, S.; Martin C. R. *J. Membrane Sci.* **1994,** 91, 1-12.